Volume 95, Number 5, September-October 1990
Journal of Research of the National Institute of Standards and Technology

Contents

Articles

Title	Authors	Page
Recommended Values of the Fundamental Physical Constants: A Status Report	**Barry N. Taylor and E. Richard Cohen**	497
An International Comparison of Absolute Radiant Power Measurement Capabilities	**Douglas B. Thomas**	525
Results of a CIE Detector Response Intercomparison	**Douglas B. Thomas and Edward F. Zalewski**	533
Effects of the International Temperature Scale of 1990 (ITS-90) on CIE Documentary Standards for Radiometry, Photometry, and Colorimetry	**Klaus D. Mielenz and Jack J. Hsia**	545
An Accurate Value for the Absorption Coefficient of Silicon at 633 nm	**Jon Geist, A. Russell Schaefer, Jun-Feng Song, Yun Hsia Wang, and Edward F. Zalewski**	549
Hard X-Ray Microscope With Submicrometer Spatial Resolution	**Masao Kuriyama, Ronald C. Dobbyn, Richard D. Spal, Harold E. Burdette, and David R. Black**	559
Software Techniques to Improve Data Reliability in Superconductor and Low-Resistance Measurements	**L. F. Goodrich and A. N. Srivastava**	575

Conference Reports

Title	Authors	Page
Workshop on Intelligent Processing for Primary Metals	**James G. Early**	591
Data Administration Management Association Symposium	**Judith Newton**	597
CIMCON '90 Conference—Computer Integrated Manufacturing (CIM) Architecture Conference (CON)	**Albert Jones**	601

News Briefs

GENERAL DEVELOPMENTS 605
NIST Seeks Proposals for Measurement Grants
Study to Help Understand Bone Demineralization
Basic Membrane Research
Bibliography of Electron Swarm Data
More Efficient Route Developed to Low-Shrinkage Polymers
Wear Mechanisms in Coal-Fueled Diesel Engines
First SEMPA Images of Magneto-Optical Recording Media
Secure Data Network System (SDNS) Reports Published
Revision to FIPS 120, Graphical Kernel System (GKS), Proposed
FIPS 100 Being Revised
FIPS for Programming Language C Proposed
American Society for Metals Adopts NIST-Developed Software to Further its Phase Diagram Publications
Frequency Stabilization of Erbium Fiber Laser Offers Potential for Wavelength Standard
NIST Work Leads to Adoption of Three ASTM Standards on Electromigration Measurements
New Video Can Help Save Energy and Dollars
Characterizing Clocks and Oscillators
Atmospheric Attenuation Measurements Studied
Electromagnetic Properties of Superconductors
Measurement Needs for New Technologies in Electronics
Electrical Engineering/Electronics Bulletin Available
NIST Expands Security Bulletin Board
PHIGS Conformance Test Available
Basics of Chemical Instrumentation Explained
Coaxial Intrinsic Impedance Standards Described
NIST, APL Study Automated Electronics Assembly
New Accreditation Program Announced for Testing Labs
Guidelines Issued for Pressure Vessel Safety Assessment
Industrial Firm to Consult With NIST on Polymers
Risk Assessment the DOE Way
Measuring Flow in The Space Shuttle
Nine Grants Awarded for State Technology Programs
Is Your Office User-Friendly?
Directory Published on Weights and Measures Labs
Automated Stress Analysis of Solder Joints Using Inspection Data
Refractory Materials at Ultra-High Temperatures
New Ceramic Phases Characterized in Collaborative Program
New Standard for Polymer Processing

Consortium on Automated Analytical Laboratory Systems (CAALS) Meets at NIST
First Infrared Spectra of Dimer Ions
User Interface Component of the Applications Portability Profile as a Federal Information Processing Standard (FIPS) Approved
New Publication Describes Object Database Management Systems
Magnetoresistive Recording Head Fabricated, Measured
NIST Develops New Optically Pumped Integrated-Optic Laser
NIST, Industry Apply Expert System to Screen Production-Line Integrated Circuit Wafers
Ego-Motion Field Theory Developed

CALIBRATION SERVICES 615

Inexpensive Frequency Calibration Service Available
NIST Establishes Special-Test Services for Complex Permittivity Measurement

STANDARD REFERENCE MATERIALS 616

Materials Can Help Evaluate Industrial Atmosphere
X-Ray Fluorescence Spectrometry Ore Available

STANDARD REFERENCE DATA 617

Database to Help Test Writing Recognition Devices
Standard Reference Data Products Catalog Published
PC Database Available for Hydrocarbon Mixtures
Major Expansion Made to Chemical Kinetics Database
DIPPR Database Expanded to 1,117 Compounds

Calendar 619

Volume 95, Number 5, September–October 1990
Journal of Research of the National Institute of Standards and Technology

[J. Res. Natl. Inst. Stand. Technol. **95**, 497 (1990)]

Recommended Values of the Fundamental Physical Constants: A Status Report

Volume 95 | Number 5 | September–October 1990

Barry N. Taylor

National Institute of Standards and Technology,
Gaithersburg, MD 20899

and

E. Richard Cohen

Rockwell International Science Center,
Thousand Oaks, CA 91360

We summarize the principal advances made in the fundamental physical constants field since the completion of the 1986 CODATA least-squares adjustment of the constants and discuss their implications for both the 1986 set of recommended values and the next least-squares adjustment. In general, the new results lead to values of the constants with uncertainties 5 to 7 times smaller than the uncertainties assigned the 1986 values. However, the changes in the values themselves are less than twice the 1986 assigned one-standard-deviation uncertainties and thus are not highly significant. Although much new data has become available since 1986, three new results dominate the analysis: a value of the Planck constant obtained from a realization of the watt; a value of the fine-structure constant obtained from the magnetic moment anomaly of the electron; and a value of the molar gas constant obtained from the speed of sound in argon. Because of their dominant role in determining the values and uncertainties of many of the constants, it is highly desirable that additional results of comparable uncertainty that corroborate these three data items be obtained before the next adjustment is carried out. Until then, the 1986 CODATA set of recommended values will remain the set of choice.

Key words: CODATA; conversion factors; electrical units; fundamental physical constants; Josephson effect; least-squares adjustment; quantum Hall effect; recommended values of the constants; Task Group on Fundamental Constants.

Accepted: August 10, 1990

1. Introduction

1.1 Background

In late 1986 [1] and also in 1987 [2], CODATA[1] published a report of the CODATA Task Group on Fundamental Constants prepared by the authors under the auspices and guidance of the Task Group. The report summarizes the 1986 least-squares adjustment of the fundamental physical constants and gives a set of self-consistent values for the basic constants and conversion factors of physics and chemistry derived from that adjustment. Recommended by CODATA for worldwide use throughout all of science and technology and thus widely disseminated [3], the 1986 CODATA set of recommended values replaced its immediate predecessor, that recommended for international use by CODATA in 1973. This set was based on the 1973 least-squares adjustment of the fundamental physical constants which was also carried out by the authors under the auspices and guidance of the Task Group [4,5]. The 1986 adjustment was a

[1] CODATA, the Committee on Data for Science and Technology, was established in 1966 as an interdisciplinary committee of the International Council of Scientific Unions. It seeks to improve the compilation, critical evaluation, storage, and retrieval of data of importance to science and technology.

major advance over its 1973 counterpart; the uncertainties of the recommended values were reduced by roughly an order of magnitude due to the enormous advances made throughout the precision measurement-fundamental constants field during the 13 years that elapsed between the two adjustments.

Recognizing that the fundamental physical constants field is ever advancing, that is, data affecting our knowledge of the constants are continually appearing, the CODATA Task Group[2] at its June 1988 meeting asked the authors to prepare a status report on the constants for discussion at its June 1990 meeting. This paper is a direct consequence of that request, which to some extent was motivated by the planned introduction, starting 1 January 1990, of new practical representations of the volt and ohm as defined in the International System of Units or SI. (These new representations will be discussed in sec. 2.1.7.) Another motivating factor was the recognition by the Task Group that 13 years between adjustments is probably too long and that progress in the field should be monitored more closely to help identify when a new set of recommended values should be introduced; the 1973 set had become completely out of date well before the 1986 set was available to replace it.

The 1986 adjustment took into consideration all relevant data available up to 1 January 1986. In the intervening $4\frac{1}{2}$ years, a number of new results have been reported that have important implications for the 1986 CODATA recommended values as well as the timing of the next least-squares adjustment. We summarize these results in this paper and discuss their impact, but do not give new recommended values for any constants. One reason is that because the output values of a least-squares adjustment are correlated, the new results cannot be readily incorporated in the 1986 table of recommended values; to do so properly requires nothing less than a new least-squares adjustment. More important, although the new results can lead to significant reductions in the uncertainties assigned to many of the 1986 recommended values, it is not deemed appropriate to replace the 1986 set so soon after its introduction. There are two reasons for this view. First, it takes considerable time for a new set of recommended values to diffuse throughout all of science and technology; handbooks, textbooks, encyclopedias, and other reference works are not revised yearly. Second, the 1986 values adequately serve the needs of the vast majority of users—those few users who require the most up-to-date and accurate values of the constants can consult the primary literature as well as seek advice and guidance from the authors. Based on past experience, it would seem that 6–8 years between adjustments is reasonable; it is not so short an interval that the current set of recommended values has had insufficient time to become widely adopted, or so long that the current set has become totally obsolete. In the final analysis, however, scientific progress should be the deciding factor. If the advances made since the last adjustment would lead to changes in the recommended values several times the one-standard-deviation uncertainties assigned to these values, then a new adjustment may well be immediately called for. If the new results would only lead to reductions in the uncertainties of the recommended values, which as we shall see is the situation at present, then there is considerably less motivation for introducing a new set of values and it is appropriate to wait a longer period. On this basis, we believe that the 1986 set of values should remain the most up-to-date, consistent set available for the next several years and that it will not be necessary to introduce a new set of constants to replace the 1986 set before 1994.

In discussing the new results and their impact, we shall follow to the fullest possible extent the notation, terminology, and order of topics of the 1986 adjustment, reference [2] in particular. To keep this paper to a reasonable length, it is assumed that the reader is familiar with or has reference [2] in hand. After a few brief comments concerning the status of the least-squares evaluation procedure in section 1.2, we review in section 2 the status of the auxiliary constants and stochastic input data. It will be recalled that quantities in the auxiliary constant category are either defined constants such as c (speed of light in vacuum=299 792 458 m/s exactly) and μ_0 (permittivity of vacuum=$4\pi\times10^{-7}$ N/A^2 exactly) with no uncertainty, or constants such as R_∞ (Rydberg constant for infinite mass) with assigned uncertainties sufficiently small in comparison with the uncertainties assigned the stochastic input data with which they are associated in the adjustment that they can be taken as exact. In other words, the auxiliary constants are not subject to adjustment in contrast to the stochastic data. In the 1986 adjustment the uncertainty of each auxiliary constant was no greater than 0.02

[2] The current members of the CODATA Task Group on Fundamental Constants are T. J. Quinn (Chairman), E. R. Cohen, T. Endo, B. Kramer, B. A. Mamyrin, B. N. Oleinik, B. W. Petley, H. Preston-Thomas, and B. N. Taylor.

parts-per-million or ppm.[3] In contrast, the uncertainties assigned the 38 items of stochastic input data considered in the 1986 adjustment were in the range 0.065 to 9.7 ppm. The 38 items were of 12 distinct types with the number of items of each type ranging from one to six.

Since this is a status report and not a description of a new least-squares adjustment, our summary of the data in section 2 is not exhaustive and the data are not critically evaluated; we discuss the significant new results only and assume the values and uncertainties as reported are correct. We are therefore addressing the question: If the new results reported since the completion of the 1986 adjustment are taken at face value, what are the implications for the 1986 recommended values? When known, anticipated future results are indicated to provide guidance as to when the next adjustment should be carried out. Where appropriate, the new data are compared with their 1986 counterparts and the 1986 recommended values. The data are further compared and analyzed in section 3, and the implied changes in the 1986 recommended values and their uncertainties as obtained from least-squares analyses that may well preview the next CODATA adjustment are presented in this section as well. Our conclusions are given in section 4.

1.2 Data Selection and Evaluation Procedures

Grabe [6] has taken issue with the statistical approaches generally used to treat experimental data, in particular, those employed in the 1986 least-squares adjustment of the constants [7]. He prefers a more conservative approach based on what he terms "abandoning the randomization of systematic errors" [6] that would lead to recommended values of the constants with larger assigned uncertainties. Grabe's proposed treatment has been extensively rebutted by one of the authors (ERC) in private correspondence and in a brief note [8]. Artbauer [9] has proposed an "interval" approach to the evaluation of measurement uncertainty that, if applied to the least-squares adjustment of the constants, would also likely lead to recommended values with larger uncertainties. At this point, there is little justification for abandoning what has been done in the past; the perceived need by some for recommended values of the constants with "safe" uncertainties was refuted by one of the authors (BNT) 20 years ago [10]. That is not to say that further work to improve the statistical procedures used in a least-squares adjustment should be abandoned; indeed, the authors plan to carry out such work over the next several years with emphasis on refining the statistical techniques used in the 1986 adjustment. But it should be borne in mind that the cornerstone of a successful fundamental constants adjustment is the critical review of each experimental and theoretical result considered for inclusion in the adjustment. Discussions and correspondence with the researchers who have carried out the measurements and calculations are crucial to this process and the evaluator must not accept their *a priori* assigned uncertainties uncritically. By comparison, the particular statistical procedures used in the adjustment play a secondary role.

[3] Throughout, all uncertainties are one-standard-deviation estimates.

2. Review of the Data

2.1 Auxiliary Constants

Because the uncertainties of the auxiliary constants in a least-squares adjustment are generally 10–20 times less than the uncertainties of the stochastic input data, as might be expected, the new results discussed in this section have little impact on the vast majority of the 1986 recommended values. Moreover, it is unlikely that any quantity in the auxiliary constant category in the 1986 adjustment will become a stochastic input datum in the next adjustment.

2.1.1 The Speed of Light and the Definition of the Meter Principal among the list of recommended radiations given by the International Committee of Weights and Measures (CIPM) [11] for realizing the meter is the He-Ne laser stabilized by saturated absorption on CH_4 with the adopted frequency $f=88\ 376\ 181\ 608$ kHz. However, recent measurements [12–15] have shown that this value is too large by about 9 parts in 10^{11}, or twice the 4.4×10^{-11} uncertainty assigned to it by the CIPM. This implies that the frequencies adopted for the other CIPM recommended radiations, which are in the more important visible portion of the spectrum, are also in error by this amount. Nevertheless, because the smallest uncertainty assigned by the CIPM to these frequencies is 2 parts in 10^{10}, the impact is minor. In fact, the only fundamental-constant experiment at present that requires the realization of the meter with an uncertainty of less than 1 part in 10^9 is the determination of R_∞ (to be discussed in sec. 2.1.4). However, in this case the uncertainty in realizing the meter is the limiting factor.

2.1.2 Proton-Electron Mass Ratio The 1986 recommended value and that used as an auxiliary

constant in the adjustment, $m_p/m_e = 1836.152\ 701(37)$ (0.020 ppm), was obtained by van Dyck and colleagues at the University of Washington from Penning-trap ion-cyclotron resonance measurements. It has recently been confirmed to well within the current 0.05-ppm uncertainty of the experiments of Gabrielse and colleagues [16] working at CERN who are using similar techniques but a radically different geometry to measure the antiproton-proton mass ratio [17]. A value of m_p/m_e with a 0.13-ppm uncertainty that also confirms the 1986 recommended value has been obtained from the H-D isotopic shifts of three transitions as measured in a recent Rydberg constant experiment (see sec. 2.1.4). van Dyck and colleagues are continuing their measurements of m_p/m_e and believe that the present 0.020-ppm uncertainty can be reduced by an order of magnitude. An improved result from Gabrielse and coworkers may also be expected.

2.1.3 Relative Atomic Masses and Mass Ratios The 1983 Atomic Mass Table of Wapstra and Audi used in the 1986 adjustment remains the most complete table of values published to date. The 1986 Audi-Wapstra Mid-Stream Mass Evaluation was distributed as a private report [18] and was not fully published [19]. The effect on the fundamental constants of the small differences between the 1986 and 1983 values is negligible. For example, the value of the atomic mass of ^{1}H from the 1986 Mid-Stream Mass Evaluation implies the value 1.007 276 468(7) u for the atomic mass of the proton, compared with the 1983 value of 1.007 276 470(12) u. For the atomic mass of the neutron, the corresponding values are 1.008 664 914(8) u and 1.008 664 904(14) u. Advances in cyclotron resonance measurements of single ions in a Penning trap promise to provide improved mass values during the next several years. As an example, van Dyck and colleagues [20] have measured directly the ratio $m(^{12}C^{4+})/m_p$ to obtain 1.007 276 468(3) u for the proton atomic mass. A new mass adjustment and atomic mass table to replace that of 1983 is expected to be available in the early 1990s.

The accurate measurement of mass in kilograms is important in a number of fundamental constant experiments, for example, determining the Avogadro constant N_A by the x-ray crystal density method or determining the Planck constant h using a balance that compares electrical and mechanical power. Although the SI unit of mass, the international prototype of the kilogram, has cleaning and stability-related problems [21], these are sufficiently small at present (e.g., ~1 part in 10^8) relative to the uncertainties of such experiments that they can be ignored. However, anticipated improvements in these experiments may confront the kilogram's limitations and eventually lead to a new definition of the SI unit of mass based on an invariant of nature such as the mass of an elementary particle or atom, or other fundamental constant [22].

2.1.4 Rydberg Constant The 1986 recommended value, $R_\infty - 10\ 973\ 731\ \mathrm{m}^{-1} = 0.534(13)\ \mathrm{m}^{-1}$, was based to a large extent on the 1981 value (suitably corrected for the new meter definition) $0.539(12)\ \mathrm{m}^{-1}$ [4] obtained by Amin et al. at Yale from their single photon measurements of the wavelengths of the Balmer-α lines in H and D. The experiment was subsequently repeated with a number of improvements, yielding the result $0.569(7)\ \mathrm{m}^{-1}$ as reported by Zhao et al. in late 1986 [23]. The cause of the difference has yet to be identified. However, a number of other measurements of R_∞ with uncertainties in the parts in 10^{10} range have been reported, and all agree with this higher value (see table 1 and fig. 1).

Biraben et al. [24] at the Ecole Normale Supérieure using Doppler-free, two-photon spectroscopy of H and D Rydberg levels ($2S-nD$, $n=8,10$) obtained $0.569(6)\ \mathrm{m}^{-1}$. Zhao et al. [25] also measured the $2S-4P$ Balmer-β transition in H and D in a modification of their earlier Yale experiment and obtained $0.573(3)\ \mathrm{m}^{-1}$. Boshier et al. [26] at the University of Oxford measured the $1S-2S$ transition in H and D using Doppler-free, two-photon spectroscopy to find $0.573(3)\ \mathrm{m}^{-1}$. In a similar experiment, McIntyre et al. [27] at Stanford University obtained $0.569(8)\ \mathrm{m}^{-1}$. (An earlier version of this experiment at Stanford by Beausoleil et al. [28] in which the uncertainty was assigned more optimistically gave $0.571(7)\ \mathrm{m}^{-1}$.)

The most recent result and that with the smallest quoted uncertainty,

$$R_\infty = 10\ 973\ 731.5709(18)\ \mathrm{m}^{-1}\ (1.7\times10^{-10}) \quad (1)$$

was obtained by Biraben et al. [29,30] from an improved version of their earlier experiment using Rydberg levels. It is this work that has yielded the value of m_p/m_e with an uncertainty of 0.13 ppm mentioned in section 2.1.2. The 1.6×10^{-10} uncertainty they assigned to the realization of the meter at visible frequencies based on the 633-nm $^{127}I_2$ stabilized laser [11] is the main source of the 1.7×10^{-10} relative uncertainty in their value of R_∞; if it could be neglected, the relative uncertainty of their result would be 4 times smaller or 4.3×10^{-11}.

[4] To simplify comparisons, we quote $R_\infty - 10\ 973\ 731\ \mathrm{m}^{-1}$ rather than R_∞ itself.

Table 1. Summary of values of the Rydberg constant R_∞

Authors, publication date, reference	Transition	Reported value and uncertainty (R_∞/m^{-1}−10 973 731)	Relative uncertainty (parts in 10^{10})
Cohen and Taylor CODATA 1986 recommended value [2]		0.534(13)	12
Zhao et al., 1986 [23]	H, D, 2S–3P	0.5689(71)	6.5
Biraben et al., 1986 [24]	H, D, 2S–8,10D	0.5692(60)	5.5
Beausoleil et al., 1987 [28]	H, 1S–2S	0.5715(67)	6.1
Zhao et al., 1989 [25]	H, D, 2S–4P	0.5731(29)	2.6
Boshier et al., 1989 [26]	H, D, 1S–2S	0.5731(31)	2.8
McIntyre et al., 1989 [27]	H, 1S–2S	0.5686(78)	7.1
Biraben et al., 1989 [29,30]	H, D, 2S–8,10,12 D	0.5709(18)	1.7

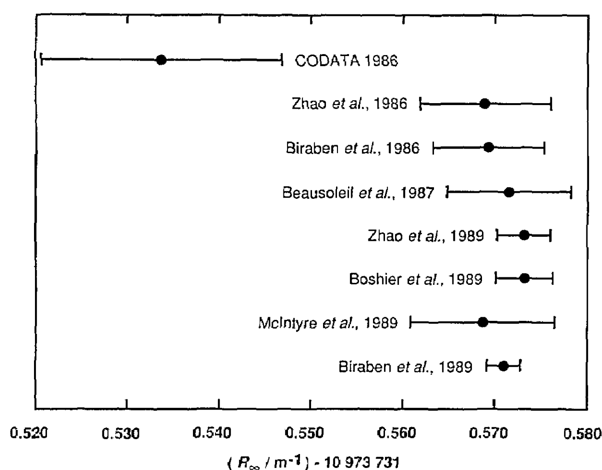

Figure 1. Graphical comparison of the values of the Rydberg constant for infinite mass R_∞ given in table 1.

These and any other R_∞ results that become available will be critically reviewed as part of the next CODATA adjustment. Although it is likely to lead to some changes in values and assigned uncertainties, these should be at the 1–2 parts in 10^{10} level at most and thus not large enough to alter the excellent agreement apparent in table 1 and figure 1. The changes are expected to arise mainly from a uniform treatment of the frequencies assigned to the reference lasers and the theory of the hydrogen atom energy levels.

The recent Biraben et al. value of R_∞ [eq (1)] exceeds the 1986 recommended value by 0.0034 ppm or 2.8 times the 0.0012 ppm uncertainty assigned the 1986 value. Although clearly a significant change, it is sufficiently small relative to the uncertainties of the stochastic input data with which R_∞ was associated in the 1986 adjustment, and the uncertainties of those recommended values derived with the aid of R_∞, that its effect on the 1986 set of values is inconsequential.

2.1.5 *g* Factor of the Free Electron and Muon The University of Washington group has improved its Penning-trap measurements of the magnetic moment anomalies of the electron and positron: $a_e=(\mu_e/\mu_B)-1=(g_e/2)-1$, where μ_e is the electron magnetic moment and μ_B is the Bohr magneton. The new results are [31]

$$a_e(e^-)=1\ 159\ 652\ 188.4(4.3)\times 10^{-12}\ (0.0037\ \text{ppm}) \qquad (2a)$$

$$a_e(e^+)=1\ 159\ 652\ 187.9(4.3)\times 10^{-12}\ (0.0037\ \text{ppm}), \qquad (2b)$$

and $g_e(e^-)/g_e(e^+)=1+(0.5\pm 2.1)\times 10^{-12}$. The uncertainties of the two anomalies are dominated by the common 4×10^{-12} (0.0034 ppm) uncertainty assigned to each to take into account the possible effect of microwave cavity resonances on the measured cyclotron resonance frequencies. The agreement of the two g-factors is the most accurate demonstration to date of charged particle-antiparticle symmetry.

The value of a_e used in the 1986 adjustment, 1 159 652 193(10)$\times 10^{-12}$ (0.0086 ppm), was an earlier result of the University of Washington group but with their originally assigned 4×10^{-12} uncertainty (0.0034 ppm) expanded by a factor of 2.5 to allow for the cavity resonance problem. A new method developed to observe these resonances now provides a sound basis for the 4×10^{-12} uncertainty included in eq (2) for this effect. The current and earlier results are clearly in excellent agreement. In particular, the 1986 recommended value of $g_e/2$ exceeds the value implied by eq (2a) by only 5 parts in 10^{12}, which is entirely negligible.

Very recent measurements in a new, low-Q Penning trap [32] have apparently uncovered a slow magnetic field oscillation induced by a nearby elevator [33]. The simple mean of 14 runs with a nonstatistical distribution falling almost uniformally between limits 0.012 ppm apart yields $a_e(e^-)$=1 159 652 185.5(4.0)$\times 10^{-12}$, which is still consistent with eq (2). Work to understand the observed distribution of values is continuing.

The 1986 value of $g_\mu/2$ is unchanged. A new experiment to determine a_μ with an uncertainty of only 0.35 ppm, some 20 times smaller than the current uncertainty, is being undertaken at Brookhaven National Laboratory by V. W. Hughes and collaborators. This will yield a value of $g_\mu/2=1+a_\mu$ with an uncertainty of 4.1 parts in 10^{10} compared with the present 8.4 parts in 10^9.

2.1.6 Electron and Nuclear Magnetic Moment Ratios The 1986 values of μ_e/μ_p, μ_p/μ_B, and μ'_p/μ_B with their respective 0.010, 0.010, and 0.011 ppm uncertainties remain unchanged. Although μ_e/μ_B is required in the derivation of μ_p/μ_B and μ'_p/μ_B, its 5×10^{-12} increase is too small to have a meaningful effect.

The 1986 recommended value for the deuteron-proton magnetic moment ratio μ_d/μ_p is based on the simple mean of two results: that of Phillips, Kleppner, and Walther (PKW) obtained from the ratio of the g factors for the deuteron and electron in deuterium; and that of Neronov and Barzakh (NB) obtained from the ratio of NMR frequencies in HD. Because the two values differed by more than could reasonably be expected from their *a priori* assigned uncertainties, their simple mean rather than their weighted mean was taken as the recommended value. Recently, Gorshkov et al. [34] carried out new NMR experiments and discovered a systematic error in the NB value. Their new result, μ_d/μ_p=0.307 012 2081(4), agrees well with that of PKW but has a 10-times smaller uncertainty. It is 0.015 ppm larger than the 1986 recommended value and has an uncertainty that is 13 times smaller than the 0.017 ppm of the 1986 value. This implies that the 1986 recommended values and uncertainties of quantities derived from μ_d/μ_p, particularly μ_d/μ_B, μ_d/μ_N, and μ_d/μ_e, will also need to be changed accordingly.

2.1.7 "As Maintained" Volt and Ohm Standards In the 1986 adjustment, electric unit-dependent quantities such as the Faraday F and gyromagnetic ratio of the proton γ_p were expressed in terms of the practical laboratory unit of voltage V_{76-BI} defined by the Josephson effect and the adopted value 483 594.0 GHz/V_{76-BI} for the Josephson frequency-voltage quotient; and in terms of the practical laboratory unit of resistance Ω_{BI85} defined as the value of Ω_{69-BI} on 1 January 1985, where Ω_{69-BI} was the time-dependent unit of resistance maintained at the International Bureau of Weights and Measures (BIPM) by means of a group of standard resistors. These noncoherent units were then related to their coherent SI counterparts through the relations $V_{76-BI}=K_V$ V and $\Omega_{BI85}=K_\Omega$ Ω with the quantities K_V and K_Ω taken as unknowns in the least-squares adjustment.

During the years 1986 to 1988, extraordinary advances were made in measuring the Josephson frequency-voltage quotient and quantized Hall resistance (QHR) in SI units and in calibrating laboratory voltage and resistance standards in terms of these quantum effects. These advances led the CIPM, upon the recommendation of its Consultative Committee on Electricity (CCE), to introduce new representations of the volt and ohm for worldwide use starting 1 January 1990 [35,36]. The new representation of the volt is based on the Josephson effect using the value

$$K_{J-90}=483\ 597.9 \text{ GHz/V exactly} \tag{3}$$

for the Josephson constant K_J, where $U_J(n)=nf/K_J$. ($U_J(n)$, n an integer, is the voltage of the nth constant-current voltage step induced in a Josephson device by radiation of frequency f. K_J is thus the frequency-voltage quotient of the nth step times the step number.) Similarly, the new representation of the ohm is based on the (integral) quantum Hall effect using the value

$$R_{K-90}=25\ 812.807\ \Omega \text{ exactly} \tag{4}$$

for the von Klitzing constant R_K, where $R_H(i)=U_H(i)/I=R_K/i$. ($R_H(i)$ is the quantized Hall resistance of the ith plateau, i an integer, and is equal to the quotient of the Hall voltage of the ith

plateau $U_H(i)$ divided by the current I through the Hall device. R_K is thus the Hall voltage-current quotient or resistance of the ith plateau times the plateau number.)

Equations (3) and (4) imply that $K_J = 483\ 597.9$ GHz/V_{90} exactly and $R_K = 25\ 812.807\ \Omega_{90}$ exactly, where

$$V_{90} = (K_{J-90}/K_J)\ \mathrm{V} = K_V\ \mathrm{V} \tag{5}$$

$$\Omega_{90} = (R_K/R_{K-90})\ \Omega = K_\Omega\ \Omega. \tag{6}$$

The quantities V_{90} and Ω_{90} are printed in italic type in recognition of the fact that they are physical quantities. (The corresponding quantities were taken as non-SI units in references [1,2].) They are exactly defined by K_{J-90} and R_{K-90}. In practice, laboratory voltage and resistance standards can be calibrated in terms of V_{90} and Ω_{90} with relative uncertainties considerably less than 0.01 ppm. This is especially true if a Josephson array voltage standard is used [37]; and if the CCE guidelines for making reliable QHR measurements are followed [38] and a cryogenic current comparator is employed [39]. These calibration uncertainties must be included, however, in the total uncertainty assigned any quantity measured in terms of such standards.

Fortunately, expressing electric unit-dependent quantities in terms of V_{90} and Ω_{90}, or in terms of $A_{90} = V_{90}/\Omega_{90}$, $W_{90} = V_{90}^2/\Omega_{90}$, and $C_{90} = A_{90}$ s, is a relatively straightforward procedure since most measurements of such quantities that are presently of interest have been carried out in terms of laboratory standards calibrated in terms of, or traceable to, the Josephson and quantum Hall effects. Because $\Omega_{69-\mathrm{BI}}$ is known from the calculable capacitor ohm realizations of the CSIRO/NML [40] to have been varying over the 25 years prior to 1 January 1990 at a constant linear rate given by [41]

$$\mathrm{d}\Omega_{69-\mathrm{BI}}/\mathrm{d}t = (-0.0614 \pm 0.0011)\ \mu\Omega/\mathrm{a}, \tag{7}$$

even those few results obtained well before the discovery of the QHE that need to be considered can be reexpressed in terms of Ω_{90}. (The value given in eq (7) is well supported by the value $\mathrm{d}\Omega_{69-\mathrm{BI}}/\mathrm{d}t = (-0.0579 \pm 0.0047)\ \mu\Omega/\mathrm{a}$ obtained from BIPM QHR measurements [42] but differs somewhat from the value used in the 1986 adjustment because of new data and a reevaluation of the older data [40,41].) The drift rates prior to 1 January 1990 of other national resistance units based on precision standard resistors, such as that of the NIST [43,44], are also adequately known for this purpose.

The Josephson and von Klitzing constants are believed to be related to other fundamental constants through

$$K_J = 2e/h \tag{8}$$

$$R_K = h/e^2 = \mu_0 c \alpha^{-1}/2, \tag{9}$$

where α^{-1} is the inverse fine-structure constant $\simeq 137$. Since μ_0 and c are defined constants, in principle a value of R_K with a given relative uncertainty yields a value of α^{-1} with the same relative uncertainty, and vice versa. It is also useful to note that $K_J R_K = 2/e$ and $K_J^2 R_K = 4/h$. Equations (8) and (9) were assumed to be exact in the 1986 adjustment and no substantiated experimental or theoretical evidence to the contrary has appeared in the last $4\frac{1}{2}$ years. In fact, considerable new experimental data has been obtained from comparisons of different Josephson and QHE devices that reinforces the view that these equations are correct (see reference [36] for a listing of the appropriate papers). Unless there is a truly startling and unexpected discovery in the next few years, the next set of recommended values of the constants will no doubt also be based on the assumed exactness of these relations.

On the other hand, from a purely physics standpoint, it is of interest to ask the question: What can the fundamental constants tell us about the accuracy of eqs (8) and (9)? One can, of course, compare values of $2e/h$ obtained from appropriate combinations of other constants with values of K_J obtained from force balance experiments; and values of α^{-1} obtained from quantum electrodynamics (QED) with values of R_K obtained from calculable capacitor ohm realizations. But the more rigorous way to answer this question is to carry out least-squares adjustments that do not assume the equalities expressed in eqs (8) and (9). In such adjustments, K_J and/or R_K are taken as phenomenological constants unrelated to e and h. The adjusted values obtained for them may then be compared with the adjusted values of $2e/h$ and h/e^2 resulting from the same adjustment. Such considerations are beyond the scope of this report and will not be discussed further. However, they are the subject of a forthcoming paper [45] and will likely be an integral part of the next CODATA adjustment.

The conventional values K_{J-90} and R_{K-90} [eqs (3) and (4)] recommended by the CCE and adopted by the CIPM were obtained by two CCE working groups from an analysis of all the relevant data available by 15 June 1988. In the analysis, which is thoroughly documented in reference [36], it was assumed for the purpose of including data from measurements of fundamental constants in the derivation of the conventional values of K_J and R_K that eqs (8) and (9) are exact. The goal, of course, was to use the best data available to derive values (within certain constraints [36]) that were as close to the SI values as possible so that the new representations would closely approximate the (SI) volt and ohm.

The working groups and the 15 June 1988 cutoff date were established by the CCE at its 17th meeting held in September 1986. The decision of the CCE to proceed with the introduction of new volt and ohm representations based on the Josephson and quantum Hall effects starting 1 January 1990 stimulated the reporting of new and significant results by the cutoff date. In many cases, the new data supplanted similar data used in the 1986 least-squares adjustment. However, as we anticipated (and hoped), the 1986 adjustment has proved to be more reliable than some of its predecessors. K_{J-90} exceeds the 1986 recommended value of $2e/h$ by only 0.47 ppm or 1.6 times the 0.30-ppm one-standard-deviation uncertainty of the 1986 value; and R_{K-90} exceeds the 1986 value of h/e^2 by only 0.052 ppm or 1.2 times its 0.045 ppm uncertainty. This reasonable agreement indicates that the new stochastic input data that have become available since the 1 January 1986 cutoff date of the 1986 adjustment will not lead to major changes in the 1986 recommended values. But the new data will lead to significant reductions in the uncertainties of many of these values, a fact not readily apparent from the 0.4-ppm and 0.2-ppm one-standard-deviation uncertainties conservatively assigned by the CIPM and CCE to the ratios K_{J-90}/K_J and R_K/R_{K-90}, respectively [35,36]. Indeed, these uncertainties are actually larger than the 0.30-ppm and 0.045-ppm uncertainties of the corresponding 1986 recommended values.

2.1.8 Acceleration Due to Gravity Knowledge of the local value of the acceleration due to gravity g is still not a limiting factor in any experiment that requires it, for example, the determination of K_J by comparing a mechanical force with an electrostatic force using a volt balance. However, anticipated future advances in measuring $h=4/K_J^2R_K$ by comparing mechanical and electrical power using a moving coil balance (to be discussed in sec. 2.2.2) may well require knowing g at the site of the balance with a relative uncertainty of $\sim 3\times 10^{-9}$. Although modern absolute gravimeters based on either the direct free-fall or symmetrical rise and fall methods are believed to have this capability [46], the results of the second international comparison of absolute gravimeters carried out at the BIPM in 1985 [47] imply an uncertainty 3–5 times larger. The results of the third international comparison conducted at BIPM in 1989 [48] are apparently more encouraging, however.

2.2 Primary Stochastic Input Data

Table 2 gives the principal items of stochastic input data of current interest. (See the Appendix for the main laboratory abbreviations used in table 2 and throughout this paper.) Since our purpose is not to carry out a new adjustment of the constants but only to obtain an overview of the impact of the most significant recent results on the 1986 recommended values, as stated in section 1.1, the data are not critically evaluated and our summary of the available data is not exhaustive. This means that the values and uncertainties of some of the listed items may change in the future, and items of data that are only of marginal or historical interest because of their comparatively large uncertainties or because they are known to be in error have been omitted. Further, no attempt has been made to estimate the effective degrees of freedom for each datum as needed for some of the data analysis algorithms used in the 1986 adjustment since the standard least-squares algorithm is deemed adequate for our purpose. Although the new results now available imply that the 12 distinct types of data considered in the 1986 adjustment may be somewhat different in the next adjustment, we discuss them under the 1986 data-type headings for ease of understanding. The following comments apply to the data of table 2, which takes full advantage of the paper by Taylor and Witt [36] documenting the data analysis that led to the values of K_{J-90} and R_{K-90} adopted by the CCE and CIPM (see sec. 2.1.7). It should also be recognized that some of these data are first results of on-going experiments and eventually will be superseded by newer results.

2.2.1 Direct Ohm Determinations Data items 1.1, 1.2, and 1.3 in table 2 are the only three currently available, direct, calculable capacitor-based measurements of R_K in SI units with uncertainties of less than 0.1 ppm. They were reported in 1988

Table 2. Summary of principal items of stochastic input data

Data type and item no.	Measurement date	Identification	Value	Relative uncertainty (ppm)
1. Ohm, Ω_{90}			Ω	
1.1	1985–1988	CSIRO/NML (Australia)	1.000 000 092(66)	0.066
1.2	1985–1988	NPL (UK)	1.000 000 085(54)	0.054
1.3	1983–1988	NIST (USA)	1.000 000 009(24)	0.024
2. Watt, W_{90}			W	
2.1	1987–1988	NPL (UK)	0.999 999 903(136)	0.14
2.2	1988	NIST (USA)	1.000 000 24(133)	1.33
3. Volt, V_{90}			V	
3.1	1983	CSIRO/NML (Australia)	0.999 999 975(269)	0.27
3.2	1989	PTB (FRG)	1.000 000 027(274)	0.27
4. Faraday, F			C_{90}/mol	
4.1	1975–1984	NIST (USA)	96 485.384(128)	1.33
5. Proton gyromagnetic ratio, γ'_p, low			10^4 s^{-1}/T_{90}	
5.1	1986–1988	NIST (USA)	26 751.5427(29)	0.11
5.2	1987	VNIM (USSR)	26 751.5630(96)	0.36
6. Proton gyromagnetic ratio, γ'_p, high			10^4 C_{90}/kg	
6.1	1973–1974	NPL (UK)	26 751.503(27)	1.01
7. Proton gyromagnetic ratio, γ'_p			10^4 s^{-1}/T	
7.1	1988	NIM (PRC)	26 751.541(23)	0.86
7.2	1985	ASMW (GDR)	26 751.427(21)	0.80
8. Avogadro constant, N_A			10^{23} mol^{-1}	
8.1	1974–1989	NIST (USA)	6.022 1315(72)	1.19
8.2	1982–1989	PTB/CBNM (FRG, Belg.)	6.022 1341(66)	1.10
9. Inverse fine-structure constant, α^{-1}				
9.1	1987–1990	U. Wash./Cornell (USA)	137.035 992 22(94)	0.0069
9.2	1989	PTB (FRG)	137.035 993(27)	0.20
10. Muon magnetic moment, μ_μ/μ_p				
10.1	1982	Los Alamos/Yale (USA)	3.183 3461(11)	0.36
10.2	1982	SIN Switzerland	3.183 3441(17)	0.53
11. Muonium hyperfine interval, ν_{Mhfs}			kHz	
11.1	1982	Los Alamos/Yale (USA)	4 463 302.88(62)	0.14

by Small et al. [49] at the CSIRO/NML; Hartland et al. [50] at the NPL; and Shields et al. [43,44] at the NIST. Since $\Omega_{90} = (R_K/R_{K-90})\ \Omega = K_\Omega\ \Omega = (\mu_0 c \alpha^{-1}/2R_{K-90})\ \Omega$, such measurements determine Ω_{90} in units of Ω, or equivalently K_Ω, and α^{-1}. Because of their significantly smaller uncertainties and close ties to QHR measurements carried out in the same laboratories, these three values supplant the five values of Ω_{BI85} considered in the 1986 adjustment, including those obtained at the same three laboratories from earlier versions of the same experiments. Omitted from table 2 are the four other independent, similarly obtained values of Ω_{90} listed by Taylor and Witt [36] since these have uncertainties that range from 0.22 to 0.61 ppm and would carry negligible weight in any data analysis compared with data items 1.1–1.3.

The three values are in reasonable agreement. Their weighted mean is $\bar{K}_\Omega = 1.000\ 000\ 028(21)$ (0.021 ppm), where the uncertainty has been calculated on the basis of internal consistency [2] (i.e., it has not been multiplied by the Birge ratio $R_B = (\chi^2/\nu)^{1/2}$); $\chi^2 = 2.70$ for $\nu = 2$ degrees of freedom, $R_B = 1.16$, and $P_{\chi^2}(2.70|2) \simeq 0.26$. The value of α^{-1} implied by this mean value is

$$\alpha^{-1}(\bar{R}_K)=137.036\ 0005(32)\ (0.021\ \text{ppm}), \quad (10)$$

a result that exceeds the 1986 recommended value by 0.080 ppm or 1.8 times the 0.045 ppm uncertainty of the 1986 value. Since the uncertainties of the two values only differ by about a factor of 2, it may be concluded that data items 1.1 to 1.3 will influence the 1986 set of recommended values in a significant but not major way. For future reference, we note that the value of α^{-1} from the most precise of these data items, that obtained at the NIST, is

$$\alpha^{-1}(R_K)_{NIST}=137.035\ 9979(32)\ (0.024\ \text{ppm}). \quad (11)$$

This result exceeds the 1986 recommended value by 0.061 ppm or 1.4 times its 0.045 ppm uncertainty. Measurements of Ω_{90} are continuing at the NIST and additional results may be expected in the next 1–2 years.

2.2.2 Direct Ampere Determinations (now Watt Determinations) Six values of $A_{BI85}=V_{76-BI}/\Omega_{BI85}$ were initially considered for inclusion in the 1986 adjustment with uncertainties in the range 4.1 to 9.7 ppm. All were eventually discarded because of their disagreement with the other data and/or negligible weight in the adjustment. No new values of this type have become available (i.e., values of $A_{90}=V_{90}/\Omega_{90}$) or are any expected in the future. Ampere balance experiments have been replaced by more promising volt balance experiments that determine V_{90} (see sec. 2.2.3) and watt balance experiments that determine $W_{90}=A_{90}V_{90}=V_{90}^2/\Omega_{90}$. The quantity W_{90} is an important new input datum since $h=4/K_J^2R_K$, which implies

$$h=4K_W/K_{J-90}^2R_{K-90}, \quad (12)$$

where

$$W_{90}=K_W\ \text{W}=K_\Omega^{-1}K_V^2\ \text{W}. \quad (13)$$

Thus a measurement of W_{90} is actually a measurement of h in SI units, (i.e., J s). In combination with the measured value of $\Omega_{90}=K_\Omega\ \Omega$, a determination of W_{90} also gives a value of K_V, and thus of $K_J=2e/h$ in Hz/V, through the relations

$$K_V=(K_\Omega K_W)^{1/2}, \quad (14a)$$

$$K_J=2e/h=K_{J-90}/K_V. \quad (14b)$$

Data item 2.1 in table 2 was obtained by Kibble et al. at the NPL [52] from their pioneering moving-coil apparatus that allows one to realize the watt by comparing mechanical and electrical power. A new version of this experiment with the goal of reducing the uncertainty by a factor of 10 is under construction and first results should be available in 1 to 2 years. Data item 2.2 was obtained at the NIST by Olsen et al. [53] using the same method but an apparatus of considerably different geometry. This value is from their initial version of the experiment that used a room temperature, oil-cooled solenoid to generate the required magnetic field. It has now been replaced with a superconducting solenoid that can generate a much larger field and an eventual reduction in uncertainty by a factor of 50 to 100 is hoped for.

Another approach to measuring W_{90} is being vigorously pursued at the NRLM and the ETL [54]. It involves comparing mechanical and electrical energy by levitating a superconducting mass with a superconducting coil. Although no result has yet been reported, these researchers believe a relative uncertainty of $\sim 1\times 10^{-8}$ is feasible. A similar experiment in underway at the VNIIM.

The two values of W_{90} are clearly in good agreement, differing by only 0.33 ppm, but because the NPL datum, item 2.1, has an uncertainty nearly 10 times smaller than that of the NIST datum, item 2.2, the latter will carry negligible weight by comparison. Indeed, the NPL value of K_J, 483 597.903(35) GHz/V (0.073 ppm) [corresponding to $K_V=0.999\ 999\ 994(73)$ (0.073 ppm)], obtained from eq (14) using NPL data items 1.2 and 2.1, played the dominant role in determining K_{J-90} [36]. (The value of K_V and $2e/h$ implied by the NIST measurements of W_{90} and Ω_{90}, data items 2.2 and 1.3, are from eq (14) 1.000 000 12(67) (0.67 ppm) and 483 597.84(32) GHz/V (0.67 ppm), respectively.) If $\bar{K}_\Omega$, the weighted mean of data items 1.1 to 1.3 given in section 2.2.1 is used instead of data item 1.2, the NPL value of W_{90} yields

$$K_V=0.999\ 999\ 965(69)\ (0.069\ \text{ppm}) \quad (15a)$$

$$K_J=2e/h=483\ 597.917(33)\ \text{GHz/V}\ (0.069\ \text{ppm}). \quad (15b)$$

This value of $2e/h$ exceeds the 1986 recommended value by 0.51 ppm or 1.7 times the 0.30 ppm uncertainty of the 1986 value. More significant, its 0.069 ppm uncertainty is 4.3 times smaller than the 0.30 ppm uncertainty of the latter. The new type 1 and 2 data together will therefore lead to new recommended values of e, h, m_e, N_A, F, and other quantities dependent upon $2e/h$ that differ from the

1986 recommended values by less than twice the uncertainties of the 1986 values, but the uncertainties of the new recommended values will be reduced by more than a factor of four. Indeed, the NPL value of K_W gives, from eq (12), $h = 6.626\ 068\ 21(90) \times 10^{-34}$ J s (0.14 ppm), which is 1.1 ppm less than the 1986 value or 1.8 times the 0.60 ppm uncertainty of the latter. Further, the uncertainty of this value of h is 4.4 times smaller than the 0.60 ppm uncertainty of the 1986 value.

2.2.3 Direct Volt Determinations Data item 3.1 in table 2 is the final result of the liquid-mercury electrometer experiment at the CSIRO/NML of Clothier et al. [55]; a preliminary value with an uncertainty of 0.60 ppm and in good agreement with it was used as an input datum in the 1986 adjustment. Data item 3.2 is the recently reported result from the PTB volt balance experiment of Funck and Sienknecht [56]. Not listed in table 2 is the LCIE kelvin electrometer result with its 2.4 ppm uncertainty, the other direct volt balance determination initially included as an input datum in the 1986 adjustment but later deleted because of its low weight and marginal agreement with the other 1986 data. The value obtained by Bego et al. at the U. Zagreb using a volt balance, which has an assigned uncertainty of 0.35 ppm and was initially considered by the CCE Working Group on the Josephson effect [36] in their analysis of values of K_J, has also been omitted because of its known disagreement with other values and the subsequent identification by Bego and colleagues of several unsuspected systematic errors (see reference [36], Note Added in Proof). This work is continuing and a reliable result with an uncertainty of $\sim$0.3 ppm may eventually be expected.

It is clear that data items 3.1 and 3.2 agree exceedingly well with each other and with the value of K_V implied by data item 2.1 (the NPL value of W_{90}) as given in eq (15a); the maximum spread of the three values is less than 0.07 ppm. However, the watt-ohm value has an uncertainty 2.8 times smaller than that of the weighted mean of data items 3.1 and 3.2 [$\bar{K}_V = 1.000\ 000\ 000(192)$ (0.192 ppm), $\bar{K}_J = 483\ 597.900(93)$ GHz/V (0.19 ppm)] and as a consequence, carries nearly 8 times as much weight. Hence, although data items 3.1 and 3.2 confirm eq (15), they have little additional impact on the 1986 recommended values. (The values of K_J corresponding to data items 3.1 and 3.2 are 483 597.91(13) GHz/V (0.27 ppm) and 483 597.89(13) GHz/V (0.27 ppm), respectively.) Since K_{J-90} and R_{K-90} were chosen to be consistent with the SI values of K_J and R_K, V_{90}, Ω_{90}, and thus W_{90} should be very nearly equal to V, Ω, and W (i.e., K_V, K_Ω, and K_W should all be equal to 1). This is well borne out by the seven data items included under data types 1, 2, and 3.

2.2.4 Faraday Constant There have been no new results for the Faraday constant since the 1986 adjustment and to the best of our knowledge, no experiments are underway. Data item 4 is the NBS (now NIST) result included in the 1986 adjustment reexpressed in units of $C_{90} = A_{90}\ \text{s} = (V_{90}/\Omega_{90})$ s. This was accomplished using the value (-0.0529 ± 0.0040) $\mu\Omega$/a for the drift rate of Ω_{NIST} based on NIST QHR measurements made over the period 1983–1988 [44], and the fact that Ω_{NIST} (1 January 1990)$= \Omega_{90} - 1.69\ \mu\Omega$ [44]. (The electrochemical measurements in the NIST Faraday experiment were carried out in 1975.) This drift rate agrees well with the value (-0.0536 ± 0.0024) $\mu\Omega$/a reported by Shields et al. [43] based on NIST calculable capacitor ohm realizations in 1973/1974 and 1988. The consistency of the NIST value of F with the other data will be discussed in section 3.

2.2.5 Gyromagnetic Ratio (Low Field) Six values of $\gamma_p'(\text{lo})_{\text{BI85}}$ obtained at the ETL, NPL, NIM, NIST, VNIIM, and ASMW with uncertainties in the range 0.24 to 3.25 ppm were initially considered for inclusion in the 1986 adjustment. All but one, that obtained at the NIST with an uncertainty of 0.24 ppm, were eliminated because of their incompatibility with the other data and/or negligible weight in the adjustment. Since 1986, new values from the NIM, NIST, VNIIM, and ASMW have been reported. The new NIST result of Williams et al. [57] (data item 5.1) was obtained from an entirely new apparatus. It is essentially identical to the earlier NIST value, which has an uncertainty of 0.24 ppm or about twice that of the new value. Because the earlier value is not as closely tied to Ω_{90} as is the new value, it is not included in table 2. The NIST measurements are continuing and a reduction in the present 0.11-ppm uncertainty is expected. The new VNIIM result of Tarbeev et al. [58,59] (data item 5.2) was obtained after many significant improvements were incorporated in the earlier version of the experiment. It exceeds the previous VNIIM value, which was initially considered for use in the 1986 adjustment and has an assigned uncertainty of 0.62 ppm, by about 5.5 ppm. This work is also continuing.

The new values of $\gamma_p'(\text{lo})$ from the NIM and the ASMW are not listed in table 2 under data type 5 but under data type 7, γ_p' in SI units. This is because the NIM result is not closely tied to a realization of Ω_{90}, and the ASMW result is not closely tied to

either a realization of V_{90} or Ω_{90}. To express the NIM and ASMW $\gamma_p'(\text{lo})$ values in terms of A_{90} would require using the results of problematical volt and ohm transfers to the BIPM. Since both laboratories carried out new measurements of $\gamma_p'(\text{hi})$ at about the same time, it is more appropriate to use these to obtain a single value of γ_p' from each laboratory. The relevant equation is

$$\gamma_p' = [\gamma_p'(\text{lo})_{\text{LAB}}\ \gamma_p'(\text{hi})_{\text{LAB}}]^{1/2}, \quad (16)$$

where the subscript LAB is used to indicate that the practical unit of current A_{LAB} in terms of which $\gamma_p'(\text{lo})$ and $\gamma_p'(\text{hi})$ are measured must be the same for both. This laboratory current unit need not be based on the Josephson and quantum Hall effects; any battery and resistor with arbitrary but fixed values may be used to establish A_{LAB}. Data items 7.1 and 7.2 will be discussed at the end of section 2.2.6 which deals with measurements of $\gamma_p'(\text{hi})$.

The NBS and VNIIM values of $\gamma_p'(\text{lo})$, data items 5.1 and 5.2, are only marginally in agreement; they differ by (0.76 ± 0.38) ppm or 2.0 times the standard deviation of their difference. These values will be compared with the other data in section 3.

2.2.6 Gyromagnetic Ratio (High Field) The four values of $\gamma_p'(\text{hi})_{\text{BI85}}$ with uncertainties in the range 1.0 to 5.4 ppm considered for inclusion in the 1986 adjustment were obtained at the KhGIMIP, NPL, NIM, and ASMW. Because of inconsistencies with the other data and/or negligible weight, the KhGIMIP and ASMW values were eventually eliminated. As noted in section 2.2.5, new results for $\gamma_p'(\text{hi})$ have been obtained by both the NIM and the ASMW but will be combined with corresponding values of $\gamma_p'(\text{lo})$ and treated as measurements of γ_p'. Since no other new $\gamma_p'(\text{hi})$ results are available, the only datum of type 6 listed in table 2 is the NPL value of Kibble and Hunt used in the 1986 adjustment but reexpressed in terms of $C_{90} = A_{90}$ s. This was done by expressing the NPL value in terms of $\Omega_{69-\text{BI}}$ at the time of the measurement (1974), and using the value for $d\Omega_{69-\text{BI}}/dt$ given in eq (7) and the fact that $\Omega_{69-\text{BI}}(1 \text{ January } 1990) = \Omega_{90} - 1.90\ \mu\Omega$ [60].

The new results for $\gamma_p'(\text{lo})$ and $\gamma_p'(\text{hi})$ obtained at the NIM in 1988 and reported by Liu et al. [61] are

$$\gamma_p'(\text{lo}) = 26\ 751.338(20) \times 10^4\ \text{s}^{-1}/T_{\text{NIM}-88}\ (0.74\ \text{ppm}) \quad (17\text{a})$$

$$\gamma_p'(\text{hi}) = 26\ 751.743(42) \times 10^4\ C_{\text{NIM}-88}/\text{kg}\ (1.55\ \text{ppm}). \quad (17\text{b})$$

These lead, through eq (16), to data item 7.1 in table 2. Similarly, the individual values leading to data item 7.2 obtained at the ASMW in 1985 and reported by Forkert and Schlesok [62] are

$$\gamma_p'(\text{lo}) = 26\ 751.319(22) \times 10^4\ \text{s}^{-1}/T_{\text{ASMW}-85}\ (0.81\ \text{ppm}) \quad (18\text{a})$$

$$\gamma_p'(\text{hi}) = 26\ 751.534(37) \times 10^4\ C_{\text{ASMW}-85}/\text{kg}\ (1.37\ \text{ppm}). \quad (18\text{b})$$

The two values of γ_p', data items 7.1 and 7.2, are seen to be in poor agreement; they differ by (4.3 ± 1.2) ppm or 3.6 times the standard deviation of their difference. Since V_{90} and Ω_{90} are very nearly equal to V and Ω, the numerical values of $\gamma_p'(\text{lo})$, $\gamma_p'(\text{hi})$, and γ_p' should be nearly equal. With the exception of data item 7.2, and to some extent item 5.2, this is roughly the case. Consequently, item 7.2 and possibly item 5.2 may be inconsistent with the other data as well. This will be investigated further in section 3.

2.2.7 Silicon Lattice Spacing, 2.2.8 Molar Volume of Silicon At the time of the 1986 adjustment, two values of the d_{220} silicon lattice spacing were available and one value of the mean molar volume of silicon $M(\text{Si})/\rho(\text{Si})$. Because the two $d_{220}(\text{Si})$ results, one obtained at the NIST and the other at the PTB, were in gross disagreement, they could not be readily combined with each other and the NIST value of $M(\text{Si})/\rho(\text{Si})$ to obtain a single value of the Avogadro constant N_A that could be treated as a single stochastic input datum. Rather, the two different types of data were treated separately: the silicon lattice spacing measurements as two items of type 7 data and the molar volume as a single item of type 8 data. In the end, the NIST $d_{220}(\text{Si})$ value was eliminated because of its severe disagreement with the other data in the adjustment.

During the last 5 years, Deslattes and colleagues [63] at the NIST have discovered unsuspected systematic errors in the original NIST lattice spacing result and have reported [64] a preliminary value based on new data in good agreement with the value from the PTB. Further, the PTB and the CBNM [65] have recently reported a completely independent determination of $M(\text{Si})/\rho(\text{Si})$. Consequently, the d_{220} and $M(\text{Si})/\rho(\text{Si})$ values of each laboratory as obtained on their own samples now yield two entirely independent values of N_A: a NIST value and a PTB/CBNM value. The relevant equation is

$$N_A = \frac{8M(\mathrm{Si})}{\rho(\mathrm{Si})(d_{220}(\mathrm{Si})\sqrt{8})^3}, \tag{19}$$

and the two results are given as data items 8.1 and 8.2 in table 2. They agree well with one another, the PTB/CBNM value exceeding that from the NIST by only (0.43±1.62) ppm. These values will be compared to the other data in section 3. Work at the NIST to refine the value of d_{220}(Si) is continuing and a final result should be available in the near future. The PTB and the CBNM are vigorously pursuing an improved value of $M(\mathrm{Si})/\rho(\mathrm{Si})$ (the limiting factor in both N_A results) and a reduction in the uncertainty of their value of N_A by a factor of 3 to 4 in the next several years seems feasible.

2.2.9 Quantized Hall Resistance In the 1986 adjustment, six values of the quantized Hall resistance R_H (i.e., what is now termed the von Klitzing constant or R_K) expressed in terms of Ω_{BI85} constituted the type 9 stochastic input data. However, because of the uncertainties associated with the transfer of reference resistors between standards laboratories, QHR measurements that are not tied to a realization of the ohm based on a calculable capacitor and carried out in the same laboratory are not used in this report. With the 1 January 1990 introduction of the new ohm representation based on the QHE and the conventional value R_{K-90} for the von Klitzing constant, determining R_K in terms of a local laboratory unit of resistance defined in terms of a group of precision resistors serves only to calibrate the resistors in terms of the new ohm representation. Consequently, this type of stochastic data provides little useful information as far as the fundamental constants are concerned and will have a limited role to play in future adjustments. Of course, comparing transportable resistors calibrated by different laboratories in terms of Ω_{90} can serve as a useful check on the accuracy of each laboratory's realization of Ω_{90}. The 1987 international comparison of national resistance standards shows that such realizations are well in hand [41].

2.2.10 Fine-Structure Constant Our knowledge of the theoretical expression for the electron magnetic moment anomaly a_e has advanced markedly in the last 3 years due to the Herculean QED calculations of Kinoshita and coworkers [66–68]. Their most recent result is [69]

$$a_e(\mathrm{theor}) = C_1\left(\frac{\alpha}{\pi}\right) + C_2\left(\frac{\alpha}{\pi}\right)^2 + C_3\left(\frac{\alpha}{\pi}\right)^3 + C_4\left(\frac{\alpha}{\pi}\right)^4 + \ldots + \delta a_e \tag{20}$$

with $C_1 = 1/2$, $C_2 = -0.328\,478\,965\ldots$, $C_3 = 1.176\,11(42)$, $C_4 = -1.434(138)$, and $\delta a_e = 4.46\times10^{-12}$. C_1 and C_2 have been evaluated analytically, C_3 partly analytically and partly numerically, and C_4 entirely numerically. The small term δa_e is a sum of contributions arising from muon and tauon loops, and from hadronic and electroweak effects. The total uncertainty in a_e(theor) is 0.0058 ppm, 0.0046 ppm from C_3 and 0.0035 ppm from C_4. (In 1986 the corresponding uncertainties were 0.065, 0.014, and 0.063 ppm.) Together with the improved University of Washington experimental value of a_e [0.0037 ppm uncertainty, eq (2a)], eq (20) yields the value given as data item 9.1 in table 2,

$$\alpha^{-1}(a_e) = 137.035\,992\,22(94)\ (0.0069\ \mathrm{ppm}), \tag{21a}$$

which from eqs (6) and (9) is equivalent to

$$K_\Omega = 0.999\,999\,9672(69)\ (0.0069\ \mathrm{ppm}). \tag{21b}$$

The uncertainty of this new QED value of α^{-1} is nearly 10 times smaller than the 0.065 ppm of its predecessor used in the 1986 adjustment and 3.5 times smaller than the 0.024 ppm uncertainty of the next most precise single value of α^{-1} currently available, that given in eq (11) and obtained from the NIST measurement of R_K (data item 1.3). The two are in reasonable agreement; eq (11) exceeds eq (21a) by (0.041±0.025) ppm or 1.7 times the standard deviation of their difference. Further, the value of R_K implied by $\alpha^{-1}(a_e)$ through $R_K = \mu_0 c\alpha^{-1}/2$ is only 0.033 ppm smaller than R_{K-90}. This is not surprising since the NIST value of R_K and that implied by $\alpha^{-1}(a_e)$ from an earlier [36,68] but only slightly different version of eq (20) played a major role in determining R_{K-90} [36]. The 0.0069-ppm uncertainty of $\alpha^{-1}(a_e)$ is almost small enough to allow α^{-1} to be taken as an auxiliary constant at the present time, but it should be noted that $\alpha^{-1}(a_e)$ is (0.061±0.022) ppm smaller than $\alpha^{-1}(\bar{R}_K)$ [eq (10)] or 2.8 times the standard deviation of their difference. Further comparisons of $\alpha^{-1}(a_e)$ with the data of table 2 are given in section 3.

Although the new value of $\alpha^{-1}(a_e)$ is only 0.020 ppm larger than the 1986 recommended value or 0.44 times the latter's 0.045-ppm uncertainty, the 0.0069-ppm uncertainty of the new value is 6.5 times smaller than the 0.045 ppm 1986 uncertainty. The implication is that the new value of α^{-1} will not lead to any significant changes in the 1986 recommended values but will lead to a comparable and thus significant reduction in the uncertainties of a number of quantities dependent upon α^{-1}, such

as the Bohr and nuclear magnetons μ_B and μ_N in units of eV/T, the Bohr radius $a_0=\alpha/4\pi R_\infty$, the quantum of circulation $h/2m_e$, and the Compton wavelengths of the electron, proton, and neutron, $\lambda_{C,x}=h/m_x c$, x=e, p, or n. Kinoshita and colleagues plan to continue their QED calculations in order to further reduce the uncertainties of the coefficients C_3 and C_4 of eq (20).

Data item 9.2 is a new value of α^{-1} from the PTB with an uncertainty of 0.20 ppm as reported recently by Krüger et al. [70]. It is the first really high-precision result from an experiment, underway for many years, to measure $\lambda v=h/m_n$, where λ is the wavelength of neutrons of velocity v. λ is defined by back reflection from a silicon single crystal of known lattice spacing and v is determined using what is essentially a time-of-flight technique. The inverse fine-structure constant is then obtained from

$$\alpha^{-1}=[(2R_\infty/c)(m_n/m_p)(m_p/m_e)(h/m_n)]^{-1/2}. \quad (22)$$

Using the value of R_∞ given in eq (1), the 1986 recommended values for the auxiliary constants m_n/m_p and m_p/m_e, and the value $h/m_n=3.956\,0344(16)\times10^{-7}$ m^2/s (0.40 ppm) reported by Krüger et al. [70], eq (22) yields the value of α^{-1} given in table 2 as data item 9.2,

$$\alpha^{-1}=137.035\,993(27)\ (0.20\ \text{ppm}), \quad (23a)$$

or equivalently

$$K_\Omega=0.999\,999\,97(20)\ (0.20\ \text{ppm}). \quad (23b)$$

This result agrees well with all the values of α^{-1} and K_Ω discussed so far but, of course, it has a comparatively large uncertainty. The PTB researchers are continuing their measurements of h/m_n and hope for some reduction in uncertainty.

Omitted from table 2 is the value of α^{-1} derived from spectroscopic measurements of the fine structure in atomic helium. Considered for inclusion in the 1986 adjustment, it was later eliminated because it was based on an incomplete theoretical expression. Further, its uncertainty was comparatively large and hence it carried negligible weight.

2.2.11 Muon Magnetic Moment There have been no new developments in this area in the last $4\frac{1}{2}$ years; the two values of μ_μ/μ_p given in table 2 as data items 10.1 and 10.2 are the same as those used in the 1986 adjustment. V. W. Hughes of Yale University and collaborators working at Los Alamos are undertaking a new version of their earlier experiment to determine the muonium ground-state hyperfine splitting ν_{Mhfs} from which data items 10.1 and 11.1 were both obtained. A value of α^{-1} with an uncertainty of a few parts in 10^8 from μ_μ/μ_p and the experimental value of and theoretical expression for ν_{Mhfs} is anticipated. First results may be available in the early 1990s.

2.2.12 Muonium Hyperfine Splitting As for the muon magnetic moment (sec. 2.2.11), there are no new experimental results for the ground-state hyperfine splitting in muonium; the value given in table 2 as data item 11.1 is that used in the 1986 adjustment. On the other hand, there are new theoretical results from a number of workers in the USSR. Some higher-order QED terms have been calculated [71] and the terms evaluated numerically by Sapirstein et al. have now been obtained analytically [72,73]. However, the dominant uncalculated term, that arising from purely radiative corrections and of order $\alpha^2(Z\alpha)E_F$, has yet to be calculated. Its ±1 kHz estimated limit of error contributes a 0.13-ppm one-standard-deviation uncertainty to data item 11.1, which may be compared with the 0.036-ppm experimental uncertainty. This term must be calculated if the new results expected for μ_μ/μ_p and ν_{Mhfs} (see sec. 2.1.11) are to be fully useful. Fortunately, some progress is now being made in its evaluation [74]. Taking R_∞ as given in eq (1), the weighted mean of data items 10.1 and 10.2 for μ_μ/μ_p, and the 1986 recommended value of μ_p/μ_B, the updated theoretical expression for ν_{Mhfs} and the experimental value of ν_{Mhfs} (data item 11.1) yield for the inverse fine-structure constant

$$\alpha^{-1}(\text{Mhfs})=137.035\,993(22)\ (0.16\ \text{ppm}), \quad (24a)$$

or equivalently

$$K_\Omega=0.999\,999\,97(16)\ (0.16\ \text{ppm}). \quad (24b)$$

This result is identical to that obtained from h/m_n, eq (23), and thus agrees well with all other values. But again, its uncertainty is comparatively large.

2.3 Secondary Stochastic Data

No verified existing theory relates the Newtonian constant of gravitation G to other fundamental constants, hence its measured values are treated as independent stochastic quantities regardless of the size of their assigned uncertainties. On the other hand, the molar gas constant R, Boltzmann constant k, and Stefan-Boltzmann constant σ are related by the equations

$$k=R/N_A \quad (25)$$

$$\sigma=2\pi^5(R/N_A)^4/15\,h^3c^2. \quad (26)$$

Thus if directly measured values of R, k, and σ with sufficiently small uncertainties are available, they may be included as stochastic input data in a least-squares adjustment on an equal footing with the data discussed in the preceding sections. Although a new result for R with an uncertainty of 1.7 ppm has recently been obtained (see sec. 2.3.1), there are no precision measurements of k and the directly measured value of σ discussed in the 1986 adjustment with its 134 ppm uncertainty remains the best available. Because the situation regarding k and σ is unlikely to change in the foreseeable future, recommended values of these quantities will continue to be obtained from eqs (25) and (26) with N_A and h taken from the least-squares adjustment and R from its directly measured values.

2.3.1 Molar Gas Constant A new value of the molar gas constant R obtained from measurements of the speed of sound in argon at the NIST was reported in 1988 by Moldover et al. [75]. Using a spherical acoustical resonator the volume of which was obtained by weighing the mercury required to fill it, Moldover and colleagues found

$$R=8.314\,471(14)\ \text{J/(mol K)}\ (1.7\ \text{ppm}). \quad (27)$$

This result is only 4.7 ppm smaller than the 1986 recommended value or less than 0.6 times the 8.4 ppm uncertainty of the latter. (The 1986 recommended value was obtained at the NPL by measuring the speed of sound in argon also, but by means of an acoustical interferometer.) Further, the 1.7 ppm uncertainty of the NIST result is nearly 5 times smaller than the 8.4 ppm uncertainty of the 1986 value. A comparable and thus significant reduction in the uncertainties of other 1986 recommended values that are dependent upon R, such as the Boltzmann and Stefan-Boltzmann constants k and σ [eqs (25) and (26)], the molar volume of an ideal gas V_m, Loschmidt constant $n_0=N_A/V_m$, and second radiation constant $c_2=hc/k$, may be expected.

2.3.2 Stefan-Boltzmann Constant As pointed out in section 2.3, the Stefan-Boltzmann constant must still be obtained indirectly via eq (26). If the new NIST result for R, eq (27), is used to evaluate eq (26) along with the 1986 recommended values of N_A and h, then the resulting value of σ is 19 ppm less than the 1986 value or about 0.6 times the 34-ppm uncertainty of the latter. Further, this new value of σ has an uncertainty of only 6.9 ppm, which is 4.9 times smaller than the 34 ppm of the 1986 value. Only small changes in these figures occur when the values of N_A and h implied by the data of table 2 are used to evaluate eq (26) in place of the 1986 values (see sec. 3.3). One reason is that the product $(N_A\,h)^3$ depends only on auxiliary constants and α^6, which changes by less than 0.4 ppm; N_A changes by 1 ppm or less.

2.3.3 Newtonian Constant of Gravitation No new results for G have been reported; the 1986 recommended value remains unchanged. A potentially important experiment is underway at the PTB [76].

3. Data Analysis and Results

Our analysis of the data will be limited since, as stated earlier, our purpose is not to obtain new recommended values of the constants but only to survey the impact of recent results on the 1986 set of values. In section 3.1 we briefly study the compatibility of the data items of table 2 using the known relationships among them, a few such comparisons having already been made in previous sections with the aid of eqs (8), (9), (13), and (14). In section 3.2 the data are briefly investigated using the method of least-squares, possibly foreshadowing the next CODATA adjustment. Finally, in section 3.3 we give the changes in the 1986 recommended values and uncertainties of a representative group of constants as implied by the least-squares adjustments of section 3.2.

3.1 Relationships Among Data of Different Types

Some preliminary analyses of the stochastic data of table 2 were given in various subsections of section 2.2 and some inconsistencies were identified. For example, the two values of $\gamma_p'(\text{lo})$ differ by 2.0 times the standard deviation of their difference; the two values of γ_p' differ by 3.6 times the standard deviation of their difference; and $\alpha^{-1}(a_e)$ differs from the value of α^{-1} implied by the weighted mean of the three measurements of Ω_{90} by 2.8 times the standard deviation of their difference.

An efficient way of further investigating these inconsistencies and of obtaining a clear overview of the compatability of the data of table 2 is to compare the values of K_Ω and K_V that the data imply. Table 3, which lists eight values of K_Ω in order of increasing uncertainty, compares the data of type 1, 5, 9, 10, and 11 in this way; table 4, which lists 10 values of K_V in order of increasing uncertainty, does the same for the data of type 2, 3, 4, 6, 7, and 8. Because the uncertainties of the data of

Table 3. Summary of values of $K_{\Omega}=(R_K/R_{K-90})=\mu_0 c\alpha^{-1}/2R_{K-90}$ taken directly from or derived from the stochastic data of table 2 (the 1986 value excepted)

Identification	Value and uncertainty $\Delta=(K_{\Omega}-1)\times10^6$
1. $\alpha^{-1}(a_e)$ (data item 9.1)	-0.0328 ± 0.0069
2. Ω_{90}, NIST (data item 1.3)	0.009 ± 0.024
3. α^{-1} from NIST $\gamma'_p(\mathrm{lo})$ (from data item 5.1)	-0.093 ± 0.037
4. Ω_{90}, NPL (data item 1.2)	0.085 ± 0.054
5. Ω_{90}, CSIRO/NML (data item 1.1)	0.092 ± 0.066
6. α^{-1} from VNIIM $\gamma'_p(\mathrm{lo})$ (from data item 5.2)	-0.35 ± 0.12
7. $\alpha^{-1}(\mathrm{Mhfs})$ (from data items 10.1, 10.2, 11.1)	-0.03 ± 0.16
8. $\alpha^{-1}(h/m_n)$ (data item 9.2)	-0.03 ± 0.20
CODATA 1986 recommended value	-0.052 ± 0.045

Table 4. Summary of values of $K_V=K_{J-90}/K_J=K_{J-90}/(2e/h)$ taken directly from or derived from the stochastic input data of table 2 (the 1986 value excepted)

Identification	Value and uncertainty $\Delta=(1-K_V)\times10^6$
1. K_V from NPL W_{90} and Ω_{90} via $\alpha^{-1}(a_e)$ (from data items 2.1 and 9.1)	0.065 ± 0.068
2. V_{90}, CSIRO/NML (data item 3.1)	0.025 ± 0.269
3. V_{90}, PTB (data item 3.2)	-0.027 ± 0.274
4. $2e/h$ from NPL $\gamma'_p(\mathrm{hi})$ and $\alpha^{-1}(a_e)$ (from data items 6.1 and 9.1)	-0.62 ± 0.50
5. $2e/h$ from PTB/CBNM N_A and $\alpha^{-1}(a_e)$ (from data items 8.2 and 9.1)	-0.68 ± 0.55
6. $2e/h$ from NIST N_A and $\alpha^{-1}(a_e)$ (from data items 8.1 and 9.1)	-0.89 ± 0.60
7. K_V from NIST W_{90} and Ω_{90} via $\alpha^{-1}(a_e)$ (from data items 2.2 and 9.1)	-0.10 ± 0.67
8. $2e/h$ from NIST F and $\alpha^{-1}(a_e)$ (from data items 4.1 and 9.1)	0.19 ± 0.67
9. $2e/h$ from ASMW γ'_p and $\alpha^{-1}(a_e)$ (from data items 7.2 and 9.1)	-4.11 ± 0.80
10. $2e/h$ from NIM γ'_p and $\alpha^{-1}(a_e)$ (from data items 7.1 and 9.1)	0.15 ± 0.86
CODATA 1986 recommended value	-0.47 ± 0.30

the latter six types are relatively large compared with the uncertainties of the most precise values of K_Ω, these data cannot provide meaningful values of K_Ω; as far as they are concerned K_Ω, or equivalently α^{-1}, is an auxiliary constant. This will be apparent from eqs (29)-(33) to be given shortly in connection with the discussion of table 4. Figures 2 and 3, respectively, graphically compare the values of K_Ω and K_V listed in tables 3 and 4. *Note that the values in both the tables and figures are given in the form* $\Delta=(K_\Omega-1)\times10^6$ *and* $\Delta=(1-K_V)\times10^6$ *since* Δ *is then the implied ppm change in* R_{K-90} *and* K_{J-90}, *respectively.*

The eight values of K_Ω in table 3 or the values of α^{-1} from which they have been derived using the relation $K_\Omega=\mu_0 c\alpha^{-1}/2R_{K-90}$ have already been mentioned in various subsections of section 2.2 except Nos. 3 and 6. These were obtained from the NIST and VNIIM values of $\gamma_p'(\text{lo})$ expressed in units of s^{-1}/T_{90} (data items 5.1 and 5.2 of table 2) using the relation

$$\alpha^{-1}=\left[\frac{K_{J-90}\,R_{K-90}(\mu_p'/\mu_B)}{2\mu_0\,R_\infty\,\gamma_p'(\text{lo})_{90}}\right]^{1/3}, \qquad (28)$$

and taking the 1986 recommended value for μ_p'/μ_B and eq (1) for R_∞. Because of the comparatively small uncertainties of these two auxiliary constants and the cube root, the uncertainty of the value of α^{-1} and thus of K_Ω derived from eq (28) is 1/3 that of $\gamma_p'(\text{lo})_{90}$. The value of K_Ω derived from the NIST $\gamma_p'(\text{lo})_{90}$ result is thus the third most precise value listed in table 3, but the value from $\alpha^{-1}(a_e)$ (No. 1) is still 5.4 times more precise. Indeed, as noted previously, the uncertainty of this value is even 3.5 times smaller than the uncertainty of the next most precise value (No. 2), that obtained from the NIST measurement of Ω_{90} (data item 1.3 of table 2). This means that $\alpha^{-1}(a_e)$ will essentially determine the final value of K_Ω and thus α^{-1} in any least-squares adjustment in which it is included.

Table 3 and figure 2 show that the other seven values of K_Ω differ from value No. 1 by less than twice the standard deviation of their difference except No. 4 (NPL Ω_{90}, data item 1.2) and No. 6 (VNIIM $\gamma_p'(\text{lo})$, data item 5.2), which differ from No. 1 by 2.2 and 2.6 standard deviations, respectively. Thus, while the data are not in gross disagreement, the inconsistencies are clearly larger than one would like.

The values of K_V listed in table 4 and graphically compared in figure 3, with the exception of the CSIRO/NML and PTB direct measurements of V_{90} (Nos. 2 and 3 of table 4, data items 3.1 and 3.2), were obtained using $\alpha^{-1}(a_e)$ or equivalently, the value of K_Ω it implies [eq (21b)]. Although there are significant differences among the various values of K_Ω given in table 3, these are sufficiently small that their effect on the derived values of K_V is relatively minor. Equation (14a) was used to derive the

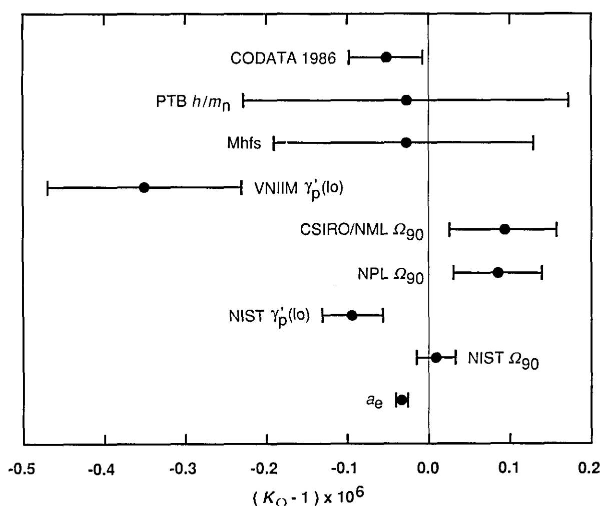

Figure 2. Graphical comparison of the stochastic input data through a comparison of values of $K_\Omega=(R_K/R_{K-90})=\mu_0 c\alpha^{-1}/2R_{K-90}$ given in table 3. With the exception of the 1986 CODATA recommended value, these values are taken directly from or are derived from the stochastic data of table 2.

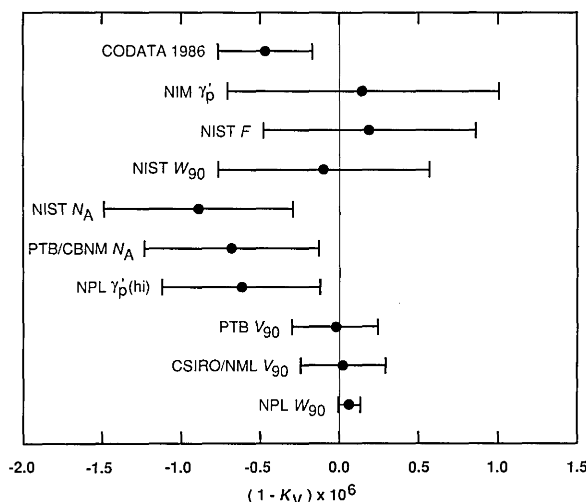

Figure 3. Graphical comparison of the stochastic input data through a comparison of values of $K_V=(K_{J-90}/K_J)=K_{J-90}/(2e/h)$ given in table 4. With the exception of the 1986 CODATA recommended value, these values are taken directly from or are derived from the stochastic data of table 2. (Because its severe disagreement with the other values of K_V is obvious, value No. 9 of table 4, that derived from the ASMW value of γ_p' (data item 7.2 of table 2), has been omitted from the figure to allow the use of a higher resolution scale.)

values of K_V from the NPL and NIST measurements of W_{90} (Nos. 1 and 7, data items 2.1 and 2.2). Written as a relation involving $2e/h$ and α^{-1}, eq (14a) becomes

$$\frac{2e}{h}=\left[\frac{\mu_0 c\alpha^{-1}(W_{90}/\mathrm{W})}{2K_{J-90}^2 R_{K-90}}\right]^{-1/2} \tag{29}$$

The following equation was used to derive the value of $K_J=2e/h$ and thus $K_V=K_{J-90}/K_J$ from the NIST measurement of the Faraday constant expressed in units of $C_{90}=A_{90}$ s (No. 8, data item 4.1):

$$\frac{2e}{h}=\left[\frac{8K_{J-90}R_{K-90}R_\infty\alpha^{-1}(m_p/m_e)F_{90}}{\mu_0 c^2 M_p}\right]^{1/2}, \tag{30}$$

where we have taken the 1986 recommended value for m_p/m_e and the new University of Washington value for M_p given in section 2.1.3. The similar equation used to derive the value of $2e/h$ and thus K_V from the NPL high-field measurement of γ_p' in units of C_{90}/kg (No. 4, data item 6.1) is

$$\frac{2e}{h}=\left[\frac{8K_{J-90}R_{K-90}R_\infty\alpha^{-1}\gamma_p'(\mathrm{hi})_{90}}{\mu_0 c^2(\mu_p'/\mu_B)}\right]^{1/2}. \tag{31}$$

The relation employed to derive the values of $2e/h$ from the ASMW and NIM values of γ_p' (Nos. 9 and 10, data items 7.2 and 7.1) is

$$\frac{2e}{h}=\frac{4R_\infty\alpha^{-2}\gamma_p'}{c(\mu_p'/\mu_B)}. \tag{32}$$

Finally, the equation used to derive the values of $2e/h$ from the NIST and PTB/CBNM measurements of N_A (Nos. 5 and 6, data items 8.1 and 8.2) is

$$\frac{2e}{h}=\left[\frac{16R_\infty\alpha^{-1}(m_p/m_e)N_A}{\mu_0 c^2 M_p}\right]^{1/2}. \tag{33}$$

Since the assigned uncertainties of the measured values of the five quantities W_{90}/W, F_{90}, $\gamma_p'(\mathrm{hi})_{90}$, γ_p', and N_A lie in the range 0.14 to 1.2 ppm (see table 2), and the assigned uncertainty of $\alpha^{-1}(a_e)$ is only 0.0069 ppm, eqs (29)-(33) clearly indicate that as far as these data are concerned, $\alpha^{-1}(a_e)$ may be treated as an auxiliary constant.

Table 4 and figure 3 show that the other nine values of K_V differ from the most precise value, that obtained from the NPL measurement of W_{90} (No. 1, data item 2.1), by at most 1.6 times the standard deviation of their difference except No. 9. This value of K_V, obtained from the ASMW measurement of γ_p' (data item 7.2), differs from the NPL W_{90} value by 5.2 times the standard deviation of their difference. This is a severe discrepancy and implies that the ASMW datum will likely need to be eliminated. Although the remaining data are consistent, there is a disparity in their uncertainties similar to that of the values of K_Ω given in table 3. For example, the uncertainty of the most precise value is 4.0 times smaller than the uncertainties of the next two most precise values, the CSIRO/NML and PTB measurements of V_{90} (Nos. 2 and 3, data items 3.1 and 3.2). This means, as was noted in section 2.2.3, that the NPL W_{90} result will to a large extent determine the value of K_V and thus $K_J=2e/h$ in any least-squares adjustment in which it is included.

In summary, we see that the data fall into two groups: those results that mainly determine K_Ω and those that mainly determine K_V. Each group is dominated by a single value significantly more precise than the other data in the same group, implying that eliminating these other data would have little effect. Each of the dominant values is supported by the other data in its group, although the support is weaker in the K_Ω case than in the K_V case. In the next section, the data are further examined by the method of least squares.

3.2 Multivariate Analysis of the Data

The $N=20$ data items of table 2, of 11 distinct types, may be expressed with the aid of auxiliary constants in terms of $M=3$ adjustable constants or unknowns, namely, K_Ω, K_V, and μ_μ/μ_p. The observational equation for each data type, 11 in all, is shown in table 5. (These equations follow from many of the relations already given, for example, eqs (5), (6), (14a), and (28)-(33).) By comparison, in the 1986 adjustment $N=38$ data items of 12 distinct types were expressed in terms of the five unknowns α^{-1}, K_V, K_Ω, $d_{220}(\mathrm{Si})$, and μ_μ/μ_p, where $K_V=\mathrm{V}_{76-\mathrm{BI}}/\mathrm{V}$ and $K_\Omega=\Omega_{\mathrm{BI85}}/\Omega$ (see sec. 2.1.7). Our decision to include only QHR measurements that are tied to a realization of the ohm based on a calculable capacitor; and the elimination of the discrepancy between the NIST and PTB values of $d_{220}(\mathrm{Si})$ along with the completion by the PTB and the CBNM of their independent measurement of the silicon molar volume $M(\mathrm{Si})/\rho(\mathrm{Si})$ (see sec. 2.2.7-2.2.8), have allowed the number of unknowns to be reduced from five to three.

In fact, the number of unknowns or variables could be reduced to two: K_Ω and K_V. This is because the 0.16 ppm uncertainty [see eq (24a)] of the value of α^{-1} implied by the two direct measure-

Table 5. The 11 distinct observational equations for the least-squares analysis of the stochastic data of table 2 taking K_Ω, K_V, and μ_μ/μ_p as the unknowns

1. $\Omega_{90}=K_\Omega\ \Omega$

2. $W_{90}=K_\Omega^{-1}\ K_V^2\ \mathrm{W}$

3. $V_{90}=K_V\ \mathrm{V}$

4. $F_{90}=\dfrac{\mu_0^2\,c^3\,K_{J-90}\,M_p}{16R_{K-90}^2\,R_\infty(m_p/m_e)}K_\Omega^{-1}\,K_V^{-2}$

5. $\gamma_p'(\mathrm{lo})_{90}=\dfrac{\mu_0^2\,c^3\,K_{J-90}\,(\mu_p'/\mu_B)}{16R_{K-90}^2\,R_\infty}K_\Omega^{-3}$

6. $\gamma_p'(\mathrm{hi})_{90}=\dfrac{\mu_0^2\,c^3\,K_{J-90}\,(\mu_p'/\mu_B)}{16R_{K-90}^2\,R_\infty}K_\Omega^{-1}\,K_V^{-2}$

7. $\gamma_p'=\dfrac{\mu_0^2\,c^3\,K_{J-90}\,(\mu_p'/\mu_B)}{16R_{K-90}^2\,R_\infty}K_\Omega^{-2}\,K_V^{-1}$

8. $N_A=\dfrac{\mu_0^2\,c^3\,K_{J-90}^2\,M_p}{32R_{K-90}\,R_\infty(m_p/m_e)}K_\Omega^{-1}\,K_V^{-2}$

9. $\alpha^{-1}=\dfrac{2R_{K-90}}{\mu_0\,c}K_\Omega$

10. $\mu_\mu/\mu_p=\mu_\mu/\mu_p$

11. $\nu_{\mathrm{Mhfs}}=\dfrac{4\mu_0^2\,c^3\,R_\infty(\mu_p/\mu_B)q}{3R_{K-90}^2(1+m_e/m_\mu)^3}K_\Omega^{-2}\,(\mu_\mu/\mu_p)$

$q=1.000\ 957\ 65(14)$

ments of μ_μ/μ_p (data items 10.1 and 10.2) and ν_{Mhfs} (data item 11.1) is so much larger than the 0.0069 ppm uncertainty of $\alpha^{-1}(a_e)$ that α^{-1}(Mhfs) contributes negligibly to the adjusted value of α^{-1}. One could just as well delete data items 10.1, 10.2, and 11.1, determine an adjusted value of α^{-1} from a two-variable K_Ω-K_V least-squares adjustment, use it and ν_{Mhfs} to determine a "muonium" value of μ_μ/μ_p, and then obtain a weighted mean value for μ_μ/μ_p from the "muonium" value and two direct values. An even more extreme approach would be to determine K_Ω from an appropriate weighted mean of the values given in table 3, use this result where needed to derive the values of K_V given in table 4, and then determine K_V from an appropriate weighted mean of these values. This is legitimate since, as discussed in section 3.1, α^{-1} may be viewed as an auxiliary constant as far as the data of type 2, 3, 4, 6, 7, and 8 are concerned provided it has a sufficiently small uncertainty. However, because we wish to investigate the effect of deleting various items of stochastic input data, including $\alpha^{-1}(a_e)$, we treat the data using only three-variable K_Ω-K_V-μ_μ/μ_p adjustments.[5]

The standard least-squares algorithm, the only one to be employed in the present study as indicated in the introductory paragraph of section 2.2, yields when applied to the 20 data items of table 2 $\chi^2=54.1$ for $\nu=N-M=17$ degrees of freedom; $R_B=1.78$ and $P_{\chi^2}(54.1|17)\simeq 1\times 10^{-5}$. This large value of χ^2 is due in large part to data item 7.2, the ASMW value of γ_p', which was previously shown to be discrepant; it is responsible for 49 percent of χ^2 but contributes only 0.6 percent to the determination of the adjusted value of γ_p'. When deleted, χ^2 is reduced to 27.6 for $\nu=16$, $R_B=1.31$, and $P_{\chi^2}(27.6|16)\simeq 0.036$. The dominant contributor to χ^2 is now data item 5.2, the VNIIM value of $\gamma_p'(\mathrm{lo})_{90}$; it is responsible for 25 percent of χ^2 but contributes less than 0.3 percent to the determination of $\gamma_p'(\mathrm{lo})_{90}$. When it is deleted, χ^2 becomes 20.7 for $\nu=15$, $R_B=1.17$, and $P_{\chi^2}(20.7|15)\simeq 0.15$. This adjustment, which will be referred to as Adjustment No. 1, gives the following values for the three adjustable constants or unknowns K_Ω, K_V, and μ_μ/μ_p:

$$K_\Omega-1=(-0.0285\pm 0.0064)\ \mathrm{ppm} \quad (34a)$$

$$1-K_V=(0.026\pm 0.062)\ \mathrm{ppm} \quad (34b)$$

$$\mu_\mu/\mu_p=3.183\ 345\ 48(40)\ (0.13\ \mathrm{ppm}), \quad (34c)$$

where the uncertainties have been computed on the basis of internal consistency. That is, they have not been multiplied by R_B, an approach followed throughout this and the next section in order not to allow the relatively minor inconsistencies in the data mask or distort the impact of the new results on the 1986 recommended values and their uncertainties. Further to this aim, we do not follow the principle used in the 1986 adjustment and delete data items that contribute in a marginal way to a particular adjustment (e.g., less than a few percent to the determination of their own value). If we did so, it would require deleting different items for different adjustments, thereby clouding the comparison of their results. For example, in Adjustment No. 4 to be discussed below, only data item 9.2 would be deleted on this basis while in Adjustment No. 1, data items 1.1, 1.2, 2.2, 4.1, 6.1, 7.1, 8.1, 8.2, and 9.2 would be so deleted.

[5] The choice of these three variables for the least squares analysis is not unique; we could have taken, for example, α, h, and μ_μ/μ_p equally as well.

Equations (34a) and (34b) imply that the new representation of the ohm based on the QHE and R_{K-90} is smaller than the (SI) ohm by (0.0285±0.0064) $\mu\Omega$; and that the new representation of the (SI) volt based on the Josephson effect and K_{J-90} is smaller than the (SI) volt by (0.026±0.062) μV. These differences, inconsequential as far as present day electrical metrology is concerned, imply that R_{K-90} would need to be decreased by 0.029 ppm and K_{J-90} would need to be increased by 0.026 ppm to bring the new ohm and volt representations into exact conformity with the presently available data as treated in Adjustment No. 1.

It is of interest to investigate the impact of deleting the two dominant data items, the NPL value of W_{90} and $\alpha^{-1}(a_e)$ (data items 2.1 and 9.1), first separately and then together. The results are given in table 6, along with those from Adjustment No. 1. Data items 7.2 and 5.2 remain sufficiently discrepant that they must also be deleted from Adjustment Nos. 2–4. An indication of the dominant role played by the NPL value of W_{90} and $\alpha^{-1}(a_e)$ is the significantly smaller uncertainties of the values of K_Ω and K_V resulting from Adjustment No. 1 compared with the uncertainties of the values resulting from Adjustment No. 4 (2.8 and 2.5 times smaller, respectively); and the significant differences in the values of K_Ω and K_V themselves resulting from the two adjustments (0.027 ppm and 0.18 ppm for K_Ω and K_V, respectively, or 4.3 and 2.9 times the uncertainties of these quantities resulting from Adjustment No. 1).

Table 6 also clearly shows the independence of the two groups of data as discussed in connection with tables 3 and 4: deleting the NPL value of W_{90} has essentially no effect upon K_Ω and thus α^{-1} (compare Adjustment No. 2 with No. 1), and deleting $\alpha^{-1}(a_e)$ has only a minor effect on K_V and thus $2e/h$ (compare Adjustment No. 3 with No. 1); deleting both yields nearly the same values of K_Ω and K_V obtained when they are deleted separately (compare Adjustment No. 4 with Nos. 2 and 3).

3.3 Changes in the 1986 Recommended Values and Their Uncertainties

Table 7 gives the changes in the 1986 recommended values and uncertainties of an important and representative group of fundamental constants as implied by Adjustment Nos. 1–4 of table 6 discussed in the previous section (the molar gas constant R, Boltzmann constant k, and Stefan-Boltzmann constant σ are discussed in sections 2.3, 2.3.1, and 2.3.2). The values and uncertainties of these constants are calculated in the usual way [2,5] from the adjusted values of the unknowns K_Ω, K_V, and μ_μ/μ_p resulting from the indicated adjustment, their variances and covariances, and auxiliary constants as appropriate. Similar patterns of behavior are observed among these constants because they depend on K_Ω and K_V in a similar way. For example, because both F and γ_p' are directly proportional to $K_\Omega^{-2} K_V^{-1}$, the entries for these quantities in all four columns of each of the four adjustments are nearly identical. Similarly, since the

Table 6. Summary of results of four least-squares adjustments involving the stochastic input data of table 2

	Adjustment No. 1	Adjustment No. 2 (NPL W_{90} deleted)	Adjustment No. 3 ($\alpha^{-1}(a_e)$ deleted)	Adjustment No. 4 (NPL W_{90}, $\alpha^{-1}(a_e)$ deleted)
$K_\Omega - 1$ (ppm)	−0.0285±0.0064	−0.0287±0.0064	0.000±0.018	−0.001±0.018
$1 - K_V$ (ppm)	0.026±0.062	−0.16±0.15	0.015±0.062	−0.15±0.15
μ_μ/μ_p	3.183 345 48(40) (0.13 ppm)	3.183 345 48(40) (0.13 ppm)	3.183 345 63(41) (0.13 ppm)	3.183 345 63(41) (0.13 ppm)
Total data items deleted	5.2, 7.2	NPL W_{90} (2.1), 5.2, 7.2	$\alpha^{-1}(a_e)$ (9.1), 5.2, 7.2	NPL W_{90} (2.1), $\alpha^{-1}(a_e)$ (9.1), 5.2, 7.2
χ^2; ν; R_B	20.7; 15; 1.17	18.9; 14; 1.16	17.7; 14; 1.12	16.2; 13; 1.12
$P_{\chi^2}(\chi^2 \mid \nu)$	0.15	0.17	0.22	0.24

Table 7. Changes in the 1986 recommended values and uncertainties of a representative group of constants implied by the new results reported since the completion of the 1986 adjustment

Quantity	1 std. dev. uncer. of 1986 recom. value (σ_{86}) in ppm	ppm change in 1986 recommended value (δ), corresponding number of standard deviations (δ/σ_{86}), new ppm uncertainty (σ_{90}), and ratio of 1986 uncertainty to new uncertainty[a] (σ_{86}/σ_{90})															
		Adjustment No. 1				Adjustment No. 2 (NPL W_{90} deleted)				Adjustment No. 3 ($\alpha^{-1}(a_e)$ deleted)				Adjustment No. 4 (NPL W_{90}, $\alpha^{-1}(a_e)$ deleted)			
	σ_{86}	δ	δ/σ_{86}	σ_{90}	σ_{86}/σ_{90}	δ	δ/σ_{86}	σ_{90}	σ_{86}/σ_{90}	δ	δ/σ_{86}	σ_{90}	σ_{86}/σ_{90}	δ	δ/σ_{86}	σ_{90}	σ_{86}/σ_{90}
h	0.60	−1.02	−1.7	0.12	4.8	−0.65	−1.1	0.30	2.0	−1.03	−1.7	0.12	4.8	−0.69	−1.2	0.31	2.0
e	0.30	−0.52	−1.7	0.062	4.9	−0.34	−1.1	0.15	2.0	−0.54	−1.8	0.063	4.8	−0.37	−1.2	0.15	2.0
m_e	0.59	−0.97	−1.6	0.12	4.7	−0.60	−1.0	0.30	1.9	−0.92	−1.6	0.13	4.6	−0.59	−1.0	0.30	1.9
α^{-1}, R_K	0.045	0.024	0.5	0.0064	6.9	0.024	0.5	0.0064	6.9	0.053	1.2	0.018	2.5	0.051	1.1	0.018	2.5
N_A	0.59	0.97	1.6	0.12	4.7	0.60	1.0	0.30	1.9	0.92	1.6	0.13	4.6	0.58	1.0	0.30	1.9
F	0.30	0.45	1.5	0.064	4.7	0.26	0.9	0.15	2.0	0.38	1.2	0.075	4.0	0.21	0.7	0.16	1.9
R	8.4	−4.7	−0.6	1.7	4.9	−4.7	−0.6	1.7	4.9	−4.7	−0.6	1.7	4.9	−4.7	−0.6	1.7	4.9
k	8.5	−5.7	−0.7	1.7	4.9	−5.3	−0.6	1.7	4.9	−5.6	−0.7	1.7	4.9	−5.3	−0.6	1.7	4.9
σ	34	−20	−0.6	6.9	4.9	−19	−0.6	6.9	4.9	−19	−0.6	6.9	4.9	−19	−0.6	6.9	4.9
K_J	0.30	0.50	1.7	0.062	4.8	0.32	1.1	0.15	1.9	0.49	1.6	0.062	4.7	0.32	1.1	0.15	1.9
μ_B	0.34	−0.57	−1.7	0.064	5.2	−0.39	−1.2	0.15	2.2	−0.65	−1.9	0.078	4.3	−0.48	−1.4	0.16	2.1
λ_C	0.089	−0.051	−0.6	0.013	6.9	−0.051	−0.6	0.013	6.9	−0.109	−1.2	0.036	2.5	−0.106	−1.2	0.036	2.5
γ_p'	0.30	0.45	1.5	0.064	4.7	0.26	0.9	0.15	2.0	0.38	1.2	0.075	4.0	0.21	0.7	0.16	1.9
m_μ/m_e	0.15	0.00	0.0	0.13	1.2	0.00	0.0	0.13	1.2	−0.05	−0.4	0.13	1.1	−0.05	−0.3	0.13	1.1

[a] See section 3.2 for a full description of Adjustment Nos. 1–4.

electron Compton wavelength $\lambda_C \propto K_\Omega^{-2}$ and $\alpha^{-1} \propto K_\Omega$, the entry for λ_C in column 1 of each adjustment is essentially −2 times the entry in column 1 for α^{-1}; the entry in column 2 for λ_C is −1 times the entry in column 2 for α^{-1}; the entry in column 3 for λ_C is 2 times the entry in column 3 for α^{-1}; and the entries in column 4 are the same for both λ_C and α^{-1}. If we had chosen to include in table 7 other constants that can be expressed in terms of the fine-structure constant (and auxiliary constants), such as the Bohr radius, the quantum of circulation, the Compton wavelengths of the proton and neutron, the classical electron radius, and the Thomson cross section [2], their entries would have followed a pattern related to that of α^{-1}. In particular, all would show the same 6.9 times reduction in uncertainty characteristic of α^{-1} and λ_C in Adjustment No. 1.

The comparatively small change in the value of the muon-electron mass ratio m_μ/m_e across the four adjustments in table 7 reflects the similar small change in μ_μ/μ_p in table 6. This is because $m_\mu/m_e=(\mu_e/\mu_p)(g_\mu/g_e)/(\mu_\mu/\mu_p)$ depends only on μ_μ/μ_p and auxiliary constants. The ratio μ_μ/μ_p is determined to some extent (about 18 percent) by the two direct measurements (data items 10.1 and 10.2 of table 2) which were also used in the 1986 adjustment, but to a much greater extent (82 percent) by the "muonium" value of μ_μ/μ_p determined from α^{-1} and $\nu_{\rm Mhfs}$ (see sec. 3.2). Because the current "muonium" value is very nearly equal to its 1986 value and to the weighted mean of the two direct measurements [2], the variation in μ_μ/μ_p and thus in m_μ/m_e is unusually small.

Many of the other patterns displayed in table 6 are apparent in table 7. For example, this table once again shows that the constants fall into two groups: those strongly dependent upon α^{-1} or equivalently, K_Ω, and those strongly dependent upon K_V. Deleting the NPL value of W_{90} (see Adjustment No. 2), which plays the dominant role in determining K_V, has little impact on the values of those constants determined by K_Ω, for example, λ_C; and deleting $\alpha^{-1}(a_e)$ (see Adjustment No. 3), which plays the

dominant role in determining K_{Ω}, has little impact on the values of the constants determined to a large extent by K_V, for example m_e.

Because table 7 is relatively self explanatory, it does not require a great deal of additional comment. It is clear that the changes in the 1986 recommended values as given by Adjustment No. 1 (depicted in fig. 4), the most important case since it includes the two most precise items of stochastic input data, are significant in comparison with the uncertainties of the 1986 values but not disturbingly so (see column 2). Indeed, in light of recent past adjustments [2,4,77], changes of less than two standard deviations are a welcome sight. In contrast, the reductions in the uncertainties of the 1986 values resulting from Adjustment No. 1 (see column 4) are clearly major and perhaps even extraordinary inasmuch as only $4\frac{1}{2}$ years have elapsed since the 1 January 1986 cutoff date of the 1986 adjustment. The NPL value of W_{90}, the new University of Washington-Cornell value of $\alpha^{-1}(a_e)$, and the NIST value of R, all obtained in the last 2–3 years, are principally responsible for the large reduction factors. These factors are typically in the range 4.7 to 6.9. Without these three new results, the changes in the 1986 values are far less significant and the reductions in their uncertainties, although not inconsequential, are far less dramatic.[6] This important conclusion, perhaps the most significant of this entire report, follows from a comparison of Adjustment No. 4 with No. 1.

4. Conclusion

Physics and metrology have not stood still since 1 January 1986, the cutoff date for data to be considered for inclusion in the 1986 CODATA least-squares adjustment of the constants; many new results have been reported in the intervening $4\frac{1}{2}$ years that lead to significant changes in the 1986 set of recommended values. In fact, only 5 of the 20

[6] See the Appendix, section 5.2, for a brief discussion of the changes in the 1986 set of recommended values that arise from these three results alone.

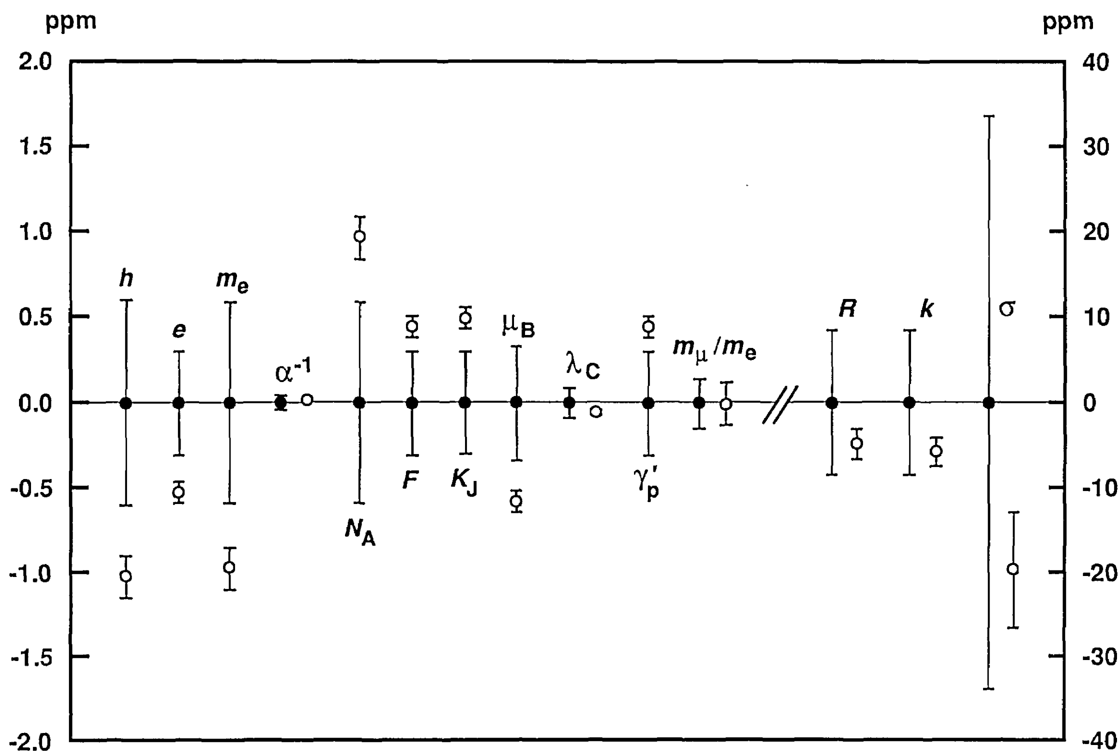

Figure 4. Graphical display of the results of Adjustment No. 1 given in table 7. The closed circles with error bars indicate the 1986 CODATA recommended values and their one-standard-deviation uncertainties; the open circles with error bars indicate the values and their one-standard-deviation uncertainties derived from the data of table 2 through Adjustment No. 1, relative to the 1986 values.

items of stochastic input data considered in this report (table 2) are the same as those considered in 1986: F, the NPL value of γ_p'(hi), the two values of μ_μ/μ_p, and the experimental value of ν_{Mhfs}. There have been changes in the auxiliary constant and secondary stochastic data categories as well. The most notable change in an auxiliary constant is that of the Rydberg. New measurements of R_∞ imply that the 1986 recommended value is too small by 2.8 times the 1.2×10^{-9} relative uncertainty assigned the 1986 value. Moreover, the 1.7×10^{-10} relative uncertainty quoted for the most precise of these is 7 times smaller. The improvement in the secondary stochastic datum R, the molar gas constant, is nearly as great: The new result for R with its 1.7 ppm uncertainty is nearly 5 times more precise than the 1986 value with its 8.4 ppm uncertainty. Fortunately, the change implied in the 1986 value, −4.7 ppm, is only 0.6 times this uncertainty. Similar changes occur in the values and uncertainties of other constants that are dependent upon R, for example, the Boltzmann constant k and Stefan-Boltzmann constant σ.

Of course, the bulk of the changes in the 1986 set of recommended values arise from the stochastic input data of table 2. Our discussion of the impact of these data as given throughout this report, but especially in section 3, may be succinctly summarized as follows (see table 7): The changes in the 1986 values are generally less than twice the uncertainties of the 1986 values; shifts in the range 1.6–1.8 standard deviations are typical. The uncertainties of the 1986 values themselves are reduced by a factor of 4.7–6.9. These changes are, however, strongly dependent upon just two new stochastic input data items: the value of W_{90} obtained from the NPL moving coil experiment (data item 2.1, table 2); and the University of Washington-Cornell value of α^{-1} obtained from the electron magnetic moment anomaly a_e (data item 9.1). If these data items are deleted, the changes in the 1986 values are in general only 1.0–1.2 standard deviations and their uncertainties are only reduced by about a factor of 2.

The strong dependence of the changes in the 1986 recommended values and their uncertainties on just three results (counting the new value of R) has significant implications for the timing of the next least-squares adjustment. While the large reduction in the 1986 uncertainties arising from these three results provides some motivation for carrying out a new adjustment sooner rather than later, their dominant role must be seen as a caution sign. We believe it is of the utmost importance to obtain corroboration of each of the three results at a comparable level of uncertainty before a new set of recommended values is introduced. This is especially true of the NPL value of W_{90} because of its significant impact on the values of a large number of constants and because it may be argued that in view of the scatter of the data upon which it is based [52], its quoted uncertainty is somewhat optimistic.

While any work that provides added confidence in these three results would be useful and is strongly encouraged, obtaining independent values with comparable uncertainties is the obvious goal. With regard to α^{-1}, further experimental work on measuring a_e currently underway at the University of Washington should clarify a number of possible systematic errors such as the cavity and "elevator" effects (see sec. 2.1.5). An independent value might also be available from the group working at CERN [16]. Kinoshita is continuing to check his monumental QED calculation of a_e(theor), but no other group is likely to repeat this effort in the foreseeable future. Nonetheless, increased effort should be devoted to improved measurements of Ω_{90} and $\gamma_p'(\mathrm{lo})_{90}$ in order to obtain values of α^{-1} with an uncertainty comparable with the current 0.0069 ppm uncertainty of $\alpha^{-1}(a_e)$, say 0.01 ppm. We therefore urge those national standards laboratories capable of carrying out calculable capacitor determinations of Ω_{90} and measurements of $\gamma_p'(\mathrm{lo})_{90}$ to exert every possible effort to reach this level of uncertainty. (This also applies to the new Los Alamos/Yale ν_{Mhfs} experiment and the calculation of ν_{Mhfs}(theor).) The fact that the NIST has already reported a value of Ω_{90} with an uncertainty of 0.024 ppm and a value of α^{-1} from $\gamma_p'(\mathrm{lo})_{90}$ with an uncertainty of 0.037 ppm provides hope that in both cases 0.01 ppm may be achievable.

With regard to W_{90}, as noted in section 2.2.2 Kibble and colleagues at the NPL are constructing a completely new and significantly improved moving coil apparatus to determine W_{90} with a relative uncertainty of ~0.01 ppm; first results are expected in 1–2 years. The similar experiment at the NIST with the same long term uncertainty goal is also being vigorously pursued and a result for W_{90} with a 0.1 ppm uncertainty could be available in the same 1–2 year time period. Since a value of W_{90} with a 0.1 ppm uncertainty provides a value of V_{90}, or equivalently K_V, with an uncertainty of 0.05 ppm, the approximate 0.3 ppm uncertainty of the volt balance experiments carried out at the CSIRO/NML, the PTB, and the U. Zagreb (see sec. 2.2.3) would have to be reduced by about a

factor of six to yield values of K_V with the same 0.05 ppm uncertainty. Similarly, the approximate 1 ppm uncertainty of the NIST and PTB/CBNM measurements of N_A would need to be reduced by about a factor of 10 to yield a value of K_V with a comparable uncertainty. While such uncertainty reductions will be difficult to achieve, we again urge those laboratories engaged in volt balance and Avogadro constant experiments to exert every possible effort to do so in view of the potential impact of the results on the next set of recommended values of the constants, as well as on replacing the kilogram [22]. This encouragement is extended also to those researchers and laboratories engaged in other approaches, for example, determining W_{90} by comparing mechanical and electrical energy through the levitation of a superconducting mass with a superconducting coil (see sec. 2.2.2).

With regard to the molar gas constant R, Moldover and colleagues at the NIST are continuing to carry out acoustical resonator measurements that may provide added confidence in the present NIST value with its 1.7 ppm uncertainty. However, what is needed is a new version of the experiment that can take full advantage of all that has been learned in the earlier version and of related research that points the way to determining the volume of the resonator from microwave resonance measurements [78] rather than from weighing the mercury required to fill it. We hope that a new effort is initiated at the NIST in the near future and that other laboratories also consider undertaking such work.

In summary, we believe it is premature to predict when the next least-squares adjustment of the constants should be carried out. While a new set of recommended values could be introduced today with uncertainties considerably smaller than those of the 1986 set, inasmuch as the 1986 set has only been available for about 4 years, we believe for the reasons given in section 1.1 that this would be premature. That the changes in the 1986 values arising from the currently available data are not highly significant, that the data are dominated by just three new results, and that there are some annoying inconsistencies among the data, supports this view. It therefore appears best to postpone the decision as to when a new set of recommended values to replace the 1986 set should be introduced until some significant progress is made in the experimental and theoretical work just discussed. This progress will no doubt strongly influence the timing of the next adjustment. Indeed, it is conceivable that new results obtained in the next several years will suggest that the introduction of a new set of recommended values be further postponed because of unacceptable inconsistencies among the data. One point about which we are certain is that the future of this field of science cannot be predicted—the discovery of a new phenomenon with the impact of the Josephson effect or the quantum Hall effect may await us just next year!

5. Appendix

5.1 Laboratory Abbreviations

The following are the laboratory abbreviations used throughout this paper.

ASMW	Amt für Standardisierung, Messwesen und Warenprüfung, Berlin, GDR
BIPM	Bureau International des Poids et Mesures, Sèvres, France
CBNM	Central Bureau for Nuclear Measurements, Geel, Belgium
CSIRO/NML	Commonwealth Scientific and Industrial Research Organization, Division of Applied Physics, National Measurement Laboratory, Lindfield, Australia
ETL	Electrotechnical Laboratory, Tsukuba, Japan
KhGIMIP	Kharkov State Scientific Research Institute of Metrology, Kharkov, USSR
LCIE	Laboratoire Central des Industries Électriques, Fontenay-aux-Roses, France
NIM	National Institute of Metrology, Beijing, PRC
NIST	National Institute of Standards and Technology (formerly National Bureau of Standards or NBS), Gaithersburg, MD, USA
NPL	National Physical Laboratory, Teddington, UK

NRLM	National Research Laboratory of Metrology, Tsukuba, Japan
PTB	Physikalisch-Technische Bundesanstalt, Braunschweig, FRG
SIN	Swiss Institute for Nuclear Research, Villigen, Switzerland
U. Zagreb	Faculty of Electrical Engineering, University of Zagreb, Yugoslavia
VNIIM	All-Union Scientific Research Institute of Metrology (Mendeleev Institute of Metrology), Leningrad, USSR

5.2 Effect of the Three Dominant New Results Alone

It is of interest to calculate the changes in the 1986 recommended values and uncertainties of the same representative group of constants listed in table 7 arising from the three dominant new results alone: $h = 6.626\,068\,21(90) \times 10^{-34}$ J s (0.14 ppm) as obtained from the NPL Measurement of W_{90} (data item 2.1 of table 2) using eqs (12) and (13); $\alpha^{-1}(a_e)$ (eq (21a), data item 9.1); and the NIST value of R, eq (27). Using relations such as $e = (2h/\mu_0 c\alpha^{-1})^{1/2}$, $K_J = 2e/h = (8/\mu_0 ch\alpha^{-1})^{1/2}$, and eqs (25) and (26) for k and σ, yields the results given in table 8. A comparison of table 8 with Adjustment No. 1 of table 7 again shows that these three results alone account for most of the observed changes in the

Table 8. Changes in the 1986 recommended values and uncertainties of a representative group of constants implied by the three dominant new results alone: the value of h obtained from the NPL determination of W_{90}, the University of Washington-Cornell value of $\alpha^{-1}(a_e)$, and the NIST value of R

Quanity	1 std. dev. uncer. of 1986 recom. value (σ_{86}) in ppm	ppm change in 1986 recommended value (δ), corresponding number of standard deviations (δ/σ_{86}), new ppm uncertainty (σ_{90}), and ratio of 1986 uncertainty to new uncertainty (σ_{86}/σ_{90})			
	σ_{86}	δ	δ/σ_{86}	σ_{90}	σ_{86}/σ_{90}
h	0.60	−1.10	−1.8	0.14	4.4
e	0.30	−0.56	−1.8	0.068	4.5
m_e	0.59	−1.05	−1.8	0.14	4.3
α^{-1}, R_K	0.045	0.020	0.4	0.0069	6.5
N_A	0.59	1.05	1.8	0.14	4.3
F	0.30	0.49	1.6	0.070	4.3
R	8.4	−4.7	−0.6	1.7	4.9
k	8.5	−5.8	−0.7	1.7	4.9
σ	34	−20	−0.6	6.9	4.9
K_J	0.30	0.54	1.8	0.068	4.4
μ_B	0.34	−0.60	−1.8	0.070	4.8
λ_C	0.089	−0.043	−0.5	0.014	6.5
γ'_p	0.30	0.50	1.6	0.070	4.3
m_μ/m_e	0.15	0.00	0.0	0.13	1.2

1986 recommended values and their uncertainties. (The value $\mu_\mu/\mu_p=3.183\,345\,46(40)$ (0.13 ppm) used to calculate the ratio m_μ/m_e is the weighted mean of the indirect "muonium" value $\mu_\mu/\mu_p=3.183\,345\,46(45)$ (0.14 ppm) as obtained from $\alpha^{-1}(a_e)$, the experimental value of ν_{Mhfs} (data item 11.1), and the theoretical expression for ν_{Mhfs} (eq (11) of table 5, see the discussion in secs. 3.2 and 3.3.); and the weighted mean of the two direct measurements $\mu_\mu/\mu_p=3.183\,345\,47(95)$ (0.30 ppm) (data items 9.1 and 9.2).)

Acknowledgment

We thank our many colleagues for helpful discussions and correspondance, especially for their willingness to share their future plans and to predict their future progress.

6. References

[1] Cohen, E. R., and Taylor, B. N., The 1986 Adjustment of the Fundamental Physical Constants, a Report of the CODATA Task Group on Fundamental Constants, CODATA Bulletin No. 63 (Pergamon, Fairview Park, Elmsford, NY 10523, or Headington Hill Hall, Oxford OX3 OBW, UK, 1986).
[2] Cohen, E. R., and Taylor, B. N., Rev. Mod. Phys. **59**, 1121 (1987).
[3] Cohen, E. R., and Taylor, B. N., J. Res. Natl. Bur. Stand. (U.S.) **92**, 85 (1987); Europhys. News **18**, 65 (1987); Phys. Today **40**, No. 8, Pt. 2, BG11 (1987); J. Phys. Chem. Ref. Data **17**, 1795 (1988).
[4] Recommended Consistent Values of the Fundamental Physical Constants, 1973, a Report of the CODATA Task Group on Fundamental Constants, CODATA Bulletin No. 11, CODATA Secretariat, 51 Blvd. de Monmorency, 75016 Paris, France, August, 1973.
[5] Cohen, E. R., and Taylor, B. N., J. Phys. Chem. Ref. Data **2**, 663 (1973).
[6] Grabe, M., Metrologia **23**, 213 (1986/1987).
[7] Grabe, M., CODATA Newslett. No. 41, 6 (July 1987).
[8] Cohen, E. R., CODATA Newslett. No. 42, 4 (Nov. 1987).
[9] Artbauer, O., Metrologia **25**, 81 (1988).
[10] Taylor, B. N., in Precision Measurement and Fundamental Constants, Langenberg, D. N., and Taylor, B. N., eds., Natl. Bur. Stand. (U.S.), Spec. Publ. 343, U.S. Govt. Printing Office, Wash. D.C. (1971), p. 495.
[11] Hudson, R. P., Metrologia **19**, 163 (1984).
[12] Clarion, A., et al., Metrologia **25**, 9 (1988).
[13] Whitford, B. G., and Hanes, G. R., IEEE Trans. Instrum. Meas. **IM-37**, 179 (1988).
[14] Kramer, G., Weiss, C. O., and Lipphardt, B., in Frequency Standards and Metrology, De Marchi, A., ed., Springer-Verlag, Berlin (1989), p. 181.
[15] Bagayev, S. N., et al., in Frequency Standards and Metrology, De Marchi, A., ed., Springer-Verlag, Berlin (1989), p. 191.
[16] Gabrielse, G., et al., Phys. Rev. Lett. **65**, 1317 (1990).
[17] Gabrielse, G., et al., Phys. Rev. Lett. **63**, 1360 (1989).
[18] This report was prepared in April 1986 by Audi, G., and Wapstra, A. H., and distributed by Haustein, P. E., Brookhaven National Laboratory, USA.
[19] Wapstra, A. H., Audi, G., and Hoekstra, R., At. Data Nucl. Data Tables **39**, 281 (1988).
[20] Moore, F. L., Farnham, D. L., Schwinberg, P. B., and van Dyck, R. S., Jr., Bull. Am. Phys. Soc. **34**, 99 (1989); Nucl. Instrum. Meth. Phys. Res. B **43**, 425 (1989).
[21] Quinn, T. J., IEEE Trans. Instrum. Meas. **IM-40** (April 1991), to be published.
[22] Taylor, B. N., IEEE Trans. Instrum. Meas. **IM-40** (April 1991), to be published.
[23] Zhao, P., Lichten, W., Layer, H. P., and Bergquist, J. C., Phys. Rev. A **34**, 5138 (1986).
[24] Biraben, F., Garreau, J. C., and Julien, L., Europhys. Lett. **2**, 925 (1986).
[25] Zhao, P., et al., Phys. Rev. A **39**, 2888 (1989).
[26] Boshier, M. G., et al., Phys. Rev. A **40**, 6169 (1989).
[27] McIntyre, D. H., et al., Phys. Rev. A **39**, 4591 (1989).
[28] Beausoleil, R. G., et al., Phys. Rev. A **35**, 4878 (1987).
[29] Biraben, F., Garreau, J. C., Julien, L., and Allegrini, M., Phys. Rev. Lett. **62**, 621 (1989).
[30] Garreau, J. C., Allegrini, M., Julien, L., and Briaben, F., J. Phys. (Paris) **51**, 2263 (1990); **51**, 2275 (1990); **51**, 2293 (1990).
[31] van Dyck, R. S., Jr., Schwinberg, P. B., and Dehmelt, H. G., Phys. Rev. Lett. **59**, 26 (1987).
[32] van Dyck, R. S., Jr., Schwinberg, P. B., and Dehmelt, H. G., Bull. Am. Phys. Soc. **33**, 2349 (1988).
[33] van Dyck, R. S., Jr., Schwinberg, P. B., and Dehmelt, H. G., Abstracts of Contributed Papers, Twelfth International Conference on Atomic Physics, University of Michigan, 29 July-3 August, 1990, Baylis, W. E., Drake, G. W. F., and McConkey, J. W., eds., p. II-8.
[34] Gorshkov, M. V., et al., Dokl. Akad. Nauk SSSR **305**, 1362 (1989) [English transl.: Sov. Phys. Dokl. **34**, 362 (1989)].
[35] Quinn, T. J., Metrologia **26**, 69 (1989).
[36] Taylor, B. N., and Witt, T. J., Metrologia **26**, 47 (1989).
[37] Reymann, D., IEEE Trans. Instrum. Meas. **IM-40** (April 1991), to be published.
[38] Delahaye, F., Metrologia **26**, 63 (1989).
[39] Delahaye, F., and Bournaud, D., IEEE Trans. Instrum. Meas. **IM-40** (April 1991), to be published.
[40] Small, G. W., IEEE Trans. Instrum. Meas. **IM-36**, 190 (1987).
[41] Witt, T. J., Delahaye, F., and Bournaud, D., IEEE Trans. Instrum. Meas. **IM-38**, 279 (1989).
[42] Delahaye, F., Satrapinsky, A., and Witt, T. J., IEEE Trans. Instrum. Meas. **IM-38**, 256 (1989).
[43] Shields, J. Q., Dziuba, R. F., and Layer, H. P., IEEE Trans. Instrum. Meas. **IM-38**, 249 (1989).
[44] Cage, M. E., Dziuba, R. F., Van Degrift, C. T., and Yu., D., IEEE Trans. Instrum. Meas. **IM-38**, 263 (1989).
[45] Taylor, B. N., and Cohen, E. R., to be published.
[46] Faller, J. E., and Marson, I., Metrologia **25**, 49 (1988).
[47] Boulanger, Yu., et al., Bur. Grav. Int. Bull. Informat. No. 59, 89 (Dec. 1986).
[48] Faller, J. E., private communication, 1990; and to be published in Bur. Grav. Int. Bull. Informat.
[49] Small, G. W., Ricketts, B. W., and Coogan, P. C., IEEE Trans. Instrum. Meas. **IM-38**, 245 (1989).
[50] Hartland, A., Jones, R. G., and Legg, D. J., Document CCE/88-9 submitted to the 18th meeting of the CCE, 1988.

[51] Cage, M. E., et al., IEEE Trans. Instrum. Meas. **IM-38**, 284 (1989).
[52] Kibble, B. P., Robinson, I. A., and Belliss, J. H., A realization of the SI watt by the NPL Moving-Coil Balance, NPL Report DES 88, Division of Electrical Science, National Physical Laboratory, Teddington, UK, May 1988.
[53] Olsen, P. T., et al., IEEE Trans. Instrum. Meas. **IM-38**, 238 (1989).
[54] Shiota, F., et al., IEEE Trans. Instrum. Meas. **IM-38**, 225 (1989).
[55] Clothier, W. K., et al., Metrologia **26**, 9 (1989).
[56] Funck, T., and Sienknecht, V., IEEE Trans. Instrum. Meas. **IM-40** (April 1991), to be published.
[57] Williams, E. R., et al., IEEE Trans. Instrum. Meas. **IM-38**, 233 (1989).
[58] Tarbeev, V. Yu., Shifrin, V. Ya., Khorev, V. N., and Studentsov, N. V., Izmeritel. Tekh. No. 4, 3 (April 1989) [English transl.: Meas. Tech. **32**, 279 (1989)].
[59] Pudalov, V. M., private communication, 1990.
[60] Witt, T. J., Projected Changes in National Reference Standards of Electromotive Force and Resistance, BIPM Report-89/7, Bur. Int. Poids Mes., Sèvre, France, 1989.
[61] Liu, H., Liu, R., Shen, P., Jin, T., Lu, Z., Du, X., and Yu, B., Document CCE/88-11 submitted to the 18th meeting of the CCE, 1988.
[62] Forkert, J., and Schlesok, W., Metrologische Abhandlungen **6**, 165 (1986) (in German).
[63] Deslattes, R. D., et. al., IEEE Trans. Instrum. Meas. **IM-36**, 166 (1987).
[64] Deslattes, R. D., in the Art of Measurement, Kramer, B., ed., VCH Publishers, Weinheim, FRG (1988), p. 193.
[65] Seyfried, P., PTB Mitt. **5**, 336 (1989) (in German).
[66] Kinoshita, T., IEEE Trans. Instrum. Meas. **IM-36**, 201 (1987).
[67] Kinoshita, T., Metrologia **25**, 223 (1988).
[68] Kinoshita, T., IEEE Trans. Instrum. Meas. **IM-38**, 172 (1989).
[69] Kinoshita, T., and Lindquist, W. B., Phys. Rev. D **42**, 636 (1990). For the reasons given by Kinoshita [Phys. Rev. Lett. **61**, 2898 (1988), Phys. Rev. D **40**, 1323 (1989)], the value of the light-by-light scattering contribution $a_{\gamma\gamma}$ to C_3 obtained by M. A. Samuel [Phys. Rev. Lett. **57**, 3133 (1986), Phys. Rev. Lett. **61**, 2899 (1988)], which disagrees with the value used by Kinoshita and Lindquist, is not considered.
[70] Krüger, E., Nistler, W., and Weirauch, W., PTB Mitt. **99**, 318 (1989) (in German). See also Nucl. Instrum. Meth. Phys. Res. A **284**, 143 (1989).
[71] Karshenboim, S. G., Shelyuto, V. A., and Eides, M. I., Yad Fiz. **49**, 493 (1989) [English transl.: Sov. J. Nucl. Phys. **49**, 309 (1989)].
[72] Karshenboim, S. G., Shelyuto, V. A., and Eides, M. I., Zh. Eksp. Teor. Fiz. **92**, 1188 (1987). [English transl.: Sov. Phys. JETP **65**, 664 (1987)].
[73] Karshenboim, S. G., Shelyuto, V. A., and Eides, M. I., Zh. Eksp. Teor. Fiz. **94**, 42 (1988). [English transl.: Sov. Phys. JETP **67**, 671 (1988)].
[74] Eides, M. I., Karshenboim, S. G., and Shelyuto, V. A., Phys. Lett. **229B**, 285 (1989).
[75] Moldover, M. R., et al., J. Res. Natl. Bur. Stand. (U.S.) **93**, 85 (1988).
[76] DeBoer, H., Haars, H., and Michaelis, W., Metrologia **24**, 171 (1987).
[77] Taylor, B. N., Parker, W. H., and Langenberg, D. N., Rev. Mod. Phys. **41**, 375 (1969).
[78] Mehl, J. B., and Moldover, M. R., Phys. Rev. A **34**, 3341 (1986).

About the authors: *Barry N. Taylor is a physicist in the NIST Center for Atomic, Molecular, and Optical Physics and Chief Editor of the NIST Journal of Research. E. Richard Cohen, also a physicist, is Distinguished Fellow at the Rockwell International Science Center.*

Volume 95, Number 5, September–October 1990
Journal of Research of the National Institute of Standards and Technology

[J. Res. Natl. Inst. Stand. Technol. 95, 525 (1990)]

An International Comparison of Absolute Radiant Power Measurement Capabilities

Volume 95 | Number 5 | September–October 1990

Douglas B. Thomas

National Institute of Standards and Technology,
Gaithersburg, MD 20899

We report the results of an intercomparison of monochromatic radiant power measurement capabilities recently completed by 11 national laboratories. The intercomparison radiometers, distributed in pairs, included an amplifier with six decades of precision gain and one of two types of silicon photodiode (*pn* or *np*-type construction). Eleven of the laboratories measured the absolute responsivity of the radiometers at 633 nm and nine at 488 nm. The standard deviation of the overall difference was 0.36% at both wavelengths. The agreement between the various participating laboratories and NIST was within the measurement accuracy stated by the participants.

Key words: absolute spectral response; intercomparison; laser power; photodetector; radiant power; radiometry; silicon photodiodes.

Accepted: July 31, 1990

1. Introduction

In 1986 an intercomparison of monochromatic radiant power measurements at 633 and 488 nm was undertaken at the request of the Comité Consultatif de Photométrie et Radiométrie (CCPR). The lead laboratory was the National Institute of Standards and Technology (NIST) (formerly the National Bureau of Stanards). The participating laboratories were: Electrotechnical Laboratory (ETL), Japan; Institut National de Métrologie (INM), France; National Institute of Measurements (NIM), Chengdu, People's Republic of China; CSIRO National Measurement Laboratory (NML), Australia; National Office of Measures (OMH), Hungary; National Physical Laboratory (NPL), United Kingdom; National Physical Research Laboratory (NPRL), South Africa; National Research Council (NRC), Canada; Physikalisch-Technische Bundesanstalt (PTB), Federal Republic of Germany; and Research Institute of Technical Physics of the Hungarian Academy of Sciences (MFKI), Hungary. The intercomparison was organized by E. F. Zalewski (formerly with NIST) and a report on the intercomparison was prepared by him and submitted to the CCPR for publication in the proceedings of the eleventh session of the CCPR [1]. This paper is a subsequent update of the analysis presented in the report to the CCPR and presents a more detailed error analysis of the data and some typographical corrections.

This was the first international comparison of monochromatic radiant power measurements using silicon photodiodes as the transfer standards. A previous intercomparison of laser power measurements [2,3] used thermal detectors as transfer standards, while an intercomparison of (spectrally total) radiant power [4] used incandescent lamps. Recent reports on the behavior of various types of silicon photodiodes under varying environmental conditions [5–8] suggest good measurement stabil-

ity can be obtained by the appropriate selection of silicon photodiode and use of an improved design of the calibration transfer device.

The intercomparison procedure will be described along with some details of the absolute radiant power measurement procedures employed in each of the participating laboratories.

2. Experimental Conditions

The comparison method consisted of each laboratory measuring the absolute spectral response of circulated silicon photodiode radiometers. The participating laboratories measured absolute responsivity at 488 and 633 nm (argon ion and helium-neon laser wavelengths) within the central portion of the photodiode's active area. NIST, as the central laboratory, measured the responsivity before and after the participating laboratory. In some cases, due to equipment problems, this protocol was not maintained. A detector responsivity comparison is equivalent to comparing each laboratory's capability of measuring radiant power. This intercomparison has added significance in radiometry arising from the new definition of the candela which enables realization of this unit from a radiant power measurement base [9].

To allow for maximum uniformity of measurement in the participating laboratories, complete radiometers were circulated that included both the photodiode and the signal processing electronics. This precluded any complications in the intercomparison arising from different amplification techniques and possible inaccuracies in gain calibrations. The signal processing electronic circuit consisted of an operational amplifier in a transimpedance configuration (current to voltage amplifier) and a buffer amplifier. The gain settings of the radiometers were variable in six precise decade steps from 0.1 mA/V to 1 nA/V. The absolute uncertainty in the gain was less than 0.1% in the 0.1 mA/V to 100 nA/V range. At the two higher gain settings the absolute uncertainty increased to 0.5 and 1%, respectively.

Stability of the transfer device is an important consideration in any intercomparison. At the time this intercomparison was being planned, it was known that the collection efficiency for minority carriers generated near the oxide-silicon interface in *pn*-silicon photodiodes could be unstable [10,11,12]. Since the collection efficiency in the *np* induced-junction type silicon photodiode is immune to changes at the oxide-silicon interface [13], it was decided that photodiodes of this type would also be circulated for the comparison. Circulating both types was deemed necessary because very little evidence concerning the stability of the new *np* type of silicon photodiode existed at that time. The two different silicon photodiodes used were a *pn* type that was manufactured by the EG&G Company[1] [14], Model UV-444B, and an *np* type incorporating the recently developed induced junction technology that was manufactured by the United Detector Technology Company (UDT) [15], Model UV-100. A total of 16 radiometers were constructed for this intercomparison.

Laser sources at power levels of the order of 1 mW were scheduled to be used at NIST and some of the other laboratories, which brought about the possibility that the *np*-type photodiodes could be operated in a slightly non-linear region, i.e., become saturated [13,16], at the higher power levels. Applying a reverse bias voltage to the photodiode extends its dynamic range [16,17]. To diminish this probable non-linearity phenomenon, the *np*-type intercomparison radiometers were biased at 4.5 V by three lithium batteries included in the circuit. Applying a reverse bias to a silicon photodiode introduces a large dark current which is considerably noisier than that of the unbiased photodiode. Some precision would therefore be sacrificed in order to obtain a dynamic range of response of the *np*-type intercomparison radiometers that would be comparable to that of the *pn* type [16].

Since lasers were to be used as the radiation source, the radiometers did not have a window covering the silicon photodiode. In the first phase of the intercomparison, the photodiodes were not sealed from possible atmospheric contaminations, but were merely covered by a dust-cap during transport. Although they were all found to be stable at 633 nm under laboratory conditions at NIST, three of the 16 photodiodes, one *pn* type and two *np* types, were found upon remeasurement at NIST to have changed significantly during transport. The *pn* type of photodiode showed a decrease in response at 633 nm of 4% and the two *np* types an increase of 8% and 9.5%. In subsequent rounds of the intercomparison, an attempt was made to more adequately protect the photodiodes by a redesigned cap that sealed off the detector from the

[1] Certain commercial equipment, instruments, or materials are identified in this paper to specify adequately the experimental procedure. Such identification does not imply recommendation or endorsement by the National Institute of Standards and Technology, nor does it imply that the materials or equipment identified are necessarily the best available for the purpose.

atmosphere and by packaging the entire radiometer in a sealed plastic bag containing a desiccant. No changes of such magnitude were observed in the subsequent rounds of the intercomparison. The satisfactory stability of the diodes used in the intercomparison (excluding those that exhibited large changes and were not included in the data analysis) can be assessed from the differences of the before and after NIST measurements. For example, at 633 nm, the average absolute value of these differences was only 0.12%.

The laboratories that received the radiometers suffering the large changes were NRC and NPL. It was also suspected that the radiometers received by PTB might have changed. All three laboratories were invited to repeat their measurements using a different pair of radiometers. In addition, PTB also repeated their measurements on the original pair of radiometers. There was no statistically significant difference in the PTB results on either pair of radiometers. Both sets of the PTB measurements are listed in table 1, but only the averages were used in the calculation of the final result. For NRC and NPL, only their second set of measurements on the more stable transfer radiometers are listed in table 1 and used in the analysis of the intercomparison. In the case of the 633-nm measurements at PTB, NRC, and NPL, it was not possible to repeat the NIST measurements after the laboratory's measurements.

The original plans for the intercomparison called for the radiometers to be measured at NIST both before and after transport to the participating laboratories. Because of difficulties with the argon-ion

Table 1. Summary of uncertainties and experimental conditions

Lab name	Wavelength	Absolute base	Uncertainties SI	Trans	(%) Prec	Total	Source	Power
ETL	633	PQE	0.5	0.005	0.04	0.50	L	40 μW
INM	633	PQE	0.12	0.08	0.05	0.15	L	70 μW
	488	PQE	0.12	0.08	0.11	0.18	M	
MFKI	633	PQE	0.15	0.2	0.1	0.27	M	1.5 μW
	488	PQE	0.15	0.2	0.1	0.27	M	1.5 μW
NIM	633	PQE	0.05	0.06	0.06	0.10	L	1 mW
	488	PQE	0.10	0.11	0.15	0.21	L	1 mW
NIST	633	PQE	0.15	0.1	0.14	0.23	L	0.1 to
	488	PQE	0.15	0.1	0.27	0.32	L	0.6 mW
NML	633	ESR	0.05	0.07	0.09	0.12	L	0.5 mW
	488	ESR	0.05	0.07	0.15	0.17	L	1.4 mW
NML[a]	633	PQE	0.1	0.1	0.15	0.21	L	0.5 mW
	488	PQE	0.2	0.1	0.2	0.30	L	1.4 mW
NPL	633	ESR	0.005	0.05	0.02	0.05	L	0.5 mW
	488	ESR	0.005	0.05	0.06	0.08	L	1 mW
NPRL	633	ESR	0.2	0.3	0.3	0.47	M	0.1 to
	488	ESR	0.2	0.3	0.3	0.47	M	200 μW
NRC	633	ESR	0.1	0.1	0.2	0.24	L	0.3 to
	488	ESR	0.1	0.1	0.15	0.21	L	0.8 mW
OMH	633	PQE	0.25	0.06	0.07	0.27	M	40 nW
	488	PQE	0.25	0.06	0.09	0.27	M	20 nW
PTB	633	ESR	0.1	0.1	0.06	0.15	L	0.2 to 1.4 mW

[a] The PQE based results of NML not used in averages.
L = laser source, M = monochromator based source.
Average uncertainty: 633—0.24%; 488—0.25%.

laser at NIST, it was not possible to perform the first set of NIST measurements at 488 nm. All 633-nm measurements (except for those of PTB, NRC, and NPL as noted above) were performed at NIST before and after transport. For all the laboratories reporting measurements at 488 nm, except NRC and NPL, the NIST measurements were performed after transport. For NPL, the 488 nm NIST measurements were performed before transport; and, for NRC, they were performed both before and after transport. The detailed timetable of the measurements is contained in reference [1]. The lack of consistent before and after NIST measurements is an unfortunate shortcoming of the intercomparison. However, as will be seen below, the results are still remarkably good.

Besides being asked to measure the absolute response of the photodiodes, the laboratories were asked to describe some of the essential features of their measurement process. A summary of the experimental conditions during this intercomparison at each participating laboratory, including NIST, is given in table 1. The uncertainty relative to SI is the laboratory's estimate of their absolute accuracy with respect to the SI units. The transfer uncertainty is the estimated error incurred in transferring a primary or base measurement to the actual intercomparison measurement. The total measurement uncertainty of a given laboratory is determined from the quadrature sum of these factors and the standard deviation of the measurements reported. The values for the various uncertainties are for one standard deviation for the measurement parameter discussed. The type of optical radiation source used in the intercomparison was either a laser, listed as L in table 1, or a monochromator system, listed as M. Approximate power levels are given in microwatts (W), milliwatts (mW) or nanowatts (nW).

The above experimental conditions listed in table 1 can be summarized as follows. Five laboratories reported using an electrical substitution radiometer as the absolute base of their measurements. Seven laboratories used the predictable quantum efficiency method, originally called the silicon photodiode self-calibration method [18,19]. One laboratory, NML, reported two sets of measurements, that is, they used both types of absolute detectors. They observed no difference in the two techniques at 633 nm and only a 0.1% difference at 488 nm [1]. Their electrical substitution radiometer results are reported in this paper.

Eight of the 11 laboratories that measured the radiometers at 633 nm used a laser at powers ranging from 0.04 to 1.4 mW. The remaining three used either a conventional source and monochromator at a power level as low as 40 nW, or an interpolation from laser-based measurements at lines other than 633 nm. Four of the nine laboratories participating in the 488-nm intercomparison reported using an argon ion laser at power levels ranging from 0.1 to 1.4 mW. Of the five remaining laboratories one reported making measurements at the 20-nW level. The dynamic range of this intercomparison covered nearly five decades of radiant power.

3. Results

The data from each participating laboratory are summarized in tables 2 and 3. Table 2 contains the results of the measurements at 633 nm and table 3 contains the results of the measurements at 488 nm. The results are plotted in figures 1 and 2, respectively. Not all laboratories received the same set of radiometers, so the results are reported as the ratio of the participating laboratory's measurement with respect to NIST's measurement of the same radiometer. Since this ratio is near unity, the percent difference in the measurements can easily be obtained as the difference from unity in the reported ratios. This data reduction of the intercomparison results assumes that the measurement uncertainties incurred at NIST are the same for all the radiometers. The random uncertainties in the NIST measurements also contribute to the level of accuracy of the intercomparison. At 633 nm the standard deviation of the NIST measurements for all the radiometers was 0.14%, and at 488 nm, 0.27%. These uncertainties, when combined in quadrature with the uncertainty of NIST with respect to SI and the transfer accuracy, give 0.23% and 0.32% overall accuracy for NIST at 633 and 488 nm, respectively.

Also included in tables 2 and 3 is the average of the (laboratory—NIST) differences in the measured responsivity for each detector type. The uncertainty shown for the average is the standard deviation of the difference with respect to NIST measurements.

Figure 1 is a plot of the ratio of the participant laboratory's responsivity measurement to that of NIST at 633 nm. The circles indicate the measurements made with the *pn*-type detectors and the triangles are the *np*-type detector measurements. The error bars are the quadrature sum of each laboratory's stated absolute accuracy, transfer accuracy, and measurement precision for this intercomparison and the appropriate matching quantities for

Table 2. Absolute responsivity measurement—633 nm

Lab name	Detector type	Lab (A/W)	NIST (A/W)	Lab/NIST	% Uncertainty in ratio
ETL	*pn*	0.4625	0.4594	1.0067	0.55
	np	0.4199	0.4149	1.0121	0.55
INM	*pn*	0.4497	0.4489	1.0018	0.27
	np	0.4144	0.4137	1.0017	0.27
MFKI	*pn*	0.4494	0.4490	1.0009	0.35
	np	0.4123	0.4134	0.9973	0.35
NIM	*pn*	0.4618	0.4609	1.0020	0.25
	np	0.4121	0.4116	1.0012	0.25
NML	*pn*	0.4567	0.4564	1.0007	0.31
	np	0.4094	0.4097	0.9993	0.31
NPL	*pn*	0.4560	0.4557	1.0007	0.23
	np	0.4145	0.4137	1.0019	0.23
NPRL	*pn*	0.4578	0.4560	1.0039	0.52
	np	0.4163	0.4138	1.0060	0.52
NRC	*pn*	0.4490	0.4486	0.9998	0.35
	np	0.4158	0.4155	1.0007	0.35
OMH	*pn*	0.4492	0.4490	1.0004	0.35
	np	0.4130	0.4134	0.9990	0.35
PTB[a]	*pn*	0.4529	0.4552	0.9949	0.27
	pn	0.4566	0.4590	0.9948	0.27
	np	0.4152	0.4168	0.9962	0.27
	np	0.4133	0.4141	0.9981	0.27

[a] PTB repeated their measurements on both the original and a second pair of silicon photodiodes because of possible detector instabilities. The average of their two measurements was used in the calculations and in figure 1.
Average percent difference (Lab—NIST): *pn*—0.12±0.30%; *np*—0.16±0.45%.
Average combined uncertainty in ratio=0.35%.

NIST. The dashed lines indicate the standard deviation for all the plotted ratio measurements.

Figure 2 is a plot of the ratio of the participant laboratory's responsivity measurement to that of NIST at 488 nm. Again the circles indicate *pn*-type detector measurements and the triangles represent *np*-type detector measurements. The error bars indicate the combined NIST and participant laboratory's accuracy and precision as in figure 1. The dashed lines indicate the standard deviation for all the plotted measurement ratios.

4. Conclusions

The interlaboratory measurement of monochromatic radiant power at two wavelengths shows excellent agreement among the participants. The ability of the national standards laboratories to measure highly coherent laser power, or the radiant power from an incoherent source transmitted by a monochromator, is within an overall standard deviation of approximately 0.4%. This result was obtained by two very different techniques for the measurement of absolute radiant power: conventional electrical substitution radiometry and the new predictable quantum efficiency of high quality silicon photodiodes. Furthermore, this level of interlaboratory agreement spans five decades of radiant power.

The interlaboratory agreement demonstrated by this intercomparison was limited in several ways. The overall accuracy of the measurements at the central laboratory limited the comparison to ap-

Table 3. Absolute responsivity measurement—488 nm

Lab name	Detector type	Lab (A/W)	NIST (A/W)	Lab/NIST	% Uncertainty in ratio
INM	*pn*	0.2616	0.2623	0.9973	0.37
	np	0.2998	0.2991	1.0023	0.37
MFKI	*pn*	0.2635	0.2623	1.0046	0.42
	np	0.3006	0.2991	1.0050	0.42
NIM	*pn*	0.2915	0.2902	1.0045	0.39
	np	0.2996	0.3011	0.9950	0.39
NML	*pn*	0.2863	0.2863	1.0000	0.44
	np	0.2994	0.3026	0.9983	0.44
NPL	*pn*	0.2827	0.2823	1.0014	0.33
	np	0.2994	0.2994	1.0000	0.33
NPRL	*pn*	0.2862	0.2838	1.0085	0.57
	np	0.3001	0.2992	1.0030	0.57
NRC	*pn*	0.2613	0.2620	0.9973	0.38
	np	0.2976	0.2983	0.9977	0.38
OMH	*pn*	0.2628	0.2623	1.0014	0.42
	np	0.2994	0.2991	1.0010	0.42

Average percent difference (Lab—NIST): *pn*—0.19+0.44%; *np*—0.03+0.32%.
Average combined uncertainty in ratio=0.42%.

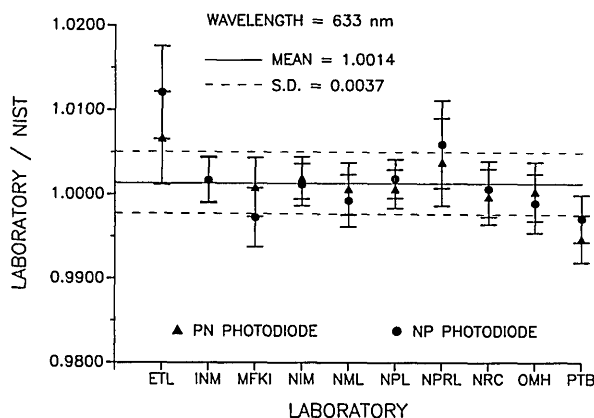

Figure 1. Ratio of participant laboratory spectral response to that determined by NIST at 633 nm; circles indicate *pn*-type detectors and the triangles are *np*-type detectors. The error bars indicate the quadrature summation of the uncertainty relative to SI, the uncertainty of the transfer and the precision of the comparison measurement for each laboratory and the appropriate quantities for NIST. The dashed lines indicate the standard deviation of the measurement for 633 nm.

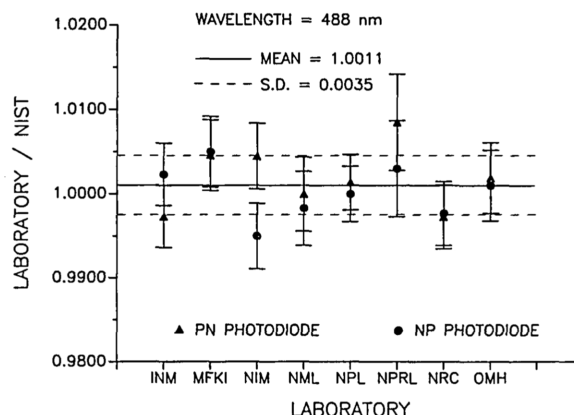

Figure 2. Ratio of the participant laboratory spectral response to that determined by NIST at 488 nm; circles indicate *pn*-type detectors and the triangles are *np*-type detectors. The error bars indicate the quadrature summation of the uncertainty relative to SI, the uncertainty of the transfer and the precision of the comparison measurement for each laboratory and the appropriate quantities for NIST. The dashed lines indicate the standard deviation of the measurements at 488 nm.

proximately 0.23% at 633 nm and 0.32% at 488 nm. At the time of this intercomparison the effect of humidity on the *pn*-type photodiodes [6] had not been clearly identified; therefore, the radiometers were not designed to avoid this effect. Finally, because of equipment difficulties, the 488-nm measurements could not be performed before shipment from the central laboratory and changes in responsivity went undetected. In spite of these limitations, this intercomparison demonstrates that high accuracy can be achieved by very different radiometric techniques.

The defects in this radiant power intercomparison can be easily avoided in future work. Calibration transfer radiometers for coherent radiation measurements [7] can now be designed to avoid the instabilities caused by humidity [6]. In addition, a measurement precision of 0.03% has been demonstrated for a radiant power measurement at wavelengths of 488 and 633 nm [7]. From the results of this radiant power intercomparison and the improvement in silicon photodiodes and radiometric techniques, we may expect to see properly employed silicon diode detectors lead to improvements in absolute radiometry and photometry in the future.

One general conclusion from this intercomparison arises from the demonstrated agreement between the electrical substitution and silicon self-calibration techniques for measuring radiant power. The silicon self-calibration technique results in a radiometer that is simpler and less expensive than an electrical substitution instrument of comparable accuracy. Although the spectral range of the self-calibration technique is limited to the visible and near visible, coupling it with other nonabsolute radiometers opens the possibility of utilizing its accuracy and ease of use over much of the optical spectrum.

Acknowledgments

The author wishes to thank the CCPR for sponsoring this intercomparison and all the national laboratories for their participation. I also wish to acknowledge NIST staff members Barbara Belzer and Warren Gladden for their assistance in the preparations for this intercomparison.

5. References

[1] Zalewski, E. F., Comparison of the National Standards of Absolute Spectral Responsivity, in Comité Consultatif de Photométrie et Radiométrie, Report of the 11th session, Appendix P4. Published by the BIPM, Pavillon de Breteuil, F-92312 Sévres Cedex, France (1986) pp. P165–P178.

[2] Honda, T., and Endo, M., IEEE J. Quantum Elect. **QE-14**, 213 (1978).

[3] Endo, M., and Honda, T., IEEE Trans. Instr. Meas. **IM-32**, 77 (1983).

[4] Betts, D. B., and Gillham, E. J., Metrologia **4**, 101 (1968).

[5] Korde, R., and Geist, J., Sol. State Elect. **30**, 89 (1987).

[6] Korde, R., and Geist, J., Appl. Opt. **26**, 5284 (1987).

[7] Thomas, D. B., and Zalewski, E. F., A radiometer for precision coherent radiation measurements, SPIE Tech. Symp. on Aerospace Sensing, Orlando, Florida, March 1989.

[8] Fox, N. P., and Martin, J. E., A Further Intercomparison of Two Cryogenic Radiometers, SPIE Tech. Symp. on Aerospace Sensing, Orlando, Florida, March 1989.

[9] In 1979 the General Conference on Weights and Measures (CGPM) accepted the suggestion of the Consultative Committee for Photometry and Radiometry (CCPR) to define the unit of luminous intensity, the candela, in terms of radiant intensity. The candela is defined as the luminous intensity in a given direction from a monochromatic source at 555 nm which has a radiant intensity in that direction of 1/683 watts per steradian. For reference see: Mielenz, Klaus, D., J. Res. Natl. Bur. Stand. (U.S.) **92**, 335 (1987).

[10] Verdebout, J., and Booker, R. L., J. Appl. Phys. **55**, 406 (1984).

[11] Key, P. J., Fox, N. P., and Rastello, M. L., Metrologia **21**, 81 (1985).

[12] Stock, K. D., and Heine, R., Optik **71**, 137 (1985).

[13] Geist, J., Liang, E., and Schaefer, A. R., J. Appl. Phys. **52**, 4879 (1981).

[14] EG&G Electro-Optics: 35 Congress St., Salem, MA 01970.

[15] United Detector Technology: 12525 Chadron Ave., Hawthorne, CA 90250.

[16] Zalewski, E. F., and Duda, C. R., Appl. Opt. **22**, 2867 (1983).

[17] Li, Tong-Bao, Some Investigation on Linearity of Si-Photodiodes, Proceedings of the 10th International Symposium of Photo-Detectors, IMEKO Secretariat H-1371, POB.457, Budapest (1982) p. 61.

[18] Zalewski, E. F., and Geist, J., Appl. Opt. **19**, 1214 (1980).

[19] Geist, J., Zalewski, E. F., and Schaefer, A. R., Appl. Opt. **19**, 3795 (1980).

About the author: Douglas B. Thomas is a physicist in the Radiometric Physics Division in the Center for Radiation Research, which is part of the NIST National Measurement Laboratory.

Volume 95, Number 5, September-October 1990
Journal of Research of the National Institute of Standards and Technology

[J. Res. Natl. Inst. Stand. Technol. 95, 533 (1990)]

Results of a CIE Detector Response Intercomparison[1]

Volume 95 Number 5 September-October 1990

This CIE Research Note was prepared for CIE Technical Committee TC 2-06 by

Douglas B. Thomas and Edward F. Zalewski[2]

National Institute of Standards and Technology,
Gaithersburg, MD 20899

A total of fifteen laboratories participated in the CIE detector response intercomparison which was designed to assess the level of agreement among participating laboratories in the absolute measurement (with respect to SI) of photodetector response in the visible spectral region. Most participants were either commercial laboratories or university laboratories with the National Institute of Standards and Technology (NIST) serving as the host laboratory. Each laboratory determined the absolute response of each of two silicon photodiode radiometers which were designed for the intercomparison by NIST. Approximately two-thirds of the laboratories reported response values which agreed with the NIST values to within ±1.0% at the two wavelengths of 488 and 633 nm.[3]

Key words: laboratory evaluation; laser; optical radiation; photodiode; spectral response.

Accepted: August 6, 1990

1. Introduction

This report provides the final results of a detector response intercomparison under the aegis of CIE Technical Committee TC 2-06 on Absolute Spectral Responsivity of Detectors. Members of the Technical Committee are listed in Appendix B of this report.

The primary purpose of the intercomparison was to assess the level of agreement among participating laboratories in the absolute measurement (with respect to SI) of photodetector response (A/W) in the visible spectral region. The method chosen to accomplish this is to have these laboratories measure the absolute response of selected radiometers at two specific wavelengths near each end of the visible spectrum. The wavelengths selected are those of the helium-neon laser (632.8 nm) and the argon ion laser (488.0 nm).

The intercomparison was implemented on the basis of the National Institute of Standards and Technology (NIST) serving as the host laboratory and providing (a) the radiometers to be used in the intercomparison, (b) instructions to participating laboratories in the use of the radiometers in absolute response measurements, and (c) data analysis and a report of the results of the intercomparison.

The intercomparison was conducted in two stages: (1) intercomparison of U.S. laboratories and (2) intercomparison of laboratories outside of the United States. All participating laboratories except two are either commercial laboratories or university laboratories. The Electrotechnical Laboratory in Ibaraki, Japan and the Van Swinden Laboratory,

[1] A CIE (Commission Internationale de l'Eclairage or International Commission on Illumination) research note. CIE headquarters in Vienna, Austria.
[2] Present address: Hughes Danbury Optical Systems, 100 Wooster Heights Road, Danbury, CT 06810.
[3] Abstracts in French and German are given in Appendix A.

The Netherlands, are national standards laboratories. The intercomparison was planned on the basis that NIST would measure the absolute response of all radiometers before shipment to the participating laboratories and then again after the radiometers were returned. The NIST absolute response value for each radiometer would be the average of the two NIST measurements.

2. The Radiometers

The radiometers used in this intercomparison were designed for ruggedness and ease of use and included commercially available silicon photodiodes. Each radiometer consists of a silicon photodiode and amplifier circuit mounted in a cylindrical aluminum housing and an external power supply.

Since it was expected that the majority of the laboratories would make their measurements using lasers, the photodiodes were not protected by a window. However, to protect each photodiode during non-use, the diodes were maintained in sealed compartments.

Two types of detectors were used: EG&G[4] model UV-444B PN photodiodes and UDT model UV-100 inversion layer photodiodes. Radiometers PI-17, PI-19, PI-20, and PI-21 have the EG&G photodiodes while radiometers PI-25 through PI-32 have the UDT photodiodes. For the UDT photodiodes, a constant reverse bias voltage (4.5 V) was supplied by lithium batteries within each radiometer. The amplifier in each radiometer has gain settings from 10^4 to 10^9 V/A with accuracies of ±0.03% except for the 10^9 range where it is ±0.5%.

Each participating U.S. laboratory received two radiometers: one with an EG&G photodiode and one with a UDT photodiode. The reason for requesting each laboratory to measure two radiometers is two-fold. (1) A second radiometer provides a backup for possible shipping damage and (2) there is a check on measurement repeatability.

After the first stage of the intercomparison was completed involving U.S. laboratories, a decision was made to use only the radiometers with the UDT photodiodes for the intercomparison involving laboratories in other countries. This decision was made when it was determined that the EG&G photodiodes exhibited a small but significant response drift at 488 nm over long periods of time (see sec. 4).

3. The Intercomparison

A total of six U.S. laboratories and nine laboratories in other countries participated in the intercomparison. Each laboratory was asked to complete a questionnaire concerning detailed information about their detector response measurement system and to use standard data forms for reporting their results. Tables 1 and 2 list the U.S. laboratories and the information each submitted about their measurements at 488 and 633 nm. Tables 3 and 4 list the corresponding information for laboratories in other countries. The information submitted covered eight measurement parameters: (1) absolute base (absolute standard(s) used), (2) standard deviation of the measurements, (3) number of measurements per radiometer, (4) type of radiation source used, (5) beam diameter of the source, (6) radiant power level at the radiometer, (7) ambient temperature during measurements, and (8) estimated uncertainty (with respect to SI) of the absolute standards used. Some laboratories used a single silicon photodiode as an absolute (standard) base for their measurements. The absolute response of these photodiodes was determined using the self-calibration method [1,2]. Two laboratories made measurements only at 633 nm. Of the fifteen laboratories participating in the intercomparison, five laboratories used lasers as radiation sources at both wavelengths and five used a tungsten lamp/filter/monochromator system at both wavelengths. The remaining laboratories used various combinations of these sources. Radiant power levels ranged from 0.16 μW to 0.7 mW.

The measurement system used at NIST for this intercomparison consists of He-Ne and Argon ion lasers, laser stabilizer, spatial filter, beam splitter, and a silicon photodiode monitor detector. Three UDT QED-200 absolute radiometers [3] were used as base standards. Figure 1 is an illustration of the system components. The NIST procedures for determining the absolute response of the intercomparison radiometers consisted basically of two steps: (1) measuring the ratio of the photocurrent of each UDT QED-200 radiometer to the photocurrent of the monitor detector at a particular laser power setting and (2) measuring the ratio of

[4] Certain commerical equipment, instruments, or materials are identified in this paper to specify adequately the experimental procedure. Such identification does not imply recommendation or endorsement by the National Institute of Standards and Technology or by the CIE, nor does it imply that the materials or equipment identified are necessarily the best available for the purpose.

Table 1. Participating U.S. laboratories. Wavelength=488 nm

	LLL	NIST	TEKX	UDT	UAZ	WEST
Absolute base	EGG	QED2	QED, UDT	QED2	QED2	
S.D. of measurements	0.24–0.35%	0.01%	0.11%	0.039–1.10%	0.003–0.018%	
No. of meas./Radiometer	5	50	3	2	48	
Radiation source	TLF	ARL	TLM	BEN	TLF	
Beam diameter	OFA	4 mm	2×5	1×5	2×3	
Power level	3.7×10^{-8} W/cm^2	0.5 mW	0.6 μW	2.0 μW	4.0 μW	
Ambient temp. (°C)	22	25–26	23.0	21.0	21.0	
Est. abs. uncertainty	0.77%	0.10%	0.17%	0.07%	0.05%	

LLL—Lawrence Livermore National Laboratory, Livermore, California.
NIST—National Institute of Standards and Technology, Gaithersburg, Maryland (Host Laboratory).
TEKX—Tektronix Corporation, Beaverton, Oregon.
UDT—United Detector Technology, Hawthorne, California.
UAZ—University of Arizona, Tucson, Arizona.
WEST—Westinghouse Electric Corporation, Baltimore, Maryland.

EGG—EG&G UV-444-BQ Photodiode.
QED—UDT QED-100 Radiometer.
QED2—UDT QED-200 Radiometer.
UDT—UDT UV-100L Photodiode.
TLF—Tungsten lamp/Filter.
ARL—Argon ion laser.
HENE—Helium-neon laser.
TLM—Tungsten lamp/Monochromator.
BEN—Bentham M300 Monochromator.
1×5—1×5 mm rectangle.
2×3—2.5×3.5 mm rectangle.
2×5—2.5×5.0 mm rectangle.
OFA—Overfill of aperture.

Table 2. Participating U.S. laboratories. Wavelength=633 nm

	LLL	NIST	TEKX	UDT	UAZ	WEST
Absolute base	EGG	QED2	QED, UDT	QED2	QED2	UDT, QED2 EGG
S.D. of measurements	0.28%	0.012%	0.015–0.12%	0.3–0.4%	0.018–0.004%	0.26–0.14%
No. of meas./Radiometer	5	50	6	2	64	3
Radiation source	TLF	HENE	TLM, HENE	BEN, HENE	TLF	HENE
Beam diameter	OFA	4 mm	2×5, 2.5 mm	1×5, 4 mm	2×3	2 mm
Power level	4.9×10^{-8} W/cm^2	0.5 mW	0.6 μW, 0.5 mW	2.0 μW, 0.5 mW	11 μW	0.44 mW
Ambient temp. (°C)	22	25–26	23.0	21.0	21.0	20.8
Est. abs. uncertainty	0.77%	0.10%	0.17%	0.07%	0.05%	0.05%

LLL—Lawrence Livermore National Laboratory, Livermore California.
NIST—National Institute of Standards and Technology, Gaithersburg, Maryland (Host Laboratory).
TEKX—Tektronix Corporation, Beaverton, Oregon.
UDT—United Detector Technology, Hawthorne, California.
UAZ—University of Arizona, Tucson, Arizona.
WEST—Westinghouse Electric Corporation, Baltimore, Maryland.

EGG—EG&G UV-444-BQ Photodiode.
QED—UDT QED-100 Radiometer.
QED2—UDT QED-200 Radiometer.
UDT—UDT UV-100L Photodiode.
TLF—Tungsten lamp/Filter.
ARL—Argon ion laser.
TLM—Tungsten lamp/Monochromator.
HENE—Helium-neon laser.
BEN—Bentham M300 Monochromator.
1×5—1×5 mm rectangle.
2×3—2.5×3.5 mm rectangle.
2×5—2.5×5.0 mm rectangle.
OFA—Overfill of aperture.

Table 3. Participating laboratories in other countries. Wavelength=488 nm

	CIP	ETL	HAM	LCIE	LNE	MAT	KROC	UDI	VSL
Absolute base	PSP	HAM2		ASP	TSP	HAM2	HAM3	EGG	QED2
S.D. of measurements	0.17–0.21%	0.04%		0.6%	0.11–0.18%	0.02%	0.52%	0.12–0.04%	0.007–0.011%
No. of meas./Radiometer	10	4		6	27,33	10	5	8-12	75
Radiation source	ARL	TLM		TLM	TLM	ARL	TLM	ARL	ARL
Beam diameter	4 mm	2×3		5 mm	6 mm	3 mm	7 mm	0.6 mm	4 mm
Power level	0.02 mW	0.16 μW		20 μW	1.5 μW	0.19 mW	2.4×10^{-3} W/m^2	0.3 mW	0.7 mW
Ambient temp. (°C)	18	23		23	23	25	23	21	23
Est. abs. uncertainty	0.17%	0.07%		0.20%	0.11 0.22%	0.07%	0.17%	0.50%	0.20%

CIP—Central Institute of Physics, Magurele-Bucharest, Romania.
ETL—Electrotechnical Laboratory, Ibaraki, Japan.
HAM—Hamamatsu Photonics K.K., Hamamatsu City, Japan.
LCIE—L.C.I.E., Fontenay-aux-Roses, France.
LNE—Laboratoire National D'Essais, Paris, France.
MAT—Matsushita Electric Industrial Co. Ltd., Moriguchi Osaka, Japan.
KROC—PRC Krochmann GMBH, Berlin, West Germany.
UDI—University College, Dublin, Ireland.
VSL—Van Swinden Laboratory, Delft, The Netherlands.

PSP—*pn* Silicon photodiode (Romanian).
HAM2—Hamamatsu S 1337 Photodiode.
HAM3—Hamamatsu S 1227 Photodiode.
ASP—Silicon photodiode.
TSP—Three silicon photodiodes.
EGG—EG&G UV-444B Photodiode.
QED2—UDT QED-200 Radiometer.
ARL—Argon ion laser.
TLM—Tungsten lamp/Monochromator.
2×3—2×3 mm rectangle.

Table 4. Participating laboratories in other countries. Wavelength=633 nm

	CIP	ETL	HAM	LCIE	LNE	MAT	KROC	UDI	VSL
Absolute base	PSP	HAM1	HAM2	ASP	TSP	HAM2	HAM3	EGG	QED2
S.D. of measurements	0.17–0.14%	0.02%	0.07–0.04%	0.6%	0.10–0.08%	0.02%	0.3–0.15%	0.07–0.08%	0.02–
No. of meas./Radiometer	10	3	10	6	21,28	10	5	6	75
Radiation source	HENE	HENE	HENE	TLM	TLM	HENE	TLM	HENE	HENE
Beam diameter	4 mm	1 mm	1.5 mm	5 mm	6 mm	3 mm	7 mm	0.6 mm	4 mm
Power level	0.1 mW	40 μW	25 μW	30 μW	2 μW	0.3 mW	1.1×10^{-2} W/m^2	0.6 mW	0.7 mW
Ambient temp. (°C)	18	23	25	23	23	25	23	18	23
Est. abs. uncertainty	0.17%	0.07%	0.17%	0.20%	0.12 0.09%	0.07%	0.17%	0.08%	0.20%

CIP—Central Institute of Physics, Magurele-Bucharest, Romania.
ETL—Electrotechnical Laboratory, Ibaraki, Japan.
HAM—Hamamatsu Photonics K.K., Hamamatsu City, Japan.
LCIE—L.C.I.E., Fontenay-aux-Roses, France.
LNE—Laboratoire National D'Essais, Paris, France.
MAT—Matsushita Electric Industrial Co. Ltd., Moriguchi Osaka, Japan.
KROC—PRC Krochmann GMBH, Berlin, West Germany.
UDI—University College, Dublin, Ireland.
VSL—Van Swinden Laboratory, Delft, The Netherlands.

PSP—*pn* Silicon photodiode (Romanian).
HAM1—Hamamatsu S 1723 Photodiode.
HAM2—Hamamatsu S 1337 Photodiode.
ASP—Silicon photodiode.
TSP—Three silicon photodiodes.
HAM3—Hamamatsu S 1227 Photodiode.
EGG—EG&G UV-444B Photodiode.
QED2—UDT QED-200 Radiometer.
HENE—Helium-neon laser.
TLM—Tungsten lamp/Monochromator.

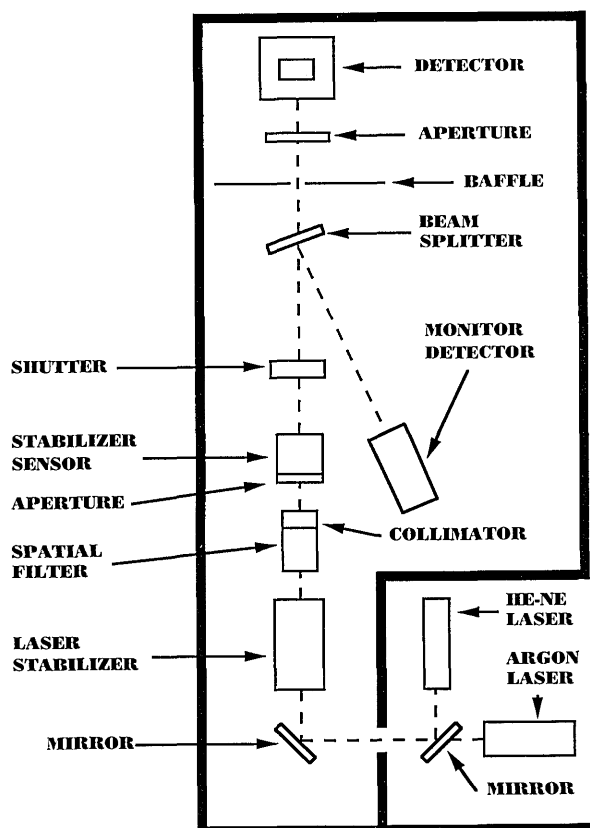

Figure 1. NIST laser based detector calibration facility.

the photocurrent of the intercomparison radiometers to the monitor detector at the same power level in (1). Since the UDT QED-200 radiometers are 100% quantum efficient (with voltage bias) at the wavelengths and power levels stated, the power (watts) can be accurately measured and the absolute response (amperes/watt) of each of the intercomparison radiometers can be determined. Details concerning the system and the measurement procedure are further described in [4]. The NIST absolute base was compared to other international standards laboratories in a recent detector response intercomparison sponsored by the Consultative Committee on Photometry and Radiometry (CCPR) [5]. In the CCPR intercomparison, the absolute response of a select group of silicon photodiode radiometers were measured by 10 international standards laboratories and also by NIST which served as the host laboratory. The ratios of the NIST response values to the mean of the response values of the other participating laboratories were 1.0011±0.0035 and 1.0014±0.0037 at the two wavelengths of 488 and 633 nm, respectively.

Since the absolute response values reported by each of the participating laboratories were compared to the response values determined at NIST, it was essential for NIST to measure the response of each set of radiometers *before* it was shipped to the participating laboratory and then measured again *after* the radiometers were returned. The *before* and *after* measurements by NIST were made to determine if any significant changes occurred in the radiometers during shipment.

4. Data Analysis

Tables 5 and 6 list the laboratory designations, date of measurement, radiometer descriptions, and absolute responsivities reported by the U.S. laboratories and laboratories in other countries, respectively. Each set of response values for a participating laboratory includes the corresponding *before* and *after* values determined by NIST. The NIST value for each radiometer was taken as the average of the *before* and *after* respective values. The *before* and *after* NIST values indicate that some of the radiometers had undergone a small but significant change in response between shipments to and from the laboratories. For example, at 488 nm, the response value for radiometer PI-20 (laboratory C, table 5) decreased from 0.2814 to 0.2787 over the period 7/87 to 2/88 as measured by NIST. This is a decrease of 0.96%. All ratios reported represent an average of the *before* and *after* values.

Since three of the four radiometers with the EG&G type photodiode showed small but significant decreases in response at 488 nm over a 7-month period, it was decided to use only the radiometers with the UV-100 type photodiodes for the second phase of the intercomparison (foreign laboratories).

Table 7 is a listing of the participating laboratories by code letter, the absolute response values reported by each laboratory, the absolute response values as determined by NIST, and the ratios of the response values.

Figures 2 and 3 are plots of the ratios of the response values (A/W) determined by each of the participating laboratories to the respective response values (A/W) determined by NIST at 488 and 633 nm. The solid line on each plot is the mean of all the ratios at the respective wavelength and the dashed lines are the standard deviation of the mean. Table 8 is a summary of the standard deviations of the measurements and the estimated uncertainty (with respect to SI) of the absolute standards used by each of the participating laboratories. Also listed are the *before/after* change in absolute response for each detector as measured by NIST and

Table 5. U.S. laboratories

Laboratory	Date	Responsivity (488 nm)		Responsivity (633 nm)	
				PI-20	**PI-25**
NIST	7/87			0.4551	0.4152
LAB A	7/87			0.4555	0.4154
NIST	7/87			0.4548	0.4153
		PI-21	**PI-27**	**PI-21**	**PI-27**
NIST	7/87	0.2830	0.2994	0.4550	0.4140
LAB B	9/87	0.2857	0.2990	0.4608	0.4208
NIST	12/87	0.2824	0.2986	0.4546	0.4141
		PI-20	**PI-25**	**PI-20**	**PI-25**
NIST	7/87	0.2814	0.2982	0.4548	0.4153
LAB C	9/87	0.2802	0.2987	0.4547	0.4151
NIST	2/88	0.2787	0.2984	0.4545	0.4153
		PI-19	**PI-28**	**PI-19**	**PI-28**
NIST	7/87	0.2596	0.2965	0.4472	0.4165
LAB D	11/87	0.2570	0.3006	0.4468	0.4168
NIST	2/88	0.2551	0.2969	0.4467	0.4169
		PI-17	**PI-30**	**PI-17**	**PI-30**
NIST	7/87	0.2849	0.3021	0.4580	0.4108
LAB E	12/87	0.2799	0.3003	0.4521	0.4027
NIST	2/88	0.2830	0.3025	0.4576	0.4105

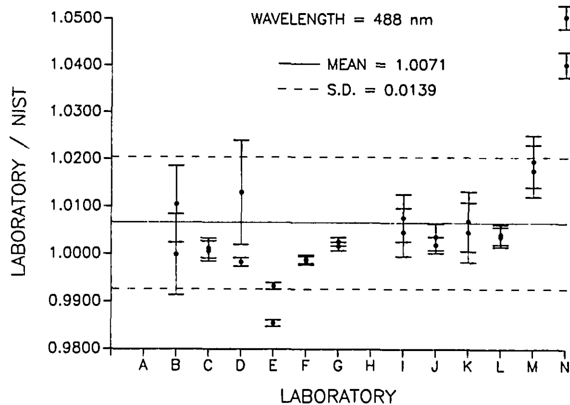

Figure 2. Ratio of the participant laboratory spectral response to that determined by NIST at 488 nm. The error bars indicate the quadrature summation of the measurement and absolute uncertainties of each participant laboratory, the *before/after* response change for each radiometer, and the NIST measurement and absolute uncertainties. The dashed lines indicate the standard deviation of the ratio values.

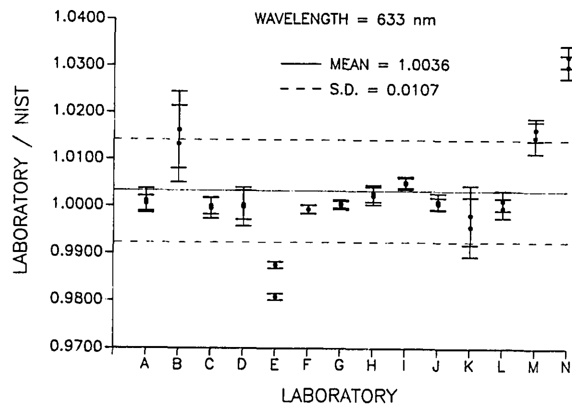

Figure 3. Ratio of the participant laboratory spectral response to that determined by NIST at 633 nm. The error bars indicate the quadrature summation of the measurement and absolute uncertainties of each participant laboratory, the *before/after* response change for each radiometer, and the NIST measurement and absolute uncertainties. The dashed lines indicate the standard deviation of the ratio values.

Table 6. Laboratories in other countries

Laboratory	Date	Responsivity (488 nm)		Responsivity (633 nm)	
		PI-28	**PI-31**	**PI-28**	**PI-31**
NIST	2/88	0.2969	0.3014		
NIST	8/88			0.4169	0.4125
LAB F	10/88	0.2964	0.3008	0.4166	0.4124
NIST	12/88			0.4169	0.4129
NIST	1/89	0.2967	0.3009		
		PI-28	**PI-31**	**PI-28**	**PI-31**
NIST	2/88	0.2969	0.3014		
NIST	8/88			0.4169	0.4125
LAB G	11/88	0.2973	0.3019	0.4170	0.4129
NIST	12/88			0.4169	0.4129
NIST	1/89	0.2967	0.3009		
				PI-28	**PI-31**
NIST	8/88			0.4169	0.4125
LAB H	12/88			0.4178	0.4138
NIST	12/88			0.4169	0.4129
		PI-25	**PI-32**	**PI-25**	**PI-32**
NIST	2/88	0.2983	0.2599		
NIST	8/88			0.4153	0.4515
LAB I	11/88	0.2999	0.2622	0.4171	0.4538
NIST	12/88			0.4148	0.4514
NIST	1/89	0.2987	0.2605		
		PI-28	**PI-31**	**PI-28**	**PI-31**
NIST	12/88			0.4169	0.4129
NIST	1/89	0.2967	0.3009		
LAB J	5/89	0.2972	0.3020	0.4172	0.4130
NIST	8/89			0.4168	0.4127
NIST	9/89	0.2966	0.3009		
		PI-28	**PI-31**	**PI-28**	**PI-31**
NIST	12/88			0.4169	0.4129
NIST	1/89	0.2967	0.3009		
LAB K	7/89	0.2980	0.3030	0.4160	0.4110
NIST	8/89			0.4168	0.4127
NIST	9/89	0.2966	0.3009		
		PI-25	**PI-32**	**PI-25**	**PI-32**
NIST	12/88			0.4148	0.4514
NIST	1/89	0.2987	0.2605		
LAB L	6/89	0.2995	0.2617	0.4153	0.4511
NIST	8/89			0.4148	0.4512
NIST	9/89	0.2982	0.2607		
		PI-27	**PI-29**	**PI-27**	**PI-29**
NIST	8/88			0.4145	0.4149
NIST	2/89	0.2989	0.2991		
LAB M	4/89	0.3043	0.3049	0.4205	0.4216
NIST	8/89			0.4144	0.4147
NIST	9/89	0.2992	0.2988		
		PI-26	**PI-30**	**PI-26**	**PI-30**
NIST	7/88	0.2667	0.3020		
NIST	8/88			0.4454	0.4108
LAB N	12/88	0.2805	0.3144	0.4583	0.4240
NIST	8/89			0.4446	0.4107
NIST	9/89	0.2672	0.3023		

Table 7. Response ratios

Laboratory (RAD. #)	488 nm Resp. Lab.	488 nm Resp. NIST	488 nm Lab./NIST	633 nm Resp. Lab.	633 nm Resp. NIST	633 nm Lab./NIST
A (PI-20)				0.4555	0.4550	1.0011
A (PI-25)				0.4154	0.4152	1.0005
B (PI-21)	0.2857	0.2827	1.0106	0.4608	0.4548	1.0132
B (PI-27)	0.2990	0.2990	1.0000	0.4208	0.4141	1.0162
C (PI-20)	0.2802	0.2806	0.9986	0.4547	0.4547	1.0000
C (PI-25)	0.2987	0.2983	1.0013	0.4151	0.4153	0.9995
D (PI-19)	0.2570	0.2570	1.0000	0.4468	0.4469	0.9998
D (PI-28)	0.3006	0.2967	1.0131	0.4168	0.4167	1.0002
E (PI-17)	0.2799	0.2836	0.9870	0.4521	0.4578	0.9875
E (PI-30)	0.3003	0.3023	0.9934	0.4027	0.4106	0.9808
F (PI-28)	0.2964	0.2968	0.9987	0.4166	0.4169	0.9993
F (PI-31)	0.3008	0.3011	0.9990	0.4124	0.4127	0.9993
G (PI-28)	0.2973	0.2968	1.0017	0.4170	0.4169	1.0002
G (PI-31)	0.3019	0.3011	1.0027	0.4129	0.4127	1.0005
H (PI-28)				0.4178	0.4169	1.0022
H (PI-31)				0.4138	0.4127	1.0027
I (PI-25)	0.2999	0.2985	1.0047	0.4171	0.4151	1.0048
I (PI-32)	0.2622	0.2602	1.0077	0.4538	0.4515	1.0051
J (PI-28)	0.2972	0.2966	1.0020	0.4172	0.4168	1.0010
J (PI-31)	0.3020	0.3009	1.0037	0.4130	0.4128	1.0005
K (PI-28)	0.2980	0.2966	1.0047	0.4160	0.4168	0.9981
K (PI-31)	0.3030	0.3009	1.0070	0.4110	0.4128	0.9956
L (PI-25)	0.2995	0.2984	1.0037	0.4153	0.4148	1.0012
L (PI-32)	0.2617	0.2606	1.0042	0.4511	0.4513	0.9996
M (PI-27)	0.3043	0.2990	1.0177	0.4205	0.4144	1.0147
M (PI-29)	0.3049	0.2990	1.0197	0.4216	0.4148	1.0164
N (PI-26)	0.2805	0.2670	1.0506	0.4583	0.4450	1.0299
N (PI-30)	0.3144	0.3022	1.0404	0.4240	0.4108	1.0321

the absolute response ratio uncertainty. The absolute response ratio uncertainty is the quadrature summation of the measurement and absolute uncertainties of each participant laboratory, the *before/after* response change for each radiometer, and the NIST measurement and absolute uncertainties. The error bars in figures 2 and 3 indicate the absolute response ratio uncertainty for each laboratory.

5. Conclusion

In general, it can be concluded that most of the response values reported by the laboratories were in good agreement with NIST. At 488 nm, the mean of all participating laboratories was 0.71% higher than the corresponding NIST values with a standard deviation of 1.39%. Similarly, at 633 nm, the mean of all laboratory values was higher than

Table 8. Summary of uncertainties

Laboratory	Measurement standard deviation (1 sigma)	Absolute uncertainty (1 sigma)	Before/After response change (%/100)	Ratio uncertainty (1 sigma)
		488 nm		
LLL	0.0024	0.0077	0.0021	0.0084
	0.0035	0.0077	0.0027	0.0089
NIST	0.0001	0.0010		
	0.0001	0.0010		
TEKX	0.0011	0.0017	0.0096	0.0099
	0.0011	0.0017	0.0007	0.0024
UDT	0.00039	0.0007	0.0175	0.0175
	0.0110	0.0007	0.0013	0.0111
UAZ	0.00003	0.0005	0.0067	0.0068
	0.00018	0.0005	0.0013	0.0017
CIP	0.0017	0.0017	0.0019	0.0032
	0.0021	0.0017	0.0010	0.0031
ETL	0.0004	0.0007	0.0007	0.0015
	0.0004	0.0007	0.0017	0.0021
LCIE	0.0060	0.0020	0.0003	0.0064
	0.0060	0.0020	0.0000	0.0064
LNE	0.0011	0.0011	0.0003	0.0019
	0.0018	0.0022	0.0000	0.0030
MAT	0.0002	0.0007	0.0007	0.0014
	0.0002	0.0007	0.0017	0.0021
KROC	0.0052	0.0017	0.0010	0.0057
	0.0052	0.0017	0.0010	0.0057
UDI	0.0012	0.0050	0.0013	0.0054
	0.0004	0.0050	0.0023	0.0056
VSL	0.00007	0.0020	0.0017	0.0028
	0.00011	0.0020	0.0008	0.0024
		633 nm		
LLL	0.0028	0.0077	0.0009	0.0083
	0.0028	0.0077	0.0002	0.0083
NIST	0.00012	0.0010		
	0.00012	0.0010		
TEKX	0.00015	0.0017	0.0007	0.0021
	0.0012	0.0017	0.0000	0.0023
UDT	0.0040	0.0007	0.0011	0.0043
	0.0030	0.0007	0.0010	0.0034
UAZ	0.00018	0.0005	0.0009	0.0014
	0.00004	0.0005	0.0007	0.0013
WEST	0.0026	0.0005	0.0007	0.0029
	0.0014	0.0005	0.0002	0.0018
CIP	0.0017	0.0017	0.0018	0.0032
	0.0014	0.0017	0.0002	0.0024
ETL	0.0002	0.0007	0.0000	0.0012
	0.0002	0.0007	0.0010	0.0016
HAM	0.0007	0.0017	0.0000	0.0021
	0.0004	0.0017	0.0010	0.0022
LCIE	0.0060	0.0020	0.0002	0.0064
	0.0060	0.0020	0.0005	0.0064
LNE	0.0010	0.0012	0.0002	0.0019
	0.0008	0.0009	0.0005	0.0016
MAT	0.0002	0.0007	0.0000	0.0012
	0.0002	0.0007	0.0010	0.0016
KROC	0.0030	0.0017	0.0002	0.0036
	0.0015	0.0017	0.0005	0.0025
UDI	0.0007	0.0008	0.0012	0.0019
	0.0008	0.0008	0.0002	0.0015
VSL	0.0002	0.0020	0.0000	0.0022
	0.0002	0.0020	0.0005	0.0023

the NIST values by 0.36% with a standard deviation of 1.07%. All laboratories participating in this intercomparison (except laboratory N) reported values at both wavelengths within ±2.0% of the NIST values and nine of the 14 laboratories reported values at both wavelengths within ±1.0% of the NIST values. This can be considered good agreement among the laboratories when one considers the variety of sources, procedures, and testing environments involved in this intercomparison.

6. Appendix A

Resumé

Quinze laboratoires situes tant aux Etats-Unis que dans d'autres pays du monde entier ont pris part, dans le cadre de la CIE, a une comparaison de mesures de sensibilite de detecteurs qui avait pour but de determiner le niveau d'accord existant entre les laboratoires participants, pour la mesure de la sensibilite absolue (par rapport au SI) des photodetecteurs dans le domaine visible. La plupart des particpants etaient des laboratoires industriels ou des laboratoires universitaires. Le National Institute of Standards and Technology (NIST) jouait le role de laboratoire pilote. Chaque laboratoire a determine la sensibilite absolute de deux radiometres equipes de photodiodes au silicium, et specialement realises pour cette comparaison par le NIST. Les resultats fournis par environ les 2/3 des laboratoires sont en accord avec ceux du NIST dans la limite d'incertitude de ±1% pour les longueurs d'onde de 488 et 633 nm.

Zusammenfassung

Insqesamt fuenfzehn Laboratorien haben an CIE Vergleichsmessungen von optischen Strahlungsempfaengern teilgenommen. Der Vergleich bezweckte die Uebereinstimmung unter den teilnehmenden Laboratorien in der Absolutmessung (relativ zu SI Einheiten) der Empfindlichkeit von Halbleiter-Empfaengern im sichtbaren Spektralgebiet zu bestimmen. Die Mehrzahl der Teilnehmer waren Industrie- oder Universitaetslaboratorien. Das U.S. National Institute of Standards and Technology (NIST) war das Zentrallaboratorium. Jedes Labor bestimmte die absolute Empfindlichkeit von je zwei speziell fuer den Vargleich entwickelten NIST Radiometern mit Silizium-Photodioden. Ungefaehr zwei Drittel der von den einzelnen Laboratorien gemessenen Empflichkeiten fielen innerhalb ±1% der NIST Werte bei 488 und 633 nm.

7. Appendix B

The following is a listing of the members of CIE Technical Committee TC 2-06 on Absolute Spectral Responsivity of Detectors. An asterisk (*) identifies those members who made the detector measurements for this intercomparison.

* Philip Armatis, Lawrence Livermore National Laboratory, Livermore, California, United States.
* Douglas Thomas, National Institute of Standards and Technology, Gaithersburg, Maryland, United States.

Albert Parr, National Institute of Standards and Technology, Gaithersburg, Maryland, United States.

Edward Zalewski, formerly of the National Institute of Standards and Technology, Gaithersburg, Maryland, United States.

* Ken Futornick, Tektronix Corporation, Beaverton, Oregon, United States.
* Richard Duda, United Detector Technology, Hawthorne, California, United States.
* James Palmer, University of Arizona, Tucson, Arizona, United States.
* Carroll Hughes III, Westinghouse Electric Corporation, Baltimore, Maryland United States.

James Christy, Hughes Electronics Corp., Tucson, Arizona, United States.

Ted Schrode, United States.

Kurt Scott, Atlas Electric Devices Company, Chicago, Illinois, United States.

* Dan Sporea, Central Institute of Physics, Magurele-Bucharest, Romania.
* Yasuo Mishima, Electrotechnical Laboratory, Ibaraki, Japan.
* Keiji Suyama, Hamamatsu Photonics K.K., Hamamatsu City, Japan.
* Yoshihiro Ohno, Matsushita Electric Industrial Co. Ltd., Moriguchi Osaka, Japan.
* B. Jean, Laboratoire Central des Industries Electriques, Fontenay-aux-Roses, France.
* Beatrice Chommeloux, Laboratoire National D'Essais, Paris, France.

Brigitte Mercier, Institute National de Metrologie, Paris, France.

* Gyorgy Czibula, PRC Krochmann GMBH, Berlin, West Germany.

J. Krochmann, PRC Krochmann GMBH, Berlin, West Germany.

* Eon O'Mongain, University College, Dublin, Ireland.
Maurice Goodman, University College, Dublin, Ireland.
* Jan de Vreede, Van Swinden Laboratory, Delft, The Netherlands.
Pieter Bloembergen, Van Swinden Laboratory, Delft, The Netherlands.
Antonio Corrons, Institute de Optica, Madrid, Spain.
Dominique Crommelynck, Royal Meteorological Institute of Belgium, Brussels, Belgium.
John Moore, National Physical Laboratory, Teddington, United Kingdom.
Juraji Zatkovic, Czechoslovak Institute of Metrology/CSMO, Bratislava, Czechoslovakia.
F. Hengstberger, NPRL/SCIR, Pretoria, South Africa.
Li Tong-Bao, National Institute of Measurement and Testing Technology, Chengdu, China.

8. References

[1] Zalewski, E. F., and Geist, J., Appl. Opt. **19**, 1214 (1980).
[2] Geist, J., Zalewski, E. F., and Schaefer, R., Appl. Opt. **19**, 3795 (1980).
[3] Zalewski, E. F., and Duda, C. Richard, Appl. Opt. **22**, 2867 (1983).
[4] Thomas, D. B., and Zalewski, E. F., A Radiometer For Precision Coherent Radiation Measurements, SPIE Tech. Symp. on Aerospace Sensing, Orlando, Florida, March 1989.
[5] Annual Report of the Consultative Committee on Photometry and Radiometry, International Bureau of Weights and Measures, Sevres Cedex, France (1986).

About the authors: *Douglas B. Thomas is a physicist in the Radiometric Physics Division in the Center for Radiation Research, which is part of the NIST National Measurements Laboratory. Edward F. Zalewski is a Senior Staff Engineer in the Advanced Developments Laboratory of Hughes Danbury Optical Systems.*

[J. Res. Natl. Inst. Stand. Technol. 95, 545 (1990)]

Effects of the International Temperature Scale of 1990 (ITS-90) on CIE Documentary Standards for Radiometry, Photometry, and Colorimetry[1]

Volume 95 | Number 5 | September-October 1990

Klaus D. Mielenz and Jack J. Hsia

National Institute of Standards and Technology,
Gaithersburg, MD 20899

The differences between ITS-90 and IPTS-68 above 1235 K are described. It is shown that none of the following CIE definitions or recommendations require revision because of the introduction of the ITS-90: International Lighting Vocabulary definitions; CIE Standard Illuminants A, D_{65}, other illuminants; and sources for realizing CIE Illuminants. The effect of the ITS-90 on previously calibrated sources for realizing CIE illuminants is negligibly small.[2]

Key words: CIE Standard Illuminants A; CIE Standard Illuminant D_{65}; colorimetry; ITS-90; light sources; photometry; radiometry.

Accepted: July 30, 1990

1. Difference Between ITS-90 and IPTS-68

Like its predecessors, the International Temperature Scale of 1990 (ITS-90) [1] is based on numerical values of temperature assigned to a number of defining fixed points and on standard interpolating instruments calibrated at these fixed points. In the radiation temperature region above the freezing point of silver, the ITS-90 can be realized by optical pyrometry and the temperature T_{90} is defined by the equation

$$\frac{L_\lambda(T_{90})}{L_\lambda[T_{90}(X)]}=\frac{\exp[c_{2,90}/\lambda T_{90}(X)]-1}{\exp(c_{2,90}/\lambda T_{90})-1},$$

where $T_{90}(X)$ refers to any one of the silver [$T_{90}(Ag)=1234.93$ K], the gold [$T_{90}(Au)=1337.33$ K], or the copper [$T_{90}(Cu)=1357.77$ K] freezing points, where $L_\lambda(T_{90})$ and $L_\lambda(T_{90}(X))$ are the spectral concentrations of the radiance of a blackbody at the wavelength (in vacuo) λ at T_{90} and at $T_{90}(X)$, respectively, and where $c_{2,90}=0.014388$ m·K.

In the International Practical Temperature Scale of 1968, Amended Edition of 1975 (IPTS-68) [2] the temperature T_{68} was defined by a similar equation:

$$\frac{L_\lambda(T_{68})}{L_\lambda[T_{68}(Au)]}=\frac{\exp[c_{2,68}/\lambda T_{68}(Au)]-1}{\exp(c_{2,68}/\lambda T_{68})-1},$$

where $T_{68}(Au)=1337.58$ K and $c_{2,68}=0.014388$ m·K.

From the above, the following relationships between the ITS-90 and the IPTS-68 are noted:

(1) The value assigned to the second radiation constant, c_2, has not been changed,

$$c_{2,90}=c_{2,68}=0.014388 \text{ m·K}.$$

[1] A CIE (Commission Internationale de l'Eclairage or International Commission on Illumination) research note.
[2] Abstracts in French and German are given in the Appendix.

(2) The ITS-90 gold-point assignment has been lowered by 0.25 K,

$$T_{90}(\mathrm{Au}) = T_{68}(\mathrm{Au}) - 0.25\ \mathrm{K} = 1337.33\ \mathrm{K}.$$

(3) The ITS-90 above the freezing point of silver (1234.93 K) is defined in terms of three fixed points, the freezing points of silver, gold (1337.33 K), and copper (1357.77 K). This introduces a redundancy of the new scale, whereas all previous scales were unambiguously defined in terms of the gold point alone. However, the text of the ITS-90 states that "the T_{90} values of the freezing points of silver, gold, and copper are believed to be self consistent to such a degree that the substitution of any one of them in place of one of the other two as the reference temperature $T_{90}(\mathrm{X})$ will not result in significant differences in the measured values of T_{90}".

2. Effects on CIE Definitions and Recommendations

The activities of the CIE which relate to temperature and could conceivably be affected by the adoption of the ITS-90 fall in the domain of thermal radiation and its applications in radiometry, photometry, and colorimetry. The published CIE output in these areas can be classified into two broad areas: definitions and recommendations. In what follows, it will be shown that none of these definitions and recommendations requires revision because of the introduction of the ITS-90.

2.1 CIE Definitions

2.1.1 General The output of the CIE contains a large number of definitions of the fundamental concepts, physical quantities, and technical terms used in the areas of light and lighting. These definitions have traditionally been collected in the International Lighting Vocabulary, which is now available in its fourth edition [3] as a joint publication compiled by the CIE in collaboration with the International Electrotechnical Commission (IEC). Insofar as these definitions relate to thermal radiation, they are given in terms of thermodynamic temperatures and are, therefore, independent of the International Temperature Scale and not affected by the adoption of the ITS-90. Specific examples include the definitions of color temperature, correlated color temperature, distribution temperature, radiance temperature, ratio temperature, and similar quantities which are used to assign a single temperature to the spectral power distributions of incandescent or fluorescent lamps, phases of natural daylight, and other sources which are not too different from blackbody sources.

2.1.2 CIE Standard Illuminants The definitions published by the CIE comprise, as a special class, "standards" in the form of uniquely defined data which form the basis of internationally accepted standard systems. These include "standard illuminants" for applications of colorimetry requiring the use of spectral power distributions which are representative of typical lighting conditions [4,5]. These illuminants are spectral power distributions which are not necessarily realizable by laboratory sources, and are provided by the CIE in the form of numerical tables. At the present time, there are two CIE standard illuminants.

Standard Illuminant A

CIE Standard Illuminant A is representative of domestic tungsten lighting and was originally defined as follows [6].

> "It is recommended that the following ... luminous sources be adopted for the general colorimetry of materials:
>
> "Source A. A gas-filled lamp of color temperature 2848 K ...
>
> "For calculations of the spectral energy distribution the constant, c_2, of Planck is taken equal to 14,350 micron degrees.
>
> "Source A. The spectral energy distribution of this source shall be considered for all colorimetric applications as that of a blackbody at the temperature 2848 K."

This definition was independent of the International Temperature Scale of 1927, which was in effect at the time. After the introduction of the International Temperature Scale of 1948, and once again after the IPTS-68 was introduced, the CIE followed a policy of adopting the assigned values of c_2 but preserving the relative spectral distribution of illuminant A. This was achieved by shifting the color temperature assigned to it, rather than computing new spectral distributions for the original color temperature of 2848 K. Accordingly, the spectral values of CIE standard illuminant A are to

be considered independent of the International Temperature Scale and require no adjustments in view of the adoption of the ITS-90. The color temperature assigned to standard illuminant A is a descriptive parameter which depends on the value of c_2 assigned in the International Temperature Scale. Its value is approximately 2856 K on the IPTS-68 and remains the same on the ITS-90 because the value of c_2 has not been changed.

Standard Illuminant D_{65}

This standard is representative of average daylight and is given in the form of numerical values that have been derived by Judd, MacAdam, and Wyszecki [7] from experimental data taken by others. The tabulated spectral data of illuminant D_{65} are consistent with the IPTS-68 value of c_2, and are also not affected by the introduction of the ITS-90 because c_2 was not changed. Likewise, the correlated color temperature of illuminant D_{65}, which is given as 6504 K on the IPTS-68, remains unchanged.

2.1.3 Other CIE Illuminants The CIE has also defined illuminants which do not have the status of primary CIE standards but are useful for special purposes [5]. Illuminants B (now obsolete) and C represent direct sunlight and average daylight with correlated color temperatures of approximately 4874 and 6800 K, respectively. Three illuminants, D_{50}, D_{55}, and D_{75}, have been defined in addition to standard illuminant D_{65} to represent daylight with approximate correlated color temperatures of 5000, 5500, and 7500 K. Additionally, illuminants F_1 through F_{12} have been defined to represent typical fluorescent lamps. The published relative spectral distributions of these additional illuminants [5] are consistent, within their estimated accuracies, with IPTS-68 temperatures and, therefore, with ITS-90 temperatures as well.

2.2 CIE Recommendations

2.2.1 General The CIE recommendations [5] concerning the calculation of color temperature and related quantities are dependent on the International Temperature Scale, in that a numerical value of c_2 is usually specified in these recommendations. However, the change from IPTS-68 to ITS-90 temperatures does not affect any of these recommendations because the value of c_2 remains the same in the new scale.

2.2.2 Recommended Sources for Producing CIE Illuminants The CIE has recommended specific sources [4,5] which can be used for practical realizations of the spectral distributions defined by CIE illuminants.

For example, the CIE recommends that Standard Illuminant A be realized by means of a gas-filled tungsten-filament lamp known as "Source A" which is operated at a correlated color temperature (2856 K on the IPTS-68) equal to the color temperature associated with Standard Illuminant A. This definition requires no change with the introduction of the ITS-90 because the color temperature associated with Standard Illuminant A has not changed.

At present, no source is recommended for realizing CIE Standard Illuminant D_{65}. However, the CIE has recommended a method [8] for assessing sources intended for this purpose. The description of this method does not rely on the International Temperature Scale and, therefore, requires no revision.

Illuminants B and C can be realized by combining Source A with specially formulated liquid filters [5]. The specifications of these filters are independent of the International Temperature scale and require no revision.

There are no CIE recommendations for realizing the D and F illuminants mentioned in section 2.1.3.

3. Effects on Calibrated Sources

Although none of the CIE recommendations for laboratory realizations of CIE Standard Illuminants are affected by the adoption of the ITS-90, it should be noted that sources that have previously been calibrated in accordance with these recommendations do not exactly produce the standard spectral distributions. Because the ITS-90 gold-point assignment is closer to the thermodynamic temperature of this fixed point, a source calibrated on the IPTS-68 and operated at a given radiance temperature T_{68} will have the ITS-90 kelvin temperature

$$T_{90}=T_{68}-0.25 * (T_{68}/1337.33)^2$$

[9] and will therefore produce a skewed spectral distribution. For example, a Source-A type lamp having the required correlated color temperature of 2856 K on the IPTS-68 will operate at the ITS-90 temperature 2855 K. Its spectral distribution, normalized to 100.00 at 560 nm, will be 0.07% lower than that of Standard Illuminant A at 460 nm, and 0.05% higher at 660 nm. These differences are small compared to the state-of-the-art

calibration uncertainties, so that no adjustments or corrections will be necessary in practice.

4. Appendix

Résumé

Les différences entre ITS-90 et IPTS-68 au delá de 1235 K sont décrites. Il est montré qu'aucune des suivantes définitions ou recommendations de la CIE nécessite de révision à cause de l'introduction du ITS-90: Les définitions du Vocabulaire Internationale de l'Eclairge, les Illuminants Standards A, D_{65}, et autres illuminants; et les sources pour la réalisation d'illuminants CIE. L'effet du ITS-90 sur les sources précédement calibrées pur réaliser les Illuminants CIE est néligeablement faible.

Zusammenfassung

Nach einer Diskussion der Unterschiede zwischen der ITS-90 und der IPTS-68 im Temperaturbereich ueber 1235 K wird gezeigt, dass die Einfuehrung der ITS-90 keine Revision der folgenden CIE Definitionen oder Empfehlungen erforderlich macht: Definitionen des Internationalen Worterbuchs der Lichttechnik; Normlichtarten A, D65, und andere; und CIE Normlichtquellen. Der Einfluss der ITS-90 auf bereits geeichte Normlichtquellen ist vernachlassigbar klein.

5. References

[1] Preston-Thomas, H., Metrologia **27**, 3 (1990).
[2] Preston-Thomas, H., Metrologia **12**, 7 (1976).
[3] CIE Publication 17.4, International Lighting Vocabulary, 1987.
[4] CIE Publication S 001, Colorimetric Illuminants, 1986a.
[5] CIE Publication 15.2, Colorimetry, Second Edition, 1986b.
[6] CIE, Recueil des Travaux et Comptes Rendu des Seances, 8th Session, Cambridge, England (1931) pp. 19–22.
[7] Judd, D. B., MacAdam, D. L., and Wyszecki, G., J. Opt. Soc. Amer. **54**, 1031 (1964).
[8] CIE Publication 51, A Method for Assessing the Quality of Daylight Simulators for Colorimetry, 1981.
[9] Mielenz, K. D., Saunders, R. D., and Shumaker, J. B., J. Res. Natl. Inst. Stand. Technol. **95**, 49 (1990).

About the authors: *Klaus D. Mielenz is Chief of the Radiometric Physics Division of the NIST Center for Radiation Research and Jack J. Hsia is a Group Leader in the Divsision. Klaus D. Mielenz is also the Director and Jack J. Hsia is the Secretary of CIE Division 2 on Physical Measurement of Light and Radiation.*

Volume 95, Number 5, September–October 1990
Journal of Research of the National Institute of Standards and Technology

[J. Res. Natl. Inst. Stand. Technol. 95, 549 (1990)]

An Accurate Value for the Absorption Coefficient of Silicon at 633 nm

Volume 95 | Number 5 | September–October 1990

Jon Geist

National Institute of Standards and Technology,
Gaithersburg, MD 20899

A. Russell Schaefer

Science Applications International Corporation,
4161 Campus Point Court,
San Diego, CA 92121

Jun-Feng Song, Yun Hsia Wang, and Edward F. Zalewski[1]

National Institute of Standards and Technology,
Gaithersburg, MD 20899

High-accuracy transmission measurements at an optical wavelength of 633 nm and mechanical measurements of the thickness of a 13-μm thick silicon-crystal film have been used to calculate the absorption and extinction coefficients of silicon at 633 nm. The results are 3105 ± 62 cm^{-1} and 0.01564 ± 0.00031, respectively. These results are about 15% less than current handbook data for the same quantities, but are in good agreement with a recent fit to one set of data described in the literature.

Key words: absorption coefficient; etch stop; extinction coefficient; HeNe; high accuracy; silicon.

Accepted: July 6, 1990

1. Introduction

The absorption coefficient [1] α at wavelength λ is related to k, the imaginary part of the index of refraction, also called the extinction coefficient, by

$$\alpha = 4\pi k/\lambda, \tag{1}$$

where λ is the vacuum wavelength of the incident radiation, which is related to the photon energy $h\nu$ of the radiation by

$$\lambda h\nu = 1.23985 \text{ eV } \mu\text{m}. \tag{2}$$

For silicon, k spectra have been derived from a Kramers-Kronig analysis of reflectance data [2], by inversion of ellipsometric data [3], and from α spectra derived from transmission measurements [4,5]. Neither ellipsometry nor a Kramers-Kronig analysis is well suited to the determination of small values of k, so for silicon most k values quoted below about 2.5 eV have been determined from transmission measurements. Since the differences among the various data sets are fairly large, Taft [6] measured the absorption coefficient at the Hg

[1] Present address: Hughes Danbury Optical Systems, 100 Wooster Heights Road, Danbury, CT 06810.

546.1-nm line (2.27 eV) for use in reducing ellipsometric data on oxide films on silicon wafers. However, at this time there is no consensus as to the correct spectra. This is illustrated by the fact that two recent compilations contain spectra that differ by much more than 20% at some wavelengths [7,8].

We have carried out a measurement similar to that of Taft at the 633-nm HeNe laser line. Our purpose was twofold. First, we wanted a smaller uncertainty at 633 nm than could be obtained from any of the published or compiled data. Second, we wanted to test the use of 1) an amplitude-stabilized laser as a radiation source, 2) extremely linear silicon photodiodes as the radiation detector, 3) recently perfected etching techniques for sample preparation, and 4) state-of-the-art mechanical measurements of sample thickness.

The advantage of using amplitude-stabilized lasers in conjunction with extremely linear photodiodes is that it allows very precise transmission measurements to be carried out over a very large dynamic range with very high wavelength accuracy and resolution. This was demonstrated recently in connection with a search for evidence of the second indirect gap in the silicon absorption coefficient spectrum [9].

The work reported here supplements the high-precision work reported in reference [9] by showing what additional steps are necessary to achieve high accuracy. Combining the techniques described here with those described in reference [9] should allow high-precision, high-accuracy measurements over a large range of transmittance.

There are two reasons why a large range of transmittance is desirable. Since the absorption coefficient of silicon changes by many orders of magnitude over the region of the indirect transition, the dynamic range over which accurate transmittances can be measured determines the number of samples needed to cover the whole spectral range. Second, there are certain advantages that accrue directly from calculating the absorption coefficient from small values of transmittance. The transmission of an optically thick sample is given by the simple expression

$$t=(1-r_f)\,(1-r_b)\,\exp(-\alpha\, x), \tag{3}$$

where r_f and r_b are the reflectances of the front and back surfaces of the sample, respectively, and x is the sample thickness. Therefore,

$$\frac{d\alpha}{\alpha}=-\frac{dx}{x}-\frac{1}{\alpha x}\left[\frac{dt}{t}+\frac{dr_f}{(1-r_f)}+\frac{dr_b}{(1-r_b)}\right]. \tag{4}$$

Thus, the relative uncertainty in α will have its minimum value at the largest value of $\alpha\, x$ (smallest transmittance) for which the relative uncertainties in the transmittance and reflectances are independent of the transmittance.

In the following sections, we describe the silicon sample, the optical measurements, the mechanical measurements, the data reduction, and the uncertainty analysis that were used to derive the absorption and extinction coefficient values reported here.

2. Silicon Sample

The sample whose transmittance we measured was a 2-cm by 2-cm by 13-μm free standing film of silicon that was prepared as follows. A uniform thickness, p-type, epitaxial layer doped with about 10^{14} B atoms per cm^3 (50 Ω-cm resistivity) was grown to a nominal thickness of 15 μm on a 100-mm diameter p^+ (0.01 Ω-cm) silicon wafer with (100) surface orientation. A nominal 25- by 25-mm square sample was cut from the wafer, and masked with wax so as to leave the central 2- by 2-cm area of heavily doped substrate exposed. The masked sample was then mounted on a sapphire carrier disk and etched in a rotating-drum mixture of 1 part HF, 3 parts nitric acid, and 8 parts acetic acid [10]. After about 8 h, it was removed and cleaned. The result was a free-standing film, approximately 15-μm thick, suspended in a 0.64-mm thick, 1.9-mm wide silicon frame.

The sample was glued onto a flexible piece of plastic over a 2- by 2-cm hole cut in the plastic so that the etched side faced the plastic. The plastic served as a convenient handle for aligning and mounting the sample, and as a strain relief for the sample during handling. Although the sample was reasonably robust due to the frame, it still could be damaged by rough handling, and the plastic served to minimize stress on it during handling.

3. Experimental Measurements

3.1 Absolute Transmission and Reflection Measurements

The absolute transmission measurements were carried out using the experimental setup shown in figure 1. A HeNe laser emitting 633-nm radiation was used as the source of radiation. The beam was passed through an electro-optical modulator and focused with a microscope objective onto a pin-

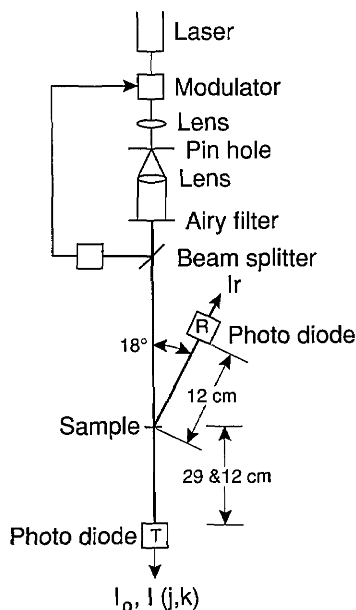

Figure 1. Apparatus for measuring the transmittance and reflectance of the silicon sample at the 633-nm HeNe laser line.

hole aperture in an opaque screen. The radiation diffracted through the pin hole was collimated with a beam-expanding telescope to produce an Airy disk about 6 mm in diameter. An opaque screen with a 6-mm diameter hole (Airy Filter) was aligned with the first dark ring in the Airy pattern so that only the Airy disk passed through the aperture. This provided a fairly clean and uniform beam of about 40 μW of 633-nm radiation. A beam splitter reflected some of this radiation to a photodiode whose output controlled the transmittance of the modulator so as to maintain a constant power in the beam to within about 0.1% over a period of hours [11].

The amplitude-stabilized laser beam passed through the sample-holder section of a computer-controlled translation stage and was incident on a photodiode having a 1- by 1-cm active area that was located in position T in figure 1. The photocurrent I_0 from this photodiode was measured with a high-accuracy digital voltmeter and a trans-impedance amplifier. In this and all other photocurrent measurements, the measured value was corrected by subtracting the dark current that was measured with the laser light shuttered and the rest of the apparatus in the same configuration as during the photocurrent measurement.

3.1.1 Direct Transmittance and Reflectance The plastic sheet to which the sample was attached was positioned on the sample holder such that the laser radiation was incident on the etched side of the sample, and the bottom and top sides of the sample were parallel to one, and perpendicular to another of the directions of motion of the translation stage on which the holder was mounted. The plastic sheet was fastened to the sample holder in this position with removable transparent tape. In this position the photodiode was 29 cm from the sample. The stages were then translated so that the 6-mm diameter HeNe radiation beam was centered on the nominal center of the sample, and the photocurrent $I_d(j,k), j=-1, 0, 1, k=-1, 0, 1$, due to the directly transmitted radiation, was recorded as a function of the position of the sample over a 3 by 3 grid of points on the sample having a 2-mm grid spacing, with the center of the grid pattern coincident with the nominal center of the sample.

The plastic sheet with the sample was removed from the sample holder and remounted as described above, but with the laser radiation incident on the polished surface, and the translation stage rotated about 9° off of the perpendicular to the direction of the laser beam to allow the reflectance of the sample to be measured by the photodiode in position R in figure 1. The resulting photocurrent I_r reflected from the nominal center of the sample was recorded. The photodiode was relocated to position T in figure 1, but at 12 instead of 29 cm from the sample, and the photocurrent I from the radiation directly transmitted through the center of the sample was measured.

The photocurrent I was 1.7% greater than $I_d(0,0)$, which was measured at the nominal center of the sample when the etched side of the sample faced the laser and the photodiode was 29 cm from the sample. This difference could be caused by a failure to irradiate exactly the same area of the sample when aligning the laser beam with the nominal center of the sample, or by the different angle of incidence for the different measurements. It could also be caused by slightly more scattered radiation falling on the photodiode when located 12 cm from the sample than when located 29 cm from the sample. In any event, the difference between I and $I_d(0,0)$ was not due to laser drift. After the measurement described above, the sample was removed from the sample holder and I_0 was remeasured. The two measurements of I_0 agreed to within 0.1%, indicating the stability of the amplitude-stabilized laser beam.

3.1.2 Scattered Transmittance A scattermeter package [12] consisting of a box-shaped array of photodiodes with a 1- by 1-cm hole in the center of the array as shown in figure 2 was used to measure the transmitted radiation that was scattered out of

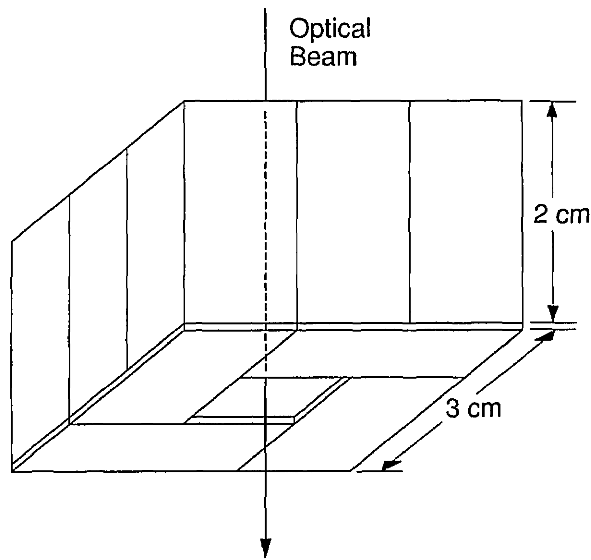

Figure 2. Illustration of the box-shaped scattermeter made from an array of photodiodes to measure the scattered component of the transmitted HeNe laser radiation.

the directly transmitted beam. First, the photodiode used to measure the directly transmitted radiation was removed. Then, with the sample still out of the sample holder, the scattermeter was aligned in the beam so that it collected all of the beam on its interior surface, and the photocurrent I_{S0} was recorded. The sample was then remounted, as described above, with the etched surface facing the scattermeter. The scattermeter was then located 10 cm from the sample as shown in figure 3, so that the 1- by 1-cm opening in the top of the scattermeter was in the position previously occupied by the photodiode measuring the directly transmitted radiation. The photocurrent I_{S1} was recorded. The scattermeter was then moved so that its base was only 2.2 cm from the sample, care being taken to keep the directly transmitted beam in the center of the 1- by 1-cm opening in the top of the scattermeter. The photocurrent I_{S2} was recorded. The results, which are $I_{S1}/I_0=0.060\%$ and $I_{S2}/I_0=0.094\%$, were used in the calculation of the total transmittance as described next.

3.1.3 Transmittance and Reflectance Data Reduction The transmittance $t(j,k)$, $j=-1$, 0, 1, $k=-1$, 0, 1 of the sample at the same nine points on the 3 by 3 grid where the direct transmittance was measured was calculated as

$$t(j,k)=\frac{I_d(j,k)}{I_d(0,0)}\left[\frac{I}{I_0}+\frac{I_{S1}+I_{S2}}{I_{S0}}\right], \tag{5}$$

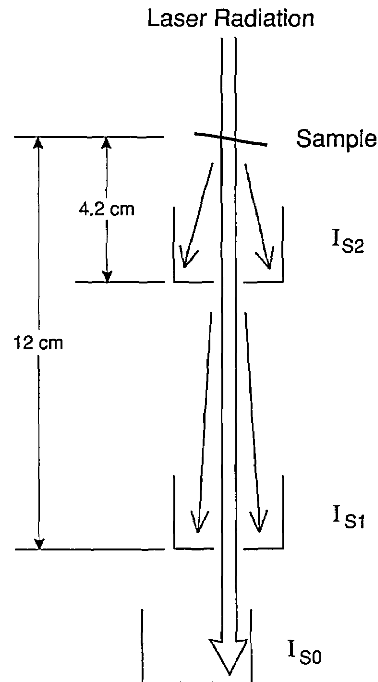

Figure 3. Illustration of the use of the scattermeter shown in figure 2 to measure some scattered components of the transmitted HeNe laser radiation.

on the assumption that the transmittance of the sample was independent of whether the radiation was transmitted from the etched surface to the polished surface, or vice versa, and that the transmitted radiation that was scattered scaled with the directly transmitted radiation. The $t(j,k)$ values calculated from eq (5) are listed in table 1.

Table 1. The absolute transmittance $t(j,k)$ measured on the silicon sample described in this paper

	$t(j,k)$		
$k \backslash j$	−1	0	1
1	0.00802	0.00778	0.00824
0	0.00786	0.00783	0.00816
−1	0.00766	0.00768	0.00800

The polished side of the sample, which faced the laser beam, was smooth enough to reflect specularly with negligible scattering. Moreover, when the radiation was incident on the polished side of the sample, the fraction that was reflected from the

etched side was attenuated by $(1-r)^2 \exp(-2\alpha x) < 2\times10^{-4}$ as it was transmitted through the polished face of the sample to the etched face, and back again. Therefore, the scattered component of radiation reflected from the etched surface was negligible compared to the radiation reflected specularly from the polished surface, and no attempt was made to measure it.

The reflectances of both faces of the sample were calculated as

$$r_b = r_f = I_r/I_0 = 0.3454, \qquad (6)$$

under the assumption that the roughness of the etched surface was not large enough to change the reflectance of the surface significantly, even though it was large enough to scatter a significant amount of radiation out of the directly transmitted beam. How this assumption was tested is described in the next section.

3.2 Mechanical Measurements

3.2.1 Surface Roughness The characterization of the roughness of the etched surface of the sample was carried out by measuring the roughness along five lines located on the sample as shown in figure 4 using the NIST Stylus/Computerized System [13], in which a high-resolution TALYSTEP[2] stylus instrument is calibrated on the 200,000 × vertical magnification range against a 0.0291-μm step-height standard that was measured interferometrically. To allow the fine structure of the surface to be resolved, a stylus width of 0.15 μm with a loading of 0.15 mgf (1.5 μN) was used. The TALYSTEP ISO filter (2CR) was used, and the cut-off wavelength was 0.0976 mm (25% attenuation). The traversing speed was 0.122 mm/s over a distance of 0.4 mm. Since the instrument's high-frequency response is 85 Hz, the surface profile could be detected over a wavelength range extending from about 1.44 μm (corresponding to the frequency response of the instrument) to 97.6 μm (the filter cut-off wavelength). The root-mean-square surface roughnesses R_q over this wavelength range varied from 7.2 to 10.0 nm for the five lines, while the arithmetic average roughness R_a varied from 6.3 to 8.1 nm. This is not large enough to disturb the mechanical thickness measurements described next, nor to change the reflectance of the surface, but it is large enough to scatter both transmitted and reflected radiation significantly out of the respective direct and specular directions.

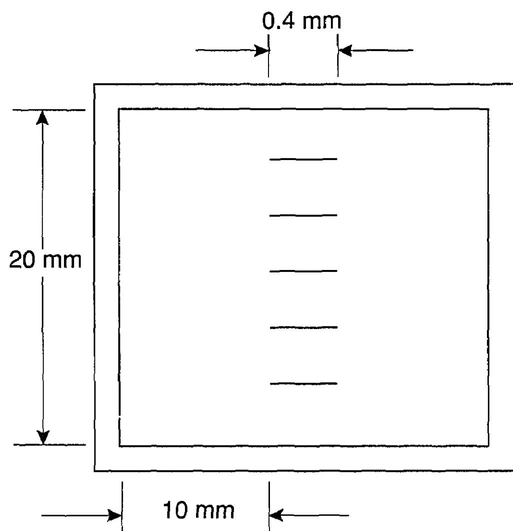

Figure 4. Illustration of the location on the sample of the surface roughness measurements. Note that the length of the surface roughness scans is exaggerated in this figure.

3.2.2 Sample Thickness We used a high-accuracy laser-interferometer micrometer (GCA LASERULER) having a resolution of 0.01 μm and an uncertainty of ±0.13 μm to measure the thickness of the sample. For these measurements, the micrometer was fitted with a 0.2-in (5.1-mm) diameter, hemispherical, steel-tipped probe, and a steel surface plate of nominal 130-mm diameter was centered under the probe. The digital output from the laser-interferometer that was connected to the probe shaft was set to zero when the probe was driven against the surface plate with the probe-driving mechanism. The probe was then raised from the surface plate and driven against it, and the zero-point height recorded six times. The probe was again raised, the sample placed on the surface plate with its polished surface down, and the probe driven to within a millimeter of the etched surface. In this position, the sample location was adjusted to be nominally centered under the probe as determined by sighting along the diagonals of the sample.

[2] Certain commercial equipment, instruments, or materials are identified in this paper to specify adequately the experimental procedure. Such identification does not imply recommendation or endorsement by the National Institute of Standards and Technology, nor does it imply that the materials or equipment identified are necessarily the best available for the purpose.

The probe was then lowered and raised six times, and the sample thickness was recorded each time. The zero-point thickness measurements were then repeated six times. The thickness h was calculated from the difference of the mean of the thickness measurements and the mean of zero-point measurements. The value determined in this way was $h=12.86\pm0.02$ μm, where the stated uncertainty is one standard deviation of the reported value. The purpose of this value was to serve as a consistency check on the data on the variation of thickness over the sample that is described next.

A small piece of graph paper was fastened to the surface plate with removable transparent tape in such a way that one corner of the plastic sheet to which the sample was fastened fell in the center of the graph paper when the sample was nominally centered under the micrometer probe. The graph paper did not extend under the sample for any position of the sample that allowed the probe to touch the etched surface of the sample. The plastic sheet was then aligned so that one edge was parallel to one of the lines on the graph paper, one corner was aligned with a point where horizontal and vertical lines on the graph paper crossed, and the micrometer probe was located over the etched portion of the sample near one corner. The plastic sheet was then translated over an 8 by 8 grid with a 2-mm grid spacing and the height $z(m,n)$, $m=0, ..., 7$, $n=0, ..., 7$, of the sample measured at each grid point. After the measurement of $z(m,n)$ at each grid point, the plastic sheet was returned to the starting point (0,0) and the thickness $z(0,0;m,n)$ was remeasured to monitor indirectly any zero drift in the digital readout of the micrometer.

When the measurements described above were completed, the plastic sheet was removed and a zero-point reading was taken. The zero-point reading had drifted by 0.32 μm during the set of 64 grid point and 64 reference-point measurements, but the reference-point measurements indicated that it had reached even larger values a few times during the measurements. Therefore, the reference-point measurements were used in making the zero-point corrections to the thickness map data.

The plastic sheet was then alternately aligned at the point (1,3) and removed three times, so that three measurements of sample thickness followed by three measurements of the zero-point value could be recorded. The thickness $h(1,3)=12.79\pm0.00$ μm of the sample at the point (1,3) was calculated as the mean of the sample thickness measurements minus the mean of the zero-point readings. The uncertainty was calculated in the same way as it was for the measurement at the nominal center of the sample that was described at the beginning of this section.

Finally, the thickness $h(m,n)$ of the sample at each grid point was calculated as

$$h(m,n)=h(1,3)+[z(m,n)-z(0,0;m,n)] -[z(1,3)-z(0,0;1,3)]. \quad (7)$$

Table 2 shows the $h(m,n)$ data obtained from eq (7). Figure 5 shows as crosses the approximate location of the 8 by 8 grid where the $h(m,n)$ data were measured on the sample as determined by observing the location of the sides of the micrometer probe relative to the corners of the sample after the

Table 2. The thickness $h(m,n)$ of the sample at points located at the approximate positions indicated in figure 5

	$h(m,n)$ in μm							
$n \backslash m$	0	1	2	3	4	5	6	7
7	10.97	11.59	11.49	11.99	12.11	11.75	13.29	10.70
6	12.42	12.66	12.80	12.58	12.60	12.56	12.24	11.68
5	12.89	12.82	13.15	12.83	12.44	12.66	12.76	11.93
4	12.94	13.01	12.79	12.81	12.54	12.80	12.88	11.84
3	12.97	12.79	12.71	12.96	12.81	12.79	12.85	11.80
2	12.95	13.05	12.95	12.66	13.02	12.88	12.50	11.68
1	12.95	12.90	13.05	13.14	12.73	12.58	12.56	11.59
0	12.17	12.61	12.68	12.74	12.55	12.30	11.97	11.36

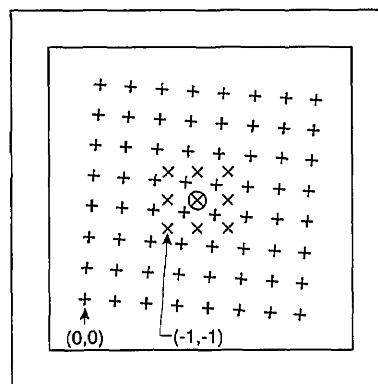

Figure 5. Approximate relative locations of the thickness measurements (+) and the transmittance measurements (×) relative to the center (circled ×) of the sample.

measurement described above was completed. For comparison, figure 5 also shows as ×'s the nominal location of the transmittance measurements reported earlier in this paper. The circled × is the point (0,0) for the transmittance data, and it is also the nominal location of the thickness measurement reported earlier in this section as a consistency check. That value, $h=12.86\pm0.02$ μm, agrees to within 0.1 μm with the expected value on the basis of the data shown in table 2.

3.2.3 Elastic Compression Correction All of the silicon thicknesses reported so far contain an error due to the elastic compression of the hemispherical probe tip and the surface that it contacts under the load of a thickness or zero-reference measurement. The true thickness of the sample h_t is related to the difference h between the sample-in and sample-out measurement by $h_t=h+\Delta h$, where $\Delta h=\alpha_2-\alpha_1$, as is illustrated in figure 6. To calculate Δh, we used the equation for the elastic compression α_i of a sphere in contact with a flat surface,

$$\alpha_i=\frac{(3\ \pi\ p\ [V_{\text{flat}}+V_{\text{sphere}}])^{2/3}}{2\ D^{1/3}}, \tag{8}$$

where p is the total applied force, D is the diameter of the sphere, and

$$V_j=(1-\sigma_j^2)/\ (\pi\ E_j), \tag{9}$$

where σ_j is Poisson's ratio of the jth material, and E_j is the modulus of elasticity of the jth material.

Reference [14] gives 0.956×10^{-8} in^2/lbf (1.39 pm^2/N) for V_{steel}. References [15] and [16] give 0.44 and 1.56×10^6 lbf/in^2 (3.0 and 10.8 GN/m2) for σ_{Si} and E_{Si}, respectively, without indicating the crystallographic direction to which the values actually apply. For forces applied to a (100) surface silicon, E_{Si} is given by

$$E_{\text{Si}}=(C_{11}+2\ C_{12})\cdot(C_{11}-C_{12})/(C_{11}+C_{12}), \tag{10}$$

where C_{kl} are the tensor stiffness constants of silicon [17]. Reference [18] gives values for C_{kl} from which we calculated $E_{\text{Si}}=18.9\times10^6$ lbf/in^2 (130 GN/m^2). The diameter of the tip of the hemispherical probe was measured to be 0.20 in (5.1 mm), and the force applied during a thickness measurement was measured to be 0.154 lbf (0.658 N). Using the above values, we calculated $\Delta h=0.035$ μm and assigned plus or minus the calculated value as a conservative uncertainty.

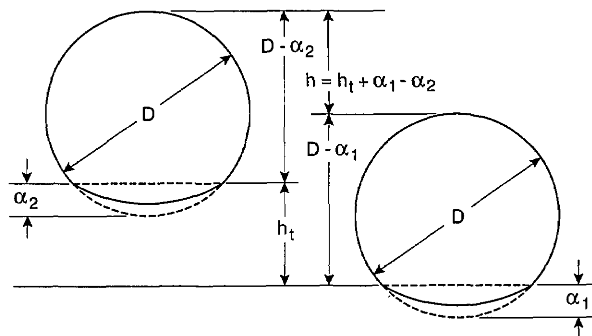

Figure 6. Illustration showing the relation between the true thickness h_t of the sample and the measured thickness h due to the difference in compression between the sample-in and sample-out measurements with the laser micrometer.

4. Data Reduction and Uncertainty Analysis

4.1 Absorption Coefficient

An absorption coefficient value was calculated for each of the transmittance measurements by inverting eq (3) with $r_f=r_b=0.3454$, as indicated in eq (6), to obtain

$$\alpha(j,k)=\frac{-\ln\{t(j,k)/[(1-r_f)(1-r_b)]\}}{x(j,k)+\Delta h}, \tag{11}$$

where

$$x(j,k)=\frac{\left[\sum_{m=j+2}^{m=j+5}\sum_{n=k+2}^{n=k+5} w(m-j-3,n-k-3)\ h(m,n)\right]}{108}, \tag{12}$$

for $j=-1,\ 0,\ 1,\ k=-1,\ 0,\ 1$, and where the weights $w(u,v)$ for $u=-1,\ 0,\ 1,\ 2,\ v=-1,\ 0,\ 1,\ 2$ are listed in table 3. These weights were chosen as illustrated in figure 7 to average the measured sample thickness over approximately the same 6-mm diameter area in the center of the sample as was used in the transmittance measurements. Table 4 lists the resulting average thicknesses $x(j,k)$, and table 5 lists the absorption coefficient values obtained from eq (11).

4.2 Uncertainty Analysis

The uncertainty in the absorption coefficient can be calculated from the total differential in eq (4).

Table 3. The weights $w(u,v)$ used in calculating average thickness of the sample over the regions irradiated during the transmittance measurements

	$108 \cdot w(u,v)$			
$u \backslash v$	−1	−0	1	2
2	0	3	1	0
1	7	16	14	1
0	11	16	16	3
−1	2	11	7	0

Table 4. The average thickness $x(j,k)$ of the sample over the same areas for which the transmittance data are shown in table 1

	$x(j,k)$ in μm		
$k \backslash j$	−1	0	1
−1	12.87	12.75	12.69
0	12.84	12.78	12.79
1	12.89	12.88	12.81

Table 5. The absorption coefficients $\alpha(j,k)$ of silicon at 633 nm determined from the data in tables 1 and 4

	$\alpha(j,k)$ in cm^{-1}		
$k \backslash j$	−1	0	1
1	3114	3106	3090
0	3114	3123	3128
−1	3099	3089	3081

First, we consider the sources of error that are common to every point (j,k). These sources of error include systematic radiometric errors in the direct and scattered transmittance measurements, and in the reflectance measurement, uncertainties associated with using the reflectance measured from the polished side of the sample to represent that from the etched side, and with using the sum of the measured scattered transmittances to represent the true scattered transmittance. Inaccuracies in the laser micrometer and the calculation of the depth Δh to which the micrometer probe penetrates into

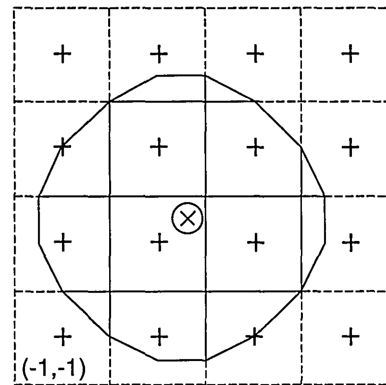

Figure 7. Illustration of the averaging of the thickness measurements to approximate the same weighting over the 6-mm diameter region as obtained from the transmittance measurements. This weighting is appropriate for the center of the sample, but is a little skewed relative to other locations of the transmittance measurements on the sample.

the silicon during the thickness measurement are also sources of error common to all of those measurements. These sources of error and our uncertainty estimates for them are listed in table 6. Also listed there is the quadrature sum of their contributions to the relative uncertainty in the absorption coefficient.

Referring to table 6 and eq (4), recall that the measured sample thickness was approximately 13 μm. Since the uncertainty associated with the laser micrometer is 0.13 μm, it contributes 1% to the uncertainty in the absorption coefficient. Similarly,

Table 6. The sources of error and associated uncertainty estimates for the sources of error that are common to the thickness and transmittance measurements at all points on the sample

Source of error	Estimated uncertainty	
dx/x		times 1
Micrometer accuracy	1.00%	1.00%
Compression correction	0.27%	0.27%
dt/t		times $1/\alpha x$
$I_d(j,k)/I_d(0,0)$	1.0%	0.25%
I/I_0	1.0%	0.25%
I_{S1}/I_{S0}	1.0%	0.25%
I_{S2}/I_{S0}	1.0%	0.25%
$(I_{S1}+I_{S2})/I_{S0}$ for true scatter	3.8%	0.95%
$dr_f/(1-r_f)$		times $1/\alpha x$
I_r/I_0	$<$0.1%	0.02%
$dr_b/(1-r_b)$		times $1/\alpha x$
Use of r_f for r_b	1.0%	0.25%
Sum in quadrature		1.79%

the 0.035-μm uncertainty assigned to the compression of the silicon, the surface plate, and the probe tip contributes 0.27%.

There is a 1% uncertainty associated with the transmittance-photocurrent ratios because the gain of the current-to-voltage converter was 100 times greater for the measurements of the numerator photocurrents than for the denominator photocurrents, and 1% is the between-range gain accuracy of the transimpedance amplifier used. An uncertainty of 25% of the measured components of the scattered transmittance was associated with the use of the sum of these quantities for the true scattered transmittance. Since the sum of the measured components of the scattered transmittance was about 15% of the total measured transmittance, the relative uncertainty is about 3.8%. An uncertainty of less than 0.1% is associated with the reflectance ratio since the same gain was used for both the numerator and the denominator photocurrents in this measurement. However, an uncertainty of 1% was associated with r_b to allow for the possibility that it was smaller than r_f due to the roughness of the etched surface. According to eq (4), each of these uncertainties is multiplied by a factor of $1/\alpha x$ (about 1/4 for this sample and wavelength) in its contribution to the uncertainty in the absorption coefficient, as shown in table 6.

Sources of error that contribute differently to the absorption coefficient values at the different points (j,k) are the random errors in the measurements of the transmittance, reflectance, and thickness. The first two are negligible at the 0.1% level. The third might not be, but its actual contribution to our data cannot be distinguished from the error associated with the variation in thickness of the sample as a function of position over its surface.

It is not really clear how to estimate the uncertainty to be associated with the variations in sample thickness. On the one hand, the thickness averaging procedure was designed to eliminate errors from this source. On the other hand, the procedure is not perfect because the transmittance values and the average thicknesses do not weight the same parts of the sample in the same way. The transmittance values weight the points of the sample within a 6-mm diameter region according to the intensity of the Airy disk. The average thicknesses weight 13 points on a 2- by 2-mm grid nonuniformly to approximate equal weighting of all points in a 6-mm diameter region. Furthermore, the centers of the corresponding regions over which the transmittance and thickness averages were computed are only approximately aligned.

4.3 Reported Value and Uncertainty

After trying a number of different approaches to the uncertainty analysis, we decided to use the average of the $\alpha(j,k)$ values in table 5 for the reported value, and to use the half-range of the values as the uncertainty. This results in a contribution of 0.76% to the relative uncertainty in the absorption coefficient. When we add this relative uncertainty in quadrature with the relative uncertainties reported in table 6, we obtain 1.94%. Therefore, we report $\alpha=3105$ cm^{-1} and $k=0.01564$ with an estimated uncertainty of 2% for silicon at a vacuum wavelength of 633.00 nm or a photon energy of 1.9587 eV.

4.4 Comparison with Existing Data

Figure 8 compares our data at 1.96 eV with some of the more noteworthy data previously reported in the 1.9- to 2.3-eV spectral region. The open circles are the handbook data of reference [7] and the closed circles are the handbook data of reference [8]. The dashed line is the data (for which no tabulated values were published) of reference [4], and the full line is data (for which no tabulated values were published) of reference [5]. The open diamond is the value reported in reference [6], along

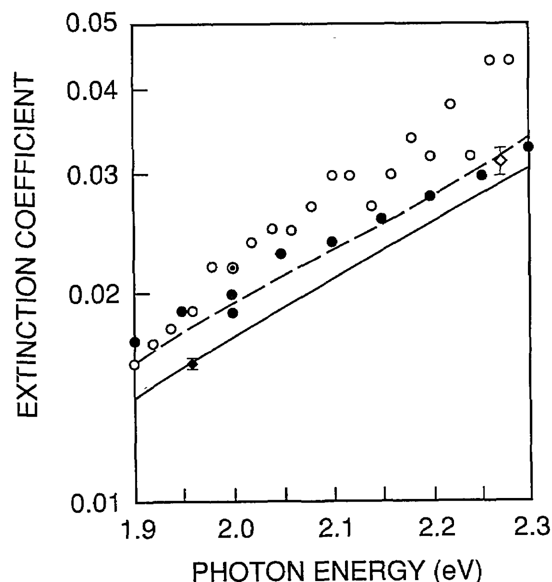

Figure 8. Comparison of Handbook data (open circles from reference [7] and closed circles from reference [8]), published data reported without tabulation (dashed line from reference [4] and continuous line from reference [5]), and single-point transmittance measurement (open diamond from reference [6]) with the value reported at 633 nm in this paper.

with the reported uncertainty. Our value is the closed diamond.

The result reported here has an estimated uncertainty that is significantly smaller than the other results shown in figure 8, due to combining a higher quality sample with more accurate and precise thickness and transmittance measurements. Two sources of uncertainty dominate the uncertainties listed in table 6. These are the measurement of the thickness of the sample and the measurement of the scattered component of the transmittance. It should be possible to improve both of these measurements to reduce the overall uncertainty to below 1%, either by using more accurate instrumentation, and/or by improving the sample quality. In either case it would be necessary to obtain a more accurate laser micometer. Other required improvements in instrumentation would include a more accurate scattermeter, and a precision translator that clamps onto both the surface plate used in the thickness measurements and the sample holder used in the transmittance measurements. The latter would allow precise alignment of the areas weighted by the transmittance and thickness measurements, as well as a finer density of points for the thickness measurements. Improvements in the sample preparation procedure that resulted in a sample having a more uniform thickness and a smoother rear surface would eliminate the requirement for the improved scattermeter and the translation stage. However, at the current time, it is not clear how to obtain the necessary improvements in sample preparation.

Acknowledgment

The authors would like to acknowledge the careful skill and craftsmanship of Robert Larsen of SAIC in production of the etched sample.

5. References

[1] Born, M., and Wolf, E., Principles of Optics, 3rd Edition, Pergamon Press, New York (1965), p. 614.
[2] Philipp, H. R., J. Appl. Phys. **43**, 2835 (1972), and personal communication of spectral values.
[3] Aspnes, D. E., and Studna, A. A., Phys. Rev. **B27**, 985 (1983).
[4] Dash, W. C., and Newman, R., Phys. Rev. **99**, 1151 (1955).
[5] Weakliem, H. A., and Redfield, D., J. Appl. Phys. **50**, 1491 (1979), and private communication of spectra values.
[6] Taft, E. A., J. Electrochem. Soc. **125**, 968 (1978).
[7] Edwards, D. F., Silicon (Si), Handbook of Optical Constants, Palik, E. D., ed., Academic Press, Orlando, Florida (1985), p. 547.
[8] Aspnes, D. E., Optical Functions of Intrinsic Si: Table of Refractive Index, Extinction Coefficient and Absorption Coefficient vs Energy (0 to 400 eV), in Properties of Silicon, EMIS Datareviews Series No. 4, INSPEC, Institution of Electrical Engineers, London, England (1988), p. 72.
[9] Geist, J., Migdall, A., and Baltes, H., Appl. Opt. **29**, 3548 (1990).
[10] Dash, W. C., J. Appl. Phys. **29**, 705 (1958).
[11] Kuhr, W., and Yeng, E., Anal. Chem. **60**, 2642 (1988).
[12] Koehler, R., Luther, J. L., and Geist, J., Appl. Opt. **29**, 3130 (1990).
[13] Teague, E. C., Evaluation, Revision, and Application of the NBS Stylus/Computer System for the Measurement of Surface Roughness, NBS Technical Note 902 (1976).
[14] Putlock, M. J., and Thwaite, E. G., Elastic Compression of Spheres and Cylinders at Point and Line Contacts, National Standards Laboratory Technical Paper No. 25, CSIRO, Australia (1969).
[15] Tegart, W. J. McGregor, Elements of Mechanical Metallurgy, MacMillan, New York (1966), p. 92.
[16] Forsythe, W. L., Smithsonian Physical Tables, 9th Edition, Smithsonian Institution, Washington, DC (1954), p. 190.
[17] Landau, L. D., and Lifshitz, E. M., Theory of Elasticity: Volume 7 of Course of Theoretical Physics, 3rd Edition, Pergamon Press, New York (1986), p. 37.
[18] Lynch, C. T., Handbook of Materials Science, Volume III: Nonmetalic Materials and Applications, CRC Press, Cleveland, Ohio (1975), p. 160.

About the authors: Jon Geist is a physicist in the Semiconductor Electronics Division of the NIST Center for Electronics and Electrical Engineering; A. Russell Schaefer is a Senoir Scientist in the Electronic Vision Systems Division of Science Applications International Corporation; Jun-Feng Song is Head of the Surface Metrology Group of the Changcheng Institute of Metrology and Measurement in Beijing China, on leave as a guest worker in the Precision Engineering Division of the NIST Center for Manufacturing Engineering; Yun Hsia Wang is a chemical engineer in the same division of the same center; and Edward F. Zalewski is a Senior Staff Engineer in the Advanced Development Laboratory of Hughes Danbury Optical Systems.

Volume 95, Number 5, September-October 1990
Journal of Research of the National Institute of Standards and Technology
[J. Res. Natl. Inst. Stand. Technol. 95, 559 (1990)]

Hard X-Ray Microscope With Submicrometer Spatial Resolution

Volume 95 Number 5 September-October 1990

Masao Kuriyama, Ronald C. Dobbyn, Richard D. Spal, Harold E. Burdette, and David R. Black

National Institute of Standards and Technology,
Gaithersburg, MD 20899

A high-resolution hard x-ray microscope is described. This system is capable of detecting line features as small as 0.6 μm in width, and resolving line pairs 1.2-μm wide and 1.2-μm apart. Three types of two-dimensional image detectors are discussed and compared for use with hard x rays in high resolution. Principles of x-ray image magnification are discussed based on x-ray optics and diffraction physics. Examples of applications are shown in microradiography with fiber reinforced composite materials (SiC in Ti_3Al Nb) and in diffraction imaging (topography) with device patterns on a silicon single crystal. High-resolution tomography has now become a reality.

Key words: CCD detectors; fiber reinforced composite; microtomography; multilayer films; x-ray lens; x-ray microscope.

Accepted: August 17, 1990

1. Introduction

New engineering has embarked on a revolutionary period leading to new materials tailored from the atomic scale upward to achieve desired functional properties. Materials scientists are now earnestly designing a variety of new configurations of matter in response to industrial desires for sophisticated properties in high-performance applications. Advances in telecommunications and computers, for example, are attributed in part to the successful fabrication of novel microelectronic and photonic device materials designed on the atomic scale. Advances in the structural materials area have also been significant. Rapid solidification, for example, produces metals having excellent combinations of strength, ductility, and corrosion resistance. New processing techniques are quickly adopted to produce improved ceramics and composite materials for sophisticated and demanding applications. Composite materials are composed of dissimilar materials and are highly vulnerable to thermal and mechanical problems during processing.

Materials science that only emphasizes the designing and processing of new materials configurations, although important and necessary, is not quite adequate to advance materials engineering which industry requires to improve productivity and quality. The structure of all materials when formed is often non-uniform locally over regions of the order of a micrometer. Heterogeneity occurring as interdiffusion layers, grain boundaries, phase interfaces, interacting dislocations, local compositional variations, regionally homogeneous strains (residual stresses), and inhomogeneous strains, etc., often alters the performance behavior of materials from their originally designed applications. Thus, successful fabrication of such tailored materials having structures not found in nature

depends entirely on structural details and their influence on properties.

Material failures are often attributed, for example, to residual stresses that may have been produced during fabrication processes. Residual stresses can be measured in some cases with limited precision. However, those are normally represented by an average value over the entire specimen or in a rather large volume. Material failure happens at local catastrophic events. Residual stress values statistically averaged over a macroscopic volume have no significance in shedding light on failure events. In microelectronic devices, where different atoms are doped into mutually coherent layers, the thickness and shape of doped layers may change so as to degrade the functional properties originally designed. What we need is a measurement technique to "see" what happens locally and pinpoint local events of significance with high spatial resolution. Once we recognize such local phenomena, we can devise methods to accurately measure physical quantities which are necessary and meaningful in relation to each local event.

This paper describes one such measurement technique using x-ray imaging for detection of microstructural flaws and defects. X-ray beams can penetrate through materials to give two-dimensional images in transmission with high resolution. The current technique described in this paper is capable of detecting lines 0.6-μm wide, and resolving line pairs 1.2-μm wide and 1.2-μm apart [1,2]. Image data are digitized and displayed on a video monitor. An example of applications to fiber-reinforced-metal-matrix composites will demonstrate that the x-ray microscope gives two-dimensional microradiographic images in high resolution for the evaluation of processed materials. An appropriate set of such two-dimensional images can be used to construct a three dimensional image of the material with sufficiently high spatial resolution [3-8]. This is high-resolution x-ray tomography.

Furthermore, examples of applications to microelectronic materials indicate that the x-ray microscope will be a powerful tool, when combined with the diffraction imaging technique, to challenge interface problems from both the scientific and the engineering aspect.

2. Area Detectors for X-Ray Imaging

For microtomography, it is essential to obtain a set of two-dimensional images in transmission with high spatial resolution and excellent signal to noise ratio in either microradiography or diffraction imaging (topography). In order to achieve high spatial resolution, a microprobe x-ray beam can be employed, and the transmitted (or diffracted) beam is received by an open-window x-ray photon counter, as either the probe beam or sample is translated in two orthogonal directions to complete a two-dimensional scan. However, the preparation of a microprobe beam requires x-ray focussing, and beam divergence is inevitable. Images from objects in a sample of a finite thickness are, therefore, expanded and overlap with one another, thus deteriorating spatial resolution, and defeating the originally desired high-resolution imaging scheme. Micrometer resolution is unreachable. Besides, it is cumbersome to complete a single two-dimensional image by scanning.

Two-dimensional array detectors offer an efficient way to obtain two-dimensional images. A microprobe beam scan in combination with a two-dimensional detector still suffers the fundamental problem with divergence in producing high resolution images, no matter how small the pixel size of the detector. A parallel beam with a sufficiently large cross section is better suited for two-dimensional imaging with these detectors.

There are three major types of image detectors currently available [9,10]. One is the combination of an image intensifier stage and either a charge-injection-device (CID) type or a charge-coupled-device (CCD) solid state image detector [11]. The intensifier stage consists of a photocathode and a photoelectron multiplier, currently being microchannel plates. X-ray photons must be converted to visible light photons by a phosphor screen that is made of a fine powder or single crystal scintillator at the photocathode. This type of detector is called an indirect image detector. The second type that belongs to a class of direct image detectors is a vidicon detector [12-15], in which a photoconductive target is scanned by an electron beam. X-ray photons change a local electric resistance of the photoconductor giving rise to a different charge separation rate, locally, when the electron beam is rastered. The vidicon detector produces images of reasonable resolution, but is poor in sensitivity at low flux levels of photons. The third is a CCD detector itself, which should belong to the class of direct imaging, although the majority of applications to hard x-ray radiation (1 keV and above) favors the use of phosphors in front of CCD detectors to avoid radiation damage in the detector device.

The CCD is an analog shift register in which an entire sequence of charge packets created by photons can be shifted simultaneously along the surface of a silicon chip by applying clock voltages to overlying insulated gate electrodes. The electric charge varies from one packet to the next. The sequence of charge packets is scanned as they move past an output electrode connected to an on-chip amplifier. In the "frame transfer" type of scientific detectors, the CCD registers are illuminated directly by the (visible or x-ray) light from the imaged scene.

For high spatial resolution, the insertion of phosphors for the conversion of x-ray photons to visible photons is not desirable. X-ray sensitive direct imaging must be used with the CCDs. Direct x-ray bombardment, on the other hand, shortens the lifetime of CCDs due to radiation damage. However, as long as a monochromatic x-ray beam with limited brilliance ($\leqslant 10^{4-5}$ photons mm^{-2} s^{-1}) is used, the lifetime does not appear to be significantly affected. We have employed a direct imaging method with frame transfer CCDs for several years. The present CCD image detectors in our synchrotron radiation laboratory are described in the following.

The CCD substrate is 50 Ωcm doped Si, which is the diode structure type and is itself a complex integrated circuit. This CCD is designed to perform high-precision *light* (not x-ray) photometry, but can be used in the x-ray photon sensitive mode, that is, the direct conversion of x-ray photons to electric charges. The surface of the detector is illuminated by 5–20-keV x-ray photons. The pixels are arrayed to give the total area of 1.032×1.032 cm with 516×516 pixels; the pixel size is 20×20 μm (smaller pixel sizes may be available commercially). The capacity of each pixel is limited to the total of 250,000 electrons, which is equivalent to about one hundred 8-keV photons, assuming 100% quantum efficiency. The depletion depth is 15 μm. The quantum efficiency is measured to be about 20% at 8-keV photon energy, where charge collection outside the depletion region has been ignored.

Readout is in the frame transfer mode with the noise of less than 25 electrons per pixel, when the detector is thermoelectrically cooled to -40 °C. The dark current is negligible for exposures of several minutes. The readout charges are digitized to 14 bits by an analog to digital converter and stored in computer memory. The readout time is 20 μs per pixel, thus requiring 5 s for full array display. The minimum integration time is currently limited to 0.1 s by the shutter speed, while the maximum integration time is longer than 1000 s, only limited by the dark current level. Digital data are recorded on a hard disk or 1/2" 9 track magnetic tape and images can be processed on the spot. No significant degradation of image quality was observed during the first 6 months. After more than 1 year of operation, some slight local lightening of images has begun to be noticeable. No serious damage has been observed to affect the lifetime. In the present experience, it is not the number of photons, but the dose rate that seems to influence the increase of the dark current in certain regions of the detector. The performance of the present detector is summarized to be 25 line pairs/mm with less than 10^7 photons/cm^2 at 5 to 20 keV energy, being operated only in the photon counting mode.

Although CCD image detectors provide an ideal image data collection method with a sufficiently small pixel size, they are not quite good enough for high-resolution imaging. Various efforts to make the pixel size smaller, e.g., less than 1 μm, are expected to face tremendous technical problems. However, the spatial resolution, limited by the pixel size, can be improved by the direct image magnification technique which is equivalent to an optical lens capable of magnifying images [16,17]. The combination of a CCD detector and an x-ray image magnifier circumvents the current technical problems associated with the reduction of pixel size in CCD detectors and makes it possible to create an x-ray microscope with less than 1-μm resolution [18].

3. Imaging Principles of Magnification in Two Dimensions

When a monochromatic x-ray beam is diffracted from the surface of a highly perfect crystal and the diffracting planes in use are not parallel to the crystal surface, the diffraction is termed asymmetric. There are three aspects of asymmetric diffraction which are important for image magnification—beam magnification, reflectivity, and the beam acceptance angle of the crystal for the diffraction [16]. Figure 1(a) shows schematically the asymmetric diffraction geometry. An incident beam of x rays is magnified in one dimension (in the plane of diffraction) by a factor m given by

$$m = \sin\,\theta_{\rm out}/\sin\,\theta_{\rm in}, \tag{1}$$

where $\theta_{\rm in}$ and $\theta_{\rm out}$ are the angles between the crystal surface and the incoming and outgoing beams,

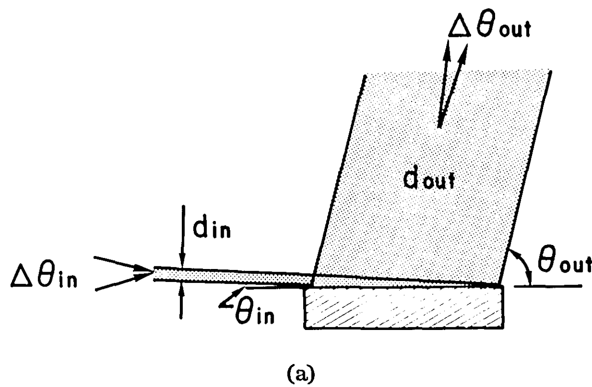

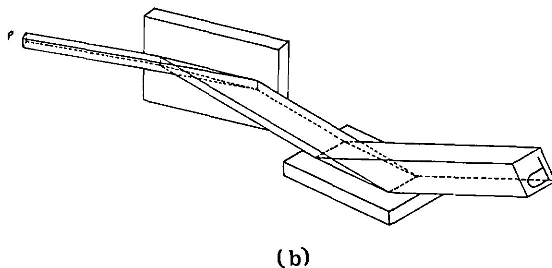

Figure 1. (a) Asymmetric Bragg diffraction showing one-dimensional magnification of an x-ray beam. The cross section of the incoming beam d_{in} is magnified by a factor m to produce the outgoing beam d_{out}, while the parallelism of the outgoing beam $\Delta\theta_{out}$ becomes more improved by the same factor m than the incoming beam $\Delta\theta_{in}$ (b) use of two asymmetric diffractions to obtain a two-dimensional (normal) magnification of images contained in an x-ray beam. Notice how the image "P" is magnified and inverted.

respectively. Obviously high magnifications are obtained when θ_{in} is very small. Alternatively the magnification factor can be written in terms of the Bragg angle for the diffraction θ_B and the angle α (cut angle) between the diffracting plane and the crystal surface as

$$m = \sin(\theta_B + \alpha)/\sin(\theta_B - \alpha). \quad (2)$$

Typically, Si (111) or (220) is used for the diffraction with various cut angle α's to provide appropriate ranges of magnification for different energies (wavelengths) of x rays. The practical levels of magnification range from about 10 to 200.

Dynamical diffraction effects that take place in perfect crystals are crucial to understanding the reason why such a geometrical principle leads to a working "magnifying lens" for x rays. In dynamical diffraction, a parallel beam of monochromatic x rays which strikes a crystal with an angle slightly off the Bragg condition can experience diffraction. The ratio of the diffracted total flux (photons/s) to the incident total flux is called the reflectivity and is a function of the deviation from the Bragg condition. This function is called the rocking curve. For a thick perfect crystal with no absorption, this ratio is unity for a range of angles centered about the Bragg condition (called the rocking curve width or range of reflection ω), and falls to zero rapidly for larger deviation from the Bragg condition. Thus, this angular range of reflection gives the beam acceptance angle of the crystal for the diffraction. Because the reflectivity is unity, regardless of the diffracting plane, the intensity (or brilliance) (photons/s·cm^2) of a parallel beam magnified in one dimension by asymmetric diffraction from a perfect crystal is decreased by a factor m^{-1} only because of the magnification of the beam area.

In dynamical diffraction from a perfect crystal, an incoming parallel beam is diffracted into a parallel beam. If the incident beam deviates from the Bragg condition by an angle ϕ, then the diffracted beam deviates from the Bragg diffracted direction by an angle $m^{-1}\phi$, since the Bragg law is "loosened" to restrict photon momentum conservation only in two dimensions, unlike the Bragg law for kinematical scattering which is equivalent to the photon momentum conservation law in three dimensions [19,20]. In reality, the incident x-ray beam has an angular divergence $\Delta\theta_{in}$ due mostly to the source size of x rays. For imaging, it is the source size rather than the beam divergence that is important. At a single point on the magnifying crystal, the source size is given by

$$\Delta\theta_{in} = H/L, \quad (3)$$

where H is the actual source height and L is the distance between the source and the single observation point. For $H = 150$ μm and $L = 15$ m, $\Delta\theta_{in}$ is about 2 arcsec. This source size can be made effectively smaller by inserting monochromator or x-ray optical systems in the optical path before the observation point. In such a case, the smaller apparent source size $\Delta\theta_{in}$, instead of eq (3), should be used in the following discussions.

Hence from the two-dimensional Bragg law, the total divergence of outgoing beams, $\Delta\theta_{out}$, becomes

$$\Delta\theta_{out} = m^{-1}\,\Delta\theta_{in}. \quad (4)$$

The higher the magnification, the more parallel becomes the outgoing beam. However, only those

rays accepted by the crystal within the angular range ω are diffracted with unity reflectivity. Rays striking the crystal outside the range ω are essentially not diffracted. Therefore, if $\Delta\theta_{in} < \omega$,

$$\Delta\theta_{out} = m^{-1}\Delta\theta_{in}, \quad (5)$$

and if $\Delta\theta_{in} \geqslant \omega$,

$$\Delta\theta_{out} = m^{-1}\omega = m^{-1/2}\omega_s, \quad (6)$$

where the acceptance angle (the rocking curve width) for asymmetrical diffraction is given by [21]

$$\omega = m^{1/2}\omega_s. \quad (7)$$

Here, ω_s is the acceptance angle for a symmetric diffraction for the same diffracting plane. For the 111 diffraction from Si with 8-keV radiation where ω_s is $\sim$5 arcsec (1 arcsec $= \pi/648\,000$rad), the maximum limit of $\Delta\theta_{out}$ is 1 arcsec for the case of magnification of 25, and $\Delta\theta_{out}$ can be smaller, if the incident beam is prepared to be less than 25 arcsec in divergence. The latter condition can easily be achieved with an appropriate monochromator system at synchrotron beam lines, discussed below.

The small value of $\Delta\theta_{out}$ guarantees the one-to-one correspondence of magnified images and the unmagnified images. This is an essential factor for making a "lens." In the case of a divergent incident beam, the intensity (brilliance) of the diffracted beam is usually called the integrated intensity because it arises from contributions over the entire acceptance angle region. The integrated intensity is proportional to ω and hence is proportional to the x-ray structure factor of a given magnifying crystal. However, if the divergence of the beam is less than ω as in the case of eq (5), the diffracted total flux (photons/s) is equal to the incident total flux and the diffracted intensity (photons/s cm^2) is decreased by only the geometrical factor m^{-1}.

Radiation from special x-ray sources, such as a synchrotron, has a powerful continuous energy spectral distribution—polychromatic (white) radiation. A "monochromatic" beam is normally prepared from such white radiation for a specific photon energy by an appropriate monochromator system. Since this beam is different in quality from the usual characteristic radiation, the effect of the radiation source size should be evaluated. The source size is defined as an angle subtended to view (through any additional x-ray optical system, such as a monochromator) the entire source from single points on the magnifying crystal. This angle now gives $\Delta\theta_{in}$ for the "monochromatic" beam prepared from white radiation. It should be noted that there is an almost uniform distribution of x-ray energies in ray trajectories within $\Delta\theta_{in}$. As in the case of the purely (say, characteristic) monochromatic beam discussed above, dynamical diffraction effects determine the energy pass-band for each ray trajectory in accordance with the acceptance angle range ω at a single point on the magnifying crystal. The average photon energy is, to be exact, different at individual single points due to the Bragg law.

The photon energy spread from one extreme edge of the beam to the other extreme is, for example, 40 eV using Si 111 asymmetric diffraction for a magnification of 25, assuming $\sim$40 arcsec as the maximum vertical divergence in the synchrotron radiation beam without the insertion of a monochromator. However, the insertion of the monochromator system (or the magnifying crystal) which utilizes asymmetric diffraction in the magnification mode reduces this divergence to a much smaller value, because the effective beam height viewed by such an asymmetric cut crystal (say, 5$\times$5 cm in size) for the diffraction is the length projected perpendicular to the beam due to the small grazing angle (say, 1°) which is about 1 mm and equivalent to $\Delta\theta_{in} = 10$ arcsec. The energy spread in actual use is thus determined by the two extreme edges of the monochromator crystal in the magnification mode and ultimately by the extreme two edges of the magnifying crystal. It should be noted, however, that this energy spread is evaluated from the beam *divergence*, not the source size.

On the other hand, the pass-band ΔE_{in} at the observation point is determined by the smallest of the pass-bands of crystals acting as x-ray optical elements in the optical path. This pass-band is described by the same ω as defined before for such a crystal, and is given by

$$\Delta E_{in}/E = \omega \cot \theta_B, \quad (8)$$

where θ_B is the Bragg angle for the x rays impinging on the observation point with the average energy E. For Si 111 diffraction with $m = 25$ using the 8-keV monochromatization, eq (8) gives $\Delta E_{in} = 3$ eV with $\omega \sim 25$ arcsec. Hence, even in a single ray trajectory of the beam path, the energy dispersion given by eq (8) is inevitable for the "monochromatic" beam, because the beam in this trajectory contains a continuous energy spectrum. Since $\Delta E_{out} = \Delta E_{in}$ in elastic scattering, $\Delta\theta_{out}$ is not affected. For the "monochromatic" beam, spatial resolution (particularly in diffraction imaging) is,

therefore, affected by the pass-band as well as the source size $\Delta\theta_{in}$. The dispersive arrangement of the monochromator system is required to reduce the pass-band.

If the x-ray energy of "monochromatic" beams can be tuned to any desired value, it is easily seen from eq (1) that the magnification factor of the same magnifying crystal can be varied at will, thus providing an image-zooming capability which is quite useful as described later.

For two-dimensional imaging, two one-dimensional magnifying crystals are arranged in two orthogonal directions to obtain an undistorted image of the sample which is placed in front of the magnifying crystals [16,22]. As illustrated in figure 1(b), detailed structures of the sample in the beam, shown as a little P, are now magnified, shown as a large P, and received by a CCD image detector. To guarantee undistorted images, care must be taken with the mutual alignment of these crystals. The plane of diffraction, defined as the plane containing the incoming beam and the normal to the diffracting plane (and also the outgoing beam) for each of the two successive diffractions must be orthogonal. Hence the first diffraction magnifies the beam horizontally and the second in a perpendicular direction. The distance between the sample and the "lenses" and between each lens must be minimized.

Since the reciprocity theorem holds for x rays, this system compresses the image in the demagnification mode. This mode of operation can provide very small, intense beams for other applications, including x-ray lithography.

4. A Hard X-Ray Microscope

The combination of the x-ray sensitive CCD detector and the x-ray image magnification technique now produces a hard x-ray microscope capable of resolving micrometer features [18]. A photograph of such a microscope is shown in figure 2. Asymmetrically-cut x-ray optical elements, A and B, are orthogonally aligned to function as the objective lenses of the microscope. Control of these optical elements is provided by their respective rotators, C and D, which are step motors driven with a step size of 0.9 arcsec. The beam containing the object image impinges, via the objective lenses, on an x-ray sensitive CCD array, E, which has been described previously. The carrousel mounted on the CCD camera head, E, holds a PIN (photo) diode, F, for alignment of the optical elements, A and B. The x-ray sensitive area of the PIN diode is 4×4 mm and is completely light-tight. Also mounted on the carrousel are a lead foil (0.15-cm thick) shutter, G, to protect the CCD camera, and a clear-line-of-sight aperture, H, to receive the image on the camera. The carrousel is controlled by the main computer which controls beam optics including a monochromator system. A shutter for the image exposure is separately set in front of the sample and is controlled by the CCD camera computer. The assembly of the camera head and the carrousel is mounted on a rotator, I, which rotates at various speeds with 60 arcsec/step. The entire microscope assembly is mounted on a rotator J (not shown), which is located on the left side of this figure. This rotator is similar to I. I and J are controlled by the main computer for beam optics.

The microscope is aligned for operation, using the main computer and the readout from the PIN diode, F. Scan-and-search-peak routines are applied to the first lens A and the second B in sequence by rotating the angular position of the PIN diode in appropriate scattering angles. During the operation, slits which are located in the monochromator system are set just inside the magnified image of the incident beam. After a series of routine operations are completed, the CCD area detector is rotated in place of the PIN diode. The refinement of the angles of A and B follows under the observation of the image on a monitor screen of the CCD detector to "tweak up" the microscope system.

For the orthogonality alignment of A and B, the importance of which was discussed earlier, insert a gold 25×25 μm grid mesh in the sample holder, and adjust the setting of B with respect to A, using an auxiliary dc motor connected to one of the arcs of the goniometer head that holds B, while viewing the two-dimensional image on the CCD monitor screen. Rows and columns of the mesh image must become perpendicular to each other. Obviously, when the magnification factor of the microscope is increased by increasing the x-ray energy, the orthogonality must be refined.

For the x-ray microscope, a parallel monochromatic incident beam is highly desirable. Such a beam can be prepared by an asymmetric-cut monochromator crystal with characteristic radiation [11], and by a monochromator system consisting of a crystal, functioning as a prism, and another crystal, functioning as a monochromator, with synchrotron radiation [2,23]. These crystals can be prepared for symmetrical and/or asymmetrical diffraction. In the present use, these crystals are aligned in the non-dispersive mode (note a com-

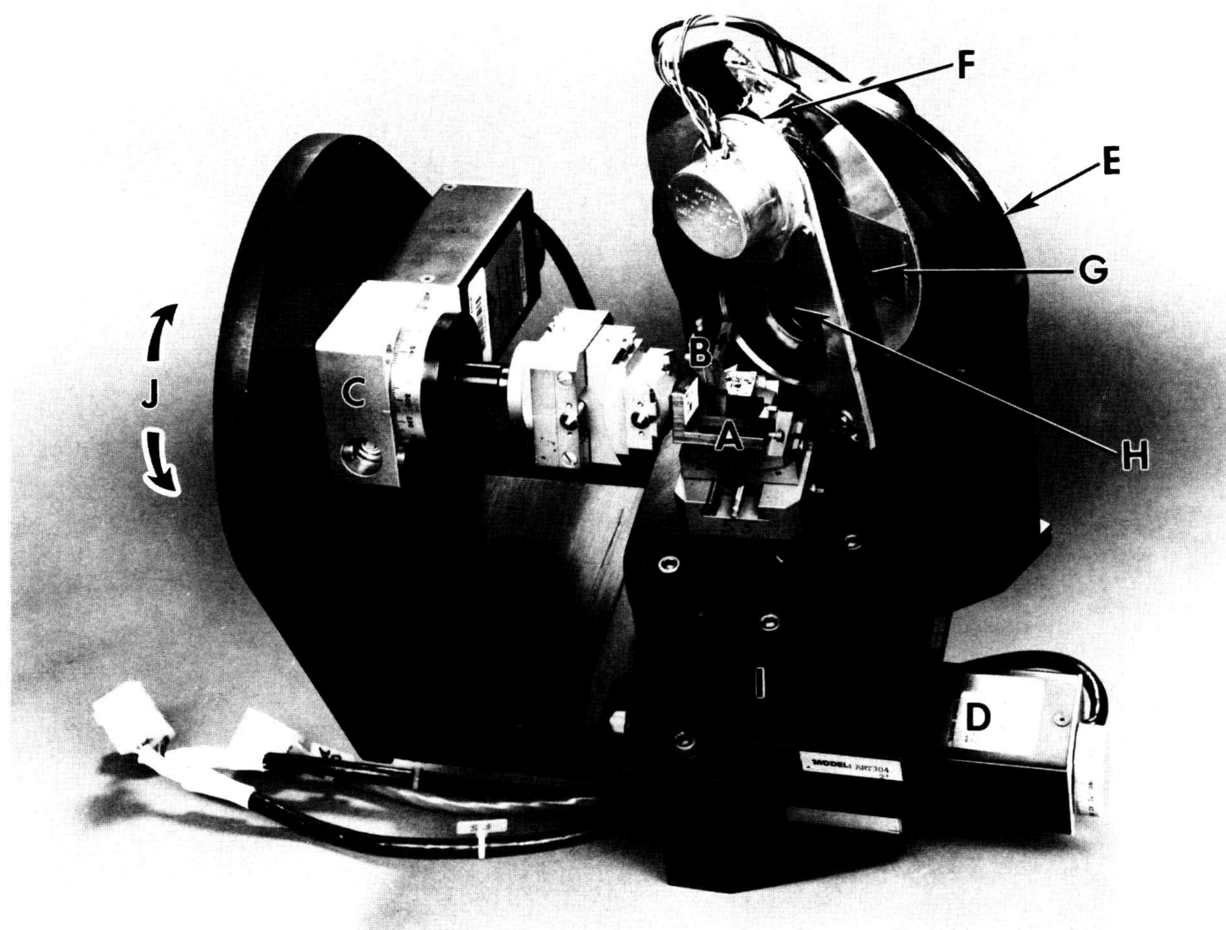

Figure 2. The high-resolution hard x-ray microscope capable of detecting submicrometer features. A and B are asymmetrically-cut x-ray diffraction optics controlled by microstepping rotators C and D. E is an x-ray sensitive CCD array. The carrousel mounted on the CCD camera head holds a photodiode F, a lead foil shutter G and a clear-line-of-sight aperture H. I is the rotator for the camera assembly and J is another rotator (not shown) that mounts the entire microscope assembly.

ment in a previous section). Preliminary calculations and experiments have indicated that the asymmetric (m) and asymmetric ($1/m$) arrangement for these crystals gives a better condition for photon flux, but the symmetric ($m=1$) and symmetric arrangement is superior with respect to spatial resolution.

Figure 3 shows what has been achieved with the x-ray microscope to date. This is a microradiographic image of a pattern of 0.15-μm thick Pd lines, of various widths, deposited on a 0.38-mm-thick Si wafer. The image was obtained at a magnification of 79 and a wavelength of 1.0 Å (12.25 keV). At this magnification, one CCD pixel represents 0.25 μm. The 11 evenly spaced lines are 1-μm wide and 50-μm long, with a center-to-center spacing of 5 μm. The single line above the 11 lines is 0.6 μm wide. The submicrometer feature is clearly visible for the first time. The image in figure 3 has been normalized to a blank field to correct for intensity variations due to blemishes in the magnifier crystals and non-uniform illumination. This is another advantage of CCD cameras which store digital image data for further image processing and quantitative analyses. Figure 4 shows a plot of the average pixel intensity for each (horizontal) row of pixels, superimposed on the view of figure 4. The dips in intensity for the 11 1-μm lines have an average full-width half maximum (FWHM) of 1.4 μm, while the dip (shown on the left) for the 0.6-μm line has a FWHM of 1.0 μm, in good agreement with the predictions of geometrical optics. However, the secondary dip between each 1-μm primary dip cannot be explained by geometrical

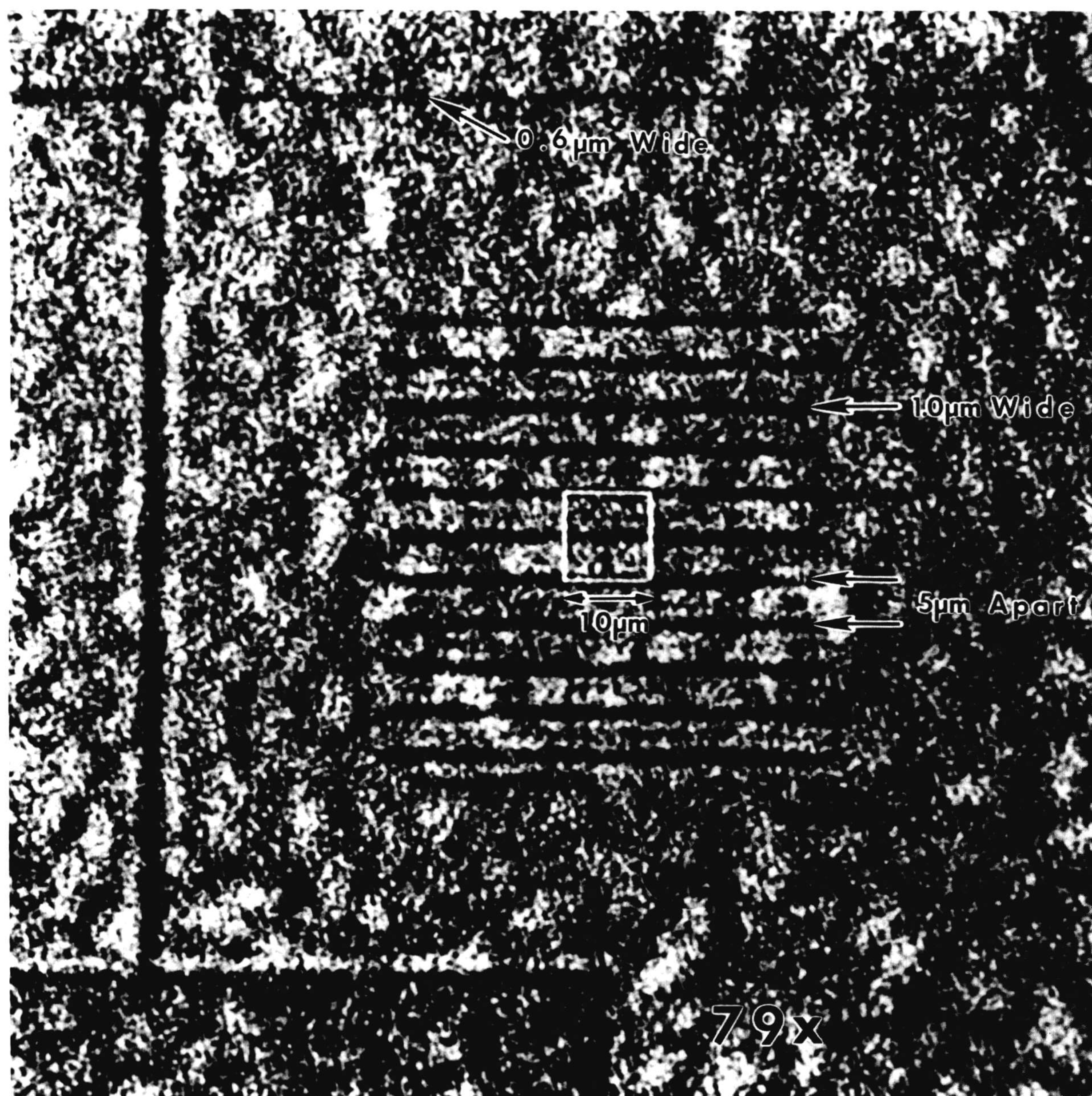

Figure 3. A radiographic image of a pattern of Pd lines on Si. This image was obtained with a magnification of 79 and a wavelength of 1.0 Å (12.3 keV). At this magnification, one CCD pixel represents 0.25 µm.

optics, and are, at present, attributed to Fresnel diffraction.

For the evaluation of spatial resolution, line pairs of various widths and spacings should be used. Figure 5 (a), (b), and (c) show the images taken from Pd line pair patterns with the microscope operated at a magnification of 79× at 12.25 keV. The images of line pairs, (a) 1.4-µm wide and 1.4-µm apart and (b) 1.2-µm wide and 1.2-µm apart, clearly show well-resolved patterns, while the image of line pairs, (c) 1.0-µm wide and 1.0-µm apart, is hardly discernible. Although the microscope is able to show isolated submicrometer features as evidenced in figures 3 and 4, the resolution of the microscope should be considered to be 1.2-µm. It should be noted that the Si substrates on which Pd line pair patterns were prepared show many features of microstructure and may have degraded the crispness of the patterns and their images particularly when the features become less than 1 µm.

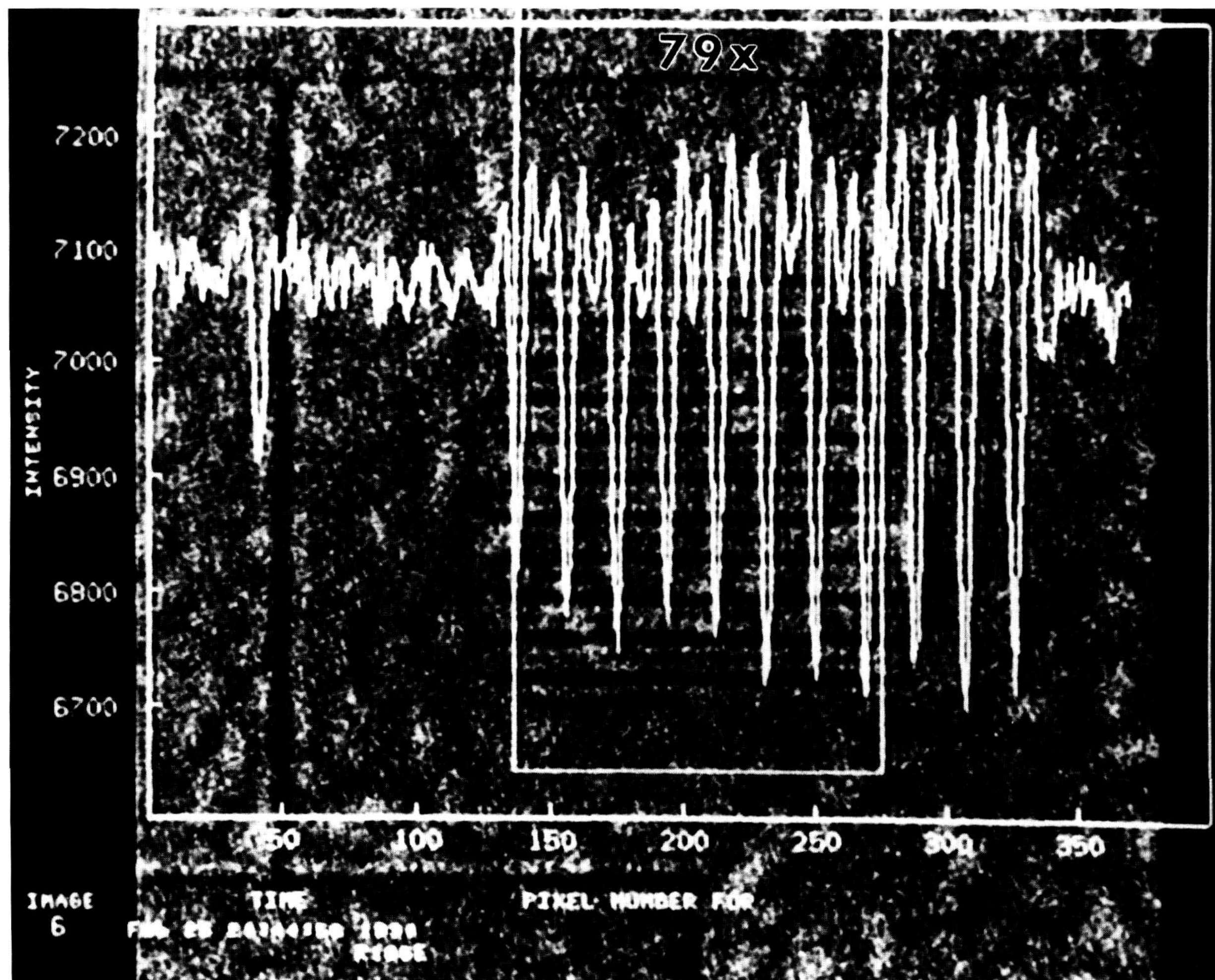

Figure 4. A plot of the average intensity. The average pixel intensity for each horizontal row of pixels is plotted, superimposed on the view seen in figure 3.

The synchrotron beam line that was used in this work has not yet been equipped with a monochromator system to control the horizontal source size. In this beam line, the horizontal source size of the synchrotron radiation is twice as much as the vertical source size. To evaluate the source size effect, the Pd pattern used in figure 4 was placed in two orthogonal orientations. The pattern object was placed 4 mm from the edge of the first lens A. Figure 6 (a) and (b) show the images taken at a magnification of 79×, (a) the line pattern being placed horizontally to detect the vertical source size effect and (b) being placed vertically for the horizontal source size effect. Also shown are the plots of the average pixel intensity for each horizontal and vertical row of pixels, respectively. The broadening or blurring of image (b) is easily recognizable, indicating that the width of each line image is twice as much as those observed in figure 6 a in agreement with the prediction based on the source size of the synchrotron radiation in use.

5. Applications

In the microradiographic mode, the hard radiation microscope has many applications in the detection of flaws and defects in all sorts of materials including advanced structural and functional material components, dental, medical and biotechnological materials and in the development of new processing and chemical treatments for these materials, as examples in the dental research area indicate [24,25].

An example of straightforward applications to microradiography is the evaluation of processed

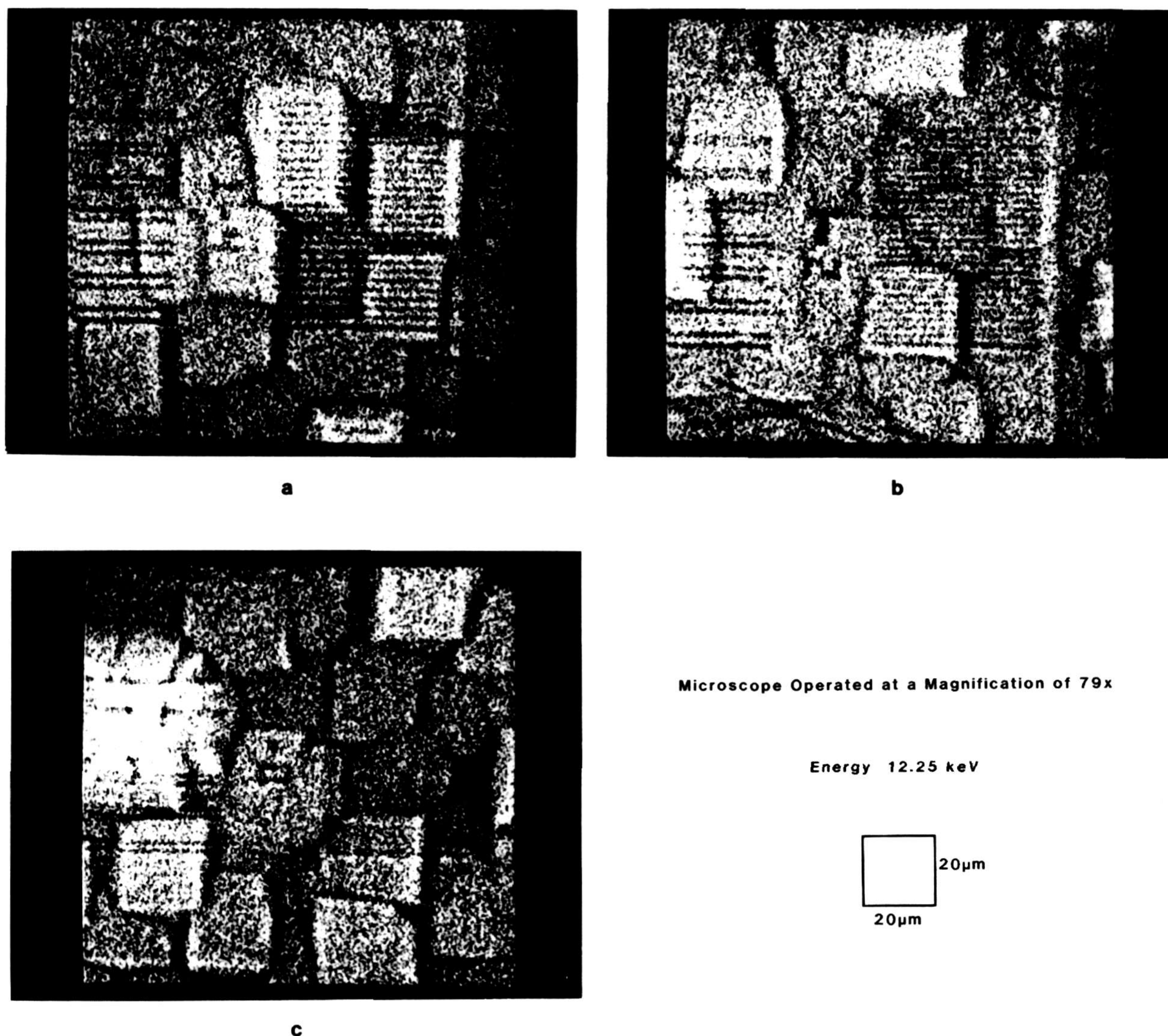

Figure 5. Images of various line pair patterns with the microscope operated at a magnification of 79× at 12.25 keV, (a) 1.4-μm wide and 1.4-μm apart, (b) 1.2-μm wide and 1.2-μm apart, and (c) 1.0-μm wide and 1.0-μm apart.

materials. Here a reinforced Ti_3Al Nb metal matrix composite material is used to image a single SiC fiber with the microscope operated at a magnification of 55× and 12.15 keV. The thickness of the sample is about 1.7 mm. The x-ray beam is transmitted through the sample in a direction parallel to the fiber axis. Figure 7 shows a microradiograph of a single fiber, roughly 130 μm in diameter, surrounded by a Ti_3Al Nb matrix. A graphite core is at the center. The detailed structure of SiC appears as a bundle composed of layers with great clarity; no pixel images are registered discernibly. The CCD pixel size is equivalent to 0.45 μm under this magnification.

As in the operation of an optical microscope, the zooming capability of the x-ray microscope is indispensable to first locate such a small object in a wide field of view, using a lower magnification, and then to increase a magnification of the microscope to desired levels. Also necessary is the capability to manipulate the sample orientation while viewing images. In the present application to a single fiber, it is difficult to determine when the x-ray beam is really parallel to the fiber. Figure 8 (a), (b), and (c) show three different views of the fiber with an increment of 0.1° inclined from the x-ray beam. Each shows slightly different aspects of the SiC layers.

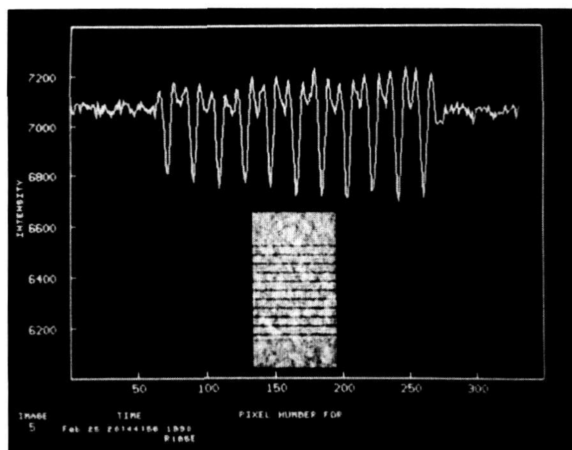

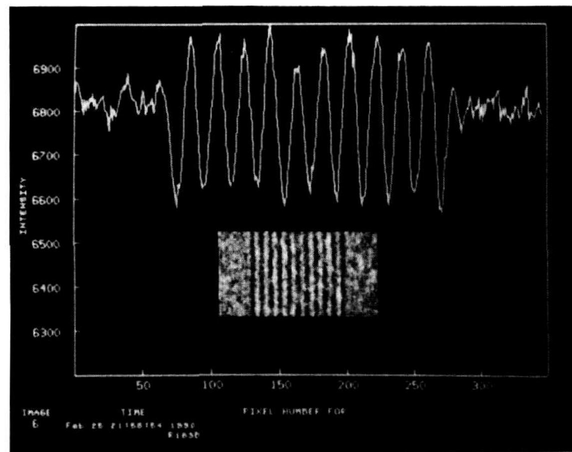

Figure 6. The effect of the vertical and horizontal source sizes. Images were obtained at a magnification of 79× and 12.25 keV, (a) the line pattern is oriented horizontally for the vertical source size effect, (b) oriented vertically for the horizontal source size effect.

The application of this microscope is not limited to microradiography. Device features used in microelectronics and photonics are prepared by a sequence of depositions of a few atoms at a time and doping in appropriate time intervals. These features are almost perfectly lattice-matched to each other and to the substrate. It is difficult to create images with good contrast from mutually coherent features consisting of similar materials. The physical shape of these features, if visible in microradiography, may not give clues for the understanding of phenomena actually taking place. For example [2], figure 9 shows a microradiographic image with 22× magnification at 8.3 keV of the Pd pattern shown in figure 3. This shows the physical shape of object features. Since Pd is more absorbing than the Si substrate, contrast is good.

Because this substrate is a single crystal and the Pd pattern is epitaxially coherent it can be brought into a Bragg condition. In transmission two diffracted images appear [1]: one in the forward direction of the incident beam is called the O-beam image, and the other in the Bragg diffracted direction is called the H-beam image. Without moving the microscope from the position set for microradiography, the O-beam image can be viewed on the monitor screen merely by rotating the sample. Figure 10 shows the O-beam image taken in transmission for the 220 diffraction with the microscope set for the same magnification, 22× at 8.3 keV, as figure 9. In dynamical diffraction, a strain field acts as a scattering center and produces a black and white image [1]. The black/white contrast is expected to be inverted in the H-beam image. This contrast inversion has been confirmed by moving the microscope to view the H-beam image. Therefore, there are interfacial strains around the features. The direction of the atomic shifts in these strained areas can be analyzed in detail.

The ability to reveal strain features in diffraction imaging along with micrographic views of the object can now be utilized to a full extent not only in a qualitative but in a quantitative way to study interface problems. The above example with the Pd pattern opens up an opportunity to challenge the problems associated with advanced microelectronic devices, as described in a previous paper [18]. Since these materials are often highly perfect single crystals, x rays can pass through more than one-half millimeter thick samples, almost regardless of x-ray energy, when the sample is set for Bragg diffraction due to the anomalous transmission or Borrmann effect [1,26,27]. In this mode of imaging—phase contrast microscopy, the important feature is that those transmitted images in diffraction represent true transverse cross sectional images of the layers [1,18].

As demonstrated so far, the hard x-ray microscope is indeed capable of producing two-dimensional images with 1 μm or less spatial resolution in microradiography and diffraction imaging. A set of two-dimensional images is easily collected as a function of rotational angle, as shown in figure 8. A tomographic image can be reconstructed from this set of high-resolution two-dimensional images. To reconstruct a three-dimensional image with 1-μm spatial resolution, the increment of the sample rotational angle is, for example, roughly 0.8° for a

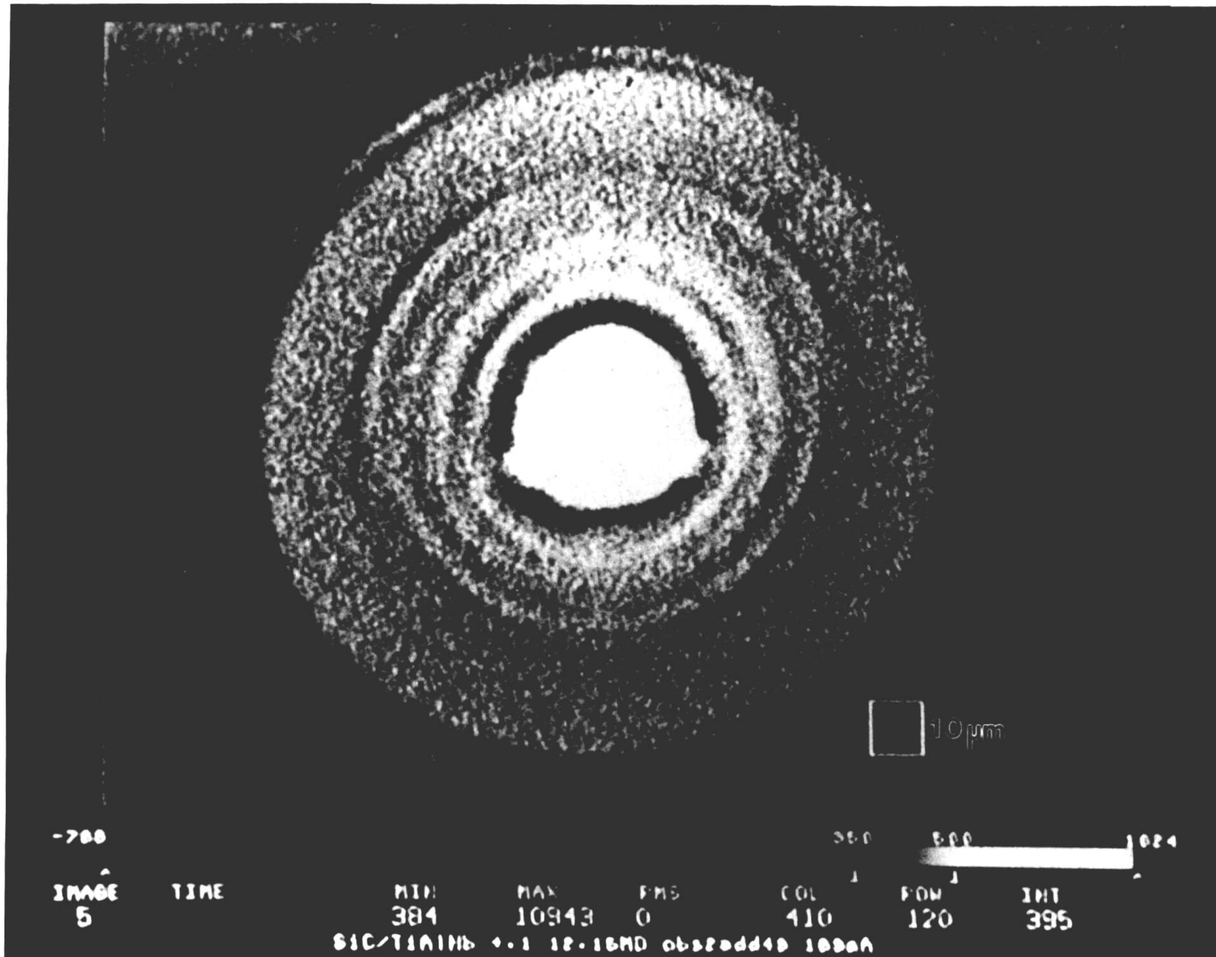

Figure 7. An image of a single SiC fiber in a reinforced Ti_3Al Nb metal matrix composite at a magnification of 55× and 12.15 keV. The thickness of the sample is about 1.7 mm. The diameter of the fiber is about 130 μm. A graphite core is at the center.

cylindrical sample 100 μm in radius. Obviously, the larger the sample, the smaller the required angular increment. The rotator currently in use can easily provide this capability with a well-fixed rotational center controlled by a set of submicrometer translators. Algorithms are available for tomographic reconstruction. A working microtomographic system capable of reaching 1 μm or less spatial resolution has become a reality with the hard radiation microscope described in this paper.

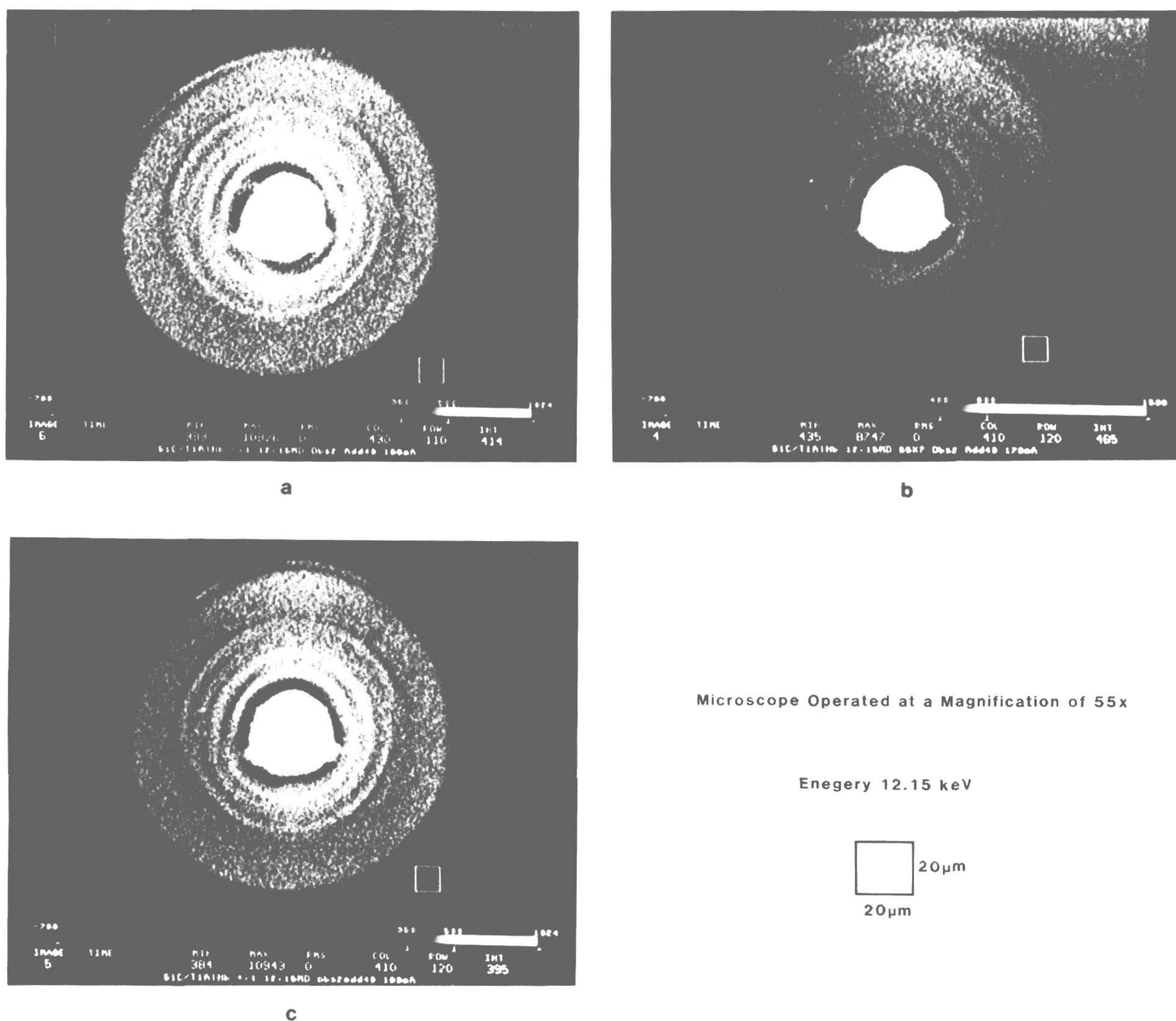

Figure 8. Three views of the SiC fiber at a magnification of 55× and 12.15 keV. The sample is oriented (a) −0.1°, (b) 0.0°, and (c) +0.1° off from the x-ray beam direction.

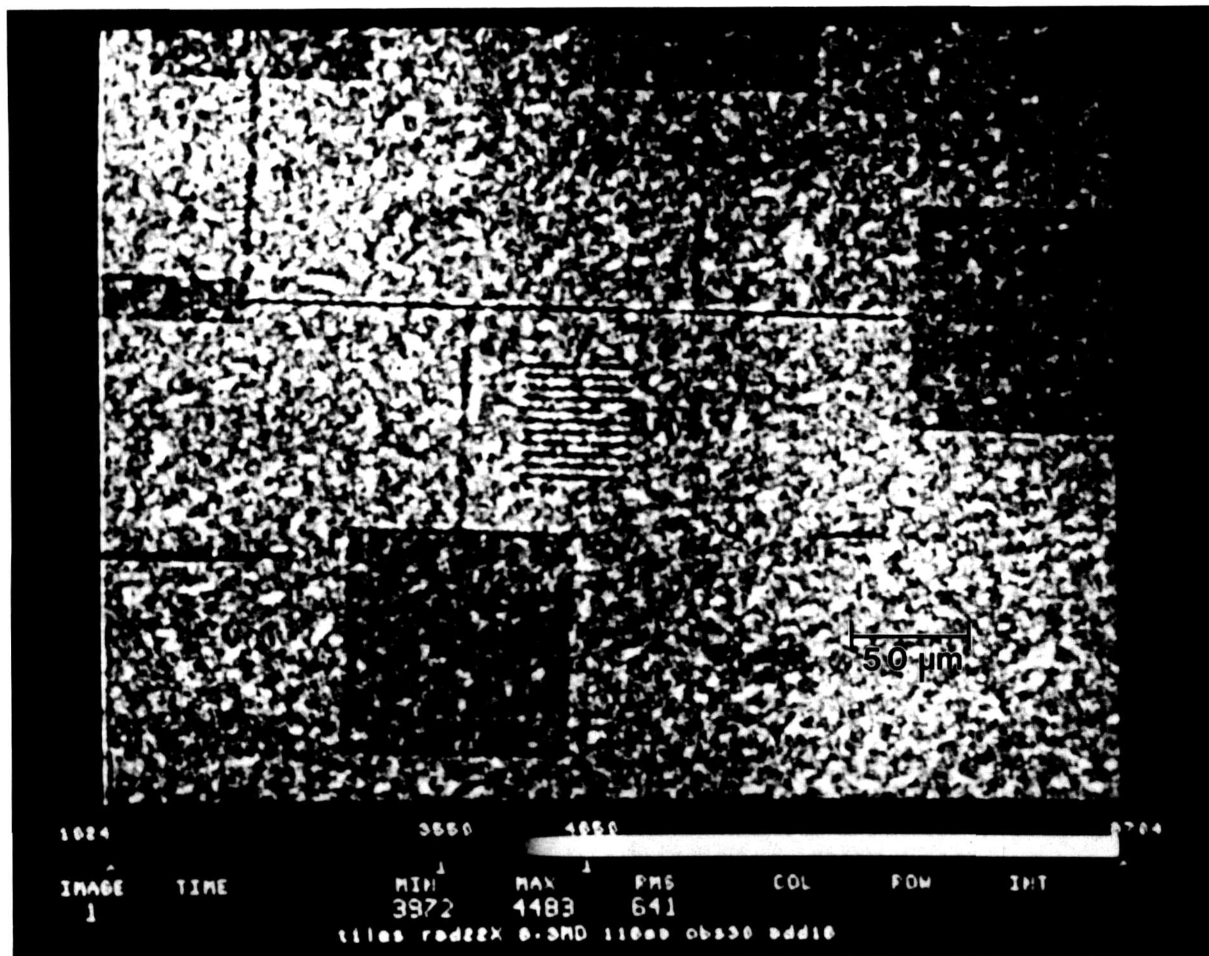

Figure 9. A radiographic image of another section of Pd pattern with a magnification of 22× at 8.3 keV.

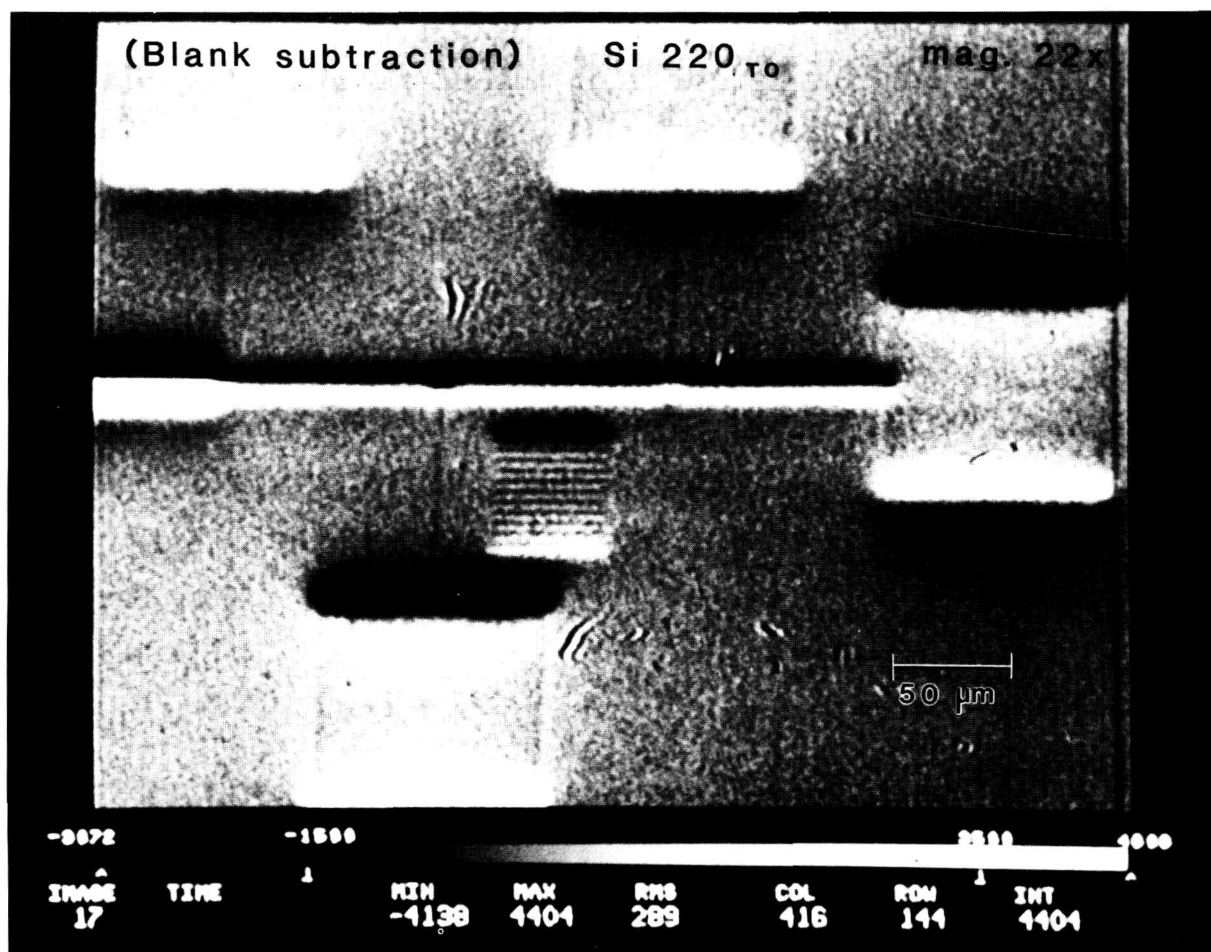

Figure 10. The O-beam image of the Pd pattern for the 220 diffraction in transmission with the same magnification of the microscope as the companion radiographic image in figure 9.

Acknowledgment

The authors thank I. C. Bassignana and S. Eicher, Bell-Northern Research Ltd, for Pd pattern samples.

7. References

[1] Kuriyama, M., Steiner, B. W., and Dobbyn, R. C., Ann. Rev. Mater. Sci. **19**, 183 (1989).
[2] Kuriyama, M., Proc. of the International Symposium on X-ray Synchrotron Radiation and Advanced Science and Technology, the Institute of Physical and Chemical Research (RIKEN), Tokyo (1990) p. 109, and Nucl. Instrum. Meth. (1991) in press.
[3] Bowen, D. K., Elliott, J. S., Stock, S. R., and Dover, S. D., Proc. SPIE **691**, 94 (1986).
[4] Flannery, B. P, Deckman, H. W., Roberge, W. G., and D'Amico, K. L., Science **237**, 1439 (1987).
[5] Sakamoto, K., Suzuki, Y., Hirano, T., and Usami, K., Japn. J. Appl. Phys. **27**, 127 (1988).
[6] Kinney, J. H., Johnson, Q. C., Nichols, M. C., Bonse, U., Saroyan, R. A., Nusshardt, R., and Pahl, R., Rev. Sci. Instrum. **60**, 2471 (1989).
[7] Hirano, T., Usami, K., and Sakamoto, K., Rev. Sci. Instrum. **60**, 2482 (1989).
[8] Kinney, J. H., Stock, S. R., Nichols, M. C., Bonse, U., Breunig, T. M., Saroyan, R. A., Nusshardt, R., Johnson, O. C., Busch, F., Antolovich, S. D., J. Mater. Res. **5**, 1123 (1990).
[9] Green, R. E., Jr., Adv. X-Ray Anal. **14**, 311 (1971) and **20**, 211 (1977).
[10] Rose, A., and Weimer, P. K., Physics Today, September (1989) p. 24.
[11] Boettinger, W. J., Burdette, H. E., Kuriyama, M., and Green, R. E., Jr., Rev. Sci. Instrum. **47**, 906 (1976).
[12] Chikawa, J., and Fujimoto, I., Appl. Phys. Lett. **13**, 387 (1968).
[13] Chikawa, J., Real-Time Radiologic Imaging: Medical and Industrial Applications, ASTM Special Tech. Publ. 716, ASTM, Philadelphia (1980) p. 209.

[14] Hartmann, W., Markewitz, G., Rettenmaier, V., and Queisser, H. J., Appl. Phys. Lett. **27**, 308 (1975).
[15] Hartmann, W., Real-time Radiologic Imaging: Medical and Industrial Applications, ASTM Spec. Tech. Publ. 716, ASTM, Philadelphia (1980) p. 201.
[16] Boettinger, W. J., Burdette, H. E., and Kuriyama, M., Rev. Sci. Instrum. **50**, 26 (1979).
[17] Kuriyama, M., Boettinger, W. J., and Burdette, H. E., Real-time Radiologic Imaging: Medical and Industrial Applications, ed. by Garrett, D. A., and Bracher, D. A., ASTM Spec. Tech. Publ. 716, ASTM, Philadelphia (1980) p. 113.
[18] Kuriyama, M., Dobbyn, R. C., and Spal, R. D., Rigaku J. 7 (1990) in press.
[19] Kuriyama, M., and Boettinger, W. J., Acta Cryst. **A32**, 511 (1976).
[20] Ashkin, M., and Kuriyama, M., J. Phys. Soc. Japn. **21**, 1549 (1966).
[21] For example, Warren, B. E., X-Ray Diffraction, Addison-Wesley, Reading, MA (1969) p. 324.
[22] Boettinger, W. J., Dobbyn, R. C., Burdette, H. E., and Kuriyama, M., Nucl. Instrum. Meth. **195**, 355 (1982).
[23] Spal, R., Dobbyn, R. C., Burdette, H. E., Long, G. G., Boettinger, W. J., and Kuriyama, M., Nucl. Instrum. Meth. **222**, 189 (1984).
[24] Takagi, S., Chow, L. C., Brown, W. E., Dobbyn, R. C., and Kuriyama, M., J. Dental Res. **64**, 866 (1985).
[25] Kuriyama, M., Dobbyn, R. C., Takagi, S., and Chow, L. C., Med. Phys. **14**, 968 (1987).
[26] Borrmann, G., Phys. Z. **42**, 157 (1941).
[27] Kuriyama, M., Phys. Status Solidi **24**, 743 (1967).

About the authors: *Masao Kuriyama is leader of the Synchrotron Radiation Group of the Materials Science and Engineering Laboratory at NIST. Ronald C. Dobbyn, Harold E. Burdette, and David R. Black are scientists in that group. They divide their time between Gaithersburg and the National Synchrotron Light Source at Brookhaven National Laboratory, where they have specially instrumented a beam line to perform materials science work such as described in the article. Richard D. Spal is a scientist in-residence at the National Synchrotron Light Source at Brookhaven National Laboratory and provides on-site maintenance of the beam line.*

Volume 95, Number 5, September–October 1990
Journal of Research of the National Institute of Standards and Technology

[J. Res. Natl. Inst. Stand. Technol. **95**, 575 (1990)]

Software Techniques to Improve Data Reliability in Superconductor and Low-Resistance Measurements

Volume 95 | Number 5 | September–October 1990

L. F. Goodrich and A. N. Srivastava

National Institute of Standards and Technology,
Boulder, CO 80303

Software techniques have been developed to take low-amplitude data in various patterns, assign a figure of merit to a set of data readings, edit data for erroneous readings (or other experimental variations), and to alert the experimenter if the detected errors are beyond the scope of the software. Erroneous voltage readings from digital voltmeters, intermittent electrical connections, and an array of similar variations in data have been detected through the use of a data editor. The fixed-limit data editor removes readings that are inconsistent with the distribution of the majority of the data readings. The frequency of erroneous readings from a particular digital voltmeter ranges from 1 error per 100 000 readings to 1 error per 100 readings. The magnitude of the error can be as large as 3% of full scale with a zero volt input to the voltmeter. It may be necessary to have multiple meters measuring voltages in the same circuit in order to generate these erroneous readings. A systematic study was performed on the occurrence of the internally-generated erroneous voltmeter readings, and it was determined that the amount that a reading was in error scaled with one of a few parameters. The software techniques described here have been used in a variety of measurements, such as resistance-versus-temperature measurements made on cryoconductors or superconductors, and voltage-versus-current measurements made on superconductors to determine the critical current.

Key words: critical current; cryoconductor; editor; errors; figure of merit; measurement system; outlier; resistivity; software; statistics; superconductor.

Accepted: August 13, 1990

1. Introduction

In this age of computerized data acquisition, a computer and digital voltmeter[1] are found in most modern measurement systems. These innovations have removed some of the subjective screening of data (that is, the determination of the validity of a set of data readings) which took place earlier with little forethought. Computers have also made the collection of vast amounts of data possible in a short period of time. While this is often desirable, the computer may give a number with as many digits as desired, with unknown significance. Thus, it is conceivable that the numerical output of a computer could be a mixture of both erroneous and correct data. Objective screening is difficult to introduce into software because of the variety of circumstances under which data acquisition takes place. Also, different levels of variation of the data

[1] Certain commercial equipment, instruments, or materials mentioned in this paper might be indirectly identified by their particular properties. Such identification does not imply recommendation or endorsement by the National Institute of Standards and Technology, nor does it imply that the materials or equipment identified are necessarily the best available for the purpose.

readings tend to complicate the software. Since implementing screening software of this type is rather complicated, there is always the chance that the software will create errors. Therefore, a simple and expedient method to screen data is needed to improve data reliability.

In order to obtain reliable data, hardware tests of software techniques have been developed. These tests can be used to determine the integrity of both the software techniques and the hardware components of a measurement system [1]. One test that may be used to judge the performance of the software and the hardware components of a measurement system is the ability of the system to measure a null (zero) voltage. This is often quite challenging when voltage measurements are being made on superconductor samples. In this case, the ability of the system to measure zero volts is essential to obtain realistic and reliable data.

Another test that would investigate different aspects of the measurement system can be performed with the use of a dummy sample with finite resistance. In some cases, the system may measure a null voltage satisfactorily, but it may not measure a low-amplitude signal accurately. Null and finite resistance tests have proven to be invaluable in determining the integrity of the software and hardware components of a measurement system against thermal electric noise, common mode, random occurrences, and ground loop voltages.

Time constraints are often imposed upon the experimenter. These constraints may be present due to a combination of monetary and experimental problems. There are many relevant time constants of an experiment, such as the time needed to take a single reading from a meter, the thermal time constant, the system settling time, and the system drift time. Data acquisition would be a relatively simple task if time constraints of this type were not problematic. Since experimental constraints are usually not at nominal levels, efficient time management is of utmost importance.

The techniques described here have been useful in several types of low voltage measurements [2,3,4,5]. For example, they have been used to detect such experimental events as erroneous voltage readings, intermittent electrical connections, sample motion in a magnetic field, rapid changes in temperature, changes near a temperature transition on a superconductor, lack of thermal equilibrium, periodic and random electrical noise, and movements of humans near a sensitive experiment.

The software is designed to alert the operator (either through audio or visual means) if a problem is detected during data acquisition, thus making it easier to deduce the source of the problem and implement a solution. The software can also be designed to flag data for future editing, or in some cases, throw it away and attempt to take data again. In some cases, for example near temperature transitions, it is beneficial to store all of the measurements since data subsequently acquired may not have a smaller variation. It may also happen that the readings that were thrown away were the most interesting. In other cases, it may be necessary to perform repeat determinations until the variation of these data lies within the preset limits. In general, readings should not be eliminated from a data set without due consideration. Eliminating valid readings will affect uncertainty calculations.

The reliability of an experiment can be significantly affected by the pattern in which data is acquired. For example, in resistance-versus temperature-experiments, sample temperatures and transient settling times should be taken into consideration when determining the pattern in which data is to be acquired. Experiments have been performed in order to measure resistance as a function of temperature with transport dc current on superconductors, copper, copper alloy, and high strength, high conductivity metals. In these experiments, a forward-reverse-forward current data pattern was used. The pattern in which data is acquired can significantly change from experiment to experiment. For example, if voltage-current (V-I) measurements are being made on a superconductor, it is advantageous to create a data pattern generator which calculates current set-points that result in equally-spaced voltage readings on a logarithmic scale. This type of current distribution is necessary in order to fully characterize the extremely nonlinear voltage-current characteristics of a superconductor.

1.1 Terminology

Throughout this paper, a "reading" is defined to be a single measurement taken from a digital voltmeter. A set of readings is said to be "edited" if any erroneous readings have been removed from the set. A "data point" is a numerical compilation of a number of edited readings (an average of edited readings, for example), and a "data set" is simply a collection of related datapoints.

A set of "parallel readings" (as opposed to a set of consecutive readings) refer to a set of single readings that are taken in a sequential manner from different meters. For example, given three meters

X, Y, and Z, a parallel reading pattern would be X(1), Y(1), Z(1); X(2), Y(2), Z(2); ...; X(n), Y(n), Z(n), where n denotes the number of readings taken per meter. A set of "consecutive readings," on the other hand, refer to a set of readings that are consecutively taken from different meters. In this case, the reading pattern would be X(1), X(2), ..., X(n); Y(1), Y(2), ..., Y(n); Z(1), Z(2), ..., Z(n).

A "data run" (or simply a "run") is a compilation of several data sets taken under various experimental conditions, for example, voltage readings at different temperatures, or critical current measurements at different magnetic fields. A post-run analysis may be desired to further analyze both the raw readings as well as the edited data sets.

A reading is said to be an "outlier" if it is inconsistent with the distribution of the majority of the readings. The difference between the correct reading and the outlying reading is called the "error." A "data editor" is used to determine whether or not an outlier has occurred.

A "measurement system" consists of both hardware and software components. A block diagram of one of the measurement systems used in this experiment is shown in figure 1.

2. Software Techniques

The function of the software described in this paper is threefold. It can be used to assign a figure of merit to a particular data point, implement a particular pattern of data acquisition, and determine whether or not an outlier occurred. The software has been designed to provide feedback to the user (through audio and visual methods) in the event that an outlier occurred, or if the standard deviation of the majority of the readings is high. Software of this type is important not only for the determination of an occurrence of an erroneous voltage reading—it can also be used to correlate the experiment's environment with an error in the data readings. It is necessary to design software editors to detect the presence of an outlier since outliers occur somewhat randomly, and are perhaps the most common source of errors in experimental work. Although the software discussed here is general in design, it has been empirically developed for superconductor and low-resistance measurements. More sophisticated statistical methods may be available [6], but the editor described here is simple, expedient, and sufficient for this type of measurement.

Given the set of time constraints under which many experiments are performed, it is prudent to do computations, generate a printout and a plot during settling times. The ratio of the time used to acquire data to the time needed for the measurement system to settle must be considered. It is inefficient to have a data acquisition time that is much less than the system settling time. A real time data editor must be simple enough so that the computation time is small, yet effective enough so that outliers and experimental variations in the data can be identified and the experimenter alerted.

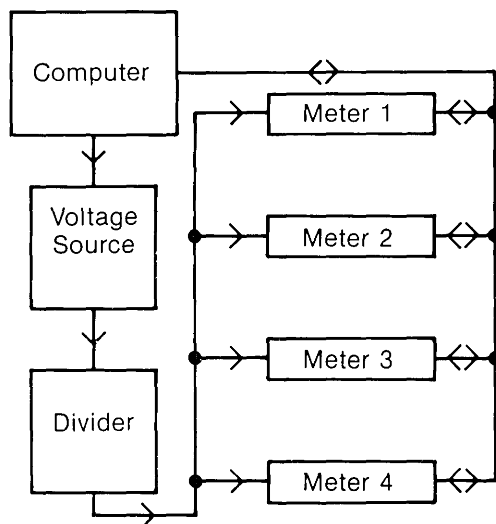

Figure 1. Block diagram of measurement system.

2.1 Fixed Limit Editor

The fixed limit editor may be used for routine measurements under relatively low or known noise conditions. The editor limits would define an upper and lower bound for the acceptable variations in data readings.

After a collection of readings has been taken during an experiment, it is stored in matrix form on a permanent mass storage medium for future use (perhaps by a post-run analysis routine). One column of the reading matrix is extracted and stored in vector form. The readings in this vector are sorted from the smallest value to the largest value.

The preset editor limits are applied about the median of a sorted reading vector. Those readings that are within the upper and lower limits of the editor are used to calculate the average and the standard deviation of the edited readings. Any outliers that may be present in the readings appear

either above the upper editor limit, or below the lower editor limit. If the number of readings outside the bounds of the editor is greater than the larger of two readings, or 3% of the total readings, the user should be alerted either through audio or visual means. If a similar number of readings is consistently found to be outside the bounds of the editor, the user should increase the allowed range for the readings, if they are consistent with the distribution of the majority of the readings.

Before the actual experiment is performed, a preliminary experiment should be conducted to determine a typical standard deviation using a large number of readings per data point. The preset editor limits should be five to ten times the standard deviation of these readings. In superconductor measurements, the extremely nonlinear voltage-current (*V-I*) characteristics can result in an increase in signal variation with voltage. In this case, two data points should be considered: zero current, and a current that results in a sample voltage that is near the typical maximum. A subsequent calculation of the standard deviation of the voltage readings would lead to appropriate editor limits. This preliminary experiment should be conducted periodically so that any changes in the measurement system can be accounted for in the editor limits. The time constants of the experiment can also be determined during this preliminary experiment. During the actual experiment, the number of readings that are taken per point could be reduced, so that the experiment can be performed more efficiently. During these measurements, it is important to monitor the relationship between the standard deviation and the editor limits to determine changes in noise conditions.

2.2 Data Patterns and Figures of Merit

Depending upon the type of measurements being made, the *pattern* in which data are obtained may significantly affect the ability of the experimenter to analyze the data and perform any corrections that may be necessary. Thus, it is important to implement a pattern suitable to the type of experiment being performed [5]. This reduces the number of assumptions that the experimenter must make in the data analysis.

In resistance-versus-temperature measurements on superconductors, copper, and copper alloys, a data pattern as depicted in figure 2 was incorporated in the software. A four-wire measurement with current reversals to correct for thermal-electric and offset voltages was used. This assumes that the current is constant and has a known magnitude. The software was designed to measure voltage, temperature, and time in parallel.

In the resistance-versus-temperature measurements, the data pattern of forward-reverse-forward current was used. In this data pattern, current is first injected into the sample in one direction (defined as the forward direction), and a number of voltage readings from the voltmeter are acquired on a computer. The current is reversed and an additional time is allotted for the settling of any transient effects in the system (region s in fig. 2). After the system has settled, voltage readings are obtained for the reverse current. The current is switched back to the forward direction and another fixed settling time is allotted for transient effects to decay. Finally, data corresponding to the forward current is obtained. This pattern could be continued or repeated after an experimental parameter has changed. For example, in the resistance-versus-temperature experiment, after the sample temperature changed by a certain amount, the forward-reverse current injection pattern was used.

In order to correct for any thermal electric effects that may be present, the two forward-current voltage readings (regions A and C, for example) are averaged to approximate the thermal effects that occurred at the approximate time of the reverse-current readings, region B in figure 2. The actual time of individual or groups of readings can be stored to avoid this approximation. This average is combined with the average of the reverse-current voltage data to give the effective voltage drop across the sample (assuming forward and reverse currents are identical in magnitude). The resulting equation for the data point value associated with regions A, B, and C is:

$$\text{data point(ABC)} = \frac{1}{2} \left| \frac{(A+C)}{2} - B \right| \tag{1}$$

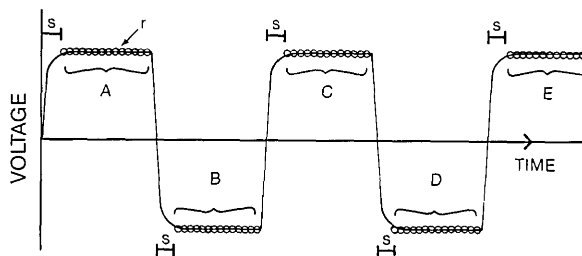

Figure 2. Data pattern of forward-reverse-forwared current.

The difference between the two forward voltages can be assigned a figure of merit for the measurement, which can be used as a basis for editing or flagging individual printouts after the data run is complete. This sequence of forward and reverse current data points can be continued as necessary. The combination of any three adjacent data points would provide an associated figure of merit (regions A, B, C; B, C, D;...). The figure of merit can be calculated using the following equation:

$$\text{Figure of Merit(ABC)} = |\text{A-C}|/(\text{data point(ABC)}), \quad (2)$$

where data point (ABC) is calculated using eq (1). Thus, a forward-reverse data pattern configuration proved to be useful in the thermal electric corrections described above.

If the forward-reverse current data pattern is not feasible in the type of experiment being performed, it may be necessary to use a "zero-forward-zero" current data pattern. For example, if the experiment prohibits the application of a negative current (a diode in the circuit, for example), or if the magnitude of the reverse current is not identical to the magnitude of the forward current, then it is necessary to use a zero-forward-zero data pattern.

2.3 Example Experiment

Several experiments have been performed using the software techniques described in the preceding section and the digital voltmeters discussed in section 3. As described in section 3, these voltmeters generate occasional erroneous readings. However, they are very suitable for superconductor and low resistance measurements. One experiment of this type was to determine the temperature dependence of a 16.6 μΩ (6000 A) shunt resistor. The results of this experiment were to be used in critical current measurements of superconductors. In critical current measurements, the magnitude of the transport current, (the current flowing through the superconductor) must be accurately measured. The transport current was calculated from the voltage across a known shunt resistor. Since the temperature of the shunt resistor increases with increasing transport current, the temperature dependence of the shunt resistor must be precisely known. The software techniques discussed earlier resulted in precision on the order of a few thousandths of a percent. A plot of the shunt resistance as a function of temperature is presented on figure 3. A current of 500 A was used (which is low compared to the resistor's 6000 A rating) in order to reduce the effect of self-heating of both resistors. A typical current drift was about 0.5 A, which is 0.1% of the total current.

In this experiment, the current supply, a known resistor, and the unknown resistor were connected in series, as is schematically shown on figure 4. Voltage leads from each resistor were fed into a scanner. Two digital voltmeters were also connected to the scanner. The scanner allowed each meter to measure either voltage signal. Precise voltage measurements and the calibrated shunt resistor can be used to determine the resistance of the unknown resistor. A data pattern of zero, forward, and zero current was used.

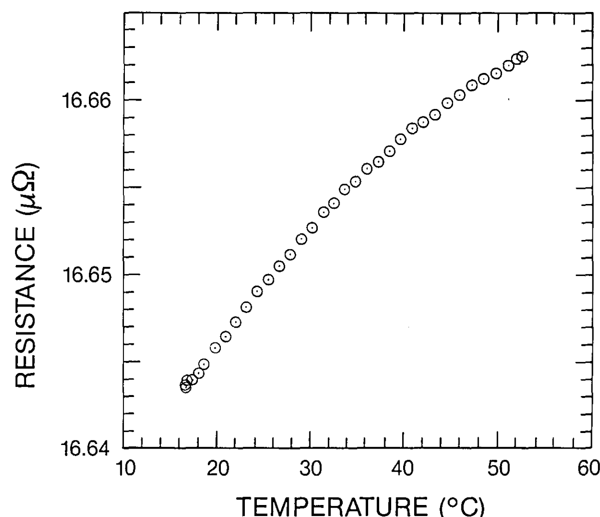

Figure 3. Shunt resistance as a function of temperature.

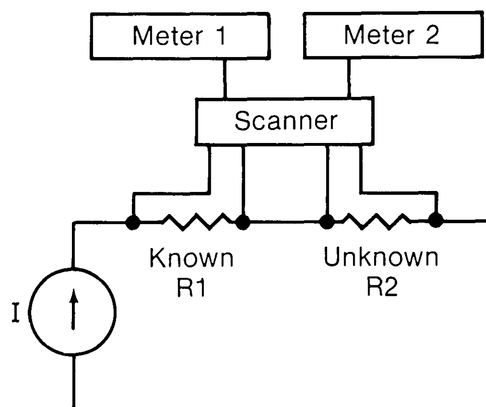

Figure 4. Block diagram of shunt resistor experiment.

Frequently, the "forward" current has a small drift in time, as is schematically presented in figure 5. (The current drift has been exaggerated in this figure.) The drift in the forward-current regions is attributed to changes in the thermal electric voltage and drift in the current. The drift in the zero-current regions is attributed to changes in the thermal electric voltage. The forward current drift can be accounted for by using the data taken with zero current. This correction can be performed by calculating a linear voltage-time fit between the readings in zero-current regions, (as indicated in fig. 5 by the dashed line), and subtracting the resulting best fit line from the readings in the forward current region. A set of calculated instantaneous resistance values can be obtained by taking the ratio of the corrected voltage and current readings. The current readings are inferred by using the voltage drop across a standard resistor. The instantaneous resistance values can be edited to remove any erroneous data, and an average and standard deviation of the instantaneous resistance readings can be subsequently calculated.

If a leakage current is present in the nominally zero current regions of the pattern, then the unknown resistance is calculated using the ratio of the change in the voltage readings to the change in the current. This technique of calculating the instantaneous resistance is only applicable if the sample is ohmic. If the sample is non-ohmic, this calculation would result in a differential resistance. It may be possible to reduce the effect of leakage current by open-circuiting the system. However, this could change the effects of the circuit ground.

Voltmeters often have calibration errors associated with them. In order to approximately cancel this error, it is useful to use a scanner to interchange the voltage signals that are being fed to the voltmeters. The approximate cancellation of linear calibration errors only takes place if the deviation between the calibration constants of the two meters is small. Since another calibration error may exist between the voltmeter ranges on a given voltmeter, the two voltmeters were kept on the same voltage range. A single meter could be used to measure the voltage across both shunt resistors and reduce the inaccuracy in the experiment. However, one meter can be used only when the current and temperature are in steady-state conditions.

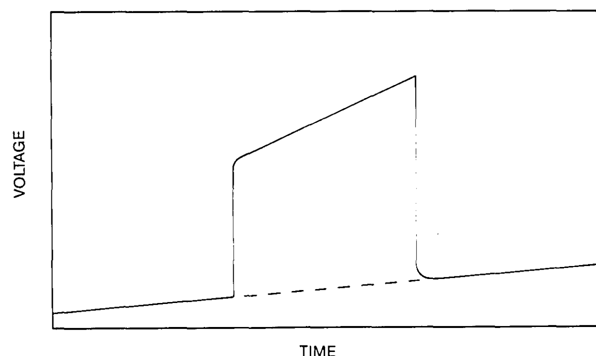

Figure 5. Data pattern of zero-forward-zero current with exaggerated current drift.

3. Erroneous Voltage Readings

The erroneous readings discussed here have provided a relevant and repeatable phenomenon that can be used to test the ability of software to discriminate erroneous from correct readings. This ability is necessary to detect experimental problems such as occasional noise spikes, human intervention, and transient conditions. If not detected, these types of experimental problems can lead to unreliable and generally unrepeatable readings. The fixed limit editor was used in this experiment to detect the presence of outliers.

This example is not intended to be a harsh labeling of digital voltmeters—it is only meant as a general caution on their use. They are clearly superior for obtaining automated, precise, and accurate measurements. If the digital voltmeters discussed here are used in conjunction with a software editor, it is not unreasonable to obtain precision on the order of a thousandths of a percent. The same model voltmeter described in this section was used to take the measurements in section 2.3.

3.1 Observation of Outliers

During voltage calibrations and resistance versus temperature measurements, it was observed that the digital voltmeters would occasionally give an erroneous reading. This phenomenon was first noted during attempts to reduce the variation of voltage readings being made during resistance-versus-temperature measurements. The voltmeter's manufacturer stated in their Operator's Manual that the meter occasionally exhibits "internally generated noise spikes." Averaging more readings (20 to 50 readings) and using longer settling times between current reversals did little to alleviate this problem. It was also discovered that turning off the voltmeter's signal filtering capability had a beneficial effect. The voltage readings were plotted using

an automatic plotting routine. Occasionally, the limits of the voltage axis were significantly changed to accommodate what turned out to be outlying points.

3.2 Digital Voltmeter

The internal digital filter on this particular voltmeter switches on and off based on a comparison of the new reading and the accumulated running average. A scheme of this type is used so that if there is a rapid change in voltage readings, like a current reversal, the meter can quickly respond. However, the filter can generate a series of erroneous readings if a single outlying reading occurs. This results in a series of readings that approach the correct reading within arbitrarily small differences, thus making it difficult or impossible to edit the filtered readings. Also, using the internal digital filter creates some uncertainty with respect to the appropriate time to assign to a voltmeter reading. Editing filtered data is especially difficult when a few (10 to 50) readings are taken. Thus, it is beneficial to take data with the filter off, and edit the data using the computer before averaging. Using the filter when manually reading the meter display is advisable since it is difficult to average the displayed reading. If the filter is used in conjunction with a computer, the resultant readings will have an artificially low standard deviation.

3.3 Systematic Study of Erroneous Readings

The outliers were observed on one particular voltmeter model. Four meters of this model were tested extensively, and two other meters had limited testing. A voltage source and a resistive divider were used to generate an input signal which was split into four digital voltmeters. A block diagram of the system used is given in figure 1. The voltage divider in figure 1 was omitted for the larger signals. Each meter had the same input signal and should therefore measure the same value within calibration limits. An input voltage level was set and allowed to settle for about 10 min. A set of 1000 readings were taken in parallel from each of four meters. This allowed for an effective reading rate for each meter of 3.6 readings per second on the millivolt ranges, which is close to the ideal single meter reading rate of 4.0 readings per second. The effective rate was about 7.3 readings per second on the voltage ranges compared to the ideal reading rate of 8.0 readings per second. Thus, a total of 4000 readings were taken in 278 s on the millivolt ranges, and 137 s on the voltage ranges.

Next, the median reading was determined for each meter and the average and standard deviation calculated from the readings that were within preset limits of the respective median reading. A statistical summary of the readings on each meter and the location of any outlier that may have occurred were stored. If an outlier occurred during the data acquisition, a printout was made that included the average, standard deviation, and the maximum and minimum reading for each meter. The maximum and minimum readings were calculated after the outlying reading(s) was removed from the data point.

In order to obtain statistically significant results, a vast number of voltmeter readings had to be acquired, edited, and analyzed. In total, 2.4 million readings were taken for each data run, (there were 600 data sets consisting of 1000 readings taken from each of 4 meters) and more than 14 data runs were made. A few runs have been chosen for illustrative purposes here. Two of these runs depict the differences between the millivolt and volt ranges (in particular the 2-mV and 2-V ranges) of the voltmeters.

3.4 Data Plots

Three figures have been included here for each of the 2-V and 2-mV data sets to illustrate various characteristics of the outliers. The 2-V data set corresponds to the "a" figures and the 2-mV data set corresponds to the "b" figures. The number of outliers within each data set, along with a histogram of the spacing between adjacent outliers over all data sets has been displayed in figures 6a, 6b, 7a, and 7b. A statistical summary of the edited readings is presented in figures 8a and 8b.

Figures 6a and 6b illustrate the relative frequency of an outlier in a data set. Most data sets have no outliers. The majority of the outliers occur in data sets that contain multiple outliers. Therefore, the outliers seem to occur in bursts. The outliers on a particular meter seem to occur independently of outliers on other meters. For example, on figure 6a, the errors made by meters 1 and 2 were independent of each other in the sense that they did not occur in the same data set. If an error was present on all four meters at the same time, the error may be attributed to a variation in the input signal. A similar comparison of the other meters show that the errors are not correlated with a variation in input signal. There were only a few cases in which two of the four meters had adjacent

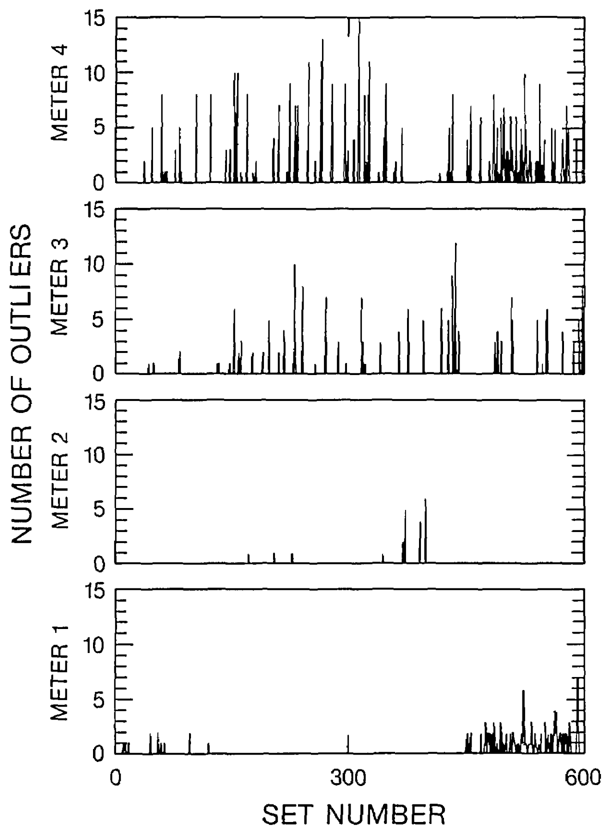

Figure 6a. Number of outliers as a function of data set number, 2-V range, filter off.

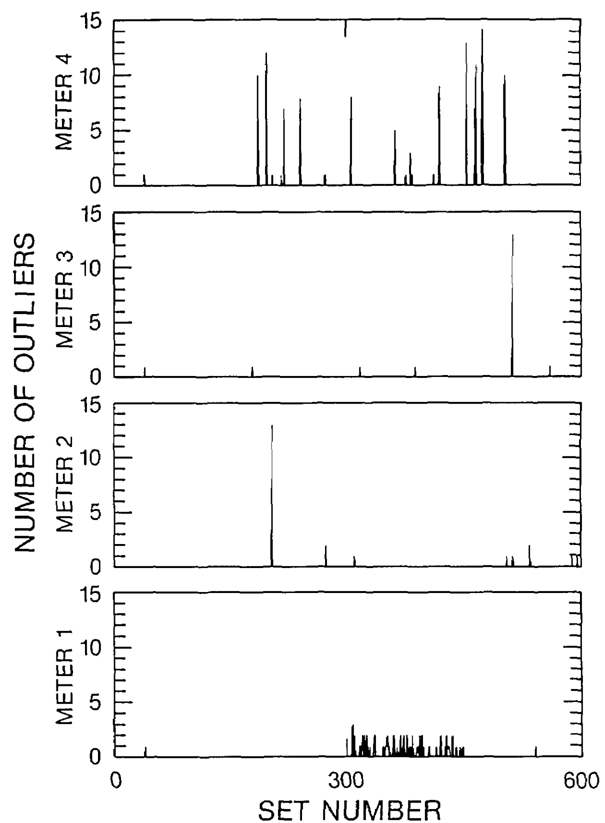

Figure 6b. Number of outliers as a function of data set number, 2-mV range, filter off.

outlying readings. Figure 6b clearly indicates the independence of the errors made by the meters. Near set 300, meter 1 had bursts of approximately 2 error readings per 1000 readings, while the other meters did not show any errors in those data sets. Figures 6a and 6b have similar overall characteristics, although the 2-V data set had more outliers than the 2-mV data set.

Figures 7a and 7b display a histogram of the separation between adjacent outliers within each of the 600 data sets. Most of the outliers within a data set are separated by at least 20 correct readings. This is relevant when considering the likelihood of a large number of outliers in a small data set. Thus, it is not likely that a set of 15 readings would contain a significant number of outliers.

Figures 8a and 8b display the distribution of the maximum and minimum values of the edited voltage readings about the average of the data set. The middle line in each plot indicates the standard deviation of the data sets. All of these values were computed after removing the outliers from the data set. Meter 1 on figure 8a shows a larger variation of voltage readings between sets 38 and 152. This increase may be attributed either to poor connections of voltmeter to voltage source or an increase in the internal noise of the meter. As can be seen from figure 8a, the increase in noise diminishes after data set 152. Although the variation in the signal was larger, the limits of the fixed limit data editor were such that most of the readings were not classified as outliers, as can be seen in figure 6a. Meter 2 has a different characteristic when compared to the other meters on figure 8b. However, meter 2 had the lowest frequency of outliers on the millivolt range. There were some relatively high minimum and maximum values on figure 8a and 8b that are attributed to random events which have magnitudes that were within the limits of the editor.

Figure 9 is included to illustrate the combined effect of the meter's internal digital filter and the occurrence of an outlier. This graph displays the relative error (in μV) as a function of the reading number. A single outlier probably occurred near the leading edge of each of the three sharp spikes. The meter's internal digital filter may have switched off as it received the erroneous reading, but it did not switch off again after the erroneous

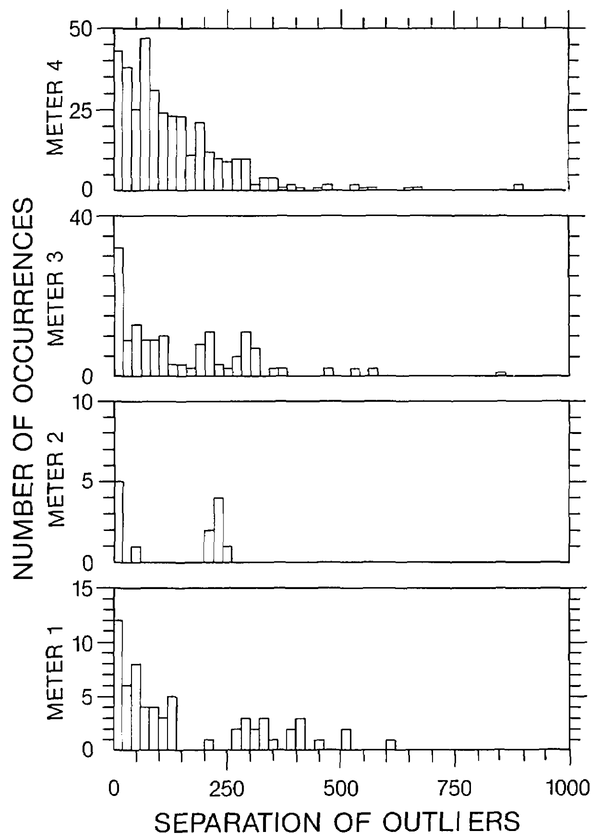

Figure 7a. Number of outliers as a function of outliers separation, 2-V range, filter off.

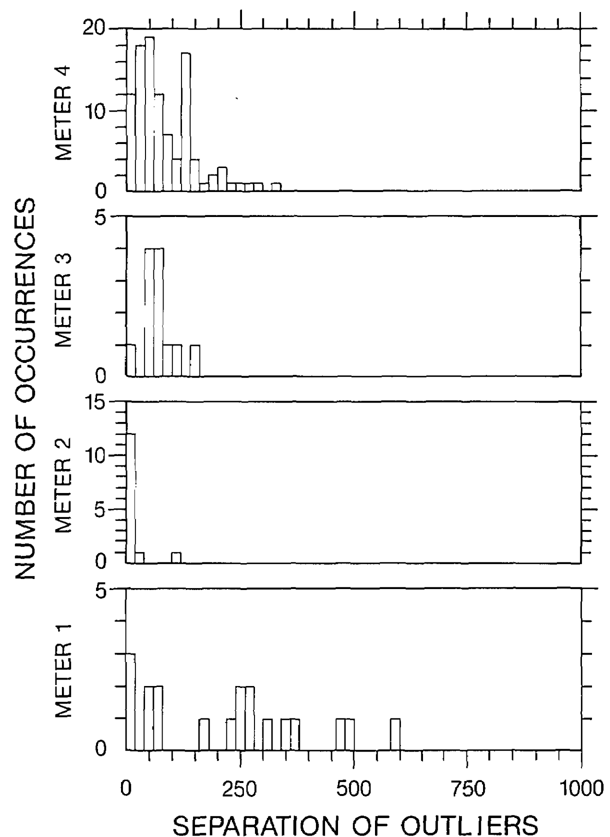

Figure 7b. Number of outliers as a function of outlier separation, 2-mV range, filter off.

reading. Consequently, the subsequent readings indicate an apparent integration or accumulating average that approaches the correct reading. These examples were somewhat atypical. More often, the filter switched off twice, creating an isolated point. In general, the frequency of the outliers was about the same with and without the digital filter. There were more errors with the filter on. These errors were most probably due to an occasional integration of a single error.

3.5 Data Tables

The observed errors scaled as a function of one of the following three parameters: the bias level (actual input signal), the selected voltage range of the voltmeter, and the difference between the maximum allowable value of the selected range and the input signal. In 99.07% of the cases, the error was a fixed percentage of one of these parameters (tables 1a through 2b). Tables 3a and 3b show the magnitude of the error caused by an outlier, along with the number of standard deviations the error is above the correct readings.

Each of the tables 1a through 2b contains the meter number, the type of error, (an error due to the bias level, voltage range, etc.) and the percentage category (0.6%, 3.0%, etc). The table entries are the actual percentage error, and the number of such errors is indicated in parentheses.

As mentioned earlier, the outliers were a fixed percentage of one of the above parameters. Out of the 9.6 million readings represented in these four tables, 2162 readings were outliers (approximately 1 in 4440 readings). Of the 2162 outliers, 2142 (99.07%) outliers can be characterized as an error due to either the bias level, the voltage range, or a difference in the voltage range and the bias level. Of the remaining 20 outliers, 3 can be attributed to the simultaneous occurrence of two outliers from the above categories. For example, one of these outliers could be categorized into a −2.4% of bias error. An outlier of this type can be attributed to a simultaneous occurrence of a +3.0% of bias error and a −0.6% of bias error. The remaining 17 outliers can be attributed to infrequent random events.

The errors listed above were infrequent when compared to the total number of readings that were

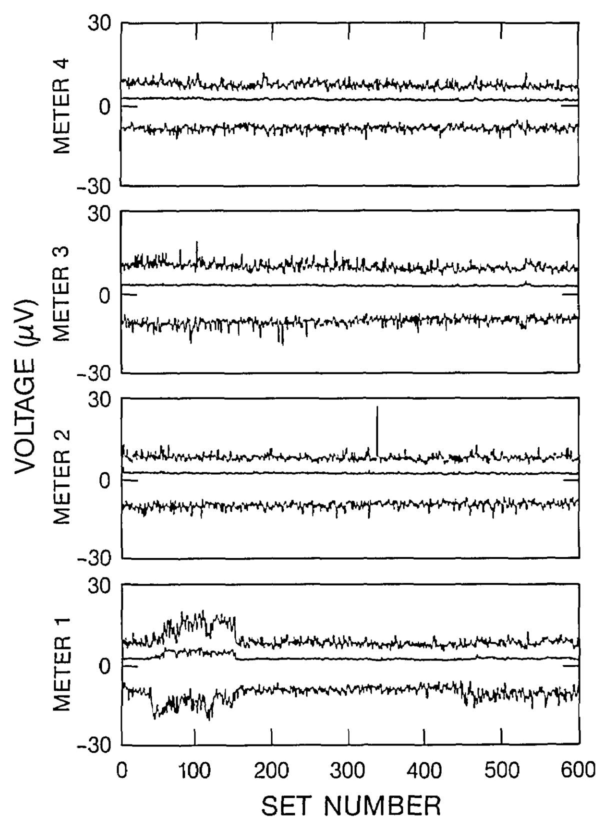

Figure 8a. Edited voltage reading as a function of data set number, 2-V range, filter off.

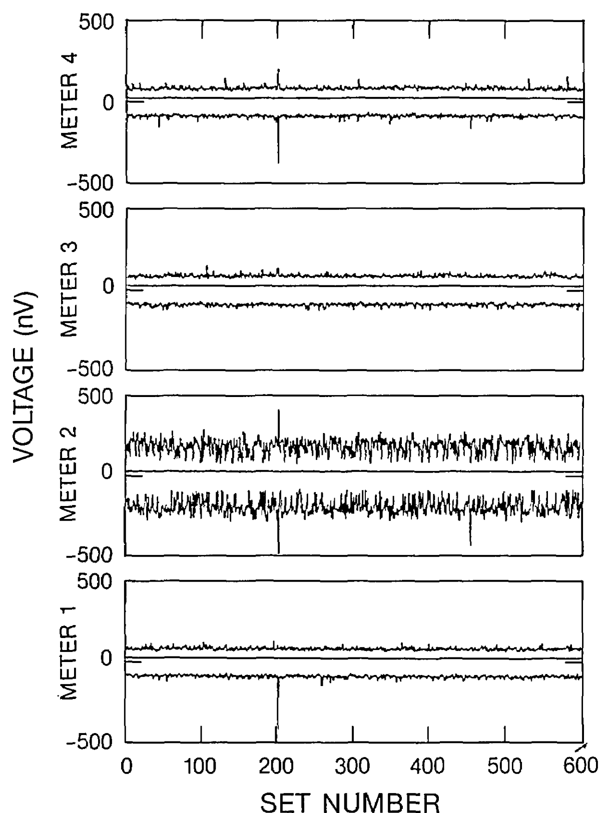

Figure 8b. Edited voltage reading as a function of data set number, 2-mV range, filter off.

taken from the voltmeter. However, after a single error occurred, the chance that more errors would occur on the same meter increased, as indicated in figures 6a and 6b. Thus, if an experiment's time constraints dictate that a relatively small number of readings be taken per data point, the occurrence of one or more outliers in the readings could significantly affect the computed average. For example, on the highest voltage scale, a 3% of range error could result in an outlier with a 60-V magnitude. Thus, if the correct reading was 15 V, the outlying reading would be 75 V. As another example, if the actual reading is 1 μV on the 2-mV range, a 3% of range error outlier would have a magnitude of 60 μV, resulting in a 61-μV erroneous reading. Erroneous readings of this type would significantly alter the unedited average.

A comparison of the error patterns on the 2-mV and the 20-mV range of the meters (with the same bias level) exhibits the different scaling of the bias and the range dependent errors. The 2-V and the 20-V ranges also exhibit a similar scaling of errors. There were some slight systematic differences between the percentage scaling of the errors for different meters. A similar pattern continued for the 200-mV and the 200-V ranges. The highest voltmeter range was 1000 V, but the errors scaled as though this range was 2000 V. Other data sets with the internal digital filter on showed the same scaling of errors.

The standard deviation of the outliers in each error category was approximately the same as the standard deviation of the allowed readings (see figs. 8a and 8b). For example, on the millivolt ranges of the meter, standard deviations of 27 nV and 28 nV were typical for the outliers and the allowed readings, respectively. Similarly, on the voltage ranges, standard deviations of 4 μV for the outliers and standard deviations of 3 μV were typical. The voltage difference between the correct readings and the outliers was significant compared to the standard deviation. For example, with a 0.6-mV bias on the 2-V range, the lowest error would be 3.6 μV (the actual outlier reading would be 0.6036 mV, which is 0.6% of bias). Thus, the lowest error in this case would be 128 times the standard deviation of the correct readings.

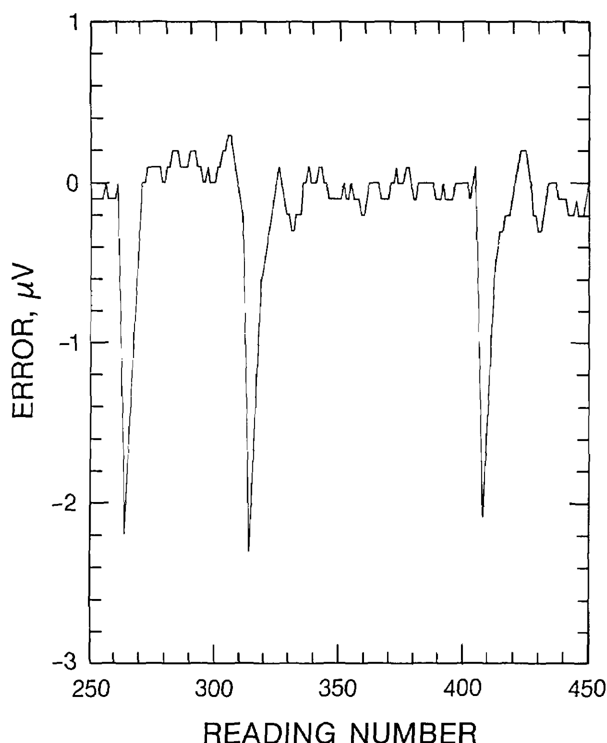

Figure 9. An occurrence of outliers with the internal digital filter on.

Tables 3a and 3b show the error value and the number of standard deviations that the error is above the correct readings for the 2-mV and the 2-V ranges. Standard deviations of 28 nV and 3 μV were typical for the correct readings for the 2-mV range and the 2-V range, respectively. Notice that most of the errors are hundreds or thousands of standard deviations above the correct readings. At these signal levels, these errors were clearly extreme outliers. At lower signal levels, the 0.6% of bias error can be difficult to identify.

3.6 Discussion of Erroneous Voltmeter Readings

The voltmeters were transmitting data to the computer via a standard IEEE bus cable. Since the errors were visually observed on the voltmeter's display, it was deduced that the IEEE cable was not the source of these errors.

The regular patterns of the errors suggest that the source of the errors were not due to thermal electric effects. However, an effort was made to reduce the thermal effects by allowing for long settling times (between 10 and 60 min) between experiment setup and actual data acquisition. Also, leadshot bags were placed under and on top of the voltmeter lead connections in order to reduce thermal effects.

The manufacturer of the voltmeter is currently in the process of identifying the source of the erroneous readings. The manufacturer will also verify that this problem is limited to the situation in which multiple units of a particular model are used to measure voltages at the same time in an experiment. Erroneous readings have not been observed when only a single meter is used.

It is suggested that the outliers result from analog-to-digital conversion errors due to the discrete nature of the errors. In a typical experiment, multiple meters are used to measure different voltages in the same circuit. Even in this case, erroneous readings have been observed. The voltmeters that were used in these experiments are one of the most sensitive instruments presently available. Thus, they are probably pushing the present "state-of-the-art" in voltage measurements.

4. General Discussion

Although excellent commercial software packages for data acquisition may be available to experimenters, often they cannot be modified for specialized measurements. Invariably, due to the specialized nature of many experimental setups, data acquisition software must be designed by the experimenter. As is true for any sophisticated computer program, the experimenter must fully test the software under various conditions before proceeding further. Otherwise, it may be possible that the software either generates errors, or allows erroneous measurements in the system.

The editor discussed in this paper has been developed to remove those readings that are inconsistent with the distribution of the majority of the readings during data acquisition. The editor is designed to warn the user if the standard deviation of the edited readings is high, or if the number of points removed by the editor is greater than the larger of two readings or 3% of the total number of readings. These tolerances are a function of the inherent noise of the measurement system, the sensitivity of the measurement system, and the number of readings in a data set. If the editor warns the user that the number of discarded readings exceeds the tolerance, the user can investigate the source of the errors and determine a method to rectify the problem. There may be experiments in which a tolerance of 1% or less is appropriate. In this case, it

Table 1a. Percentage errors (number of occurrences in parentheses) for the 2-mV range, 4 bias levels, no filter

Meter	Bias, mV	% of bias +0.6	% of bias −3.0	% of range +3.1	% of balance −3.2
1	0.0				−3.051 (1)
	0.2				
	0.6	0.560 (33)	−2.969 (35)		
	1.5		−2.968 (1)		
2	0.0				
	0.2				−3.278 (2)
	0.6	0.684 (1)			
	1.5	0.695 (2)	−3.098 (1)	3.200 (3)	
3	0.0				−3.066 (1)
	0.2		−2.972 (1)		
	0.6	0.572 (1)	−2.971 (1)		
	1.5	0.565 (6)	−2.971 (8)		
4	0.0			3.097 (1)	
	0.2	0.597 (18)	−3.004 (18)	3.101 (1)	−3.166 (1)
	0.6	0.597 (14)	−2.999 (12)	3.097 (1)	−3.349 (1)
	1.5	0.595 (23)	−3.000 (32)		

Notes: 234 outlyers for this data set. 15 points did not fit in a pattern.

Table 1b. Percentage errors (number of occurrences in parentheses) for the 20-mV range, 4 bias levels, no filter

Meter	Bias, mV	% of bias +0.6	% of bias −3.0	% of range +3.1	% of balance −3.2
1	0.0				
	0.2	0.558 (34)	−2.977 (39)		
	0.6	0.562 (23)	−2.969 (44)		
	1.5	0.563 (1)	−3.000 (2)		
2	0.0				
	0.2				−3.204 (1)
	0.6		−3.088 (1)		
	1.5				
3	0.0				
	0.2	0.571 (12)	−2.961 (18)		
	0.6	0.569 (3)	−2.968 (7)		−3.082 (1)
	1.5	0.567 (23)	−2.971 (21)		
4	0.0				
	0.2	0.600 (4)	−2.985 (5)		
	0.6	0.592 (12)	−2.997 (13)		−3.116 (1)
	1.5	0.592 (27)	−2.997 (33)	3.097 (1)	

Notes: 326 outlyers for this data set.

will be necessary to adjust the editor so that the operator is not desensitized by being frequently alerted. Although the editor may eliminate some data from calculations during data acquisition, the software routine should be designed to store all of the data for future analysis using more sophisticated techniques.

It is necessary to use some type of outlier rejection rule [6] when analyzing data taken when outliers may be present. The rejection rule that best suits an experiment may be affected by the details of the measurement system, especially under low signal-to-noise ratio conditions. The fixed-limit editor described here may not be optimum; however it

Table 2a. Percentage errors (number of occurrences in parentheses) for the 2-V range, 4 bias levels, no filter

Meter	Bias, V	% of bias	% of balance	
		0.6	+3.0	−3.1
1	0.0		2.966 (13)	
	0.2			
	0.6			
	1.5	0.561 (65)	2.967 (65)	
2	0.0			
	0.2	0.696 (2)	3.092 (1)	
	0.6	0.696 (8)	3.092 (10)	
	1.5			
3	0.0		2.972 (6)	−3.063 (1)
	0.2	0.567 (35)	2.972 (22)	−3.126 (3)
	0.6	0.566 (27)	2.972 (43)	−3.304 (2)
	1.5	0.566 (43)	3.000 (16)	
4	0.0		2.999 (46)	−3.092 (3)
	0.2	0.595 (70)	2.999 (67)	−3.157 (1)
	0.6	0.596 (46)	2.999 (36)	−3.346 (1)
	1.5	0.596 (106)	3.000 (85)	

Notes: 826 outlyers for this data set. 3 points did not fit in a pattern.

Table 2b. Percentage errors (number of occurrences in parentheses) for the 20-V range, 4 bias levels, no filter

Meter	Bias, V	% of bias	% of balance	
		0.6	+3.0	−3.1
1	0.0		2.966 (70)	
	0.2	0.557 (41)	2.966 (33)	
	0.6			
	1.5	0.559 (1)		
2	0.0			
	0.2	0.693 (3)		
	0.6	0.694 (9)	3.090 (14)	
	1.5	0.695 (53)	3.091 (49)	
3	0.0		2.972 (19)	
	0.2	0.565 (20)	2.972 (22)	
	0.6	0.566 (32)	2.972 (25)	
	1.5	0.566 (63)	2.972 (45)	
4	0.0		2.998 (32)	
	0.2	0.597 (43)	2.998 (37)	−3.097 (1)
	0.6	0.595 (66)	2.998 (55)	
	1.5	0.595 (21)	2.998 (20)	

Notes: 776 outlyers for this data set. 2 points did not fit in a pattern.

is clearly better than not using an editor. The editor limits can be adjusted so that only extreme outliers are rejected.

5. Conclusions

A software routine can create a data pattern, assign a figure of merit to a data point, compute edited averages and standard deviations, and store the

Table 3a. Error values in μV, and the number of standard deviations above the edited readings (in parentheses) for the 2-mV range on meter 4, using a typical standard deviation of 28 nV for the edited readings

Bias, mV	% of bias +0.6	% of bias −3.0	% of range +3.1	% of balance −3.2
0.0			61.9 (2210)	−65.2[a] (2330)
0.2	1.19 (43)	−6.0 (214)	62.0 (2210)	−57.0 (2040)
0.6	3.58 (128)	−18.0 (643)	61.9 (2210)	−46.8 (1670)
1.5	8.9 (318)	−45.0 (1610)	62.0[a] (2210)	−16.3[a] (582)

[a] These errors were not observed in the experiment.

Table 3b. Error values in mV, and the number of standard deviations above the edited readings (in parentheses) for the 2-V range on meter 4, using a typical standard deviation of 3 μV for the edited readings

Bias, V	% of bias 0.6	% of balance +3.0	% of balance −3.1
0.0		60.0 (20000)	−78.4 (26100)
0.2	1.19 (397)	54.0 (18000)	−56.8 (18900)
0.6	3.58 (1200)	42.0 (14000)	−46.8 (15600)
1.5	8.94 (2980)	15.0 (5000)	−16.0[a] (5300)

[a] This error was not observed in the experiment.

analyzed data. A summary printout of the data taken during a particular experiment also proves to be beneficial. It is wise to store as much raw (unedited) data as possible, so that it can be analyzed later when the time constraints imposed by the experiment are no longer present. At that time, a more sophisticated statistical analysis method could be used.

Data reliability is affected by experimental events such as intermittent electrical connections, sample motion in a magnetic field, rapid changes in temperature, periodic and random electrical noise, and movements of humans near a sensitive experiment. In addition, internally generated erroneous voltmeter readings have been observed. These particular errors scale with one of the following parameters: the bias level, the selected voltage range of the voltmeter, or the difference between the maximum allowable value of the selected range and the input signal. A typical error may be more than 100 times the standard deviation of the correct readings. Thus, a few erroneous readings can significantly affect the average of a collection of readings unless a data editor is in use. The fixed-limit editor has been developed to remove occasional erroneous readings that are inconsistent with the distribution of the majority of the readings. This editor is simple and expedient.

The software should give the user feedback on the experiment not only through data tables, but through audio and video signals as well. A system of this type could allow the experimenter to ascertain the source of an error, and possibly correct it. Unless a data editor is implemented in a data acquisition software routine, it is difficult to determine whether or not errors have occurred. High precision data can be obtained using an editor in the presence of outlying readings.

Acknowledgments

The authors acknowledge the contribution of C. A. Thompson and F. Fickett for discussions on software techniques, T. M. Larson for discussions on analog-digital converters, and T. C. Stauffer and R. M. Folsom for assistance with measurements and drafting.

This work was supported in part by the Department of Energy, Office of Fusion Energy and Division of High Energy Physics.

6. References

[1] Goodrich, L. F., and Bray, S. L, Adv. Cryo. Eng.-Mater. **36A**, 43 (1990).
[2] Fickett, F. R., and Capobianco, T. E., Conductors for Advanced Energy Systems, INCRA 321B, International Copper Research Association, New York (1987).
[3] Moreland, J., and Goodrich, L. F., IEEE Trans. Magn. **25**, 2056 (1989).

[4] Goodrich, L. F., and Bray, S. L., Cryogenics **30**, 667 (1990).
[5] Thompson, C. A., and Fickett, F. R., Adv. Cryo. Eng.-Mater. **36A**, 663 (1990).
[6] Hampel, F. A., Technometrics **27**, 95 (1985).

About the authors: *Dr. Loren F. Goodrich is a physicist in the Superconductor and Magnetic Measurements Group of the Electromagnetic Technology Division at NIST-Boulder. Ashok N. Srivastava is an Electrical Engineering student at the University of Colorado at Boulder and works part-time in the Superconductor and Magnetic Measurement Group at NIST-Boulder.*

Volume 95, Number 5, September-October 1990
Journal of Research of the National Institute of Standards and Technology

Conference Reports

WORKSHOP ON INTELLIGENT PROCESSING FOR PRIMARY METALS Gaithersburg, MD August 29–30, 1989

Report prepared by

James G. Early

Scientific Advisor to the Director,
Materials Science and Engineering Laboratory,
National Institute of Standards and Technology,
Gaithersburg, MD 20899

The Materials Science and Engineering Laboratory (MSEL) of the National Institute of Standards and Technology (NIST), the Office of Industrial Programs of the Department of Energy (DOE), and the American Iron and Steel Institute (AISI) co-sponsored a Workshop on Intelligent Processing for Primary Metals held at NIST on August 29–30, 1989. Attendance was by invitation and the more than 80 participants were primarily senior technical staff and managers from steel, aluminum, and copper companies.

Although the United States is a leading contributor to the world's materials science base, it is beginning to lag in the cost-effective implementation of this knowledge. U.S. industry does not enjoy leadership in the introduction of new materials technologies into consumer products, as it does in defense systems. Other nations have initiated government-industry programs aimed at the development of advanced processing technology. Advanced manufacturing techniques increasingly demand materials of greater reliability and uniformity at competitive cost. Specific demands for properties and performance can be met by control of the processing of the material from synthesis or raw material production to forming/finishing.

Such process control, or "Intelligent Processing of Materials" (IPM), is based on four elements: a process model that relates specific materials properties at each stage of the processing to the final properties; sensors (measurement technology) which can measure the appropriate materials properties in real-time during processing; materials property data which must be coupled with the real-time measurements in the process model; and rapid computational capability for incorporation of sensor data, process model evaluation, and process variable control into an integrated, automated control strategy. The IPM concept differs greatly from conventional automated materials processing. In conventional practice, only the process variables (temperature, pressure, etc.) are automatically controlled to pre-set values which, nevertheless, still allow the microstructure and properties of the material to deviate significantly from the desired values. A critical feature of intelligent processing is the shift from off-line measurements on finished products to on-line measurements in real-time to control processing.

The past 5 years have witnessed extensive advances in the enabling technologies needed for intelligent processing of materials. These include: advanced sensors for on-line monitoring of material and process parameters, the knowledge base and materials characterization techniques to develop process models relating process parameters

to material properties, and hierarchical computer control strategies for implementing artificial intelligence/expert systems concepts. Several recent national programs have been initiated to integrate elements of these advances to control the processing of advanced materials such as gallium arsenide crystals, powder metals, and composites. Similar opportunities now appear to exist in the primary metals industries.

The goal of this industry-led workshop was to highlight the recent advances in sensing, modeling, and process control, to identify areas of need in the primary metals industries, and to develop a strategy for implementation of research results. Industry, university, and government participants assessed information provided by researchers and operating staff from industry to develop a research agenda for coupling the advancing state of materials processing in the primary metals industries.

1. History of the Workshop

The genesis of this workshop may be traced to two events. First, the signing into law in late 1988 of the Steel and Aluminum Energy Conservation and Technology Competitiveness Act that authorizes DOE and NIST to carry out coordinated programs in support of the primary metals industries, primarily steel, aluminum, and copper. NIST would concentrate on providing instrumentation and measurement R&D. The second event was the January 1989 forum at Northwestern University to identify long-range research opportunities for the North American steel industry. The industry participants concluded that research opportunities could best be addressed in the context of three specific long-range development projects: direct production of liquid steel, near-net shape casting, and finishing and coating operations.

To capitalize on these events, planning was initiated through a steering committee, chaired by Lyle H. Schwartz, Director, MSEL/NIST, with representatives from steel, aluminum, and copper trade associations, individual companies, the academic community, and Federal agencies. The consensus was to attempt to address the process control needs of the broad spectrum of primary metal industries and the role of intelligent processing concepts in solving these needs by focusing on three generic areas: primary metal production/refining, production of near-net shape products, and finishing/coating to final properties. Emphasis would be on future, advanced processes and technologies.

2. The Workshop

The Organizing Committee, chaired by James G. Early, MSEL/NIST, was pleased to have participation by representatives of the aluminum and copper industries because the workshop structure is applicable to the processing of these metals. An overlap or commonality of process control needs is likely in some areas of processing. The success of this workshop could lead to other industries using this approach to develop process control priorities. Although the strategy was to achieve a workshop relevant to steel, aluminum and copper, the program contained a strong orientation toward steel-related issues. Since early in this decade, the steel industry has worked to develop a consensus on technical advances needed to improve traditional production practices and on identifying the future steel-making technologies. Thus, the steel industry was particularly well-positioned to play an important role and make major contributions to the workshop resulting in the strong emphasis on steel.

The core of the workshop was organized into three working sessions:

I. Direct Liquid Metal Production

II. Near-Net Shape Casting

III. Finishing and Coating

Within these areas, the key elements of intelligent processing were stressed. The relationships between fundamentals and processing were explored through the integration of process modeling, sensor technology, and control strategies. Leading off the first day of the Workshop was an introduction to intelligent processing of materials concepts through applications to aerospace and other advanced materials followed by an overview of the process control research needs for the production of steel and aluminum. The three working sessions, responsible for Direct Liquid Metal Production, Near-Net Shape Casting, and Finishing/Coating, took place in the afternoon of the first day and the morning of the second day to permit a wide range of inputs from the participants. Coordinated presentations were given in these working sessions on the status of sensors, process models, and control approaches, the available technology, and the benefits to relevant research. After the morning sessions on the second day, a brief, verbal synopsis of the deliberations in each of the three working sessions was presented to the assembled workshop participants.

Between the first and second days working sessions, Deputy Secretary of Commerce Thomas J. Murrin, spoke to the Workshop on "New Metals Technologies: Making the Government-Industry Connection Work." In his remarks, Mr. Murrin discussed the three key issues facing industry as it develops new metals technologies: the need to improve the quality of products and services; the need to take advantage of new technologies being developed overseas; and the need for continued and expanded government-industry-labor cooperation. While the metals industry's health will be determined primarily by its own efforts, there are appropriate areas in which the Federal Government can contribute. Deputy Secretary Murrin reported on a number of policy initiatives underway related to taxes and tax credits, antitrust laws, and a broad review of technology-innovation policies and programs to determine if other changes are needed.

3. Plenary Session

The first session was devoted to a series of invited presentations to prepare the participants in the three working sessions with the necessary background and global view needed to achieve the Workshop goal. The first speaker, W. Barker (DARPA) described the concept of intelligent processing of materials and reviewed the national programs supported by DARPA. In a companion talk, D. Backman (General Electric Company) reviewed the application of IPM concepts to advanced aerospace materials. The industry perspective was presented in the final two talks: I. Hughes (Inland Steel) "Long Range Research - North American Steel's Competitive Edge"; and R. Bonewitz (Alcoa) "Sensor, Process Models, and Control Needs in the Aluminum Industry."

4. Direct Liquid Metal Production Session

Co-Chairmen:

A. W. Cramb
Carnegie-Mellon University

J. Kor
Timken Company

The session was organized into two parts: the first part was an information exchange between experts on sensor technology, process control, modeling, and the application of advanced computer decision making techniques, while the second part was to define and prioritize specific needs in the area of intelligent processing of liquid metals. Within each area specific needs were identified. Speakers included: J. Kor (Timken Company); P. Koros (LTV Steel Company); J. Fay (ASARCO, Inc.); A. McLean (University of Toronto); D. Hardesty (Sandia National Laboratory); C. Alcock (Notre Dame University); Y. Kim (Lehigh University); R. Guthrie (McGill University); M. Shah (IBM); and S. Ray (NIST).

The sensor area was considered to be the area of highest importance and it was the consensus of the group that sensor development and implementation should be the major focus of any endeavor. Three separate groups of sensors were distinguished: continuous temperature sensors; continuous chemical sensors for liquid metal and hot, dirty gases; and, physical sensors to measure reaction intensity. The area of process modeling was identified as the second most important area for research at this time. Two separate groups of needs were outlined: Process Control Models; and In-Detail Process Models. In the area of process control there was a concern that current "Artificial Intelligence" techniques might not be applicable to on-line control in a broad sense; however, in certain well-defined circumstances it may be useful. In addition, it was felt that the computer science involved in process control and decision making was sufficiently rapid that a mechanism should be set up so that appropriate advances can be implemented within the industry in a reasonable time frame. Three separate groups of needs were identified: Operator Feedback and Instruction; System Integration; and Technology Transfer. A copper industry participant reported that many of the sensors discussed would also be of use to the copper industry and further identified the sensors that overlapped those needed by the steel industry.

5. Near-Net Shape Casting Session

Co-Chairmen:

W. E. Eckhart, Jr.
U.S. Department of Energy

R. Sussman
ARMCO, Inc.

This session was conducted in two parts. The first day was characterized by presentations made by experts in their respective fields. Each presentation generated a modest number of questions within the subject area. It is noteworthy that no process-specific problems were detailed during the first-day

presentations, to the disappointment of some of the participants. The second day of this session was started by brief presentations made by individuals having hands-on experience with near-net shape casting of metal. Despite the obvious differences between the various casting methods, needs were categorized into three distinct areas: liquid metal handling, casting, and strip collection. Speakers included: M. R. Moore (USS Division of USX); R. A. Gleixner (Battelle Memorial Laboratories); L. T. Shiang (Inland Steel Company); Y. Sahai (Ohio State University); H. N. G. Wadley (University of Virginia); and J. A. Walton (ARMCO, Inc.).

Eight sensors were identified as critical to the successful development of a commercial strip casting process: continuous temperature measurement of the meet; continuous temperature of the substrate surface; rapid on-line strip thickness sensing; on-line hot strip inspection system; continuous topographic sensing of substrate; liquid metal level sensor; liquid metal inclusion sensor; and liquid metal nitrogen sensor. It was recognized that each of these must be employed in a manner in which it could be actively used to control the outcome of the process, and not merely in a passive role to provide information. Attempts were made to determine the range and precision needed for each of the sensors. In many cases, the identified range was quite accurate, but the estimated precision reflected that required of the product; the sensor may require greater sensitivity. In the area of mathematical modeling, it was agreed that most models are process-specific. Nonetheless, there exist many commercially available models of the two principal phenomena involved in near-net shape casting, heat transfer and fluid flow. It was determined after considerable discussion that the industry would benefit from a comprehensive review of such models currently available, along with their respective strengths and weaknesses, and a strategy for implementation of selected models. In the area of process control, it was recognized that the overall state of knowledge of near-net shape casting makes it difficult to design a comprehensive control system at this stage of development. It was determined that it would be meritorious to undertake an intelligent process simulation project to serve as a model for the metals industry. Shortly after the close of the workshop, a participant from the copper industry submitted an analysis that summarized similarities and differences in the sensor/model/control needs for copper and steel near-net shape casting.

6. Finishing and Coating Session

Co-Chairmen:

D. Watanapongse
Inland Steel

A. Van Clark, Jr.
NIST

The session consisted of two meetings designed to facilitate interaction between national experts and industry experts. The goal of the first meeting was to understand and assess the states of knowledge in intelligent processing; namely, product/process knowledge, process modeling, sensors, integrated process control, and artificial intelligence. The product/process relationships for steel substrates and coated steel were presented along with the needs for future improvements. Subsequent presentations were in sensor development, process modeling, and advanced control. The goal of the second meeting was to address the issues and resolutions that can enhance the success of future research programs to develop and apply intelligent processing technologies. Speakers included: D. Reinbold (Bethlehem Steel); P. Southwick (Inland Steel); S. Denner (National Steel); K. Brimacombe (University of British Columbia); J. Monchalin (IMRI Canada); A. V. Clark, Jr. (NIST); L. Lowry (Jet Propulsion Laboratory); and A. Meystel (Drexel University).

Although there is a wide range of sensor needs in the finishing and coating processes, five sensors were identified as having highest priority: continuous temperature measurement of strip; on-line measurement of chemical composition and phase identification in coatings; measurement of surface topography and surface chemistry of strip; measurement of lubricant film thickness; and measurement of mechanical properties/microstructure. Further attempts to prioritize among the five or to define specific ranges and accuracy of the sensors were considered inappropriate by the group because sensor requirements must be specified as an integral part of process modeling and control system development. Attempts were made, however, to estimate the developmental time for the sensors based on current understanding of available principles and technologies. In the coating processes, much work is needed to understand and model coating adherence mechanisms for a range of coating materials, steel substrates, surface morphology, and processing parameters. In addition, press performance of coated materials in terms of stampabil-

ity and powdering characteristics must be studied and modeled. Engineered surfaces and microstructural engineering were cited as the important areas needing further modeling studies. Since intelligent processing involves implementation and also a wide range of multidisciplinary backgrounds, the significance of project team formation, technology transfer, designed-in safety and maintenance were discussed at length. Intelligent processing has definitive roles in the finishing and coating processes, in terms of new product and process design and on-line process control. Specific recommendations are: Develop real-time expert models for control to supplement process models; and develop implementable intelligent processing systems from hot rolling to coating, with emphasis on continuous processing.

7. Summary

The research agenda developed at this industry-led workshop is summarized in NIST Special Publication 772, "Intelligent Processing for Primary Metals." According to the participants, successful development and implementation of advanced processing concepts for the production of steel, from raw steel through finished steel products, will be enhanced through the formation of broad-based, multidisciplinary teams focusing on generalized approaches and solutions to well-defined tasks. Specific recommendations for critically-needed sensors, process models, and control strategies are reported for the three working sessions.

For information on collaborative IPM research opportunities at NIST or a copy of the workshop report, NIST Special Publication 772, send a self-addressed mailing label to Dr. James Early, Materials Building, Room B309, NIST, Gaithersburg, MD 20899.

Volume 95, Number 5, September-October 1990
Journal of Research of the National Institute of Standards and Technology

Conference Reports

DATA ADMINISTRATION MANAGEMENT ASSOCIATION SYMPOSIUM Gaithersburg, MD May 7-8, 1990

Report prepared by

Judith Newton

Information System Engineering,
National Computer Systems Laboratory,
National Institute of Standards and Technology,
Gaithersburg, MD 20899

1. Introduction

Information and information technology will form an integral part of the way business competes in the 1990s. Organizations will have to deploy their information resources effectively to succeed, exploiting information to make better decisions and gain market advantage.

The increased focus on the management of data to deliver information requires progress in data administration; an emphasis on information as a corporate resource considered independently of process.

The Data Administration Management Association (DAMA) is the professional organization for Data Administrators. An international board oversees a loose federation of local chapters in the United States and Australia. The National Capital Region Chapter (NCR DAMA) has monthly meetings from September through April, as well as a Symposium in May.

NCR DAMA held its third annual Symposium at NIST on May 7-8, 1990. The theme this year was "Future Directions in Information Management." Attended by 264 Federal and private industry data administrators, the Symposium was cosponsored by NIST and DAMA International. The keynote speakers were Professor N. Venkatraman of MIT's Sloan School of Management and Robert Curtice of A. D. Little, Inc.

This year, the Symposium was extended to 2 days to accommodate the expanded program of speakers, workshops, and tutorials. The first day included sessions addressing Management Issues and Practical Techniques. The second day was divided between four tutorials and eight workshops. The workshops, to be held on a continuing basis, are designed to be research tools which will develop useful products for the data administration community.

2. Speakers

The key topics covered by the speakers included:

1) Information technology and business transformation,
2) Selecting a data management tool strategy,
3) Developing decision support systems using a data architecture,
4) Institutionalizing data architecture,
5) Building and managing a data administration function, and
6) Data architecture: planning effectively.

3. Tutorials

The tutorials were designed to introduce participants to unfamiliar topics.

The first, James Kendrick's "The New Management Challenge—Aligning Business and Technological Choices," discussed the implementation of information management in the corporate environment on a global scale. Effecting information-based management is a political process requiring strategic alignment of business and technical choices.

Strategic alignment consists of four areas:

1) Technology exploitation—studies information technology's potential to influence the organization's policy and direction.
2) Technology leverage—considers how business strategies affect the formation of an information technology strategy and the existing organization.
3) Strategy implementation—focuses on traditional strategy and structure implementation with the additional requirement of information technology support.
4) Technology implementation—focuses on implementing information technology strategies and their effect on business structures.

Information provides corporate agility necessary to be successful in the 1990s. Strategic alignment allows organizations to adapt to changing business and technological circumstances.

Ronald Ross presented a tutorial on "Defining Business Rules on a Data-Driven Basis." Business rules can be defined to information systems through an object-oriented paradigm. Two systems defined by this paradigm are:

1) Sensory system—any system that creates, changes, or deletes data, and in so doing applies rules reflecting desired or correct behavior; and
2) Delivery System—any system that delivers data to its users, through appropriate channels (e.g., screens, reports, etc.).

Rules which are applied to these systems in an object-oriented information environment include:

1) Data-centered rule—A system that updates a stored data type cannot deliver it, and vice versa;
2) Data-precedence rule—A system cannot be built until the sensory components for the data type(s) it retrieves have been built.
3) Data-bounded rule—A sensory system may manage data for one, and only one, object type.
4) Data-encapsulation rule—The sensory system for an object must enforce all rules constraining that object, with support for each rule being rendered one and only one time.

These rules can be applied to object aging. Object state changes over time can be recorded; for example, the events in the life of an order can be tracked as the order is processed in the business systems. A business rule such as "An order cannot be completed until a payment has been received" will be captured and enforced.

The next tutorial presented a discussion of the logical development of business rule capture. Barbara von Halle addressed "Business Rules and Database Design."

Traditionally, databases have been designed to process data in the most efficient possible way without regard for the requirements of business rule enforcement. Shared data environments, however, demand attention both to data considered as a resource and to the exigencies of rules which impose restrictions on the use of data. They require a partnership between business users and information specialists.

The shared data environment consists of business facts (data structure) and a corresponding set of common business rules (data integrity). Both data elements and business rules about the data must have business custodians. In order to insure business rule compliance in the application databases, this issue must be addressed at the level of the logical data model.

The logical data model is an integrated picture of all data used by an organization. It provides a starting point for database design and/or integration of one set of data requirements into a shared data environment. By integrating business rules into the data model, a place is provided for documenting detailed business data independently from how it is stored or accessed.

Here is an example of a working methodology for designing relational databases to include business rules.

1) Identify tables.
2) Identify columns.

3) Adapt data structure to product environment: sequence of columns, space calculations, file allocations, database assignment, and database locking.
4) Design for business rules about entities.
5) Design for business rules about relationships.
6) Design for additional business rules about data elements.
7) Tune: scans, clustering, hashing, indexing, etc.

The fourth tutorial was "Balancing Data and Process Modeling," given by Chris Gane. The object-oriented paradigm was taken as the reference point to integrate data flow and data structure models for information systems architecture. In this way, system developers can get the reusability benefits of object-oriented programming languages without the performance limitations.

An object-oriented modeling object consists of four components:

1) A data entity with associated relationships, attributes, and domains. This is identical with an entity in a data model. It has attributes (characteristics) and relationships with other objects.
2) A set of relevant object procedures. Some of these, such as standard data manipulation language operations, will be reusable. Complex logic may be associated with these operations.
3) A set of conditions (procedures that return only true or false). This is the place to store business rules for eventual use by generated code. These conditions may also serve to define events, which may trigger the execution of procedures.
4) Other relevant object constraints, for instance, state-transition and referential integrity constraints.

The benefits of this approach derive from the storage of all modeling information, procedures, conditions, and constraints of concern to any object in one central location. Reuse of procedures and constraints is expedited. It assists inheritance of procedures, conditions, and constraints as well as relationships and attributes. And it provides a common basis for the definition of objects and methods, independently of eventual implementation.

4. Workshops

Eight workshops were held, each oriented towards a different topic in data administration. These workshops will continue to meet, sponsored by DAMA chapters, and produce deliverables which will be of assistance to data administrators. Each will set its own timetable for meetings and development schedule for deliverables. The workshops will be centrally coordinated by a member of the International DAMA board.

The workshops and their leaders are:

1) Data Naming Standards—Arnold Barnett, Barnett Data Systems.
2) Defining the Mission and Function of Data Resource Management: Terms and Concepts—Mike Phillips, AIRS, Inc.
3) Data Oriented Deliverables Produced by a Systems Development Life Cycle—Greta Blash, Information Systems, Inc.
4) Effective Data Management in a Multiple DBMS Environment—Larry K. Dougherty, Signet Bank.
5) Essential Capabilities for CASE Tools from the Data Administration Point of View—Joe Oates, Life Cycle Technology.
6) Data Administration's Role in Supporting End User Computing—Bruce Rosen, NIST.
7) Pros and Cons of Different Data Modeling Techniques—Sashi Sood, AMS, Inc.
8) Standards and Procedures for the Data Administration Function—Judith Newton, NIST.

5. Proceedings

The proceedings of this Symposium will be released as a NIST publication. The Proceedings of the First[1] and Second[2] Annual DAMA Symposia were published by NIST and copies are still available. The Fourth Annual Symposium will be held at NIST May 14–15, 1991.

[1] Newton, Judith J., and Spielman, Frankie E., editors, Data Administration: Management and Practice, Proceedings of the First DAMA Symposium, NIST Special Publication 500-159, National Institute of Standards and Technology, Gaithersburg, MD, October, 1988.

[2] Newton, Judith J., and Spielman, Frankie E., editors, Data Administration: Standards and Techniques, Proceedings of the Second Annual DAMA Symposium, NISTIR 90-4292, National Institute of Standards and Technology, Gaithersburg, MD, April 1990.

Volume 95, Number 5, September-October 1990
Journal of Research of the National Institute of Standards and Technology

Conference Reports

CIMCON'90 CONFERENCE—COMPUTER INTEGRATED MANUFACTURING (CIM) ARCHITECTURE CONFERENCE (CON) Gaithersburg, MD May 22–24, 1990

Report prepared by

Albert Jones

Center for Manufacturing Engineering,
National Institute of Standards and Technology,
Gaithersburg, MD 20899

The National Institute of Standards and Technology Center for Manufacturing Engineering together with the Navy Manufacturing Technology Program and the Air Force WRDC/MTI program jointly sponsored the first conference to address the problems associated with designing and implementing a system architecture for Computer Integrated Manufacturing (CIM). More than 125 people attended from the United States, Canada, Denmark, England, France, Italy, Japan, the Netherlands, Switzerland, the Soviet Union, and West Germany. The conference was held in conjunction with a meeting of the international standards committee ISO TC 184/SC 5/ WG 1. This committee is looking into the possibility of developing a standard framework for CIM.

1. About the Conference

Two considerations motivated this conference. First, the initial implementation phases of early CIM programs had been completed and a great deal had been learned from those experiences. The conference provided a forum for people to describe their original architectures and implementation plans, to discuss what did and did not work, and to report on changes they might be considering in those architectures and plans.

Second, the ISO TC 184/SC 5/ WG 1 committee had just been assigned a new work item to develop a CIM architecture to aid in identifying standards needed to enable integration of all systems within the CIM enterprise. The conference gave those responsible for developing that architecture the opportunity to discuss this issue with experts from around the world and to learn about the problems involved in integrating new and existing manufacturing systems.

The conference had three major goals: to propose some architectures, to examine some implementation problems, and to discuss some design tools.

2. Opening the Conference

Albert Jones, Conference chairman and Deputy Program Director of the Automated Manufacturing Research Facility (AMRF) welcomed the conference participants. John Lyons, Director of NIST, gave the opening address. In his address, Dr. Lyons pointed out that the conference provided an opportunity for speakers to discuss research and implementation issues related to architectures for computer integrated manufacturing. He emphasized that NIST has been involved in these areas for a number of years through the

AMRF and other programs. He then discussed the new mission and direction of NIST and some of the new projects underway at NIST. Dr. Lyons concluded by stressing the importance of completing the research, development, and technology transfer chain and expressing his hope that the conference would strengthen that chain.

3. Architectures

Albert Jones and Edward Barkmeyer gave the opening paper at the conference. They described the control hierarchy, the distributed data management system, and the communications system developed in the AMRF program at NIST. Sanjay Joshi from Penn State then described how one could use control grammars to implement the control hierarchy described by Jones. He also indicated how one could decompose process plans to match the tasks assigned to the levels in that control hierarchy. Robert Boykin from CAM-I gave an overview of CAM-I's work in CIM architecture development and CIM standards in general. Clyde Van Haren, James River Corporation, presented the Reference Model developed by the International Purdue Workshop. This model includes a hierarchy for shop floor control and data flow diagrams to capture information flows. This strategy was also used to develop the RAMP architecture described by David Jung. Paul Fehrenbach of GEC Marconi Research Centre, UK, described his DtoP (Design to Product) architecture developed as part of an ESPRIT project. Allan Anderson of Honeywell gave an overview of the architectural approach being developed at Honeywell. Michel Böhms of TNO Netherlands gave some criteria for comparing various architectures.

Several European authors described a different approach based on the "matrix concept." The oldest and most famous of these, called CIM-OSA, was described by Richard Panse from IBM Germany. The CIM-OSA framework was developed by the ESPRIT AMICE Consortium. The framework is a three dimensional matrix. One dimension contains three modeling levels: requirements definition, design specification, and implementation description. The second dimension contains three levels of genericity: Generic, Partial, and Particular. The last dimension contains four views: Function, Information, Resource, and Organization. David Shorter, SD Scicon UK, compared the CIM-OSA model with the model developed in the ISO standards committee ISO TC 184/SC 5/WG 1. Bruno Vallespir, GRAI Laboratory France, also described a 36 cell matrix but with different definitions for the dimensions. Wolfram Süssenguth, Fraunhofer Institut Berlin, presented a framework that combined the CIM-OSA matrix with the WG 1 Reference Model.

Shop floor control was addressed by several authors. Two approaches were advocated: heterarchical and hierarchical. In the former, decisions are arrived at by a committee of cooperating agents. James Ting of Michigan University and Matt Johnson of DEC Italy discussed the advantages of this approach at length. In hierarchical control, entities are arranged in a tree structure with each entity having a single supervisor. Frank Biemans and Roli Wendorf of North American Philips discussed the advantages of this approach.

Both Mukasa Ssemakula from the University of Maryland and Wayne Davis of the University of Illinois described architectures for integrating higher level functions such as CAD, CAPP, MRP-II, and production planning with shop floor architectures.

4. Design Tools

Robert Young of NC State University described the $IDEF_0$ and $IDEF_1$ modeling tools and how these tools were used to upgrade existing manufacturing plants in Denmark. Bruno Vallespir reported on his efforts to integrate the IDEF tools with the French-developed GRAI tools to fill in the cells of his architecture. John Sauter of ITI described XSpec, a graphical tool which can represent both physical and control components and the messages that flow between them. Hugh Sparks from MTS Systems Corporation has integrated a graphical dataflow language and object-oriented programming techniques into a design tool called HOSE which is portable to a variety of hardware platforms. Larry Zeidner of Boston University presented the Server Network Generator which provides a distributed software development environment which allows the designer to separate the complexity of individual components from the complexity of their interconnection.

5. Implementation Issues

Richard Weston of Loughborough University, UK, described the AUTOMAIL system as an alternative to the "hard-wired" approach being used in industry today. He gave two examples of how

AUTOMAIL was used to build an integrated printed circuit board cell and manufacturing cell at a major UK computer systems company. Dirk Beeckman of Gap Gemini Sesa, Belgium, provided some results of a recent attempt to use the CIM-OSA concepts to model the FMS in the FIAT Mirafiori plant. He concentrated on the Function and Information views for the Design Specification and Requirements Definition cells in the CIM-OSA matrix. David Jung of Battelle reviewed the lesson learned from attempts to adapt the RAMP architecture to the small mechanical parts cell at the Cherry Point Naval Aviation Depot. Major Knute Hankins, U.S. Army Watervliet Arsenal, discussed the problems involved in integrating off-the-shelf software products and verifying the accuracy of the data that was used to run those packages. John Ettlie of Michigan University used several case studies to give an overview of some of the problems facing industry as they try to automate and integrate.

6. For More Information

Proceedings of CIMCON'90 (NIST Special Publication 785) is available from the Superintendent of Documents, U.S. Government Printing Office, Washington, DC 20402. Order by stock no. 003-003-03010-4 (phone 202/738-3238).

News Briefs

General Developments

NIST SEEKS PROPOSALS FOR MEASUREMENT GRANTS

NIST is seeking project proposals for its FY 1992 Precision Measurement Grants. The grants are for $30,000 for 1 year and may be renewed for up to 2 additional years. Prospective candidates must submit summaries of their proposed projects and biographical information to NIST by Feb. 1, 1991 to be considered for the current grants, which will run from October 1991 through September 1992. The Precision Measurement Grants are awarded each year to scientists in academic institutions for work in determining values for fundamental constants, investigating related physical phenomena, or developing new, fundamental measurement methods. For information, contact Dr. Barry N. Taylor, Chairman, NIST Precision Measurement Grants Committee, B160 Physics Building, NIST, Gaithersburg, MD 20899, 301/975-4220.

STUDY TO HELP UNDERSTAND BONE DEMINERALIZATION

One of the major problems potentially limiting the long-term habitability of outer space is the "demineralization" of human bone that occurs in a microgravity environment. To help understand this loss of calcium and breakdown of bone tissue, scientists need enriched calcium isotopes that can act as markers to study the calcium metabolism process in the body. Researchers from industry are teaming with NIST scientists to develop and evaluate processes aimed at producing large quantities of a marker isotope—calcium-48—inexpensively. Because calcium-48 is not abundant in nature, the isotope must be produced in the laboratory to acquire the needed amounts. Researchers hope that by using laser light to excite calcium-48 at its resonance frequency, they will be able to extract the isotope from samples. The research will be used by the National Aeronautics and Space Administration in its ongoing investigation of space effects on bone tissue. NIST facilities will be used to study specific applications of analytical techniques such as resonance ionization mass spectrometry, a method NIST used recently to trace the origin of ancient rocks.

BASIC MEMBRANE RESEARCH

The NIST membrane separations program helps to bridge the gap between the fundamental work typical of academic laboratories and the applied research of industrial organizations. NIST conducts both basic and applied research on systems that are riskier in terms of near-term payoff. Current areas of interest include gas separations, pervaporation, ultrafiltration, and general studies which include membrane sorption data for a variety of solutes, external field effects on permeation, and membrane bioreactor concepts. A recent paper, no. 40-90, outlines the programs and facilities and discusses current results and future plans. For a copy, contact Jo Emery, Division 104, NIST, Boulder, CO 80303, 303/497-3237. For more information about the program, contact Dr. John J. Pellegrino, Chemical Engineering Sciences Division, NIST, Boulder, CO 80303, 303/497-3416.

BIBLIOGRAPHY OF ELECTRON SWARM DATA

The NIST/University of Colorado Joint Institute for Laboratory Astrophysics (JILA) has published the third general bibliography on electron swarm data. It is a compilation of references to swarm data published between 1978 and mid-1989. An electron swarm is a cloud of electrons in a neutral gas under conditions such that the dominant interactions are the collisions between the electrons and

the gas atoms or molecules. Measurements include drift velocities, diffusion coefficients, rates of growth of electron density due to ionization, electron loss rates due to recombination or attachment, and the rates of excitation of the various atomic or molecular energy levels. The most important application of electron swarm data is in deriving cross sections for low energy electron impact on atoms and molecules. A Bibliography of Electron Swarm Data, 1978-1989, is available from the JILA Atomic Collision Data Center, University of Colorado, Boulder, CO 80309.

MORE EFFICIENT ROUTE DEVELOPED TO LOW-SHRINKAGE POLYMERS

A simple method has been developed by NIST scientists to produce a new class of difunctional monomers that efficiently cyclopolymerize to yield polymers with improved properties, particularly low shrinkage. Investigations have shown how the chemical composition of the monomers may be varied to control the melting temperature and molecular weight of the monomer as well as the crosslink density and glass transition temperature of the resulting polymer.

The cyclopolymers exhibit more complete polymerization and a reduced degree of polymerization shrinkage compared with conventional diacrylate-based polymeric materials. Other properties, including high-glass transition temperatures, excellent hydrolytic stability and improved processibility, make these monomers attractive for a wide range of applications.

An evaluation of the new cyclopolymerizable monomers as dental composite filling materials has demonstrated improved dimensional stability, hardness, and strength.

The same chemistry can supply multifunctional oligomers capable of several discrete cyclopolymerizations per chain to produce highly crosslinked polymers. A similar reaction also has been exploited to yield highly fluorinated functional monomers. These novel monomers can form soluble or crosslinked polymers which are extremely hydrophobic and solvent resistant. In contrast, the dicarboxylic acid derivative of the monomer provides a water soluble monomer/polymer system that may be useful in adhesive applications.

WEAR MECHANISMS IN COAL-FUELED DIESEL ENGINES

Diesel engines capable of operating directly on pulverized coal are currently under development by U.S. industry. Improved processes for the production of highly refined coal-fuels, the great abundance of coal, and diminishing supplies of crude oil are strong incentives for this effort. However, commercial success will require finding solutions to a number of technical problems, such as the high rate of wear of piston rings and cylinder liners. Researchers at NIST under the sponsorship of DOE are conducting a program to develop an understanding of the processes that are responsible for the high rates of wear. The primary mechanism appears to be that of abrasive wear due to the presence of mineral particles, such as silicates, in the coal combustion products. Although silicates can cause significant abrasion of conventional chromium plating and cast iron materials used in diesel engines, they are far less damaging to hard ceramics and ceramic-metal composite materials. Results of this program will assist in the selection and development of improved engine component materials to resist wear in the harsh coal-fuel environment. Indeed, engine developers are currently focusing on the use of such materials, probably in the form of coatings, to protect cylinder liners and piston rings from wear.

FIRST SEMPA IMAGES OF MAGNETO-OPTICAL RECORDING MEDIA

Magneto-optical disk drives are just now entering the personal computer and workstation market. This technology uses a laser and an alternating magnetic field to read and write onto a ferrimagnetic TbFeCo alloy film coating on a rotating disk. The storage density is very high, allowing over 600 megabytes to be stored in a package comparable in size to a floppy disk. However, despite intensive research, the basic magnetic domain structure of these films is poorly understood. The domains are unusually small (about 1 μm^2) and have very weak saturation magnetization.

NIST scientists were able to measure the surface magnetic microstructure of written domains in several TbFeCo alloys using scanning electron microscopy with polarization analysis (SEMPA). SEMPA, developed by NIST researchers, is capable of resolving magnetic microstructure with 50-nm spatial resolution. The instrument employs a scanning electron microscope to excite secondary electrons at surfaces. Analysis of the spin-polarization of the emitted secondary electrons generates high-resolution maps of surface magnetization.

The observations of written domains in TbFeCo alloys are the first SEMPA measurements in ferri-

magnetic systems and the first demonstration that the polarized secondary-electron cascade, which underlies the magnetic contrast in SEMPA, is dominated by the 3-*d* valence electrons from the transition metals in these alloys. The quality of the thermomagnetically written bits was investigated as a function of alloy composition and applied switching field intensity. The SEMPA measurements revealed that the demagnetizing field, which affects the nucleation and growth of domains, was the most important parameter for ensuring the regularity of the written bits.

SECURE DATA NETWORK SYSTEM (SDNS) REPORTS PUBLISHED

Three new NIST publications present the results of Phase I of the SDNS, a government/industry project sponsored by the National Security Agency (NSA). The SDNS project was initiated by NSA to investigate methods of implementing security in a distributed computer network. The results of the project consist of a set of specifications that include security services, protocols, and mechanisms for protecting user data in networks that are based on the open systems interconnection computer network model.

NIST is publishing the documents to make them broadly available and to advance their consideration as voluntary industry standards. NISTIR 90-4250, Secure Data Network System (SDNS) Network, Transport, and Message Security Protocols, includes four security protocol documents. NISTIR 90-4259, Secure Data Network System (SDNS) Access Control Documents, presents access control concepts, while key management protocols are contained in NISTIR 90-4262, Secure Data Network System (SDNS) Key Management Documents.

REVISION TO FIPS 120, GRAPHICAL KERNEL SYSTEM (GKS), PROPOSED

A revision has been proposed to FIPS 120, graphical kernel system (GKS), to add a requirement for validation of GKS implementations acquired by federal agencies. The standard adopts the American National Standard Graphical Kernel System (ANS GKS), which consists of four parts: the basic functions for computer graphics programming (ANSI X3.124-1985); the FORTRAN programming language binding for GKS (ANSI X3.124-2-1988); the Pascal programming language binding for GKS (ANSI X3.124-2-1988); and the Ada programming language binding for GKS (ANSI X3.124.3-1988). ANS GKS specifies a library of subroutines which permit the production and manipulation of two-dimensional pictures, enhancing the portability of graphics applications between different computer systems.

FIPS 100 BEING REVISED

NIST has proposed a revision to FIPS 100, interface between data terminal equipment (DTE) and data circuit-terminating equipment (DCE) for operation with packet-switched data networks (PSDNs), or between two DTEs, by dedicated circuit, and federal standard (FED-STD) 1041. The proposed revision specifies the interface between DTE such as ADP equipment and telecommunication system terminal equipment, and DCE for operation in the packet mode on PSDNs, or between two DTEs, by dedicated circuit.

The revised standard will adopt for federal agency use American National Standard (ANSI) X3.100-1989, which in turn adopts CCITT Recommendation X.25-1988, ISO 7776-1989, and ISO 8208-1987. After comments received from industry and the public have been considered, the revised FIPS will be forwarded to the Secretary of Commerce for review and approval.

FIPS FOR PROGRAMMING LANGUAGE C PROPOSED

NIST has proposed a new FIPS for programming language C, which will adopt American National Standard (ANSI) X3.159-1989. The standard specifies the form and establishes the interpretation of programs written in the C programming language. The proposed FIPS would promote portability of C programs for federal agency use on a variety of data processing systems.

AMERICAN SOCIETY FOR METALS ADOPTS NIST-DEVELOPED SOFTWARE TO FURTHER ITS PHASE DIAGRAM PUBLICATIONS

The NIST-developed software FHAZE will be used for ASM's major programs in phase diagram production. ASM has acquired computer workstations and staff to digitize data for 4,700 phase diagram graphs. The resultant high-quality graphics will be published in a second edition of Binary Alloy Phase Diagrams. Upon completion of that publication, one of the workstations will continue its role for digitizing graphs for the Journal of Phase Equilibria and the ASM Monograph series on alloy phase diagrams.

FHAZE incorporates the modern graphics capabilities of the GKS graphics standard for graphics terminals which can selectively update a screen,

and LISP-based programming methods for representing the complex graphical data structures required for metal alloy phase diagrams. The program has produced publication quality graphic output for phase diagrams in a wide range of styles and provided a means for transcribing, fitting, viewing, and organizing the data from a fundamental, i.e., thermodynamic point of view. The FHAZE software was used by ASM and NIST to produce phase diagrams for approximately 1,850 alloy systems in the two-volume first edition of Binary Alloy Phase Diagrams. At the time of its publication in 1987, it was world's most complete source of reliable data on alloy phase diagrams.

FREQUENCY STABILIZATION OF ERBIUM FIBER LASER OFFERS POTENTIAL FOR WAVELENGTH STANDARD

A NIST scientist has for the first time successfully stabilized in frequency the output from an erbium-doped optical-fiber laser that can be tuned to a single frequency over the range 1.52 to 1.57 μm, and that has an unstabilized linewidth of less than 1 MHz. These characteristics offer considerable potential for use as a wavelength standard for optical communication systems, needed especially for coherent systems and those using frequency-division multiplexing. The only laser line available previously in this wavelength range is a transition (untunable) at 1.52 μm in helium-neon. To remove long-term frequency drifts, the scientist stabilized the laser to an absorption line of acetylene near 1.53 μm by arranging to change the laser cavity length electronically in response to an error signal derived from the acetylene absorption.

NIST WORK LEADS TO ADOPTION OF THREE ASTM STANDARDS ON ELECTROMIGRATION MEASUREMENTS

NIST collaborative efforts with the semiconductor industry have resulted in the adoption of three electromigration-related standards by ASTM (formerly American Society for Testing and Materials). A NIST scientist was the originator and prime mover of these standards, which also recently have been adopted by the Electronics Industries Association Joint Electron Device Engineering Council (EIA/JEDEC) Committee 14.2 on Wafer Reliability for its wafer-level electromigration stress tests. These standards are: F 1260-89, Standard Test Method for Estimating Electromigration Median Time-to-Failure and Sigma of Integrated Circuit Metallizations; F 1259-89, Standard Guide for Design of Flat, Straight-Line Test Structures for Detecting Metallization Open-Circuit or Resistance-Increase Failure Due to Electromigration; and F 1261-89, Standard Test Method for Determining the Average Width and Cross-Sectional Area of a Straight, Thin-Film Metal Line. In response to increasing industry concerns about failures resulting from electromigration, the standards provide procedures for conducting electromigration stress tests and for designing test structures to support these tests and promote the reproducibility of the characterization of metallization interconnects in very-large-scale integrated circuits. The standards also serve to reduce disagreements between vendor and user, enhance confidence in test data among workers in the field, and lead to more effective research and development for reliability and performance improvements.

NEW VIDEO CAN HELP SAVE ENERGY AND DOLLARS

Energy-efficient buildings make dollars and sense. But tight operating and construction budgets often force tough decisions to be made on energy-conservation projects. A new video training program developed by NIST gives building professionals the basic tools needed to evaluate the cost-effectiveness of these decisions. The 1-h video is the first in a series NIST is producing for the U.S. Department of Energy (DOE). NIST economists and a DOE engineer explain basic concepts of life-cycle cost analysis and demonstrate problem-solving techniques and computer programs that can be used to calculate a building's energy consumption and the life-cycle costs of alternative designs and systems. By the end of the video, the viewer should be able to solve simple, but realistic, problems. A workbook accompanies the video. The videotape, titled Least-Cost Energy Decisions: An Introduction to Life-Cycle Cost Analysis, is available from Video Transfer Inc., 5709-B Arundel Ave., Rockville, MD 20852, 301/881-0270. VHS format is $19. Contact Video Transfer Inc. for prices on other formats.

CHARACTERIZING CLOCKS AND OSCILLATORS

Managers of calibration laboratories in private industry, universities, the military, and government agencies will be interested in a new publication from NIST. Characterization of Clocks and Oscillators (NIST TN 1337) is a collection of published papers designed as a reference for those involved in

characterizing and specifying high-performance clocks and oscillators. It is an interim replacement for NBS Monograph 140, Time and Frequency: Theory and Fundamentals, which was published in 1974. The current volume includes tutorial papers, papers on standards and definitions, and papers detailing specific measurement and analysis techniques (with corrections and notes indicating current recommended IEEE notation). Topics covered include properties of signal sources, phase noise measurements, standard terminology, stability measurement, and biases and variances. TN 1337 is available from the Superintendent of Documents, U.S. Government Printing Office, Washington, DC 20402. Order by stock no. 003-003-03019-8 for $17 prepaid.

ATMOSPHERIC ATTENUATION MEASUREMENTS STUDIED

While developing measurement methods to determine the performance of 7- to 10-GHz satellite Earth terminals, including such parameters as gain, G/T, and satellite effective isotropic radiated power, NIST researchers examined methods to correct for atmospheric attenuation effects. At 7 to 10 GHz, the principal atmospheric effects on a radio signal are the attenuations due to absorption by oxygen and water vapor molecules, and to scattering by particles of water (rain, clouds, and fog). X-Band Atmospheric Attenuation for an Earth Terminal Measurement System (NISTIR 89-3918) provides an overview of various methods to determine atmospheric attenuation (sky brightness tipping-curve method, radio source extinction curve method, and dual frequency radiometer technique) and analyzes the errors of these methods. Copies may be ordered from the National Technical Information Service, Springfield, VA 22161. Order by PB #90-100736 for $13.95 prepaid.

ELECTROMAGNETIC PROPERTIES OF SUPERCONDUCTORS

Designers and builders of high-energy physics magnets (including those for the Superconducting Super Collider) and of nuclear magnetic resonance instruments need data on the performance of superconductors and high-permeability steels. NIST has studied the effects on the superconductor critical current of mechanical loading and of the deformation resulting from fabrication. NIST also has evaluated the magnetic properties of several types of steel alloys used in these magnets and instruments. A report, Electromechanical Properties of Superconductors for High Energy Physics Applications, Part II (NISTIR 89-3912), describing NIST's findings is available from the National Technical Information Service, Springfield, VA 22161. Order by PB #90-163627 for $23. An earlier report, Electromagnetic Properties of Superconductors for High Energy Physics Applications (NISTIR 86-3061) can be ordered by PB #87-165585 for $23 prepaid.

MEASUREMENT NEEDS FOR NEW TECHNOLOGIES IN ELECTRONICS

New technologies and products based on microwaves, superconductors, lightwaves, advanced imaging technology, semiconductors, and magnetics share a common need now: more sensitive and accurate measurement techniques. A 192-page report now available from NIST devotes a chapter to the measurement role in each of eight key emerging technologies. Measurement is important to the electronics industry because it affects every phase of product realization, from research and development to manufacturing, marketing, and use. Bad measurement means wasted time and defective products. NIST managers hope the emerging technologies report will help define the research direction of measurement support for these technologies and will foster greater cooperation between NIST and industry. To receive a copy of Emerging Technologies in Electronics . . . and Their Measurement Needs: Second Edition (NISTIR 90-4260), contact the Center for Electronics and Electrical Engineering, B358 Metrology Building, NIST, Gaithersburg, MD 20899, 301/975-2220.

ELECTRICAL ENGINEERING/ELECTRONICS BULLETIN AVAILABLE

NIST measurement programs in semiconductor technology, signals and systems, electrical power, and electromagnetic interference are described in a publication now available. The Technical Progress Bulletin covers NIST's Center for Electronics and Electrical Engineering and its programs, which provide national reference standards, measurement methods, supporting theory and data, and traceability to national standards. Included are abstracts of papers and published works arranged by topic (with phone numbers of contacts). Semiconductor subjects covered include silicon materials, dimensional metrology, photodetectors, and device physics and modeling. Also included are sections on waveform, antenna, cryoelectronic, electro-optic, optical fiber, and power systems metrology. To receive the most recent issue or to be placed on

the mailing list, write to or call (stating your professional affiliation or technical interest): Technical Progress Bulletin, Center for Electronics and Electrical Engineering, B358 Metrology Building, NIST, Gaithersburg, MD 20899, 301/975-2220.

NIST EXPANDS SECURITY BULLETIN BOARD

The NIST Computer Security Bulletin Board has been expanded making it easier to access the information stored in the system. In operation since October 1989, this electronic bulletin board contains a variety of information dealing with computer security, including bibliographies of relevant publications and listings of security-related seminars and conferences. In addition, the system contains information issued by NIST and others concerning computer security incidents, such as computer virus attacks. NIST also will use the bulletin board to disseminate information about future incidents. A standard ASCII terminal or a personal computer with serial communications capability is needed to access the bulletin board. The terminal should be set up for these communications parameters: 2400, 1200, or 300 modem baud rate; 8 data bits with no parity (or 7 with even parity); and 1 stop bit. Phone 301/948-5717 to connect with the board. The system is available 24 hours a day. For further information, call NCSL Security BBS assistance at 301/975-3359 or use the message subsystem of the bulletin board.

PHIGS CONFORMANCE TEST AVAILABLE

The Programmer's Hierarchical Interactive Graphics System (PHIGS) provides a standard library of routines for use in programming three-dimensional graphics. PHIGS is a Federal Information Processing Standard (FIPS 153), which adopts a voluntary industry standard (ANSI X3.144-1988). NIST has developed a test system to help users and vendors determine whether the complex data structures used to generate the graphics displays conform to FIPS 153. A future version will include interactive tests to determine if the visual output, the picture on the screen, is correct. The test suite consists of a set of FORTRAN programs that can be easily adapted for most computer system operating environments. The PHIGS validation test costs $1,000 for the first operating environment, $1,500 for two different environments, and $2,000 for three. Four or more will cost $2,500. A user guide describing the test suite installation and operation as well as guidance on interpreting the tests results is included. To order, contact John Cugini, A266 Technology Building, NIST, Gaithersburg, MD 20899, 301/975-3248.

BASICS OF CHEMICAL INSTRUMENTATION EXPLAINED

A recent NIST publication provides an introduction to chemical instrumentation for persons working outside the field of experimental chemistry. The Basics of Chemical Instrumentation, Volume 1—Separation Methods (NISTIR 89-3933) discusses the instrumentation and techniques of all major separation methods used in chemical analysis. The discussion begins with the characteristics of mixtures and the molecular properties affecting the separation process. Topics include gas chromatography, high-performance liquid chromatography, supercritical fluid chromatography, and electrophoresis. Important calibration methods are also discussed. NISTIR 89-3933 is available from the National Technical Information Service, Springfield, VA 22161. Order by PB #90-198458 for $23 prepaid. A volume on spectroscopic methods will be available later.

COAXIAL INTRINSIC IMPEDANCE STANDARDS DESCRIBED

Today's automatic network analyzers (ANAs) have resolutions better than the accuracy of the coaxial impedance standards used to calibrate them. ANAs are used to measure critical performance parameters of many types of microwave systems and to calibrate secondary standards used to support laboratory instrumentation. NIST has published a technical report that describes how microwave impedance standards are derived from basic dimensional metrology, how they are constructed, and how they are used in calibrating coaxial air-line systems using ANAs. It provides the first selected examples of how impedance measurement uncertainties depend on the effects of dimensional (or mechanical) tolerances for 14-, 7-, and 3.5-mm coaxial devices. Coaxial Intrinsic Impedance Standards (TN 1333) is available from the Superintendent of Documents, U.S. Government Printing Office, Washington, DC 20402. Order by stock no. 003-003-02987-4 for $1.75 prepaid.

NIST, APL STUDY AUTOMATED ELECTRONICS ASSEMBLY

NIST and the Applied Physics Laboratory (APL) of the Johns Hopkins University have established a 1-year cooperative research program. The goal is to achieve productivity and quality improvements in computer-integrated manufacturing systems used for electronics assembly. Surface-mount printed-circuit boards would be a typical product. The project will include the specification of process and quality control techniques and strategies, computer hardware and software, data requirements, and interface and support standards, such as STEP (STandard for the Exchange of Product model data) and the Defense Department's CALS (Computer-aided Acquisition and Logistic Support) standards. New concepts for process control sensors will be tested. The project draws on NIST skill in process control sensors, automation, and standards technology, and APL expertise in applications and electronics manufacture.

NEW ACCREDITATION PROGRAM ANNOUNCED FOR TESTING LABS

NIST has established a laboratory accreditation program for labs that test plumbing products and devices. Labs can seek accreditation to test plumbing fixtures under ANSI Z124 standard series for plumbing plastics and to test fixture fittings and fixtures under ASME/ANSI 112 standards 18.1 and 19.2. The new program is part of the National Voluntary Laboratory Accreditation Program (NVLAP) for commercial products, which was established at the request of the International Coalition for Procurement Standards to provide buyers with a list of accredited labs that can test products to conform to contract specifications. The program also meets the needs of public authorities for energy and water conservation programs nationwide. Labs seeking accreditation for one or more of the test methods must meet all NVLAP criteria and renew their status annually to maintain accreditation. For information, contact Dr. Lawrence S. Galowin, NVLAP, A124 Building 411, NIST, Gaithersburg, MD 20899, 301/975-4022, fax: 301/975-3839.

GUIDELINES ISSUED FOR PRESSURE VESSEL SAFETY ASSESSMENT

Deterioration of certain kinds of pressure and storage vessels in the United States could result in the loss of dozens of lives and millions of dollars. A NIST study, sponsored by the Occupational Safety and Health Administration, gives an overview of stationary, unfired carbon steel and low-alloy steel pressure vessels for liquids and gases, and low-pressure storage tanks used at temperatures between −75 and 315 °C (−100 to 600 °F). These vessels are used in the process, pulp and paper, petroleum refining, and petroleum chemical industries, and for water treatment systems for boilers and steam generators. Guidelines for Pressure Vessel Safety Assessment (NIST SP 780) describes pertinent sections of ASME and API codes and standards governing vessel construction, testing, and inspection; causes of failure; and nondestructive inspection standards, practices, and methods. Data and information needed to assess the safety of these vessels and tanks are also given. SP 780 is available from the Superintendent of Documents, U.S. Government Printing Office, Washington, DC 20402. Order by stock no. 003-003-03003-1 for $4.25 prepaid.

INDUSTRIAL FIRM TO CONSULT WITH NIST ON POLYMERS

A private company has established a research associate program at NIST to consult with institute scientists on non-proprietary polymer blends of polycarbonate and poly (methyl methacrylate) (PMMA) materials. Scientists from the industrial firm will use the NIST time-resolved light-scattering instrument and small-angle neutron scattering techniques at NIST's research reactor to measure the kinetics and thermodynamics of polymer blend phase behavior. Blends of PMMA with polycarbonates or other polymers are used widely in manufacturing transparent window panels or molded into large-scale plumbing fixtures such as bath tub enclosures and shower stalls. The NIST Research Associate Program provides an opportunity for engineers and scientists from industry, universities, technical societies, and other organizations to conduct cooperative research at NIST on projects of mutual interest, with salaries paid by the sponsor.

RISK ASSESSMENT THE DOE WAY

An important part of developing a computer security program is weighing the costs of controls against the risk of loss. Controls that are more expensive than the information they protect are not cost-effective. To help achieve a balance, NIST is investigating ways to identify risks and select appropriate cost-effective computer security

measures, that include making available information on methods developed by other federal agencies. NIST recently reprinted a publication describing the risk assessment method used by the U.S. Department of Energy (DOE). The DOE approach specifies six steps, including defining the system, software, and data; identifying threats; selecting countermeasures; and obtaining management review, participation, and accountability. Included in the publication are worksheets and tables needed to carry out each step. Also included is a sample completed worksheet, a bibliography, and a glossary. U.S. Department of Energy Risk Assessment Methodology (NISTIR 4325) is available from the National Technical Information Service, Springfield, VA 22161. Order by PB #90-244484 for $23 prepaid.

MEASURING FLOW IN THE SPACE SHUTTLE

NIST scientists are solving one of the world's trickiest measurement problems—gaging the superfast flow (up to 185 ft/s) of liquid oxygen in ducts of the space shuttle main engine. Accurate measurement is important to obtain maximum fuel efficiency in the huge engine. The flow velocity is almost 10 times greater than the maximum for which commercial flowmeters are designed. To make matters worse, the ducts are continuously curved, leaving very little space to install the meters. In smaller ducts, the meter has to be inserted through an instrument port less than half an inch in diameter. A NIST researcher has designed vortex shedding flowmeters, which have been tested with both water and liquid nitrogen. Some meters have measured flows up to 180 ft/s and can fit into the instrument ports. More testing is needed, and more work is required with sensors designed to convert the flow rate into electrical signals for readouts. Two papers discussing the project are available from Jo Emery, Division 104, NIST, Boulder, CO 80303, 303/497-3237. Ask for no. 31-90.

NINE GRANTS AWARDED FOR STATE TECHNOLOGY PROGRAMS

The Commerce Department's Technology Administration (TA) has announced the award of nine grants to state governments under the Boehlert-Rockefeller Technology Extension Program. The states receiving a total of $910,845 in grants include Arkansas, Georgia, Maryland, Massachusetts, Michigan, Minnesota, New York, Pennsylvania, and Tennessee. "One of the most exciting developments of the last few years in the area of technology transfer has been the appearance of an impressive array of imaginative, aggressive programs sponsored by state and local governments," said Under Secretary Robert M. White, who heads TA. The Boehlert-Rockefeller grant program was established under the 1988 Technology Competitiveness Act and is administered by NIST, which is part of TA. This is the first year that funding has been available for such grants. The grants are made for projects that either demonstrate cooperative programs with federal laboratories that can increase the use of government-developed technology by industry, or help businesses take advantage of services and information available from NIST or its Regional Centers for the Transfer of Manufacturing Technology.

IS YOUR OFFICE USER-FRIENDLY?

What do you consider the most important feature in an office? Functionality? Privacy? Aesthetics? How important are design and furnishings? As part of its ongoing program to assist the building industry, NIST researchers recently asked these questions of office space designers and facility managers from 22 major corporations and government agencies. The survey was conducted to provide insights about how offices and workstations are planned and designed. Included were the effects of technology on design, space allocations, and systems furnishings. Among the findings: respondents rated functionality, privacy, storage, and aesthetics as the top features needed for a high-quality workplace. In comparing today's offices with those of 5 years ago, they said that design and furnishings are more important now and that more space for support activities is needed. In addition, the group felt user input to workspace and equipment planning was very important. A report, High Technology Office Evaluation Survey—A Pilot Report (NISTIR 4354), is available from the National Technical Information Service, Springfield, VA 22161. Order by PB #90-244427/AS for $17 prepaid.

DIRECTORY PUBLISHED ON WEIGHTS AND MEASURES LABS

State Weights and Measures Laboratories: State Standards Program Description and Directory (NIST SP 791) is designed to help manufacturers and others in commerce and industry locate and obtain needed measurement services. The directory is a guide to state and other labs certified by NIST that are capable of performing reliable measurements with staff trained in proper procedures. To

be certified in a particular area, each state must have a trained metrologist and an adequate facility, and must demonstrate on a continuing basis that it is capable of providing valid measurements. NIST certification indicates the laboratory is capable of providing a measurement service, but each state is responsible for verifying its measurement traceability. The directory contains the following information for each lab: the certification period, if certified by NIST; lab staff members, addresses, and telephone or fax numbers; services available; and fees, if any, for services. Copies of SP 791 are available from the Superintendent of Documents, U.S. Government Printing Office, Washington, DC 20402. Order by stock no. 003-003-03024-4 for $3.75 prepaid.

AUTOMATED STRESS ANALYSIS OF SOLDER JOINTS USING INSPECTION DATA

NIST is collaborating with the U.S. Army and private industry to develop a new procedure to assess the integrity of solder joints on certain advanced electronic packages, specifically, printed wiring boards manufactured using surface mount technology. Computer programs have been developed to convert coordinate points on the solder joint surface, obtained by advanced x-ray and optical inspection devices, into finite element meshes for stress analysis. Industry collaborators have provided trial data sets of over 1,000 *xyz* coordinate points on a solder joint surface from an x-ray laminography system and a laser vision system. Automated stress analysis will permit rapid assessment of the significance of geometrical irregularities on the reliability of the solder joints. The new method will be applied in the manufacture of products for the U.S. Army under the guidance of the Harry Diamond Laboratories.

REFRACTORY MATERIALS AT ULTRA-HIGH TEMPERATURES

Using a novel technique, under development at NIST, materials thermal stability data have been obtained for the first time at temperatures in the range of 3000-5000 K. The technique relies on use of a pulsed laser to produce the ultra-high temperatures, coupled with a high-pressure molecular beam sampling mass spectrometer system for vapor species determinations. Thermochemical data have been obtained for the refractory systems SiC and HfO2, which are under consideration for atmospheric re-entry aerospace applications at very high temperatures. The results of this work will be presented at a special Electrochemical Society Symposium on High Temperature Materials Chemistry.

NEW CERAMIC PHASES CHARACTERIZED IN COLLABORATIVE PROGRAM

Scientists from industry, academia, and NIST have begun a new collaborative program in the area of high-T_c superconductors. In this collaboration, new phases of compounds in the phase diagrams of strontium oxide, calcium oxide, bismuth oxide, and copper oxide have been synthesized, and their crystal structures are being determined to very high precision by means of neutron and x-ray diffraction. Neutron diffraction plays a critical role in this effort because of its sensitivity to light-atom positions even in the presence of heavy atoms, and the structural details that can be determined via Rietveld refinement even from polycrystalline samples.

The knowledge obtained from the elucidation of the structures of these new phases is directly related to the crystal chemistry, phase equilibria, and stability of the most important of the high-T_c superconductors discovered to date. This work will provide a part of the foundation needed for further advances in superconductor properties, critical to their technological applications.

NEW STANDARD FOR POLYMER PROCESSING

A new standard to be used in the process control of polymers has been prepared by NIST scientists. Six companies supported the development of the standard, which was produced under the auspices of ASTM subcommittee D20 on fundamental thermal properties. The new poly-propylene standard extends the temperature range of existing NIST standards used to calibrate the melt flow rate apparatus. This standard addresses the need for higher temperature calibrations brought about by recent trends to produce plastics products with higher use temperatures.

ASTM method D1238-88, Standard Test Method for Flow Rates of Thermoplastics by Extrusion Plastometer, is commonly used by both polymer resin producers and users to determine the melt flow rate of polymer resins. The melt flow rate determines the pressure needed to inject or extrude a polymeric material at a desired rate of flow.

CONSORTIUM ON AUTOMATED ANALYTICAL LABORATORY SYSTEMS (CAALS) MEETS AT NIST

A 13-member consortium, comprised of instrument manufacturers, instrumentation users, and government agencies, have joined together to promote the development of automated analytical chemistry instrumentation. The initial CAALS undertaking is to develop guidelines for creating modular instruments that can be used to build analytical systems. Two such systems are currently being created to demonstrate CAALS concepts. Future plans call for building more intelligence into these analytical systems and improving the quality assurance of the information produced, so that eventually standard analytical methods can be built around this instrumentation. CAALS will provide its instrument manufacturing members with a strong, unified basis for competing in the worldwide marketplace and will provide its members who are users of instruments with new tools to handle their ever increasing demands for chemical information.

FIRST INFRARED SPECTRA OF DIMER IONS

Experiments at NIST have yielded infrared spectra for several molecular ions and dimer ions. Although laser-based gas-phase studies have yielded infrared spectral data for some simple molecular ions, no infrared data have ever before been obtained for dimer ions. In the NIST experiments, ions and dimer ions are frozen in a large excess of solid neon. This prevents the ions from reacting with molecules in the sample. Dimer ions that have been observed include O_{4+} and O_{4-}, key reaction intermediates in the chemistry of the Earth's stratosphere. Analysis of their infrared spectra has yielded important information on their structures and chemical bonding properties. Dimer ions are important chemical reaction intermediates in high-energy systems such as discharges used for the generation of laser radiation, industrial chemical synthesis, and plasma processing of semiconductors. Infrared spectra, in addition to being of fundamental scientific interest, can provide a basis for remote sensing techniques that monitor important reaction intermediates in chemical processes.

USER INTERFACE COMPONENT OF THE APPLICATIONS PORTABILITY PROFILE AS A FEDERAL INFORMATION PROCESSING STANDARD (FIPS) APPROVED

FIPS 158, User Interface Component of the Applications Portability Profile (APP), was recently approved for federal agency use. To be effective November 15, 1990, FIPS 158 adopts the X Protocol, Xlib Interface, Xt Intrinsics, and Bitmap Distribution Format specifications of the X Window System, Version 11, Release 3 (X Window System is a trademark of MIT). The new standard should be considered for network-based bit-mapped graphic systems that are developed or acquired for government use where distributed/networked bit-mapped graphic interfaces to multi-user computer systems are required. FIPS 158 addresses the user interface functional area of the APP that is described in FIPS 151-1, POSIX: portable operating system interface for computer environments.

NEW PUBLICATION DESCRIBES OBJECT DATABASE MANAGEMENT SYSTEMS

NIST Special Publication 500-179, Object Database Management Systems: Features and Concepts, provides managers and software analysts a state-of-the-art review of object database management systems (ODBMS). The emergence of object concepts and their infusion into information systems technology spanned the 1980s, beginning with the advent of programming languages that included object concepts. More recently, object concepts have been merged with database management system technology, resulting in the production of some object database management systems. As a result, the term ODBMS is now becoming a recognized and important topic in the database community.

MAGNETORESISTIVE RECORDING HEAD FABRICATED, MEASURED

A NIST scientist has fabricated a magnetoresistive head device and measured its magnetoresistive properties in a new program for developing methods to characterize advanced thin-film recording heads used with high-coercivity magnetic media. The magnetoresistive data show the presence of abrupt jumps in the plot of resistance as a function of magnetic field. These discontinuities result from Barkhausen noise, which is produced by the interaction of magnetic domain walls with microdefects and strains in the heads and severely degrades head performance. Methods of reducing this noise using new multilayered thin films will be a major focus of the research.

NIST DEVELOPS NEW OPTICALLY PUMPED INTEGRATED-OPTIC LASER

NIST scientists have designed, constructed, and operated a new miniaturized continuous-wave laser having a wavelength of 1057 nm. The scientists used integrated-circuit fabrication techniques in

conjunction with electric-field-assisted ion exchange to form the optical waveguide that serves as the laser cavity within a thin surface layer of a small plate of neodymium-doped soda-lime-silicate glass. The resulting channel waveguide is approximately 1 cm in length, 8 μm in width, and 6 μm in depth; these dimensions make it possible to use the laser with optical fiber systems. A commercially available laser diode provides optical pumping. NIST is continuing to study the present laser, for example to investigate an anticipated tuning range of 10 nm centered at the present 1057-nm line and lasing action at 900 and 1300 nm, suggested by the existence of strong photoluminescence peaks. In addition, NIST will use the fabrication technology it has developed to construct integrated-optic lasers with other rare earth dopants and glass hosts. One goal is to discover a combination that operates near the commercially important wavelength of 1500 nm. This work is part of the NIST program to develop metrology for lightwave technology; the group anticipates commercial interest in these results.

NIST, INDUSTRY APPLY EXPERT SYSTEM TO SCREEN PRODUCTION-LINE INTEGRATED CIRCUIT WAFERS

NIST and industry developed and tested an expert system for work-in-process (WIP) wafer screening. WIP screening involves making electrical measurements on a partially fabricated integrated-circuit wafer to predict what percentage of the finished circuits on the wafer will function correctly. Wafers for which a low percentage or yield is expected are discarded or reprocessed. NIST scientists first developed an expert system to analyze WIP data and then applied it to data from 90 wafers. Two hundred and fifty parameters were measured for each of about 20 test chips on each wafer. All of these wafers had been fabricated to completion, and the yield of each wafer was entered into the expert system along with WIP data. The expert system then identified which of the 250 parameters were significant in determining the yield. It constructed a decision tree so that chips could be classified by expected yield according to the values of these significant parameters. Based on the data from the 90 wafers, the expert system was able to classify accurately chips according to their expected yield in about 80 percent of the cases. Continued development of this measurement tool is expected to cut manufacturing costs significantly by avoiding needless processing for wafers that are destined to fail.

EGO-MOTION FIELD THEORY DEVELOPED

A new theory of ego-motion and optical flow has been developed by NIST. Ego-motion is the motion of a camera through a 3-D environment. Optical flow is the flow of intensity information across the camera image plane as the camera moves. The theory describes the structure of a field in 3-D space consisting of contours and surfaces surrounding the moving camera. If static objects are placed anywhere in the surrounding space, the optical flow produced by these objects in the camera is predicted by the field theory. The field is always centered at the camera focal point and moves with the camera. The structure of the field changes as a function of the instantaneous camera motion.

NIST has tested the theory with many experiments using simulations and lab set-ups. It has been applied most heavily to obtaining a quantitative understanding of camera fixation, i.e., controlling the camera orientation during motion so that it continuously points at a single point in space. NIST is currently applying the theory to the problem of road following, where the goal is to control autonomously a vehicle so that it follows a road only using information obtained from a camera mounted on the vehicle.

Calibration Services

INEXPENSIVE FREQUENCY CALIBRATION SERVICE AVAILABLE

The NIST Automated Computer Time Service (ACTS), a dial-up service begun in 1988, can also act as an inexpensive frequency calibration service. NIST researchers have found that a frequency calibration accuracy of better than one part in a billion is readily available from a single long telephone call or from a sequence of short calls averaged over a few days. The cost of hardware and software for ACTS is only about $100 versus up to several thousand dollars for most other frequency dissemination services with this level of accuracy. Access ACTS by dialing 303/497-4774. Software

can be obtained for $36 from the Standard Reference Materials Program, Rm. 204 Building 202, NIST, Gaithersburg, MD 20899, 301/975-6776. Ask for Automated Computer Time Service, RM 8101. The system will work with modems with rates of 300 bits/s or 1200 bits/s. Modems at 300 bits/s seem to offer better stability. Paper no. 44-90 describes the service and is available from Jo Emery, Div. 104, NIST, Boulder, CO 80303, 303/497-3237.

NIST ESTABLISHES SPECIAL-TEST SERVICES FOR COMPLEX PERMITTIVITY MEASUREMENT

NIST has announced the establishment of new special-test services for dielectric material measurement. These services result from a 3-year effort to establish national traceability for measurements of electromagnetic parameters of materials. NIST has concentrated its initial work on the development of methods for measuring the permittivity, or dielectric constant, of low-loss materials. Accomplishments underlying the new service include the development of a precision resonant cavity, together with rigorous characterization of the cavity system and of its uncertainty; development of a broadband method based on a coaxial transmission line; and participation in national and international comparisons. The new services are available solely on a prearrangement basis and at present are limited to solid, low-loss dielectric materials that are linear, homogeneous, isotropic, and nonmagnetic. All measurements currently are performed at room temperature (23 °C). Two classes of dielectric measurement services are available. The most precise is a measurement in the resonant cavity near 10 GHz with an accuracy of 0.5 percent for the dielectric constant. Less accurate broadband measurements are available in 7-mm coaxial transmission line from 50 MHz to 18 GHz, in WR284 waveguide from 2.6 to 3.95 GHz, and in WR90 waveguide from 8.2 to 12.4 GHz.

Standard Reference Materials

MATERIALS CAN HELP EVALUATE INDUSTRIAL ATMOSPHERE

Regulatory agencies and others studying the toxic metal concentration of industrial environments now have a new tool to help them achieve the most accurate measurements possible. It is a series of cellulose filters, similar to the ones used to sample atmospheric specimens, each containing certified concentrations of nine metals known to be toxic at certain levels. The filters that make up this standard reference material (SRM) can be dissolved easily in acid and diluted with distilled water to the desired volume and concentration level. In solution form, the SRM can be used in atomic absorption, optical emission (plasma), spectrometry, spectrophotometry, or any other analytical techniques that require aqueous (water-based) standard solutions for calibrating instruments. Metals represented on each of the filters are barium carbonate, cadmium, chromium, iron, magnesium, nickel, lead, selenium, and zinc. Each SRM consists of six filters containing the metals and five blank filters that allow chemists to assess the ambient levels of the metals being measured. SRM 3087, Metals on Filter Media, sells for $155 and is available from the Standard Reference Materials Program, Rm. 215 Building 202, NIST, Gaithersburg, MD 20899, 301/975-6776.

X-RAY FLUORESCENCE SPECTROMETRY ORE AVAILABLE

A new fused ore x-ray fluorescence spectrometry standard has been developed by NIST for laboratories that analyze the constituent elements in rocks, ores, and clay. Standard reference material (SRM) 1834 is a silica base glass disk, 3 cm in diameter by 0.3-cm thick, for calibrating instruments. The synthetic glass material has an elemental composition similar to SRM 97a, Flint Clay, with the amount lost on ignition replaced by oxides of lithium and boron. SRM 1834 also can be used in quality-control applications and to monitor instrument stability. The new SRM has certified weight percent values for the following constituent elements: aluminum, barium, calcium, iron, magnesium, phosphorus, potassium, silicon, strontium, and titanium. SRM 1834, Fused Simulated Ore for X-Ray Fluorescence Spectrometry, is available for $298 from the Standard Reference Materials Program, Rm. 215 Building 202, NIST, Gaithersburg, MD 20899, 301/975-6776.

Standard Reference Data

DATABASE TO HELP TEST WRITING RECOGNITION DEVICES

A first-of-its-kind database containing over 1,000,000 handprinted characters has been developed by NIST to help measure the performance of systems designed to read unconstrained handwritten letters and numbers. Banks, insurance companies, and other form-processing organizations represent an enormous market for these systems. But such machines are not available, largely because of wide variations in writing style. Finding a standardized way to measure machine performance is an important link in developing the technology. To collect handwriting samples, NIST researchers asked more than 2,000 employees from the U.S. Bureau of the Census to fill out sample forms. NIST Special Database 1—Binary Images of Printed Digits, Alphas and Text is available on an ISO 9660 format CD-ROM disk for $895 from the Standard Reference Data Program, A323 Physics Building, NIST, Gaithersburg, MD 20899, 301/975-2208.

STANDARD REFERENCE DATA PRODUCTS CATALOG PUBLISHED

NIST Standard Reference Data Products 1990 Catalog (NIST Special Publication 782) provides the latest information on various data compilations, publications, and computerized databases that may be obtained from NIST and other sources. Critically evaluated data compilations for science and industry are available in the following areas: analytical chemistry, atomic physics, chemical kinetics, materials properties, molecular structure and spectroscopy, thermochemistry, and the thermophysical properties of fluids. Since 1968, the NIST Standard Reference Data Program has been responsible for coordinating on a national basis the evaluation of numerical data in the physical sciences. The evaluation of chemical and physical properties of substances and materials is carried out in the National Standard Reference Data System network of data centers. To obtain a copy of SP 782, send a self-addressed mailing label to Standard Reference Data Program, A323 Physics Building, NIST, Gaithersburg, MD 20899, 301/975-2208.

PC DATABASE AVAILABLE FOR HYDROCARBON MIXTURES

NIST scientists have developed a new database for calculating density, viscosity, and other important engineering property data of hydrocarbon mixtures petroleum, natural gas, and organic materials. The NIST Thermophysical Properties of Hydrocarbon Mixtures (Supertrapp) database is designed to provide rapid access to vital information on the storage and transportation of fluids, and for the design of new chemical processes. It is available on a floppy disk for personal computers (PCs). The interactive program allows users to calculate quickly various thermodynamic and transport properties for pure fluids or for mixtures of up to 20 components. These mixtures can be selected from a database of 116 components, mostly hydrocarbons such as ethane, hexane, and methane, and hydrocarbons as heavy as tetracosane. Some non-hydrocarbons, such as carbon dioxide, nitrogen, and oxygen, are included. NIST Standard Reference Database 4, Supertrapp, is available for $490 from the Standard Reference Data Program, A323 Physics Building, NIST, Gaithersburg, MD 20899, 301/975-2208.

MAJOR EXPANSION MADE TO CHEMICAL KINETICS DATABASE

The NIST Chemical Kinetics Database for personal computers (PCs) now contains information on the rates of more than 5,000 chemical reactions with more than 12,000 individual entries that include data on 2,400 compounds that are reactants or products. Chemists, environmentalists, and engineers will find it useful for modeling combustion systems, gas phase reactors, and chemical processes occurring in the atmosphere. These data are necessary to understand the reactions of such chemicals as fluorocarbons and their role in depleting the Earth's ozone layer. The database has increased searching speed and contains several new features, such as the simultaneous display of abstracts and graphics. Users can search by author name, add data to be plotted, and store comments and other information. PC Version 2.0 of the Chemical Kinetics Database, Standard Reference Database 17, is available for $300. It can be stored on the hard disk of any AT or XT-Class PC where it occupies 3.5 megabytes. Users of PC Version 1.0 may upgrade for $100. To order PC Version 2.0, contact the Standard Reference Data Program, A323 Physics Building, NIST, Gaithersburg, MD 20899, 301/975-2208.

DIPPR DATABASE EXPANDED TO 1,117 COMPOUNDS

The DIPPR (Design Institute for Physical Property Data) Data Compilation of Pure Compound Properties, 1990, now contains information on 39 properties for 1,117 pure chemical compounds of high industrial priority. The DIPPR database provides chemical engineers, manufacturers, and scientists with quick access to important information on the behavior of substances and their properties at various temperatures. The database includes information on the thermodynamic, physical, and transport properties of each chemical. Values are given for 26 single-valued property constants for each compound and for 13 properties as functions of temperature, calculated from correlation coefficients. The chemicals were selected by industry members of the American Institute of Chemical Engineers' (AIChE) DIPPR group and are considered to be the most important ones to industry. DIPPR, NIST Standard Reference Database 11, is available for $3,400 on standard diskettes for personal computers (PCs) or on magnetic tape. To order PC Version 5.0 or to obtain a license agreement for the database in magnetic-tape form, contact the Standard Reference Data Program, A320 Physics Building, NIST, Gaithersburg, MD 20899, 301/975-2208.

Volume 95, Number 5, September-October 1990
Journal of Research of the National Institute of Standards and Technology

Calendar

November 5–8, 1990
NORTH AMERICAN ISDN USERS' FORUM (NIU-FORUM)

Location: National Institute of Standards and Technology
Gaithersburg, MD

Integrated Services Digital Network (ISDN) is a telecommunications technology which can be used to send and receive voice, data, and pictures simultaneously over digital telephone lines. However, there is work to be done before this technology develops. User-defined applications, implementation agreements for the existing standards, and tests are needed to allow for a transparent, ubiquitous, and user-driven ISDN. NIST has formed—with private industry (both manufacturers and prospective users of ISDN technology)—a new organization to find ways to promote the implementation of ISDN standards in interoperable products and services, and to identify potential ISDN applications. This is the North American ISDN Users' Forum (NIU-Forum). This meeting of the forum will begin with tutorials on ISDN-related subjects. User's workshops will identify, define, and prioritize user applications of ISDN. Implementors' workshops will define implementation agreements for ISDN. Working group meetings will discuss issues related to the use and implementation of ISDN technology. For registration information, please call Lori Phillips on 301/975-3881. Sponsored by NIST.

Contact: Dawn Hoffman, B364 Materials Building, NIST, Gaithersburg, MD 20899, 301/975-2937.

November 26–30, 1990
EXPERIMENT DESIGN FOR SCIENTISTS AND ENGINEERS

Location: National Institute of Standards and Technology
Gaithersburg, MD

This 5-day workshop is for scientists and engineers in R&D or manufacturing with a goal of improving quality and productivity. Although some familiarity with the concepts of elementary statistics would be useful, it is not required. The workshop will de-emphasize mathematical development, and replace it with an experimentalist-based evolution of concepts and techniques with reinforcement via practical applications. The workshop covers specific designs that have proven best for three very important classes of problems: (1) how to ferret out systematically the most important factors from a large number of potential factors; (2) how to converge to an optimal operating condition starting from a best guess; and (3) how to identify settings of controllable factors that reduce variability caused by unavoidable sources of variation (Taguchi's quality engineering approach). For general information call Shirley Bremer on 301/975-2845. The workshop text is Statistics for Experimenters by Box, Hunter, and Hunter (Wiley). Sponsored by NIST.

Contact: Eric Lagergren, A337 Administration Building, NIST, Gaithersburg, MD 20899, 301/975-3245.

December 6–7, 1990

WORKSHOP ON FUNDAMENTALS OF CARBON/CARBON

Location: National Institute of Standards and Technology
Gaithersburg, MD

The objective of this workshop is to encourage fundamental research, interdisciplinary cooperation, and technology transfer to increase the understanding of mechanisms and processes relevant to new concepts for high-temperature carbon/carbon composites. The scientific issues to be covered at the workshop include mechanisms and materials for high-temperature oxidation inhibition, protective coatings, and fundamental modeling of microstructure and mechanical properties. Approximately 12 invited speakers will review the current state of the art. Poster papers are encouraged. Sponsored by the Air Force Office of Scientific Research and NIST.

Contact: David C. Cranmer, A329 Materials Building, NIST, Gaithersburg, MD 20899, 301/975-5753.

October 14–18, 1991

THIRD INTERNATIONAL SYMPOSIUM ON ESR DOSIMETRY AND APPLICATIONS

Location: National Institute of Standards and Technology
Gaithersburg, MD

This symposium will focus on current applications of electron spin resonance (ESR) spectroscopy in the general areas of ionizing radiation dosimetry, archeological dating, and instrumentation, including imaging and measurements for solid state, biological, and medical applications. The topics of discussion include solid state effects, reference dosimetry, transfer dosimetry, dating, and geology. Also, presentations of new, innovative developments in the ESR field are encouraged. Sponsored by NIST, the China University of Science and Technology, and the International Atomic Energy Agency.

Contact: Marc F. Desrosiers, C214 Radiation Physics Building, NIST, Gaithersburg, MD 20899, 301/975-5639.